The Role of *POLG* Mutations in Human Disease

Maria-Eleni Anagnostou

MRes

A thesis submitted for the degree of Doctor of Philosophy

Wellcome Trust for Mitochondrial Research

Institute of Neuroscience

Newcastle University

October 2017

Author's Declaration

This thesis is submitted to the degree of Doctor of Philosophy at Newcastle University. The research was performed at the Wellcome Trust Centre for Mitochondrial Research, Institute of Neuroscience, under the supervision of Professors Robert McFarland and Robert W. Taylor. I certify that it is my own work unless otherwise stated in the text.

This thesis includes collaborative work. All collaborative work has been fully acknowledged in the thesis, making it clear which is my own work.

The systematic review (Chapter 3) was conducted in collaboration with Dr. Ng who provided clinical and genetics data.

The work on iNPC's (Chapter 5) was performed in collaboration with Dr. Boczonadi. Specifically, Dr. Boczonadi performed the conversion of fibroblasts into iNPC's discussed in sections 5.3.1 and 5.3.2. The remaining work on iNPC's was performed by myself under the supervision of Dr. Boczonadi.

With regards to the work performed on neuropathology (Chapters 6 and 7) the data from the occipital lobe tissue of controls 2, 3 and 8 were kindly provided by Dr. Hayhurst.

I certify that none of the material offered in this thesis has been previously submitted by me for a degree or any other qualification at this or other university.

Abstract

Mitochondrial diseases due to mutations in the nuclear *Polymerase gamma* (*POLG*) gene, have emerged as a common group of disorders, collectively referred to as *POLG*-related disorders.

POLG is responsible for mitochondrial DNA (mtDNA) replication and repair. Defects in *POLG* result in secondary mtDNA defects including mtDNA depletion and deletions, which result in respiratory chain deficiency in affected tissues.

POLG-related disorders are characterised by phenotypic diversity with common neurological deficits such as epilepsy, which constitutes its predominant manifestation. Alpers' syndrome is a severe form of *POLG*-related disorders and it is a rare, early-onset, progressive encephalohepatopathy characterised by: intractable seizures, developmental delay, ataxia, visual loss and liver dysfunction. It is particularly devastating as effective treatments do not currently exist, and little is known about its molecular pathophysiology downstream from *POLG* mutations.

The aim of this work was to gain further insight into the pathogenesis of Alpers, through the characterisation of mitochondrial dysfunction in *POLG*-mutant fibroblasts, and neuropathological investigation of post-mortem brain tissue from affected patients.

Fibroblast characterisation using quantitative methodologies, revealed no evidence of mitochondrial dysfunction in primary *POLG*-mutant fibroblasts derived from patients with Alpers.

Neuropathological assessment of three cortical regions revealed extensive respiratory chain deficiencies in interneurons and to a lesser extent pyramidal neurons in patients with Alpers, which was associated with severe pyramidal neuron loss. A variable degree of astrogliosis, was also observed. Additionally, mtDNA depletion was found in tissue from adult patients with *POLG*-mutations as well as occasional mtDNA deletions.

This study provides evidence that *POLG* mutations exert a tissue-specific effect in Alpers. Mitochondrial respiratory chain deficiencies in interneurons and pyramidal neurons, combined with extensive pyramidal neuron loss may result in altered neuronal dynamics and contribute to the underlying neuropathology and clinical manifestations of Alpers.

For Kyriakos and Dimitra Filippou

Acknowledgments

Firstly, I would like to thank my supervisors Professors Robert McFarland and Robert Taylor for their guidance and support throughout my PhD and for giving me the opportunity to work on this project. I would like to express my wholehearted gratitude to Robert McFarland for his incredible patience and help throughout this PhD.

I would like to express my gratitude to Professor Sir Doug Turnbull for giving me the opportunity of being a part of the Mitochondrial Research Group.

I would like to thank all the patients involved in this study and their families and the sponsor of this project: The Ryan Stanford Appeal, as without them this work would have not been possible.

I would like to express a special 'thank you' to Dr. Nichola Lax. I am extremely grateful for her guidance and support. She showed me incredible patience and without her invaluable help and advice concerning the neuropathological study I would not have reached this stage.

I would like to thank those with whom I have collaborated throughout this project. I would like to thank Dr. Alex Laude and Dr. Trevor Booth (Bio-Imaging Unit, Newcastle University) for their technical help with the confocal microscope. Special thanks to Dr. Yi Ng for his contribution to the systematic review manuscript and his huge help with the clinical terms and findings. Thanks to Dr. Veronika Boczonadi (Institute of Genetic Medicine, Centre for Life) for her contribution and invaluable help with the iNPC's. I would like to thank Dr. Hannah Hayhurst for her contribution in the neuropathological study.

Many thanks to Dr. Amy Reeve and Dr. Eve Simcox for all the help with the fibroblasts. I would like to thank all MRG members for their help, guidance and friendship. It has been a pleasure working with such a fantastic group!

Finally, I would like to thank all my family and friends for their love and support over the last three years. My dad for being there at every step, especially during the hard times of the PhD.

Conferences

Poster presentation at North East Postgraduate (NEPG) Annual Conference 2015: **Maria-Eleni Anagnostou**, Robert W. Taylor and Robert McFarland. **Characterization of polymerase gamma (*POLG*)-mutant fibroblasts with Alpers and Alpers-like disease.**

Poster presentation at UK Neuromuscular Translational Research Conference 2016: **Anagnostou ME**., Taylor RW., McFarland R. **Characterisation of Polymerase gamma (*POLG*)-mutant fibroblasts with Alpers and Alpers-like disease.**

Oral presentation at North East Postgraduate (NEPG) Annual Conference 2016: **Maria-Eleni Anagnostou**, Robert McFarland, Doug Turnbull and Nichola Z. Lax. **Understanding the neuropathology of Alpers syndrome**.

Poster presentation at MitOX Annual Meeting 2016: **Maria-Eleni Anagnostou**, Robert McFarland, Doug Turnbull and Nichola Z. Lax**. Understanding the mechanisms contributing to Alpers neuropathology.**

Poster presentation at UK Neuromuscular Translational Research Conference 2017: **Maria-Eleni Anagnostou**, Nichola Z. Lax, Robert W. Taylor, Doug Turnbull and Robert McFarland. **Understanding the mechanisms contributing to Alpers neuropathology.**

Publications

Hayhurst H., **Anagnostou ME.**, Bogle HJ., Grady J., Taylor RW., Bindoff LA., McFarland R., Turnbull DM. and Lax NZ. **Dissecting the neuronal vulnerability underpinning Alpers' syndrome: a clinical and pathological study***. Manuscript in preparation.*

Anagnostou ME., Ng YS., Taylor RW., McFarland R. (2016): **Epilepsy due to mutations in the mitochondrial polymerase gamma (*POLG*) gene: a clinical and molecular review**. Epilepsia. Oct 57 (10): 1531-1545**.**

Olahova M., Thompson K., Hardy SA., Barbosa IA., Besse A., **Anagnostou ME**., White K., Davey T., Simpson MA., Champion M., Enns G., Schelley S., Lighowlers RN., Chrzanowska-Lightowlers ZM., McFarland R., Deshpande C., Bonnen PE. and Taylor RW (2017). **Pathogenic variants in HTRA2 cause an early-onset mitochondrial syndrome associated with 3-methylglutaconic aciduria.** J Inherit Metab Dis. Jan 40 (1): 121-130

Table of Contents

Chapter 1 Introduction 1
1.1 Mitochondria 1
1.1.1 The Mitochondrion: A Brief Introduction 1
1.1.2 Mitochondrial Structure 1
1.1.3 Mitochondrial Biogenesis 3
1.1.4 Mitochondrial Dynamics 3
1.1.5 Neuronal Mitochondria 4
1.2 Oxidative Phosphorylation (OXPHOS) 5
1.2.1 Complex I: ubiquinone oxidoreductase 7
1.2.2 Complex II: Succinate: ubiquinone oxidoreductase 10
1.2.3 Complex III: Ubiquinol: cytochrome c oxidoreductase 11
1.2.4 Complex IV: Cytochrome c oxidase 12
1.2.5 Complex V: ATP Synthase 13
1.2.6 Supercomplexes 14
1.3 Other Mitochondrial Functions 15
1.3.1 Apoptosis and Cell Death Mechanisms 15
1.3.2 Iron-Sulphur (Fe-S) Cluster Biogenesis 16
1.3.3 Production of Reactive Oxygen Species (ROS) 16
1.3.4 Calcium signalling 17
1.4 The Mitochondrial Genome 17
1.5 Mitochondrial DNA (mtDNA) Transcription and Translation 19
1.6 Mitochondrial DNA (mtDNA) Replication 20
1.7 Mitochondrial Genetics 21
1.7.1 Maternal inheritance and Bottleneck 21
1.7.2 Heteroplasmy and Threshold Effect 22
1.7.3 Mitochondrial DNA (mtDNA) Mutations and Repair Mechanisms 23
1.7.4 Mitochondrial DNA (mtDNA) Depletion 23

1.8 Mitochondrial Disease 25
1.9 Mitochondrial DNA Polymerase Gamma (POLG) 29
1.9.1 Polymerase Gamma (POLG): History, cloning and expression 29
1.9.2 Polymerase Gamma (POLG) Structure and Functions 30
1.9.3 Polymerase Gamma (POLG) Mutations 33
1.9.4 Polymerase Gamma 2 (POLG2) Mutations 37
1.9.5 Polymerase Gamma (POLG) Related Disorders 37
1.9.6 Polymerase Gamma (POLG) Mouse Models 40
1.10 Alpers' Syndrome 40
1.10.1 Clinicopathological Description and History 40
1.10.2 Early-onset Alpers 41
1.10.3 Late-onset Juvenile Alpers 42
1.10.4 Alpers and POLG 42
1.10.5 Involvement of Other Genes than POLG in Alpers 44
1.10.6 Affected Tissues 44
1.10.7 Treatment of Alpers Manifestations 45
1.11 Aims and Objectives of Study 47
Chapter 2 Materials and Methods 49
2.1 Equipment and Consumables 49
2.1.1 Equipment 49
2.1.2 Software 50
2.1.3 Consumables 51
2.2 Chemicals and Reagents 52
2.2.1 Solutions 52
2.2.2 Antibodies 54
2.2.3 Histological Reagents 55
2.2.4 Tissue Culture Reagents 56
2.2.5 Seahorse Reagents 57

2.2.6 Molecular Biology Reagents 57
2.3 Tissue Culture 59
2.3.1 Human Fibroblasts 59
2.3.2 General Cell Growth and Maintenance 60
2.3.3 Harvesting Cells 60
2.3.4 Freezing and Storage 61
2.3.5 Conversion of POLG-Mutant Human Fibroblasts into induced Neuronal Progenitors (iNPC's) 61
2.4 Live-Cell imaging 62
2.4.1 Growing Cells 62
2.4.2 Live Cell Dyes 62
2.4.3 Confocal Imaging 62
2.4.4 Mitochondrial Network Analysis 62
2.4.5 Nucleoid Analysis 63
2.4.6 Mitochondrial Membrane Potential and Motility Analysis. 63
2.5 Bioenergetics 63
2.5.1 XF Extracellular Flux Analysis Experiments 63
2.6 Neurohistopathological Methods in FFPE Brain Tissue 65
2.6.1 Patient Cohort 65
2.6.2 Control Tissue 70
2.6.3 Immunohistochemical Staining Protocol 72
2.6.4 Two-Dimensional Quantification of Neuronal Density 74
2.6.5 Immunofluorescent Identification of Respiratory Chain-Deficient Interneurons and Pyramidal Neurons 74
2.6.6 Confocal Microscopy and Image Processing 79
2.6.7 Statistics 79
2.7 Molecular Methods 80
2.7.1 Preparation of Whole Cell Lysate 80

2.7.2 Bradford Assay 80
2.7.3 SDS-PAGE 80
2.7.4 Western Blotting and Immunodetection 81
2.7.5 DNA Extraction from Human Fibroblasts 82
2.7.6 DNA Extraction from FFPE Brain Tissue 83
2.7.7 DNA Extraction from Frozen Brain Homogenate Tissue 83
2.7.8 Polymerase chain reaction (PCR) 87
2.7.9 Gel Electrophoresis 89
2.7.10 Assessment of mtDNA Copy Number and Deletions 89
Chapter 3 Epilepsy due to Mutations in the Mitochondrial Polymerase Gamma (*POLG*) Gene: A Systematic Review 91
3.1 Introduction 91
3.2 Aims and Objectives 93
3.3 Methods 94
3.3.1 Search strategy 94
3.3.2 Data extraction and statistics 94
3.4 Results 94
3.4.1 Systematic search results 94
3.4.2 Summary of clinical findings 95
3.4.3 POLG Genetics 95
3.4.4 Histopathology 97
3.4.5 MtDNA Copy Number 103
3.4.6 MtDNA Deletions/Rearrangements 108
3.4.7 Respiratory Chain (RC) Biochemistry 108
3.4.8 Genotype to Phenotype Correlations 110
3.5 Discussion 111
3.5.1 Limitations 115
3.5.2 Conclusions 115

Chapter 4 Characterisation of Human *POLG*-mutant Fibroblasts from Patients with Alpers 117
4.1 Introduction 117
4.2 Aims and Objectives 119
4.3 Results 120
4.3.1 Investigation of Mitochondrial Morphology and Dynamic Networks in POLG-mutant Fibroblasts from Patients with Alpers 122
4.3.2 Analysis of Mitochondrial Nucleoids in POLG-Mutant Fibroblasts from patients with Alpers 126
4.3.3 Motility Analysis of POLG-Mutant Fibroblasts derived from Patients with Alpers 130
4.3.4 Quantification of mtDNA Copy Number in POLG-mutant Fibroblasts from Patients with Alpers 132
4.3.5 Bioenergetics of POLG-mutant Fibroblasts with Alpers 134
4.3.6 Assessment of steady-state levels of POLG 138
4.4 Discussion 140
4.4.1 Limitations 142
4.4.2 Future Work 143
4.4.3 Conclusions 144
Chapter 5 Conversion of *POLG*-mutant Fibroblasts derived from Patients with Alpers into Induced Neuronal Progenitor Cells (iNPC's) 147
5.1 Introduction 147
5.2 Aims and Objectives 148
5.3 Results 149
5.3.1 Conversion of Human Patient-derived Fibroblasts into iNPC's using Retroviral and Sendai Virus Treatment 149
5.3.2 Conversion of POLG-mutant Fibroblasts into iNPC's using Sendai Virus 153
5.4 Discussion 155

Chapter 6 Mechanisms of Neurodegeneration in Patients with Alpers and *POLG* Mutations: Assessment of Respiratory Chain Deficiency and MtDNA Damage 159
6.1 Introduction 159
6.2 Aims 161
6.3 Results 162
6.3.1 Molecular Investigations of POLG 162
6.3.2 Mitochondrial Respiratory Chain Protein Expression within GABAergic Interneurons and Pyramidal Neurons of Patients with Alpers 163
6.3.3 Mitochondrial DNA Copy Number in Brain Tissue 183
6.3.4 Mitochondrial DNA Deletions in Brain Tissue 189
6.4 Discussion 194
6.4.1 Limitations 199
6.4.2 Future work 199
6.4.3 Conclusions 200
Chapter 7 Neuropathological Features in patients with Alpers 201
7.1 Introduction 201
7.2 Aims and Objectives 202
7.3 Results 203
7.3.1 Patient Characteristics 203
7.3.2 Gross Neuropathology Findings 205
7.3.3 Neuron loss 208
7.3.4 Astrogliosis 219
7.4 Discussion 232
7.4.1 Introduction 232
7.4.2 Astrogliosis 234
7.4.3 Limitations 235
7.4.4 Future work 235
7.4.5 Conclusions 235

Chapter 8 Final Discussion....237
8.1 Introduction....237
8.2 Major Findings....238
8.2.1 Characterisation of Mitochondrial Function in POLG-mutant Fibroblasts from Patients with Alpers....238
8.2.2 In vitro Modelling of Alpers Syndrome Secondary to POLG Mutations 240
8.2.3 Mechanisms of Epilepsy and Neurodegeneration in Alpers....241
8.3 Limitations....246
8.4 Future Work....246
8.5 Concluding Remarks....247
Appendix A....249
Appendix B....267
Bibliography....275

List of Figures

Figure 1.1: Mitochondrial structure. 3
Figure 1.2: The OXPHOS system. 7
Figure 1.3: Structure of mammalian complex I. 8
Figure 1.4: Step-wise assembly of mitochondrial complex I. 10
Figure 1.5: Crystal structure of complex II and the three prosthetic groups from porcine heart mitochondria. 11
Figure 1.6: Complex III in *S. cerevisiae*. 12
Figure 1.7: Schematic representation of complex IV. 13
Figure 1.8: Human complex V. 14
Figure 1.9: The mitochondrial genome. 18
Figure 1.10: Current model of transcription initiation in mtDNA. 19
Figure 1.11: The three models of mammalian mtDNA replication. 21
Figure 1.12: Tertiary structure of POLG catalytic subunit. 33
Figure 1.13: Mutations identified in *POLG*. 35
Figure 3.1: Flow chart of literature search and selection. 95
Figure 3.2: The ten most common *POLG* pathogenic variants identified in literature and their location within *POLG* domains. 96
Figure 3.3: Pie chart demonstrating the frequencies (%) of pathogenic *POLG* recessive mutations identified in the literature. 96
Figure 3.4: Correlation between mtDNA copy number in the liver and age of death/disease duration in patients with Alpers and *POLG*-related epilepsy reported in the literature. 105
Figure 3.5: Comparison of mtDNA copy number (% of control mean) in liver and muscle from patients with Alpers and *POLG*-related epilepsy patients. 106
Figure 3.6: Kaplan-Meier survival curves based on the different genotypes. 110
Figure 4.1: Mitochondrial networks and membrane potential in POLG-mutant fibroblasts from paediatric individuals withAlpers. 123
Figure 4.2: Mitochondrial morphology and networks in paediatric *POLG* and *FBXL4*-mutant fibroblasts. 124
Figure 4.3: Mitochondrial networks and membrane potential in *POLG*-mutant fibroblasts from adolescent individuals with Alpers. 125
Figure 4.4: Nucleoid morphology and distribution in *POLG* and *FBXL4*-mutant fibroblasts derived from patients with early-onset Alpers. 127

Figure 4.5: Nucleoid morphology and distribution in *POLG*-mutant fibroblasts from patients with late-onset Alpers.....128
Figure 4.6: Quantitative analysis of number of nucleoids in early and late-onset *POLG*-mutant and early-onset *FBXL4*-mutant fibroblasts. 129
Figure 4.7: Quantification of mitochondrial motility in *POLG*-mutant fibroblasts derived from patients with Alpers. 131
Figure 4.8: Quantification of mtDNA copy number in *POLG*-mutant fibroblasts from Alpers patients.....133
Figure 4.9: Bioenergetics of *POLG*-mutant fibroblasts derived from patients with early-onset Alpers. 135
Figure 4.10: Bioenergetics of *POLG*-mutant fibroblasts derived from a patients with later-onset Alpers. 136
Figure 4.11: Characterisation of POLG steady-state levels in fibroblast from patients with Alpers.....138
Figure 5.1: Conversion of *POLG*-mutant fibroblasts into iNPC's using retroviral treatment. 150
Figure 5.2: Conversion of *POLG*-mutant fibroblasts using Sendai virus.....152
Figure 5.3: Timeline of conversion of fibroblasts with the homozygous p.(Ala467Thr) mutations from an adolescent patient with Alpers into iNPC's using Sendai virus. .154
Figure 6.1: Agarose gel electrophoresis showing no amplification of relevant *POLG* DNA regions.....163
Figure 6.2: Quadruple immunofluorescence showing respiratory chain deficiencies involving complexes I and IV in interneurons of the occipital lobe from patients with Alpers. 168
Figure 6.3: Extensive respiratory chain deficiency involving complex I and to a lesser degree complex IV in GABAergic interneurons of the occipital lobe in patients with Alpers. 169
Figure 6.4: Quadruple immunofluorescence demonstrating complex I and IV respiratory chain deficiencies in patient interneurons from the parietal lobe of patients with Alpers.....171
Figure 6.5: Extensive respiratory chain deficiency involving complex I and to a lesser degree, complex IV in GABAergic interneurons from the parietal lobe of patients with Alpers. 172

Figure 6.6: Quadruple immunofluorescence demonstrating complex I respiratory chain protein expression in pyramidal neurons from the parietal lobe of patients with Alpers. 174
Figure 6.7: Quadruple immunofluorescence demonstrating complex IV respiratory chain protein expression in pyramidal neurons of the parietal lobe from patients with Alpers. 175
Figure 6.8: Respiratory chain deficiency involving complex I and to a lesser extent, complex IV in pyramidal neurons of the parietal lobe from patients with Alpers. 176
Figure 6.9: Quadruple immunofluorescence demonstrating complex I and complex IV respiratory chain protein deficiencies in GABAergic interneurons from the frontal lobe of patients with Alpers. 178
Figure 6.10: Respiratory chain deficiency involving complex I and to a lesser extent, complex IV in GABAergic interneurons of the frontal lobe from patients with Alpers. 179
Figure 6.11: Quadruple immunofluorescence demonstrating complex I respiratory chain protein expression in pyramidal neurons from the frontal lobe of patients with Alpers. 180
Figure 6.12: Quadruple immunofluorescence demonstrating complex IV respiratory chain protein expression in pyramidal neurons from the frontal lobe of patients with Alpers. 181
Figure 6.13: Respiratory chain protein expression of complexes I and IV in pyramidal neurons of the frontal lobe from patients with Alpers. 182
Figure 6.14: MtDNA copy number in the occipital lobe. 187
Figure 6.15: MtDNA copy number in the parietal lobe. 188
Figure 6.16: MtDNA copy number in the frontal lobe of patients with *POLG* mutations. 188
Figure 6.17: *MT-ND4* deletions in the occipital lobe of patients with *POLG* mutations. 190
Figure 6.18: *MT-ND4* deletions in the parietal lobe of patients with *POLG* mutations. 191
Figure 6.19: *MT-ND4* deletions in the frontal lobe of patients with *POLG* mutations. 192
Figure 7.1: GAD65-67 immunostaining in occipital lobe from patients with Alpers. .209
Figure 7.2: SMI-32P immunostaining in the occipital cortex of patients with Alpers. 210

Figure 7.3: Neuronal densities in occipital cortex of patients with Alpers' syndrome. 211
Figure 7.4: GAD65-67 immunostaining in the parietal cortex of patients with Alpers. 213
Figure 7.5: SMI-32P immunostaining in the parietal cortex of patients with Alpers. 214
Figure 7.6: Neuronal loss in the parietal cortex of patients with Alpers. 215
Figure 7.7: GAD65-67 immunostaining in the frontal cortex of patients with Alpers. 216
Figure 7.8: Interneuron densities in the frontal cortex from patients with Alpers. 217
Figure 7.9: Interneuron to pyramidal neuron density ratios in occipital and parietal cortices of patients with Alpers. 218
Figure 7.10: Astrogliosis of the grey matter in the occipital lobe of patients with Alpers' syndrome. 221
Figure 7.11: Astrogliosis of the white matter in the occipital lobe of patients with Alpers' syndrome. 222
Figure 7.12: Astrogliosis of the grey matter in the parietal lobe of patients with Alpers. 224
Figure 7.13: Astrogliosis of the white matter in the parietal lobe of patients with Alpers. 225
Figure 7.14: Astrogliosis of the grey matter in the frontal lobe of patients with Alpers. 227
Figure 7.15: Astrogliosis of the white matter in the frontal lobe from patients with Alpers. 228
Figure 8.1: Proposed mechanism underlying epilepsy and neurodegeneration in Alpers modified from previously published hypotheses. 244

List of Tables

Table 1.1: Clinical syndromes of mitochondrial disease. 28
Table 1.2: Clinical description of mitochondrial disorders. 38
Table 2.1: Human Fibroblasts used in this study. 59
Table 2.2: Medium formulations. 60
Table 2.3: Compounds used in seahorse extracellular flux analyser. 64
Table 2.4: Patient details used in the neuropathology study. 69
Table 2.5: Neuropathological details of the controls used in this study. 71
Table 2.6: Primary antibodies used for immunohistochemistry. 73
Table 2.7: Primary and secondary antibodies used for immunofluorescence staining. 78
Table 2.8: Reagents and volumes used for SDS-PAGE. 81
Table 2.9: Primary antibodies used for immunodetection. 82
Table 2.10: Details of patients and controls used in the study of mtDNA damage. ... 86
Table 2.11: Primer sequences used to amplify the nuclear DNA regions spanning the sites containing the individual point mutations in the *POLG* gene. 88
Table 2.12: Primer sequences used to amplify the previous PCR product. 88
Table 2.13: Primer locations and sequences used for real-time PCR. 90
Table 2.14: Probe locations and sequences used for real-time PCR. 90
Table 3.1: Summary of histological abnormalities identified in different brain regions (including cerebral cortex, cerebellum, basal ganglia, thalamus, brainstem and hippocampus) from patients with Alpers and *POLG*-related epilepsy. 100
Table 3.2: Summary of histopathological findings in brain, liver and muscle from patients with Alpers and *POLG*-related epilepsy. 103
Table 3.3: Descriptive statistics for mtDNA copy number from liver, muscle, blood and fibroblasts from patients with Alpers and *POLG*-related epilepsy reported in the literature. 107
Table 3.4: MtDNA copy number in liver, muscle, blood and fibroblasts from patients with Alpers and *POLG*-related epilepsy. 107
Table 4.1: Characteristics of patient and control fibroblasts used in this study. 121
Table 4.2: Summary of mtDNA copy number (% of control mean) in *POLG*-mutant fibroblasts. 134
Table 4.3: Bioenergetic capacity of *POLG*-mutant fibroblasts. 137
Table 5.1:Characteristics of patient and control fibroblasts used in this study. 149

Table 6.1: Details of patients used in the study of respiratory chain protein expression.. 165
Table 6.2: Details of controls used in the study of respiratory chain protein expression. 166
Table 6.3: Details of patients and controls used in the study of mtDNA damage. ...185
Table 6.4: Calculated percentage (%) mtDNA copy number relative to the control mean for occipital, parietal and frontal lobes. 189
Table 6.5: Summary of mtDNA copy number and deletions. Key: N/A=not applicable. 193
Table 7.1: Patient details used in this study. 204
Table 7.2: Control details used in this study. 205
Table 7.3: Gross neuropathology findings from patients with Alpers. 207
Table 7.4: Summary of neuron loss and astrogliosis. Key: N/A=not applicable. 231

Abbreviations

A	Adenine
ACAD9	Acyl-CoA Dehydrogenase Family, Member 9 Protein
ACTH	Adrenocorticotrophic Hormone
AD	Alzheimer's Disease
ADP	Adenosine Diphosphate
adPEO	Autosomal Dominant Progressive External Ophthalmoplegia
AHS	Alpers-Huttenlocher Syndrome
AID	Accessory Interacting Subdomain
Ala	Alanine
AMPK	Adenosine Monophosphate-Activated Protein Kinase
ANS	Ataxia Neuropathy Spectrum
ANT1	Adenine Nucleotide Translocase Isoform 1
AP	Apurimidinic
APS	Adenosine 5'-Phosphosulphate
arPEO	Autosomal Recessive Progressive External Ophthalmoplegia
Asp	Aspartate
ATP	Adenosine 5'-Triphosphate
B2M	Beta-2 Microglobulin
BAX	Bcl-2 Associated X Protein
Bcl-2	B-cell Lymphoma 2
BER	Base Excision Repair
BN-PAGE	Blue Native Polyacrylamide Gel Electrophoresis
bp	Base Pair
BSA	Bovine serum albumin
C	Cytosine
Ca^{2+}	Calcium
CARS2	Cysteinyl-tRNA Synthetase 2
CMT2A	Charcot-Marie-Tooth Disease Type 2A
c-Myc	Myelocytomatosis Viral Oncogene
CNS	Central Nervous System

CO_2	Carbon Dioxide
COX	Cytochrome Oxidase
CPEO	Chronic Progressive External Ophthalmoplegia
CRISPR	Clustered Regularly Interspaced Short Palindromic Repeats
Ct	Threshold Cycle
CT Scan	Computerised Tomography Scan
DAB	Diaminobenzidine
DEPC	Diethylpyrocarbonate
DGUOK	Deoxyguanosine Kinase
D-Loop	Displacement Loop
DMSO	Dimethyl Sulfoxide
DNA	Deoxyribonucleic Acid
dNTP	Deoxyribonucleotide Triphosphate
DPX	Distyrene Plasticizer Xylene
Drp1	Dynamin Related Protein 1
ECSIT	Evolutionary Conserved Signalling Intermediate in Toll Pathway Protein
EDTA	Ethylenediaminetetraacetic Acid
EEG	Electroencephalography
EM	Electron Microscopy
EPC	Epilepsia Partialis Continua
ETC	Electron Transport Chain
FAD	Flavin Adenine Dinucleotide
FARS2	Phenylalanine tRNA Synthetase 2
FBXL4	F-Box and Leucine Rich Repeat Protein 4
FCCP	Carbonyl Cyanide-4-(Trifluoromethoxy) Phenylhydrazone
FCS	Fetal Calf Serum
Fe	Iron
FENN	Focal Energy Dependent Neuronal Necrosis
Fe-S	Iron-Sulphur
FFPE	Formalin Fixed Paraffin Embedded
G	Guanine
g	Gram
GABA	Gamma Aminobutyric Acid

GAD	Glutamic Acid Decarboxylase
GFAP	Glial Fibrillary Acid Protein
Glu	Glutamine
Gly	Glycine
GSK-3	Glycogen Synthase Kinase 3
H^+	Hydrogen Ion
H_2O	Water
HCl	Hydrochloric Acid
HRP	Horseradish Peroxidase
HSP	Heavy Strand Promoter
IgG	Immunoglobulin G
IMM	Inner Mitochondrial Membrane
IMS	Intermembrane Space
iNPC	Induced Neuronal Progenitor Cells
iPSC	Induced Pluripotent Stem Cells
kb	Kilobases
kDa	Kilo Dalton
KLF4	Kruppel Like Factor 4
KOS	Polycistronic Vector (acronym for genes hKLF4, hc-MYC and hOCT3/4)
KSS	Kearns-Sayre Syndrome
Leu	Leucine
LHON	Leber Hereditary Optic Neuropathy
LS	Leigh Syndrome
LSP	Light Strand Promoter
M	Molar
MCHS	Myocerebrohepatopathy Spectrum
MCU	Mitochondrial Calcium Uniporter
MDa	Mega Dalton
MELAS	Mitochondrial Encephalopathy, Lactic Acidosis, and Stroke-like Episodes
MEMSA	Myoclonic Epilepsy Myopathy Sensory Ataxia
MERRF	Myoclonic Epilepsy with Ragged Red Fibres
Mfn	Mitofusin

$MgCl_2$	Magnesium Chloride
MIRAS	Mitochondrial Recessive Ataxia Syndrome
ml	Millilitre
mm	Millimetre
MMR	Mismatch Repair
mPTP	Mitochondrial Permeability Transition Pore
MRI	Magnetic Resonance Imaging
mRNA	Messenger RNA
MT	Mitochondrial
mtDNA	Mitochondrial DNA
MTERF1	Mitochondrial Transcription Termination Factor 1
mtIF3	Mitochondrial Translation Initiation Factor 3
MTS	Mitochondrial Targeting Sequence
mt-SSB	Mitochondrial Single Stranded Binding Protein
MTTs	Mitochondrial tRNA Genes
MYC	Myelocytomatosis Viral Oncogene
NAD	Nicotinamide Adenine Dinucleotide
NARP	Neuropathy, Ataxia, and Retinitis Pigmentosa
NARS2	Asparaginyl tRNA Synthetase 2
NBTR	Newcastle Brain Tissue Resource
ND1	NADH dehydrogenase Subunit 1
ND2	NADH Dehydrogenase Subunit 2
ND4	NADH dehydrogenase Subunit 4
ND6	NADH Dehydrogenase Subunit 6
ND8	NADH Dehydrogenase Subunit 8
nDNA	Nuclear DNA
NDUFA	NADH Dehydrogenase (Ubiquinone) 1 α Subcomplex
NDUFAB	NADH Dehydrogenase (Ubiquinone) 1 α/β subcomplex
NDUFAF	NADH Dehydrogenase (Ubiquinone) Assembly Factor
NDUFB	NADH Dehydrogenase (Ubiquinone) 1 β Subcomplex
NDUFS	NADH Dehydrogenase (Ubiquinone) Fe-S Protein
NDUFV	NADH Dehydrogenase (Ubiquinone) Flavoprotein
NDUFA13	NADH dehydrogenase 1 Alpha Subcomplex Subunit 13
NDUFB8	NADH dehydrogenase 1 Beta Subcomplex Subunit 8

NEAA	Non Essential Amino Acids
nm	Nanometres
NPA	No Primary Antibody
O_2	Molecular Oxygen
OCR	Oxygen Consumption Rate
OCT3/4	Octamer Binding Transcription Factor 3/4
O_H	Origin of Heavy strand Replication
O_L	Origin of Light Strand Replication
OMM	Outer Mitochondrial Membrane
OPA1	Optic Atrophy 1
OXPHOS	Oxidative Phosphorylation
PARS2	Prolyl tRNA Synthetase 2
PBS	Phosphate Buffered Saline
PBST	Phosphate Buffered Saline with Tween
PCR	Polymerase Chain Reaction
PD	Parkinson Disease
Pen/Strep	Penicillin/Streptomycin
PFA	Paraformaldehyde
PGC1-α	Peroxisome Proliferator-activated Receptor γ, Coactivator 1 Alpha
Pink1	PTEN-induced Putative Kinase 1
PMI	Post Mortem Interval
PMSF	Phenylmethanesulfonyl Fluoride
POLG	Mitochondrial Polymerase Gamma
POLG2	Mitochondrial Polymerase Gamma 2, Accessory Subunit
POLRMT	Mitochondrial RNA Polymerase
Pro	Proline
PVDF	Polyvinylidene fluoride
Q	Ubiquinone
QH_2	Ubiquinol
qPCR	Real-Time Polymerase Chain Reaction
RC	Respiratory Chain
RITOLS	RNA Incorporated Through the Lagging Strand
RNA	Ribonucleic Acid

ROCK	Rho-Associated Coil-Coiled Containing Proteinase K
ROI	Region of Interest
ROS	Reactive Oxygen Species
RRM2B	Ribonucleotide Reductase M2B
rRNA	Ribosomal RNA
RT	Room Temperature
SD	Standard Deviation
SDHA	Succinate Dehydrogenase Complex Flavoprotein Subunit A
SDHB	Succinate Dehydrogenase Complex Flavoprotein Subunit B
SDHC	Succinate Dehydrogenase Complex Flavoprotein Subunit C
SDHD	Succinate Dehydrogenase Complex Flavoprotein Subunit D
SDS-PAGE	Sodium Dodecyl Sulfate Polyacrylamide Gel Electrophoresis
SE	Status Epilepticus
Ser	Serine
SLE	Stroke-Like Episode
SOX2	SRY Related High Morbidity Group Box Protein 2
SRC	Spare Respiratory Capacity
SSBP1	Single-Stranded Binding Protein 1
SUCLA2	Succinate-CoA ligase ADP-forming Beta Subunit
SUCLG1	Succinate CoA-ligase Alpha Subunit
T	Thymine
TAE	Tris-Acetate EDTA Buffer
TBS	Tris-Buffered Saline
TBST	Tris- Buffered Saline with Tween
TCA	Tricarboxylic Acid Cycle
TEFM	Mitochondrial Transcription Elongation Factor
TEMED	Tetramethylethylenediamine
TFAM	Mitochondrial Transcription Factor A
TFB2M	Mitochondrial Transcription Factor B2
TGF-β	Transforming Growth Factor Beta
Thr	Threonine
TK2	Thymidine Kinase 2
TMRM	Tetramethyl Rhodamine Methyl Ester

TNFR1	Tumour Necrosis Factor Receptor 1
TWNK	Twinkle mtDNA Helicase
Trp	Tryptophan
TYMP	Thymidine Phosphorylase
U	Uracil
VDAC	Voltage-dependent Anion Channels
µl	Microlitre
µm	Micrometres

Chapter 1 Introduction

1.1 Mitochondria

1.1.1 The Mitochondrion: A Brief Introduction

Mitochondria are dynamic, intracellular organelles, present in the cytoplasm of all nucleated cells. Mitochondria are highly abundant in eukaryotic cells, comprising of approximately 20% of the total cell volume, (Martin and Mentel, 2010) highlighting their biological importance. Their major role involves energy production in the form of adenosine triphosphate (ATP), through the process of Oxidative Phosphorylation (OXPHOS). It is estimated that approximately 90% of cellular energy requirements are met by OXPHOS (Herrera *et al.*, 2015). In addition to their role in energy production, mitochondria are major regulators of: apoptosis (Orrenius, 2004), iron-sulphur (Fe-S) biogenesis (Rouault, 2012), production of Reactive Oxygen Species (ROS) (Sena and Chandel, 2012) and calcium handling (Rizzuto *et al.*, 2012).

Various theories exist regarding mitochondrial evolution, however these remain controversial. The ‘endosymbiosis theory’ is the most widely accepted theory of mitochondrial evolution and states that mitochondria have evolved from an alpha eubacterial ancestor, which originated from an Archaebacterium. This alpha proteobacterium, became engulfed by a host cell through a process known as ‘endosymbiosis’; and eventually became a mitochondrion (Margulis, 1975).

Alternatively, more recent evidence proposes that mitochondria have evolved after an endosymbiotic relationship between a Eubacterium, which produced hydrogen as a waste product and a hydrogen-dependent Archaebacterium. This theory is known as the ‘hydrogen hypothesis’ (Martin and Muller, 1998).

The first association between mitochondria and cellular respiration was established in 1953 (Lazarow and Cooperstein, 1953).

1.1.2 Mitochondrial Structure

Mitochondria are dynamic, double-membraned organelles, typically oval or rod-like in shape. Mitochondria are 1-4μm in length and 0.3-0.7μm in diameter, as revealed by electron microscopy (EM) (Palade, 1953). Mitochondria comprise: a permeable outer membrane (OMM), the intermembrane space (IMS), the matrix and a selectively

permeable inner membrane (IMM); all of which exert specialised functions. A simplified structure of the mitochondria is illustrated in Figure 1.1.

The OMM is a phospholipid bilayer which resembles the composition of a eukaryotic cell's cytoplasmic membrane. The OMM allows diffusion of lipid soluble molecules into the IMS. In addition, the OMM has a high abundance of proteins known as 'porins' or voltage-dependent anion channels (VDAC) which enable transfer of proteins under 5kDa to the IMS (Lemasters and Holmuhamedov, 2006).

The IMS refers to the space between the OMM and the IMM. This space resembles the environment of the cytoplasm; however, this is highly specific to large proteins required for mitochondrial function. The IMS is pivotal as it is the site where protons are pumped from the Electron Transport Chain (ETC) to maintain the membrane potential and generate the proton gradient required for ATP synthesis.

The IMM surrounds the mitochondrial matrix and is highly abundant in proteins including cardiolipin, which are required for the biochemical processes occurring in the organelle (*Mitochondrial Dysfunction in Neurodegenerative Disorders*, 2016). Consequently, the IMM is impermeable to polar molecules and anions compared to the permeable nature of OMM. The deep invaginations of the IMM give rise to highly folded structures (known as cristae) that project to surround the mitochondrial matrix (Palade, 1953). This is the site where both the mitochondrial DNA (mtDNA) and RNA lie and are attached to the IMM. The matrix is also the site where the Citric Acid Cycle (TCA) takes place during aerobic respiration. The presence of cristae increases the surface area over which OXPHOS and proton gradient maintenance occur; therefore, cristae morphology reflects the energy demands of the cell (Gautheron, 1984).

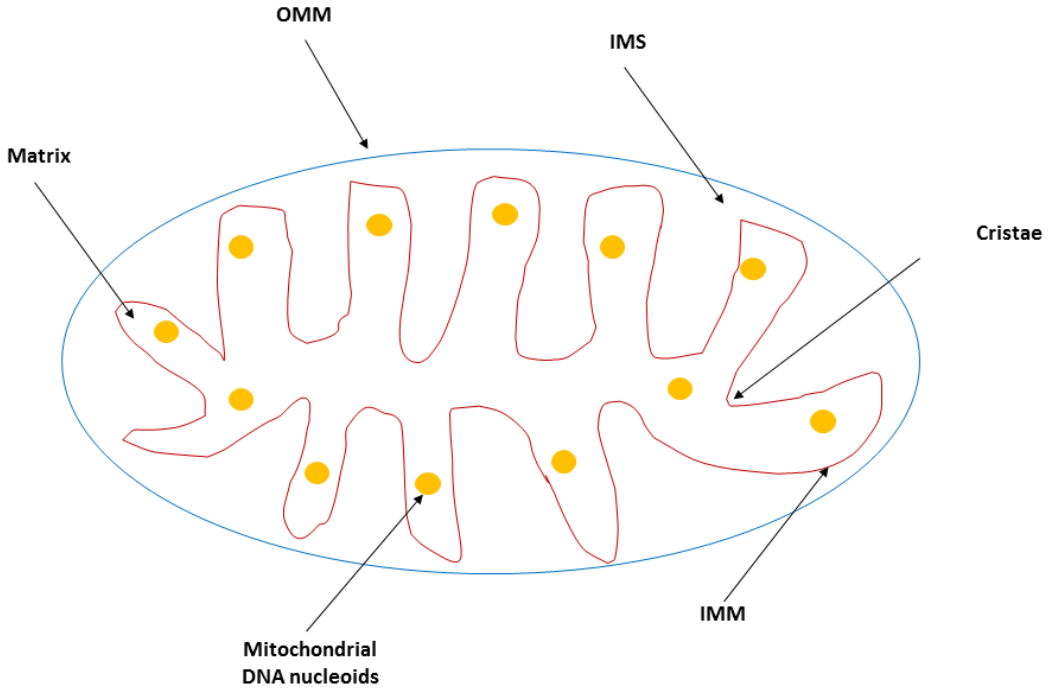

Figure 1.1: Mitochondrial structure. A typical oval-shaped mitochondrion comprising of a double membrane (OMM and IMM) which is spaced by the inter-membrane space (IMS). The inner membrane (IMM) forms cristae (highly folded) which encloses the mitochondrial matrix which contains mitochondrial nucleoids. Key: OMM=outer mitochondrial membrane; IMM=inner mitochondrial membrane; IMS=intermembrane space.

1.1.3 Mitochondrial Biogenesis

Mitochondrial number varies amongst tissues and they can increase their number and size to meet ATP requirements. The process through which mitochondria are generated from pre-existing mitochondria is known as 'biogenesis'. Mitochondrial biogenesis is tightly controlled by the Peroxisome Proliferator-Activated Receptor γ, Coactivator 1 α (PGC1-α) (Jornayvaz and Shulman, 2010). *In vivo* experiments have shown that PGC1-α expression results in the increased expression of key mitochondrial proteins (Puigserver *et al.*, 1998), which is also regulated by AMPK (AMP-Activated Protein Kinase). AMPK plays an important role as an energy sensor within the cell. Decreased AMPK activity with increasing age has been reported; suggesting reduced mitochondrial biogenesis with ageing (Reznick *et al.*, 2007). Understanding the mechanisms regulating mitochondrial biogenesis may provide insight into the process of ageing and ageing-associated disease.

1.1.4 Mitochondrial Dynamics

Mitochondria are highly dynamic organelles which frequently change shape and move around the cell to meet energy requirements. Mitochondria constantly undergo fission and fusion forming elongated tubular networks (Bereiter-Hahn, 1990; Huang

et al., 2011). Fission and fusion are two opposite processes that allow content exchange between mitochondria to maintain their size/number and location. Mitochondrial dynamics influence mtDNA stability and respiratory function and are vital for cell survival (Chan, 2012).

Fission involves the division of a single mitochondrion into two mitochondria. This occurs under stress, when cellular ATP demand is increased. Fission and mitochondrial DNA (mtDNA) replication are synchronised so that both daughter mitochondria receive sufficient mtDNA copies. Key regulators of mitochondrial fission are Dynamin Related Protein 1 (Drp1) (Bleazard *et al.*, 1999) and Endophilin B1 (Karbowski *et al.*, 2004).

Mitochondrial fusion involves the integration of two or more mitochondria into a single mitochondrion. This assimilation results in the formation of a long interconnected network. Fusion is a multi-step process involving the fusion of the outer and inner mitochondrial membranes. Fusion of the outer membranes, is regulated by Mitofusin (Mfn) 1 and 2 (Chen *et al.*, 2003a), whereas fusion of the inner membranes is controlled by Optic Atrophy 1 (OPA1) (Cipolat *et al.*, 2004).

Defects in mitochondrial dynamics have been associated with neurodegenerative diseases. For example, mutations in the fusion protein OPA1 are associated with autosomal dominant optic atrophy (Alexander *et al.*, 2000), while mutations in *Mfn2* are the underlying genetic defect in Charcot-Marie-Tooth Type 2A (CMT2A); a hereditary motor and sensory neuropathy (Zuchner *et al.*, 2004; Feely *et al.*, 2011).

Moreover, defects in mitochondrial dynamics have been linked to early disease stages in Alzheimer's disease (AD) and Parkinson's disease (PD) (Zhu *et al.*, 2013; Bose and Beal, 2016). However, the relationship between neurodegenerative diseases and altered mitochondrial dynamics has not yet been elucidated.

1.1.5 Neuronal Mitochondria

Neurons are polarized cells with very limited glycolytic capacity, therefore relying on OXPHOS for ATP production (Zsurka and Kunz, 2015). Neurons comprise a cell soma in one extremity and a pre-synaptic bouton at the other extremity, interconnected by a thin, long axon. The energy requirements vary between different neuronal regions, depending on their function. Evidence has shown that synaptic transmission is the highest energy consumption process (Harris *et al.*, 2012).

Specialised machinery is essential to distribute mitochondria to distal regions, where the ATP requirements are high. Neuronal mitochondria are generated in the cell soma and are highly motile; travelling along the axon to meet variable ATP requirements (Sheng and Cai, 2012).

Mitochondrial trafficking occurs through anterograde and retrograde motor protein-assisted transport (Sheng and Cai, 2012). Anterograde movement involves the axonal movement of mitochondria from the cell soma towards the synaptic terminals via kinesin motors. Retrograde movement is facilitated by dynein motors and the process is described as mitochondrial transport from the axon back to the cell body in order to be degraded and recycled through mitophagy (Sheng, 2014).

Efficient mitochondrial trafficking is vital not only for the recruitment and redistribution of mitochondria to sites of high ATP demand but also for the removal of depolarised mitochondria and their replacement with healthy mitochondria. Disruption of mitochondrial trafficking results in ATP depletion within neurons, insufficient mitochondrial recycling and altered Ca^{2+} buffering; all of which contribute to loss of synaptic transmission. Such defects have been associated with neurodegenerative disorders including AD, PD, Huntington's disease and Amyotrophic Lateral Sclerosis (ALS) (Sheng and Cai, 2012).

1.2 Oxidative Phosphorylation (OXPHOS)

The most fundamental and, arguably, well-known role of mitochondria is ATP production via oxidative phosphorylation (OXPHOS). This involves the aerobic synthesis of ATP from ADP and inorganic phosphate during oxidation of NADH. The number of mitochondria per cell depends on the energy demand of the tissue.

The OXPHOS machinery consists of five, multi-subunit enzyme complexes which are embedded in the IMM. These include: NADH: ubiquinone oxidoreductase (complex I), succinate: ubiquinone oxidoreductase (complex II), ubiquinol: cytochrome *c* oxidoreductase (complex III) and cytochrome *c* oxidase (complex IV). Complexes I-IV comprise the ETC and involve the transfer of electrons and reduction of water resulting in the generation of a proton gradient across the IMM. The proton gradient is then used by a fifth complex, F_0F_1 ATP synthase (complex V) to drive ATP synthesis (Mitchell, 1961). As a result, 34 molecules of ATP are produced. The basic components of the OXPHOS machinery are illustrated in Figure 1.2.

Cellular respiration is initiated by the process of glycolysis, a form of anaerobic respiration, which occurs in the cytoplasm of eukaryotic cells. The process involves the breakdown of one glucose molecule into two pyruvate molecules. During glycolysis a number of intermediate substrates are generated resulting in the production of two ATP molecules. Although only two ATP molecules are produced through anaerobic respiration, these are generated 100 times faster than the ATP molecules produced by OXPHOS (Pfeiffer *et al.*, 2001).

The pyruvate molecules produced by glycolysis are then transported to the mitochondrial matrix where pyruvate decarboxylation takes place, generating Acetyl CoA, which then enters the TCA cycle with NAD^+ and FADH substrates. Both NAD^+ and FADH are reduced into NADH and $FADH_2$, while Acetyl Co A is oxidised into Carbon Dioxide (CO_2). Electrons from the reduced substrates are passed through complexes I and II, causing the reduction of ubiquinone (Q) to ubiquinol (QH_2). Ubiquinol delivers the electrons to complex III where QH_2 is oxidised to Q, causing the reduction of the electron carrier cytochrome *c*. The electrons are then passed from cytochrome *c* to complex IV leading to cytochrome *c* oxidation and reduction of ½ O_2 molecule to H_2O. The transfer of electrons through the ETC results in the generation of protons. The latter are pumped from the matrix into the IMS, generating the electrochemical gradient used by complex V for ATP production (Lodish *et al.*, 2000).

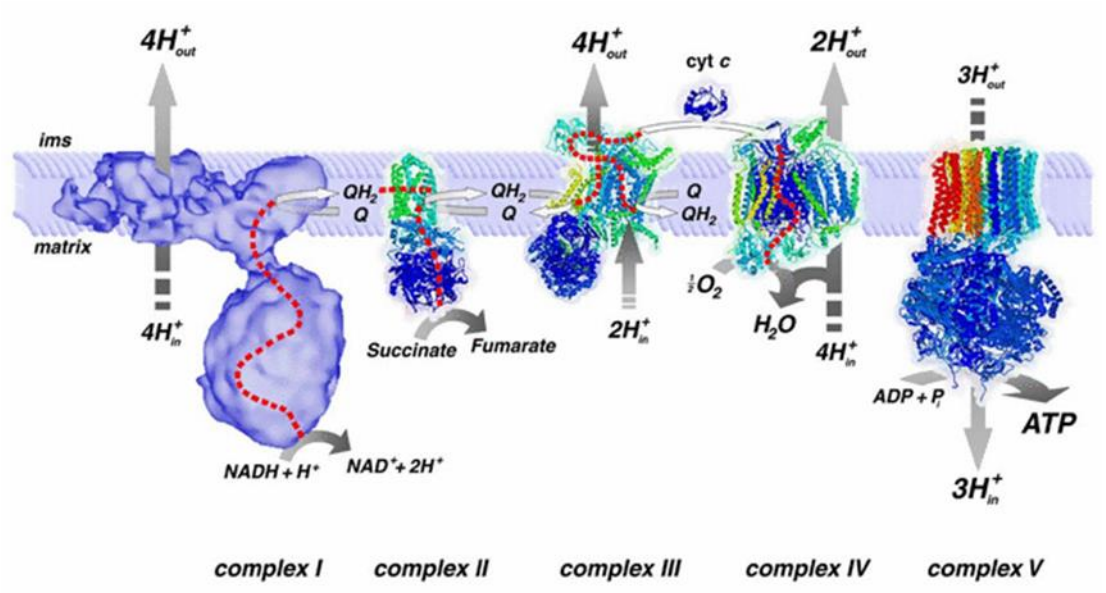

Figure 1.2: The OXPHOS system. The five complexes of the OXPHOS system are located within the IMM and undergo a series of redox reactions. Electrons enter the OXPHOS machinery at complexes I and II and are passed to complex III through reduction of ubiquinone (Q) to ubiquinol (QH_2). At complex III QH_2 is re-oxidised to Q and the electrons generated are passed to complex IV via cytochrome *c* (cyt *c*). The proton gradient resulting from the transfer of electrons through complexes I, III and IV leads to proton pumping into the matrix. An electrochemical gradient is then generated which is used by Complex V for ATP synthesis. NADH: ubiquinone oxidoreductase. Image taken from (Nijtmans *et al.*, 2004).

1.2.1 Complex I: ubiquinone oxidoreductase

Mammalian Complex I NADH ubiquinone oxidoreductase mediates oxidation of NADH to NAD^+. Two electrons are generated and passed to Q, reducing it to QH_2, prior to oxidation by complex III. As electrons are passed, translocation of four hydrogen ions occurs across the IMM into the IMS, creating an electrochemical gradient, which is the motive-force driving ATP production by complex V.

Complex I is the largest complex of the OXPHOS machinery with a molecular weight of approximately 1MDa. It exists in an L-shaped configuration with one arm embedded in the IMM and the other arm projecting into the mitochondrial matrix (see Figures 1.2 and 1.3). It consists of 44 protein subunits, from which one, NFUFAB1 is present as a dimer. Seven structural subunits are encoded by the mitochondrial DNA (mtDNA), while the remaining 37 subunits are nuclear-encoded (nDNA).

Complex I is required for oxidation of NADH, reduction of ubiquinone and proton pumping. It consists of three functional modules including Q, proximal P (a)/(b), distal P (a)/(b) and N, resulting from the assembly of all 45 subunits, which exert different functions (Guerrero-Castillo *et al.*, 2017). The N module is the site where NADH oxidation takes place. The N module harbours a Flavin Mononucleotide (FMN) which

is an electron acceptor binding to the flavoprotein NDUFV1 during NADH oxidation. Once FMN is reduced, the electrons are passed through Fe-S clusters in the N and Q modules. The Q module is the site where electron transfer to ubiquinone occurs. The P module is responsible for proton pumping. The structure of complex I and its three functional subunits are illustrated in Figure 1.3.

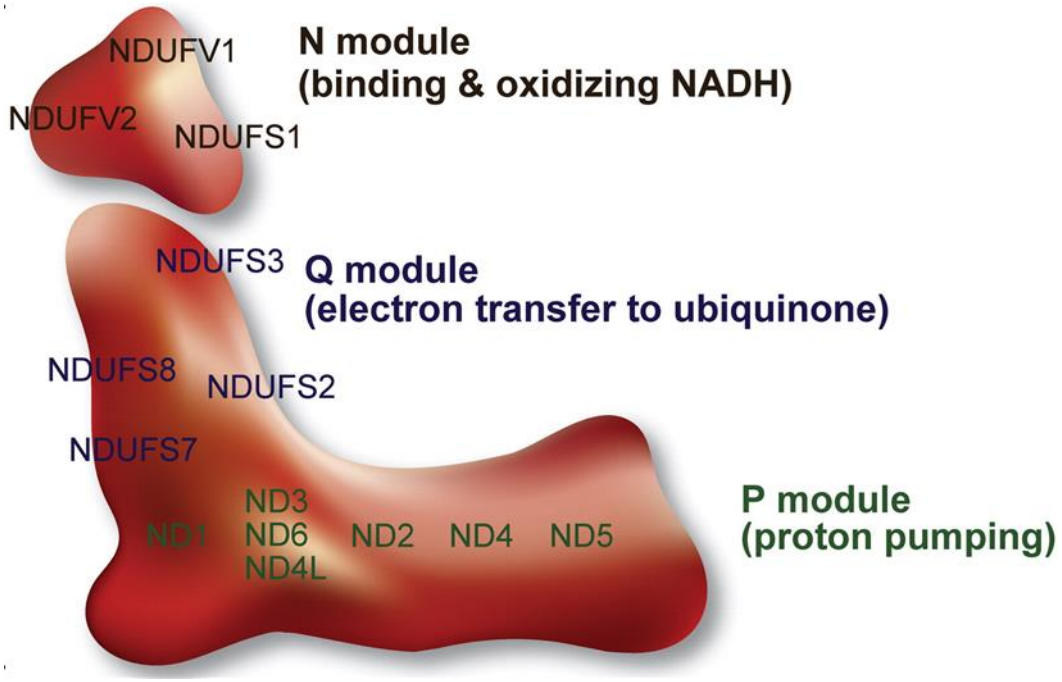

Figure 1.3: Structure of mammalian complex I. It consists of three conserved functional modules (N, Q and P). The N module is required for NADH oxidation. The Q module is the site of electron transfer and P is the proton pumping module. Both N and Q modules project to the matrix while the P module is situated within the inner mitochondrial membrane. Figure modified from (Mimaki *et al.*, 2012).

The catalytic 'core' of complex I comprises14 protein subunits. Seven protein subunits are encoded by the mtDNA including: ND1, ND2, ND3, ND4, ND4L, ND5 and ND6 and the remaining subunits are encoded by nDNA (NDUFV1, NDUFV2, NDUFS1, NDUFS2, NDUFS3, NDUFS7 and NDUFS8) (Ugalde *et al.*, 2004; Formosa *et al.*, 2017). The remaining subunits are 'accessory' and there is evidence suggesting a role in the regulation of the assembly and stabilisation of complex I (Andrews *et al.*, 2013).

The biogenesis of complex I requires at least 11 assembly factors. (Formosa *et al.*, 2017; Guerrero-Castillo *et al.*, 2017). The assembly of complex I occurs in a step-wise fashion. The assembly of protein subunits (including mtDNA and nDNA-encoded) is a coordinated process, where the assembly factors are required for maturation (Formosa *et al.*, 2017; Guerrero-Castillo *et al.*, 2017). The Q module is the first to be assembled and consists of two 'core' subunits (NDUFS2, NDUFS3). The

‘accessory’ subunits NDUFA5 and NDUFS7, NDUFA5 NDUFS7 and NDUFS8 (Guerrero-Castillo *et al.*, 2017).

Following the Q module assembly, and Q/P (a) assembly starts, assisted by the assembly factors followed by the addition of the mtDNA-encoded ND1 subunit. Subsequently, NDUFA13, NDUFA8 and NDUFA3, NDUFA9 and NDUFA1 are incorporated (Guerrero-Castillo *et al.*, 2017).

The remaining subunits comprising the proximal P (b) and distal P (a)/(b) modules form independently. NDUFC1, NDUFC2 and ND2 form first mediated by the assembly factors NDUFAF1, ECSIT, ACAD9 and COA1. This is followed by incorporation of ND3, ND6 and ND4L, resulting in the formation of proximal P (b).

The distal P (a) starts forming by the incorporation of NDUFB5, NDUFB10, NDUFB11 and NDUFB6. AT5SL is thought to modulate early stages of the distal P (a) formation, although its exact function remains unknown (Guerrero-Castillo *et al.*, 2017).

The formation of the distal P (b) module involves the incorporation of the following subunits: NDUFB2, NDUFB3, NDUFB8, NDUFB9, NDUFAB1 and ND5.

The N-module is added to the Q-P sub-complex. The incorporation of subunits NDUFS1, NDUFA2, NDUFV1, NDUFV2, NDUFV3, NDUFA12, NDUFS4, NDUFA6, NDUFA7 and NDUFAB1 occurs. Maturation of complex I requires the dissociation of the assembly factors from the intermediate complexes (Formosa *et al.*, 2017). The assembly of complex I is illustrated in Figure 1.4.

Defects in complex I protein subunits are the most commonly reported abnormality in children with mitochondrial encephalopathies. A typical example of mitochondrial disease due to complex I deficiency is Leigh Syndrome (LS), which can be a result of defects in mtDNA and nDNA-encoded subunits or assembly factors (Koopman *et al.*, 2013). The large size of this complex involving several protein subunits requiring multiple factors for correct assembly may account for its vulnerability to deficiency states in mitochondrial disease (Darin *et al.*, 2001).

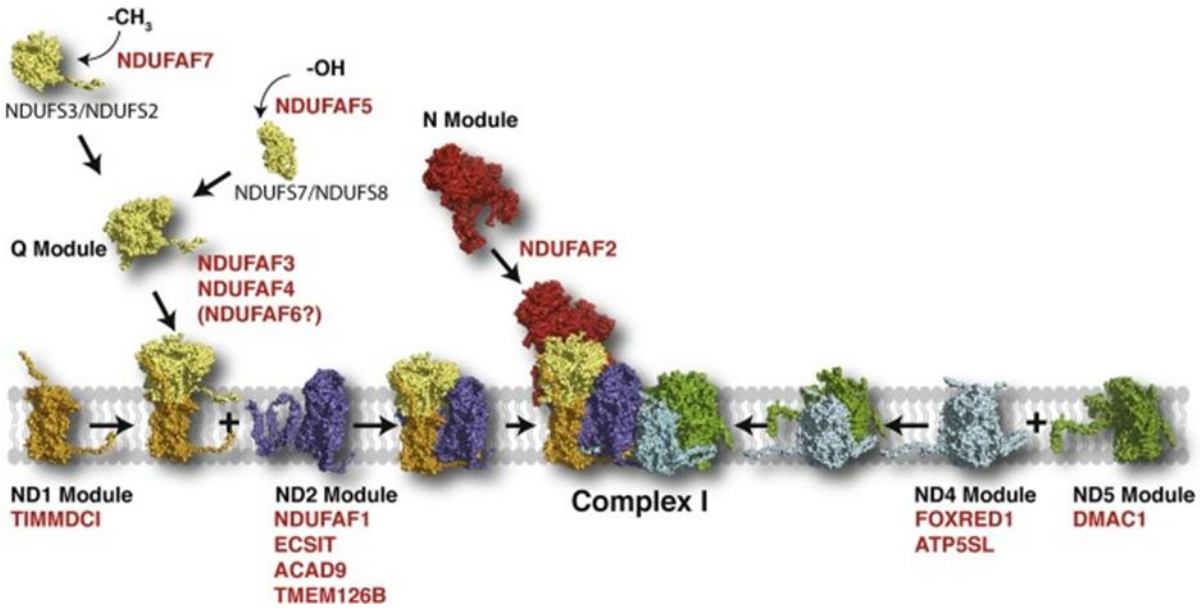

Figure 1.4: Step-wise assembly of mitochondrial complex I. Complex I consists of different modules which are assembled individually before formation of complex I and its association with complexes III and IV. The Q module involves incorporation of ND1. ND2 integrates with the Q module. ND4 and ND5 associate before they are integrated to Q/ND1/ND2 allowing the complete formation of the membrane arm of complex I. The integration of ND1 completes the assembly of complex I. The assembly factors required are indicated in red colour (Formosa et al., 2017).

1.2.2 Complex II: Succinate: ubiquinone oxidoreductase

Complex II is required for the oxidation of succinate to fumarate during the Citric Acid Cycle (TCA). The electrons generated are then passed to Q which is reduced to QH_2 during OXPHOS (Cecchini, 2003).

Complex II is the smallest complex of the OXPHOS system and consists of four protein subunits, including: SDHA, SDHB, SDHC and SDHD. All four subunits are encoded by nDNA. Hydrophilic SDHA and SDHB comprise the catalytic core of complex II, situated in the mitochondrial matrix. In contrast SDHC and SDHD are located in the IMM. Assembly of complex II is mediated by the SDHAF1 and SDHF2 assembly factors (Rutter *et al.*, 2010; Koopman *et al.*, 2013).

Complex II is characterised by the presence of three prosthetic groups including: FAD, iron-sulphur clusters (Fe-S) and haem. The [2Fe-2S] cluster is located at the N-terminus, while the [4Fe-4S] and [3Fe-3S] clusters are linked to the C-terminus (Bezawork-Geleta *et al.*). The crystal structure of complex II is illustrated in Figure 1.5.

Complex II is required for the reduction of FAD^+ to $FADH_2$ through SDHA, which oxidises succinate to fumarate. SDHB then is used for the re-oxidation and of $FADH_2$ to FAD^+ before electrons are passed from SDHC and SDHD to ubiquinone causing

its reduction to QH_2 (Rutter *et al.*, 2010). The passage of electrons through complex II is not involved in proton translocation (Cecchini, 2003).

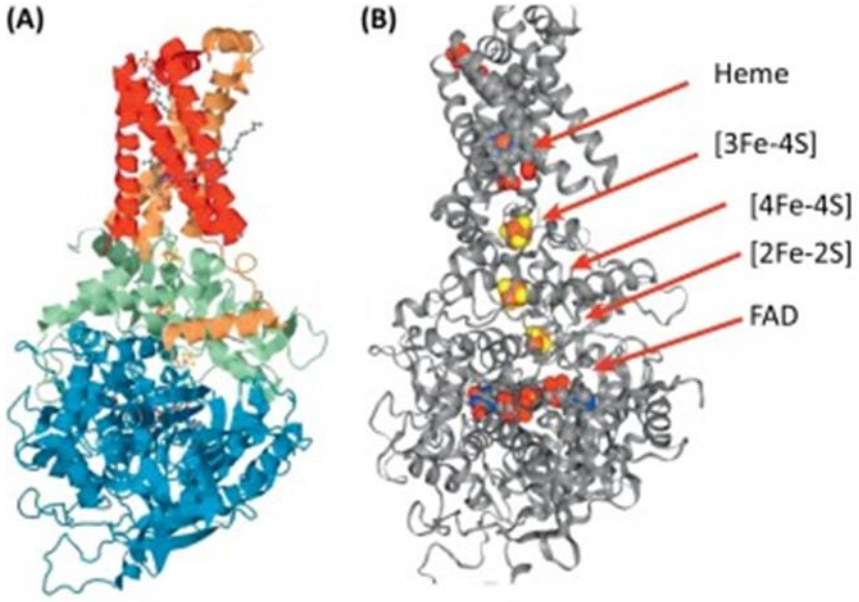

Figure 1.5: Crystal structure of complex II and the three prosthetic groups from porcine heart mitochondria. Illustration of SDH subunits including: SDHA (blue), SDHB (green), SDHC (light brown), SDHD (red). (B) Location of the three prosthetic groups in complex II. Image taken from (Bezawork-Geleta *et al.*, 2017).

1.2.3 Complex III: Ubiquinol: cytochrome c *oxidoreductase*

Complex III, ubiquinol:cytochrome *c* oxidoreductase exists as a homodimer and is responsible for the re-oxidation of QH_2 .Complex III is approximately 500kDa and consists of 11 protein subunits, of which only one, cytochrome *b*, is mtDNA-encoded. Cytochrome *b* together with cytochrome *c* and the Rieske Fe-S cluster protein constitutes the catalytic core of complex III (Saraste, 1999).

Following oxidation of QH_2, two electrons are passed from complexes I and II to complex III. The electrons passing through complex III are donated to cytochrome *c*, in a two-step reaction. The first step involves the transfer of one electron to the Fe-S cluster, which then passes to cytochrome *c* through cytochrome *c1*. The second step involves the recycling of the other electron to Q via the Q-cycle. The Q-cycle involves the oxidation of two ubiquinol molecules causing the reduction of ubiquinone through the transfer of two electrons. During the Q cycle, two protons are pumped from the matrix across the IMM to the IMS (Mitchell, 1975). Cytochrome *c*, a mobile electron carrier, passes the electrons it accepts to complex IV (Iwata *et al.*, 1998). The dimeric form of complex III in *S. cerevisiae* is illustrated in Figure 1.6.

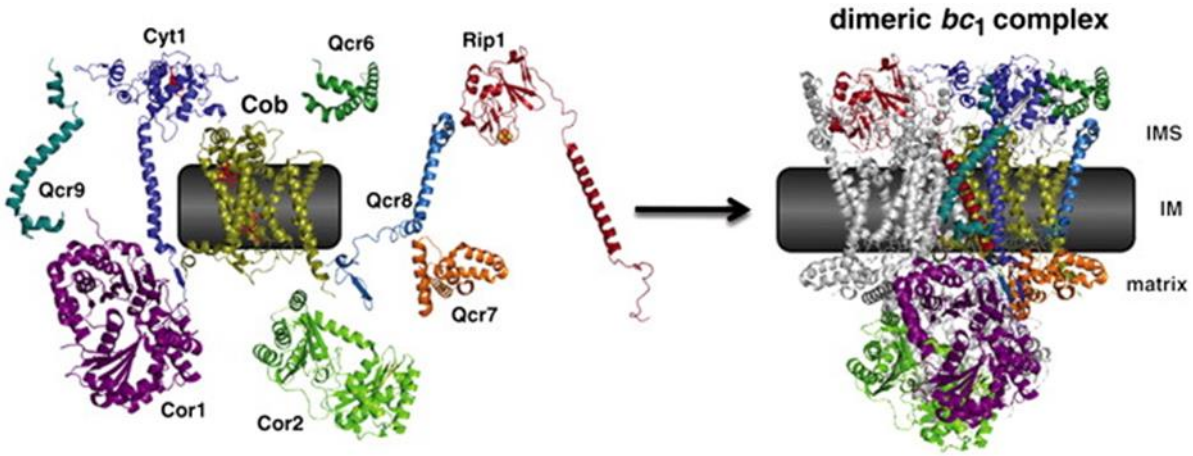

Figure 1.6: Complex III in *S. cerevisiae*. Individual monomer subunits are shown in the left. The dimeric form of complex III is shown on the right. Figure taken from (Smith *et al.*, 2012).

1.2.4 Complex IV: Cytochrome c oxidase

Complex IV is the terminal oxidase of the ETC and exists in a dimeric form. It is composed of 14 structural subunits; of which the three are the largest and are mtDNA-encoded (COXI, COXII and COXIII) and the remaining 10 are nuclear-encoded. COXI is believed to have a major role in the assembly of complex I (Mick *et al.*, 2011). Complex IV assembly is mediated by at least 18 assembly factors (Koopman *et al.*, 2013). A schematic representation of complex IV is shown in Figure 1.7.

COXI and COXII constitute the catalytic 'core' containing haem α and α_3 and two copper groups: Cu_A and Cu_B. Electrons are transferred through haem α and copper centres prior to the reduction of O_2 to H_2O. This process involves the translocation of four protons, resulting in a proton gradient, which is then used by complex V for ATP synthesis (Tsukihara *et al.*, 1996).

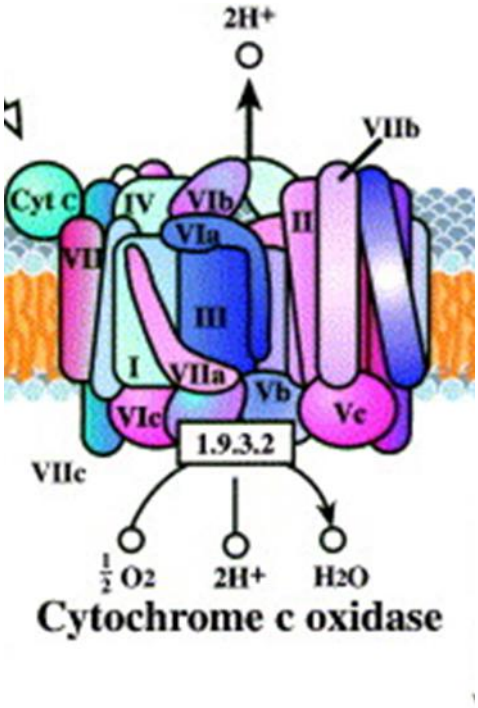

Figure 1.7: Schematic representation of complex IV. The mtDNA-encoded COXI, COXII and COXIII are shown in the centre of the structure. Cytochrome c (labelled as Cyt c), which functions as an electron carrier is shown on the left (green circle). Complex IV receives electrons from cytochrome c to form water by the combination of molecular oxygen and hydrogen ions. Image modified from (Mandavilli *et al.*, 2002).

1.2.5 Complex V: ATP Synthase

Complex V, ATP synthase is a large complex consisting of multiple subunits. Two domains are encoded by the mtDNA including ATPases 6 and 8 (Anderson *et al.*, 1981). Complex V consists of two main subunits, both of which consist of numerous proteins: F_0, which is embedded in the inner membrane and F_1, the catalytic domain, located on the matrix side of the inner membrane. The structure of human complex V is illustrated in Figure 1.8.

ATP synthase utilises the proton gradient generated from the transfer of electrons through the ETC (complexes I, II and IV). This electrochemical gradient is the force that drives protons to the F_0 subunit of ATP synthase, causing it to rotate. The F_1 subunit rotates in the opposite direction, enabling ATP production from ADP and inorganic phosphate (Yoshida *et al.*, 2001).

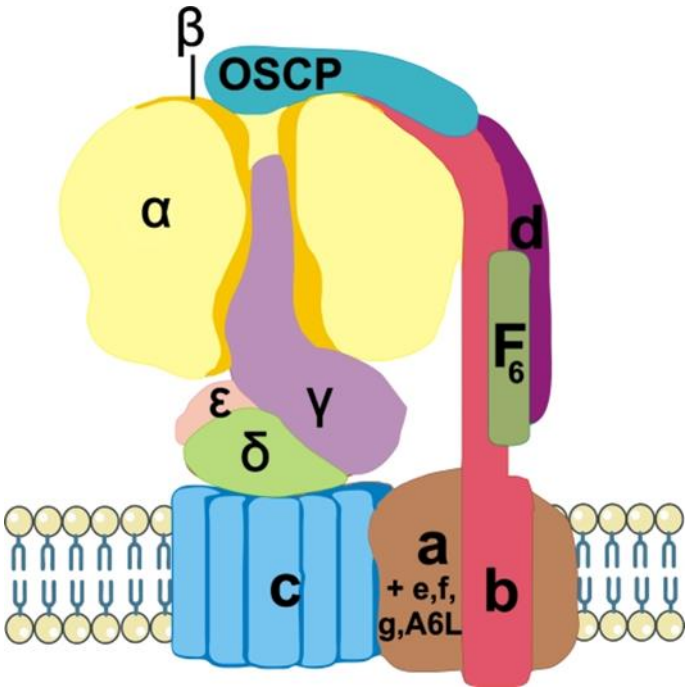

Figure 1.8: Human complex V. Complex V consists of two main subunits F_0 and F_1. F_0 is composed of subunits c, a, b, d, F6 and OSCP and four accessory including e, f, g and A6L. F1 is comprised of 5 subunits (α, β, γ, δ and ε). F_1 uses the electrochemical gradient for generation of ATP from ADP. Key: OSCP=oligomycin-sensitivity conferring protein. Image taken from (Jonckheere *et al.*, 2012).

1.2.6 Supercomplexes

The organisation of the enzymes constituting the OPXHOS system has long been debated. One theory suggests that the complexes exist as individual 'fluid-form' structures within the IMM, allowing the passage of electrons between them. However, a more recent model proposes that the complexes exist in superorganised entities, known as supercomplexes or respirasomes (Acin-Perez *et al.*, 2008). Blue-native polyacrylamide gel electrophoresis (BN-PAGE) has resolved the presence of active supercomplexes (Schagger and Pfeiffer, 2000).

Furthermore, electron microscopy (EM) studies have revealed defined interactions within the isolated supercomplexes (Schafer *et al.*, 2006) which do not form when one component is absent (Acin-Perez *et al.*, 2008). The stability of the large complex I is highly dependent on the interaction with complex III and IV (Schagger and Pfeiffer, 2000). Disruption of complex I and III is linked to oxidative stress and energy failure (Maranzana *et al.*, 2013).

1.3 Other Mitochondrial Functions

1.3.1 Apoptosis and Cell Death Mechanisms

Mitochondria have been associated with various cell death mechanisms including apoptosis, necrosis and autophagy. Mitochondrial function is crucial in all three pathways and plays a major role in neurodegenerative disease (*Mitochondrial Dysfunction in Neurodegenerative Disorders*, 2016).

Apoptosis refers to programmed cell death, which occurs naturally in multi-cellular organisms. It is a mechanism which ensures the survival of the organisms by elimination of damaged cells. Apoptosis involves morphological changes including: cell shrinkage, blebbing of the cell membrane, nuclear fragmentation and chromatin condensation (*Mitochondrial Dysfunction in Neurodegenerative Disorders*, 2016).

In mammalian cells, mitochondria are key players in two apoptotic pathways: the intrinsic pathway and the extrinsic pathway. The intrinsic pathway is highly regulated by proteins from the Bcl-2 family; enabling the release of pro-apoptotic factors from the IMS (Pradelli *et al.*, 2010).

Regulation of the extrinsic pathway is mediated by membrane-bound proteins of the tumour necrosis factor (TNF) receptor family including FAS and TNFR1. Once bound, these receptors form a signalling complex, which results in activation of caspase-8. Apoptosis is then driven by a cascade of protein interactions. These involve effector proteins of the Bcl-2 family, BAX and BK, resulting in the permeabilisation of the OMM and the release of cytochrome c from the IMS (Pradelli *et al.*, 2010; *Mitochondrial Dysfunction in Neurodegenerative Disorders*, 2016).

Necrosis is a form of premature cell death, which occurs in response to trauma or ischemia. Necrotic features include: cell swelling, disruption of cell membranes and ATP depletion. (*Mitochondrial Dysfunction in Neurodegenerative Disorders*, 2016).

Autophagy is the least characterised form of cell death. It involves the delivery of cytoplasmic components to lysosomes for their degradation. To date, the autophagic pathway has not been completely understood, however cells that are lost via autophagy reveal autophagosome accumulation. Evidence suggests that the sodium/potassium ATPase pump facilitates autophagic cell death. A special form of autophagy exists, mitophagy, the process through which unwanted or dysfunctional mitochondria are degraded. Mitophagy is mediated via the Pink1-Parkin signalling cascade (Jin and Youle, 2012; Liu and Levine, 2015).

1.3.2 Iron-Sulphur (Fe-S) Cluster Biogenesis

Iron-Sulphur (Fe-S) clusters are vital for the regulation of gene expression, DNA repair and enzyme catalysis. There are 12 different Fe-S clusters present in the ETC, which are crucial for OXPHOS as they function as electron donors and acceptors within complexes I, II and III (Wang and Pantopoulos, 2011). The process of Fe-S assembly is complex and requires multiple events. The first step involves the conversion of cysteine to alanine causing the release of sulphur by the cysteine desulphurase complex Nfs1-Isd11 (Lill *et al.*, 2012). Reduction of sulphur (S) occurs from the transfer of electrons from NADH, catalysed by ferredoxin reductase. Iron (Fe), provided by frataxin is then imported to the mitochondria via mitoferrin, a mitochondrial solute carrier protein (Paradkar *et al.*, 2009). Once Fe is transported to the IMM, the scaffold mitochondrial proteins IscU and Nfu mediate the assembly of Fe-S clusters (Tong *et al.*, 2003; *Mitochondrial Dysfunction in Neurodegenerative Disorders*, 2016).

1.3.3 Production of Reactive Oxygen Species (ROS)

The process of OXPHOS is a major source of reactive oxygen species (ROS) in the cell (Chen *et al.*, 2003b). ROS are generated through the action of complexes I and III. In brief, electrons that leak from complexes I and III react with oxygen forming superoxide which can then bind to cells and disrupt important functions (Chen *et al.*, 2003b). ROS is released from complex I across the IMM to the matrix, whereas release of ROS from complex III is bi-directional, involving release across the IMM to the matrix and the IMS (Muller *et al.*, 2004). The increased production of ROS can damage mtDNA, which is in close proximity to the ETC, where the free radicals are formed.

Mitochondrial dysfunction and increased production of ROS have been linked to neurodegenerative disease and ageing (Loeb *et al.*, 2005). The excessive production of ROS may lead to reaction with other molecules such as proteins, DNA and lipids, causing oxidative stress. The high metabolic activity of neurons makes them very susceptible to oxidative stress due to the deleterious effects of ROS (*Mitochondrial Dysfunction in Neurodegenerative Disorders*, 2016) and increase in ROS in conjunction with dysfunction of other important mitochondrial pathways, are believed to cause neuronal dysfunction and neuronal death (Zsurka and Kunz, 2015).

1.3.4 Calcium signalling

Mitochondria play a key role in the maintenance of calcium homeostasis. Intracellular calcium (Ca^{2+}) uptake into the mitochondrial matrix is mediated via a membrane potential-driven carrier, the mitochondrial calcium uniporter (MCU) (Deluca and Engstrom, 1961). Ca^{2+} first enters the mitochondria through the OMM via the VDAC pore and is then imported into the mitochondrial matrix via MCU (Kirichok *et al.*, 2004).

Ca^{2+} homeostasis is particularly important for maintaining normal neuronal function. Ca^{2+} buffering is critical to neuronal polarity, axon differentiation, neurotransmitter vesicle release and mitochondrial transport (Mattson and Partin, 1999; Macaskill *et al.*, 2009; *Mitochondrial Dysfunction in Neurodegenerative Disorders*, 2016). Research has shown that Ca^{2+} buffering has a principal role in the modulation of neuronal excitability and synaptic transmission (Pan *et al.*, 2013; Zsurka and Kunz, 2015). Therefore, mitochondrial dysfunction may contribute to altered Ca^{2+} dynamics within neurons.

1.4 The Mitochondrial Genome

Mitochondria contain their own genome, known as mitochondrial DNA (mtDNA). In humans, mitochondrial DNA (mtDNA) exists as a 16.6kb double-stranded, circular, supercoiled molecule which accounts for 1% of total cellular DNA (*Mitochondrial Dysfunction in Neurodegenerative Disorders*, 2016). The mitochondrial genome was firstly sequenced in 1981 (Anderson *et al.*, 1981), followed by a revision in 1999 (Andrews *et al.*, 1999). MtDNA resides in the mitochondrial matrix and consists of a guanine-rich heavy (H) strand and a cytosine-rich light (L) strand incorporating 37 genes. These genes encode 13 polypetides required for OXPHOS, 22 tRNAs and 2 rRNAs (12S and 16S) absolutely essential for mtDNA translation (Anderson *et al.*, 1981). A schematic diagram of the mitochondrial genome is illustrated in Figure 1.9.

ND6 and the mitochondrial tRNA genes (MTTs) are transcribed from the L-strand (Anderson *et al.*, 1981). The remaining 1,500 proteins required for mitochondria metabolism are synthesised in the cytosol and are imported into the mitochondria via specialised mechanisms including translocators of the inner and outer membranes (TIM and TOM) (Tuppen *et al.*, 2010; Calvo *et al.*, 2016).

The mitochondrial genome is characterised by unique features, making it distinguishable from the nuclear genome. It lacks introns and contains only one non-

coding region, a 1.1kb triple-strand displacement loop (D-loop). The D-loop incorporates promoters for transcription and is the site for heavy strand replication (Shadel and Clayton, 1997). These features account for the compactness of the mtDNA molecule. The close proximity of mtDNA to the OXPHOS machinery, makes it particularly susceptible to oxidative damage, accounting for its high mutation frequency compared to nDNA (Brown *et al.*, 1979; Tuppen *et al.*, 2010).

MtDNA molecules are believed to be 'naked' and are packaged into stable protein-DNA macromolecules, known as nucleoids which contain multiple mtDNA copies (6-10) (Iborra *et al.*, 2004). Nucleoids are associated with other proteins essential for mtDNA replication. These include mitochondrial single-stranded binding protein (mt-SSB), the mitochondrial transcription factor A (TFAM) and the mitochondrial DNA Polymerase Gamma (POLG) (Holt *et al.*, 2007).

In addition, mtDNA is strictly maternally inherited, with only one case of paternal mtDNA transmission being reported to date (Schwartz and Vissing, 2002).

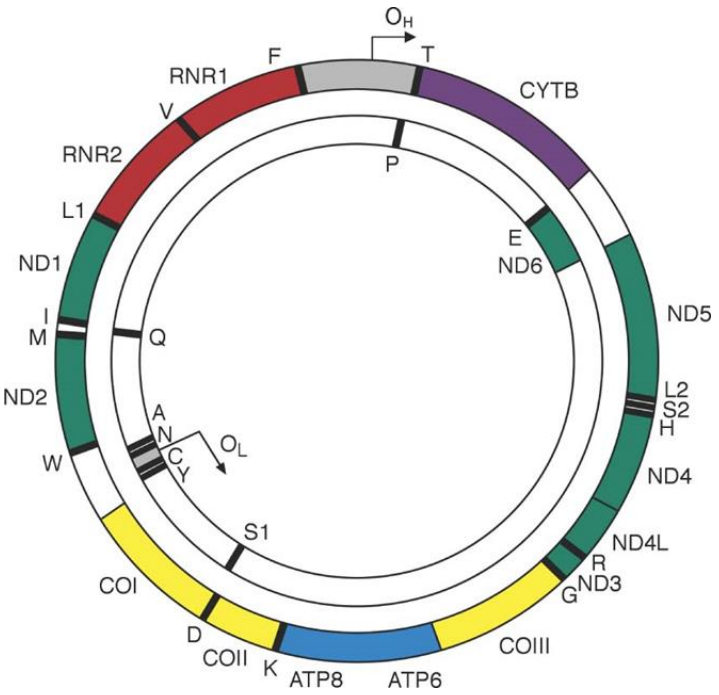

Figure 1.9: The mitochondrial genome. The mitochondrial genome is a 16.6kb circular, double stranded molecule. The outer circle represents the heavy (H) strand and the inner circle illustrates the light (L) strand. The two strands have their own replication origins: O_H on H-strand and O_L on L-strand. The mitochondrial genome consists of 37 genes which encode: 22 tRNAs (black), 2 rRNAs (red) and 13 polypeptides (genes encoding subunits of: complex I are green, complex III are magenta, complex IV are yellow and complex V are blue. In contrast to nDNA, mtDNA is devoid of introns and transcription produces a polycistronic mRNA. Image taken from (Greaves *et al.*, 2012).

1.5 Mitochondrial DNA (mtDNA) Transcription and Translation

MtDNA transcription is a multi-step process and is pivotal for ATP production given that downstream translation will enable synthesis of key peptide subunits of the OXPHOS system (see section 1.2).

Transcription is initiated at two sites, both at the Light Strand Promoter (LSP) and at the Heavy Strand Promoter (HSP). Mitochondrial RNA Polymerase (POLRMT) binds specific sequences at the LSP and HSP after specific sequences are unmasked by binding of Mitochondrial Transcription Factor A (TFAM) to mtDNA and an additional factor is required, specifically Mitochondrial Transcription Factor B2 (TFM2B) for transcription to start (see Figure 1.10) reviewed in (Gustafsson *et al.*, 2016).

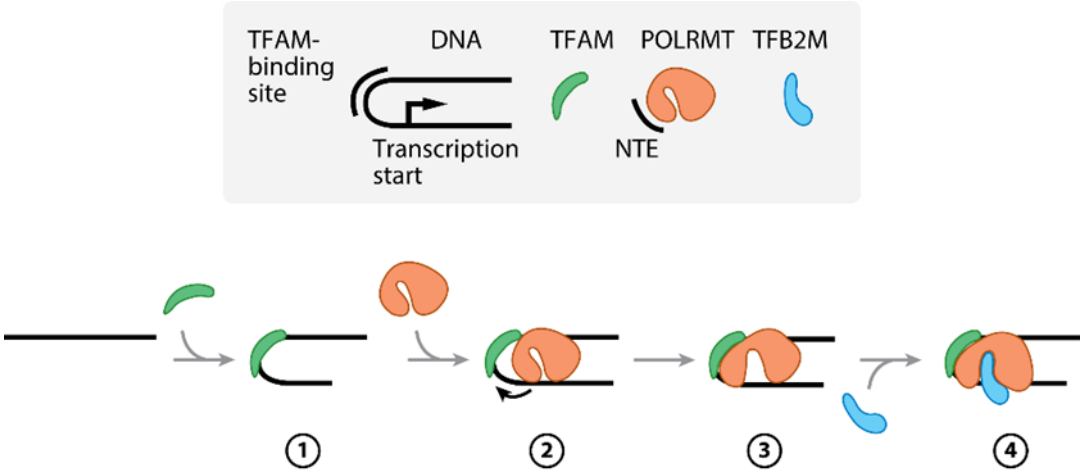

Figure 1.10: Current model of transcription initiation in mtDNA. It is proposed that 1) TFAM binds mtDNA and introduces a 180 degree bend, followed by 2) recruitment of POLRMT which binds both specific sequences in the mitochondrial DNA and TFAM, 3) changing conformation and 4) allowing assembly of TFB2M into the DNA/POLRMT/TFAM complex thus initiating transcription. Key: TFAM = mitochondrial transcription factor A; POLRMT =mitochondrial RNA polymerase; TFB2M=mitochondrial transcription factor B. Image taken from (Gustafsson *et al.,* 2016).

Once transcription has been initiated, elongation is maintained by the interaction of Mitochondrial Transcription Elongation Factor (TEFM) with the catalytic C-terminal of POLRMT until termination occurs and a full length polycistronic transcript is produced. The latter is processed to release individual RNA molecules (Gustafsson *et al.*, 2016).

Individual mRNAs are translated by the mitoribosomes, which consist of two subunits; a 28S small subunit (12S RNA and 33 proteins) and a large 39S subunit (16S RNA and 48 proteins). All proteins are nuclear-encoded (with the exception of two mtDNA-encoded rRNAs) and are imported into the matrix via specialised transporters (Anderson *et al.*, 1981).

A more extensive review of the incompletely understood processes of mitochondrial transcription and translation can be found in (Dennerlein *et al.*, 2017; Pearce *et al.*, 2017).

1.6 Mitochondrial DNA (mtDNA) Replication

Mitochondrial DNA is continuously turned-over, independently of the nDNA. Interestingly, mtDNA replication and the cell cycle do not overlap, a process known as 'relaxed replication' (Birky, 1994) (Chinnery and Samuels, 1999). The major components of the replication machinery are the catalytic subunit of DNA Polymerase Gamma (POLG), Twinkle (unwinds mtDNA), POLRMT (required for RNA primer synthesis for initiation of mtDNA replication) and mitochondrial single-stranded binding protein (mt-SSB). The mt-SSB binds, protects and stabilises ssDNA during the process of replication but also enhances Twinkle function. Evidence suggests that POLG, mt-SSB and Twinkle constitute the minimum machinery required for the full replication of mtDNA *in vitro* (Korhonen *et al.*, 2004). However, *in vivo* replication of mtDNA is facilitated by the presence and activity of POLRMT, absolutely essential for the synthesis of the required RNA primers (Fuste *et al.*, 2010).

Currently, several theories exist regarding the mechanism of mtDNA replication; however, the proposed models are still a matter of debate. The first model of replication was proposed by Clayton and colleagues and is known as the 'strand-displacement' model. In brief, this theory suggests that replication is initiated from the LSP within the D-loop. POLG then extends the RNA primers resulting in the replication of the full heavy strand. Once the POLG has replicated two-thirds of the heavy strand, the O_L region is reached on the lagging strand, forming a loop that prevents mtSSB from binding. This loop structure allows copying of the L-strand in the opposite direction. Once both strands have been synthesised, these are covalently ligated through their 5' and 3' ends to form two circular daughter mtDNA molecules (Clayton, 1982).

An alternative model known as the 'strand-coupled' model states that replication starts at the O_H region located on the H strand within the D-loop and replication occurs in a clockwise manner. Replication of the L strand occurs in the opposite direction shortly after initiation of replication. Replication is bi-directional involving the leading and lagging strands; hallmarked by the presence of intermediate segments known as Okazaki fragments (Holt *et al.*, 2000).

The latest model of replication proposed is the 'RNA Incorporated Through the Lagging Strand' (RITOLS) model. This model is similar to the 'strand-displacement model' however it states that ribonucleotides are incorporated into the lagging strand, during leading strand synthesis (Yang *et al.*, 2002; Yasukawa *et al.*, 2006). The models of mtDNA replication are illustrated in Figure 1.11.

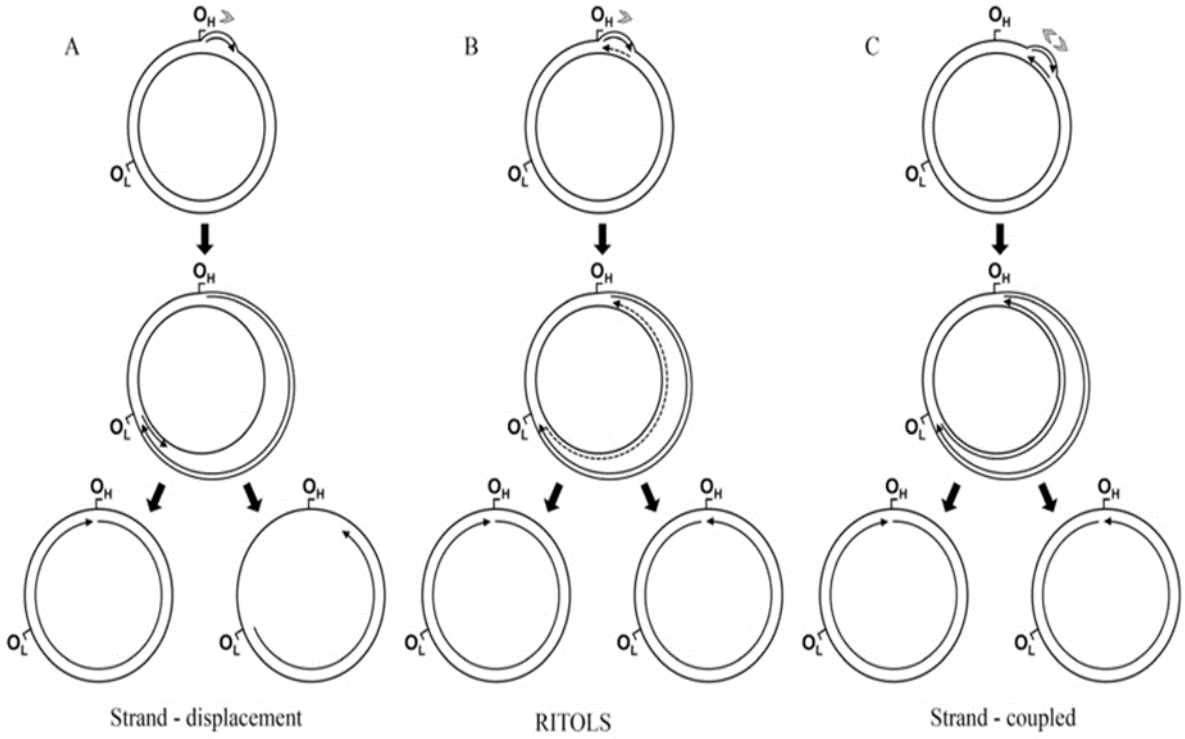

Figure 1.11: The three models of mammalian mtDNA replication. The strand-displacement model, (B) the RNA incorporated throughout the lagging strand (RITOLS) model and (C) the strand-coupled model. O_H and O_L are replication origins for the H-strand and the L-strand respectively for all models. The black arrows within the circular mtDNA molecules indicate the 5'-3' direction of mtDNA synthesis. In the RITOLS model, the dashed-line arrows represent RNA long-stretches. Image taken from (McKinney and Oliveira, 2013).

1.7 Mitochondrial Genetics

1.7.1 Maternal inheritance and Bottleneck

The mitochondrial genome is strictly inherited by the maternal germline in mammals, in the form of nucleoids. To date, only one case of paternal inheritance has been reported in humans in which, a 28-year old man with myopathy was found to harbour a 2bp mtDNA deletion in the ND2 gene; inherited from the father (Schwartz and Vissing, 2002). As paternal inheritance has not been described in any other case, there is a consensus that paternal inheritance in humans is an extremely rare event.

The paternal mtDNA is believed to be eliminated by species-specific mechanisms which may occur pre- or post-fertilisation. For example, in mammals, paternal mtDNA is destroyed by proteolytic degradation; while in flies it is eliminated during

spermatogenesis. Several theories have been proposed to explain uniparental inheritance of mtDNA. Maternal inheritance can be explained from the fact that the sperm contains only 100 copies of mtDNA compared to 100,000 mtDNA copies existing in the unfertilised oocyte. This is known as the ‘dilution effect’. Another theory states that paternal mtDNA is eliminated by ubiquitylation during mammalian zygote formation (Chinnery and Hudson, 2013).

Thus, pathogenic mutations are transmitted through the maternal line to the offspring. However, the number of mutated mtDNA molecules that are transmitted to the children vary considerably due to the ‘genetic bottleneck’. This refers to a process where mtDNA is dramatically reduced during embryonic development leading to the offspring having different mutation loads (heteroplasmy) (Chinnery and Hudson, 2013).

1.7.2 Heteroplasmy and Threshold Effect

Cells contain multiple mitochondria, which contain thousands of copies of mtDNA molecules. Homoplasmy refers to a state in which all mtDNA molecules share the same genotype (i.e. all mtDNA molecules are either wild type or mutant), whilst heteroplasmy applies when mutant mtDNA co-exists with wild type DNA in cells, tissues and organisms (Larsson and Clayton, 1995). When present, heteroplasmy is expressed as the percentage of mutant mtDNA copies per cell or tissue (Taylor and Turnbull, 2005).

Heteroplasmy has major implications in mitochondrial disease. Specifically, the levels of heteroplasmy within a cell may significantly determine the clinical phenotype expressed by the genetic defect. The levels of heteroplasmy within cells are regulated by random genetic drift via clonal expansion (Elson *et al.*, 2001), which involves the selective expansion of the mutant mtDNA. As a result, increased levels of heteroplasmy are reached in post-mitotic tissues (Chinnery and Hudson, 2013). However, a specific threshold of mutation load exists; which dictates the clinical phenotype presentation and the biochemical defect occurring. The threshold level varies considerably among individuals and is highly dependent on the metabolic demand of the tissue and the type of mutation. Typically, the threshold level for tRNA point mutations is approximately 90% (Yoneda *et al.*, 1995), while for single large-scale mtDNA deletions it drops to 70-80% (Sciacco *et al.*, 1994).

1.7.3 Mitochondrial DNA (mtDNA) Mutations and Repair Mechanisms

Unique characteristics of the mtDNA, account for its increased vulnerability to pathogenic mutations. These include: compact mtDNA structure, close proximity to the ETC and the lack of protective histones (Clayton, 1982; Richter *et al.*, 1988).

Mutations affecting directly the mtDNA can cause wide range of disorders, however mutations in nuclear genes may occur and affect mtDNA maintenance; thus causing secondary defects in mtDNA. Mutations occurring in the mitochondrial genome can exist as: point mutations, single large-scale and multiple deletions, insertions or duplications. Mutations in mtDNA are believed to occur at a 10-fold higher rate compared to the nuclear genome (Brown *et al.*, 1979). Although pathogenic mtDNA mutations are an important cause of mitochondrial disease, these are beyond the scope of this thesis.

Mitochondrial DNA repair mechanisms exist, however these are believed to exist in reduced rates compared to nDNA and exert their function through different molecular pathways. Currently, mtDNA repair mechanisms are not fully understood, except the base excision repair (BER) (Stierum *et al.*, 1999). These include: direct repair (which has only been confirmed in yeast and E.Coli) (Yasui *et al.*, 1992) mismatch repair (MMR) (Mason *et al.*, 2003) and single-strand break repair (Hegde *et al.*, 2012).

1.7.4 Mitochondrial DNA (mtDNA) Depletion

MtDNA depletion is defined as a quantitative reduction in the mtDNA copy number below 30% of normal mtDNA copy number (Rötig and Poulton, 2009). MtDNA depletion results in a group of rare heterogeneous disorders, known as mtDNA depletion disorders (MDS) which present in infancy/childhood. It has been estimated that approximately 8% of the paediatric patients with respiratory chain deficiency demonstrate mtDNA depletion (Rötig and Poulton, 2009). The first described MDS involved congenital myopathy or hepatopathy. Since then, numerous mtDNA depletion syndromes have been described and classified as: myopathic, encephalopathic, neurogastrointestinal and hepatocerebral. However, these syndromes are often overlapping due to the heterogeneous nature of the phenotypes.

MtDNA replication occurs independently of the cell cycle and the process is highly dependent on constant supply of intra-mitochondrial 2'-deoxyribonucleoside 5'-triphosphate (dNTP) pools. However, the mechanisms of dNTP synthesis required for

mtDNA replication are not well-defined to date. MtDNA depletion occurs as a result of mutations in nuclear-encoded genes involved in mtDNA replication (*POLG, TWNK*) and in mtDNA maintenance (*TK2*, *FBXL4*, *MPV17*, *SUCLA2*, *SUCLG1, TYMP*, *DGUOK*, *ANT1* and *RRM2B*). It has been suggested that defects in some of these genes lead to limited mtDNA replication, with resulting daughter cells containing fewer copies of mtDNA (Rötig and Poulton, 2009).

Interestingly, mtDNA depletion arising from mutations in the aforementioned genes seems to be tissue-specific. For example, mtDNA depletion is apparent in the liver and brain of patients with mutations in *POLG* and *DGUOK* (Naviaux *et al.*, 1999; Mandel *et al.*, 2001). In contrast, patients with mutations in *TK2* or *RRMB2* genes demonstrate depletion in the muscle (Dimmock *et al.*, 2010). Although the reasons behind tissue-specific mtDNA depletion are not fully understood, there is evidence suggesting that dNTP pools are different among different tissues/organs (Song *et al.*, 2005). Specifically, dNTP pools regulate the fidelity of mtDNA replication. Therefore, an imbalance in dNTP pools may lead to alterations in POLG activity, restricting the incorporation of dNTPs and thus mtDNA extension, leading to mtDNA replication stalling.

1.8 Mitochondrial Disease

Mitochondrial disease refers to a group of disorders characterised by genetic and phenotypic heterogeneity. Mitochondrial disease mainly arises from dysfunction in the mitochondrial respiratory chain due to mutations in either the mtDNA or nuclear genes affecting mtDNA synthesis and maintenance (Chinnery, 2014).

Mitochondrial diseases are more common than originally postulated. According to the available data, prevalence of mitochondrial disease is estimated to be 1 in 8,500 individuals (both children and adults with mtDNA or nDNA mutations) in Spain (Arpa *et al.*, 2003). A recent study from the North East of England estimated that 1 in 4300 individuals are at risk of developing adult mitochondrial disease (Gorman *et al.*, 2015). Interestingly, it has been estimated that 4.7 in 100,000 births in the Australian population may develop mitochondrial disease (Skladal *et al.*, 2003).

The first causative association of mtDNA defect and human disease was established in 1988 (Holt *et al.*, 1988) and since then, a number of mtDNA and nDNA mutations have been linked to mitochondrial disease.

Mitochondrial disease is clinically characterised by the following symptoms: neurological deficits (including epilepsy, encephalopathy and parkinsonism), proximal myopathy, exercise intolerance, external ophthalmoplegia, cardiomyopathy, diabetes mellitus, sensorineural deafness and optic atrophy. Some of the discrete clinical syndromes include: Kearns-Sayre Syndrome (KSS), Chronic Progressive External Ophthalmoplegia (CPEO), Mitochondrial Encephalomyopathy with Lactic Acidosis and Stroke-like Episodes (MELAS), Myoclonic Epilepsy with Ragged-red Fibres (MERRF), Neurogenic Weakness with Ataxia and Retinitis Pigmentosa (NARP), Leber's Hereditary Optic Neuropathy (LHON) and Leigh Syndrome (LS) (Chinnery, 2014). A summary of the clinical syndromes and their underlying genetic defects is given in Table 1.1.

Mitochondrial disease may present at any age and affect single or multiple organs, giving rise to the heterogeneous nature of its clinical presentation. Often, the clinical phenotype does not correlate with the genotype, making clinical diagnosis and management extremely challenging. Furthermore, a specific genetic defect may cause more than one phenotype depending on mutation segregation and heteroplasmy (Lax *et al.*, 2017). Currently there are no cures for mitochondrial disease; however recent research advances have enabled reproductive options

which prevent mitochondrial disease transmission to the progeny (Craven *et al.*, 2010; Hyslop *et al.*, 2016).

Neurons are highly dependent on OXPHOS for mediating synaptic transmission, as they form complex neuronal networks in the brain. This process requires a high metabolic activity; therefore neuronal cells are particularly vulnerable to energy depletion. Thus, it is not surprising that patients with mitochondrial disease manifest neurological deficits such as encephalopathy, seizures/epilepsy, migraine, stroke-like episodes, ataxia, cognitive impairment and dementia. These neurological deficits are the most frequently reported features in mitochondrial disease and account for the high morbidity and mortality rates (Lax *et al.*, 2017).

Epilepsy is a salient feature in mitochondrial disease, and frequently occurs as the presenting feature and is associated with poor prognosis (Lax *et al.*, 2017). The exact incidence of epilepsy in patients with mitochondrial disease is unknown, however it has been estimated that it occurs in approximately 60% of patients with confirmed biochemical defects (Khurana *et al.*, 2008). A study performed in the UK has shown that approximately 23.1% of 182 adults with confirmed genetic diagnosis of mitochondrial disease develop epilepsy (Whittaker *et al.*, 2015). In the paediatric population, the prevalence of epilepsy is estimated to be approximately 32% (Debray *et al.*, 2007). It has been shown that 45% of paediatric patients died within 9 months of the onset of epilepsy (Debray *et al.*, 2007).

Dissecting the pathogenesis of epilepsy in patients with mitochondrial disease can be difficult, as often the available tissue is harvested at post-mortem and epilepsy often coincides with other neurological deficits. Therefore, it is very challenging to depict primary and secondary changes when investigating post-mortem tissue.

Neuropathological findings have shown prominent neuronal loss, astrogliosis and spongiform degeneration of grey and white matter (Hunter *et al.*, 2011; Sofou *et al.*, 2012; Rouzier *et al.*, 2014). Interestingly, a recent study performed in adult patients with mitochondrial disease has shown respiratory chain deficiencies (involving complexes I and IV) within GABAergic interneurons combined with reduced interneuron densities (Lax *et al.*, 2016). These findings suggest that respiratory chain deficiency in the inhibitory GABAergic interneurons affects the neuronal networks which may contribute to lower the threshold of seizure activity. Mitochondrial epilepsy and its pathogenesis is the major focus of this thesis and this topic is discussed in more detail in subsequent chapters.

Syndrome	Onset	Main Features	Additional Features	Underlying Genetic Defects
KSS	<20 years	PEO, retinitis pigmentosa and one of the following: cerebellar ataxia, heart block, CSF protein<1g/L.	Myopathy, bilateral deafness, dysphagia, diabetes mellitus, hypoparathyroidism and dementia.	Large single mtDNA deletion and/or duplication.
CPEO	Late-onset	External ophthalmoplegia and bilateral ptosis	Mild proximal myopathy.	Single or multiple mtDNA deletions or *POLG* mutations.
MELAS	<20 years	Stroke-like episodes, seizures and/or dementia, ragged-red fibres and/or lactic acidosis.	Diabetes mellitus, cardiomyopathy, retinitis pigmentosa, cerebellar ataxia and bilateral sensorineural deafness.	m.3243A>G mutation (80%) and other mtDNA mutations (20%)
MERRF	Typically in adolescence	Myoclonic seizures, cerebellar ataxia and myopathy.	Dementia, bilateral sensorineural deafness, optic atrophy, peripheral neuropathy and multiple lipomata.	m.8344A>G

NARP	Late-childhood or adult-onset	Neuropathy, ataxia and retinitis pigmentosa.	Motor and sensory neuropathy.	m.8993T>G
LHON	Early-onset	Bilateral visual failure	Dystonia	Point mutations in mtDNA m.11778G>A, m.3460G>A and m.14484T>C
LS	Infantile onset	Encephalopathy and seizures	Dystonia and dysphagia	Deficiencies of *NDUFS1*, *NDUFS4*, *NDUFS7*, *NDUFS8* and *NDUFV1*, *SURF1*, *COX10*, *COX15*, *SDHA*, *MT-CO3, MT-ND1, MT-ND2, MT-ND4, MT-TI, MT-TK, MT-TL1, MT-TL2, MT-TV, MT-TW, ATP6, MT-ND3, MT-ND5, MT-ND6*

Table 1.1: Clinical syndromes of mitochondrial disease. Key: KSS=kearns-sayre syndrome; CPEO=chronic progressive external ophthalmoplegia; MELAS=mitochondrial encephalopathy with lactic acidosis; MERRF=myoclonic epilepsy with ragged-red fibres; NARP=neurogenic weakness with ataxia and retinitis pigmentosa; LHON=leber hereditary optic neuropathy and LS= leigh syndrome; MT=mitochondrial.

1.9 Mitochondrial DNA Polymerase Gamma (POLG)

1.9.1 Polymerase Gamma (POLG): History, cloning and expression

The first evidence of the role of DNA Polymerase Gamma (POLG) in mtDNA replication was provided in 1987 (Lestienne, 1987). POLG is believed to be the only DNA polymerase to act in mammalian mitochondria and is pivotal for embryonic development (Hance *et al.*, 2005).

In humans, POLG exists as a heterotrimer, comprised of a large catalytic subunit and two smaller accessory subunits. The catalytic subunit is encoded by *POLG*, which is composed of 23 exons and located on chromosome 15q25 (Walker *et al.*, 1997). The accessory subunits are encoded by *POLG2* which consists of 8 exons and is located on chromosome 17q23 (Yakubovskaya *et al.*, 2006).

Human *POLG* was cloned by Ropp and Copeland in 1996. The sequence of human POLG was found to be 1,239 amino acids long with a molecular weight of 139.5kDa. Human POLG's amino acid sequence is 49%, 43% and 78% identical in *Drosophila*, *S. Cerevisiae* and *G. gallus* respectively (Ropp and Copeland, 1996; Lecrenier *et al.*, 1997).

POLG is expressed and translated in the absence of mtDNA. Specifically, *POLG* is transcribed in the nucleus, translated in the cytosol and imported into the IMM where it associates with other proteins to form the apparatus required for mtDNA replication and nucleoids (Davis *et al.*, 1996; Saneto and Naviaux, 2010).

1.9.2 Polymerase Gamma (POLG) Structure and Functions

POLG heterotrimer consists of: a 140kDa catalytic α subunit encoded by *POLG* and two 55kDa accessory β subunits which form a dimer; encoded by *POLG2*. The association of the catalytic subunit with one accessory subunit allows DNA synthesis (Lee *et al.*, 2010). POLG's structure seems to be variable among species; it exists in the form of a single catalytic subunit in yeast and as a homodimer in *Drosophila* (Yakubovskaya *et al.*, 2006).

The catalytic subunit is comprised of an N-terminal exonuclease domain which is linked through a spacer region (linker domain) to a C-terminus polymerase domain. POLG's catalytic subunit retains three distinct activities: a 3'-5' exonuclease activity, a DNA polymerase activity and a 5'-deoxyribose phosphate (dRP) lyase activity see Figure 1.12A).

The exonuclease domain (aa 171-440) possesses a 3'-5' proofreading activity and is located at the N-terminus of the catalytic subunit. It contains the highly conserved motifs I, II and III, which are essential for exonuclease activity (Olson and Kaguni, 1992; Kaguni, 2004). Motif I contains the catalytic residues Asp198 and Glu200. Based on calculations the overall fidelity of POLG is estimated as 1 error in 280,000 base pairs (Johnson and Johnson, 2001; Lee and Johnson, 2006).

The DNA polymerase domain (aa 441-475; aa 789-1239) performs the mtDNA synthesising function and is divided into three subdomains: thumb (aa 441-475; aa768-815), palm (aa 816-910; aa 1096-1239) and finger (aa 911-1095). In addition, the polymerase domain contains three conserved motifs: A, B and C. These are crucial for polymerase activity as they bind to both template mtDNA and substrate nucleotide triphosphate and mediate formation of phosphodiester bonds (Kasiviswanathan *et al.*, 2009; Lee *et al.*, 2009; Saneto and Naviaux, 2010). The active site is housed in the palm subdomain which contains the catalytic residues (Asp890 located in motif A, Glu1136 and Asp1135 both located in motif C).

The linker region is approximately 482aa in length in humans and is connected to the exonuclease and polymerase domains through long helices located at the thumb domain (Lee *et al.*, 2009). The linker region is further divided into two subdomains: the global intrinsic processivity (IP; residues 475-510 and 571-785) and the extended accessory interacting determinant (AID; residues 511-570) (Lee *et al.*, 2009). Analysis of POLG's crystalline structure revealed that the linker domain of the

catalytic subunit physically interacts with only one accessory (p55) subunit (Lee *et al.*, 2009) (Saneto and Naviaux, 2010). This feature distinguishes POLG from other DNA polymerases. The IP domain is the binding site for the upstream primer-template DNA duplex, thus enhancing intrinsic processivity (Lee *et al.*, 2009; Saneto and Naviaux, 2010).

The accessory p55 subunit binds to the catalytic subunit through the AID, providing the interface for increased processivity of the holoenzyme. The AID contains the 'L-helix 'which interacts with the C-terminal of the p55 subunit via hydrophobic bonds. Mutations located in the 'L-helix' resulted in reduced polymerase activity and processivity in the presence of p55.

Each of the p55 accessory subunits is divided into 3 domains: domain 1, 2 and 3. Domain 1 (aa 66-131; aa 183-353) is situated downstream of the Mitochondrial Targeting Sequence (MTS), located at the N-terminal), which is responsible for recognition and direction to the matrix. Domain 2 (aa 132-182) contains four helices which are important in the homodimerisation of p55. Domain 3 (aa 354-485) is located at the C-terminal of the p55 subunit and is involved in catalytic subunit binding. It has been suggested that the proximal p55 subunit enhances the interaction with the DNA; whereas the distal p55 subunit accelerates nucleotide incorporation (Saneto and Naviaux, 2010).

Both accessory p55 subunits serve as processivity factors which allow increased substrate binding and enhanced activity of the catalytic subunit. The proximal p55 subunit associates with the catalytic subunit enhancing binding interaction of the holoenzyme with the DNA strand. At the same time, the distal p55 subunit increases the rate of polymerisation (Lee *et al.*, 2010). In addition to their role as processivity factors the p55 subunits are thought to suppress exonuclease activity of the catalytic subunit, allowing integrity of the replisome at the replication fork to be maintained (Johnson and Johnson, 2001; Farge *et al.*, 2007; Saneto and Naviaux, 2010). The tertiary structure of POLG can be seen in Figure 1.12.

Despite the major role in mtDNA synthesis, POLG is crucial for 5'-3' base-excision repair via 5'-dRP lyase activity. Although 5'-dRP-lyase activity is housed in the polymerase domain, its exact location remains unknown (Longley *et al.*, 1998). The process involves a class II apurinic/apyrimidinic (AP) endonuclease which mediates cleavage of the DNA backbone on the 5' side of an abasic site.

A deoxyribophosphodiesterase then eliminates the 5' sugar-phosphate residue left by AP endonuclease. POLG then fills the gap with the incorporation of a new base, before an mtDNA ligase acts to repair the nick. Base excision repair (BER) is the predominant mechanism of mtDNA repair known to exist in mitochondria (Vasileiou *et al.*, 2017). Recently, polymerase beta (β) has been detected in mammalian mitochondrial fractions (Sykora *et al.*, 2017), suggesting that it is not only involved in the BER mechanism at the level of the nuclear genome, but also an important factor in mtDNA BER (Sykora *et al.*, 2017).

Although BER is the main mechanism known to exist in mitochondria, other repair mechanisms exist which include single-strand base repair (el-Khamisy and Caldecott, 2007), double-strand break repair (Bacman *et al.*, 2009) and mismatch repair (Mason *et al.*, 2003). Nucleotide excision repair has not been yet detected in mitochondria (Vasileiou *et al.*, 2017).

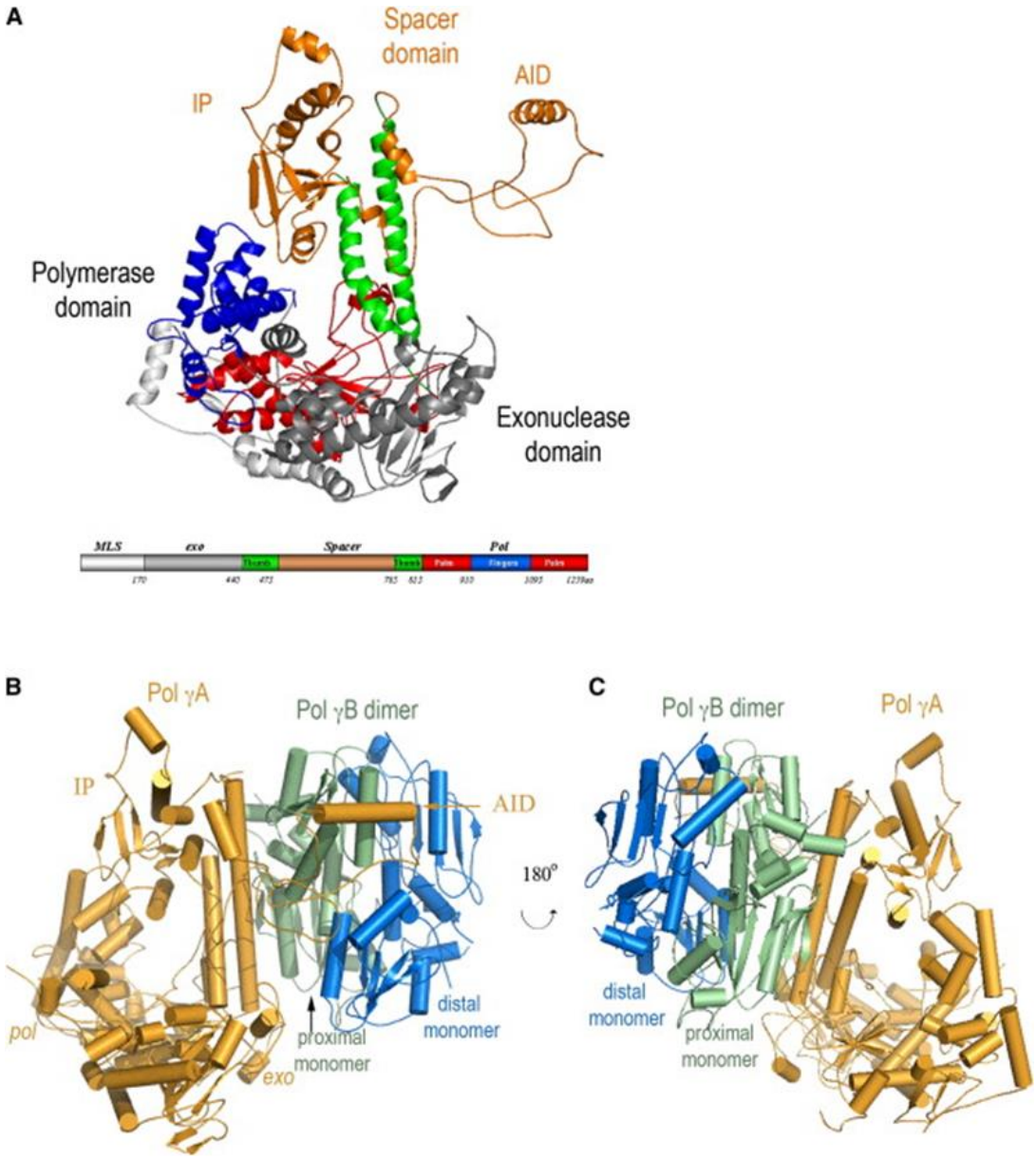

Figure 1.12: Tertiary structure of POLG catalytic subunit. The different domains are illustrated: exonuclease (grey), linker domain (orange) and polymerase (pol, blue). (B) Structure of the POLG heterotrimer containing the catalytic subunit p140 (orange) and the proximal (green) and distal (blue) p55 monomers. Figure modified from (Lee et al., 2009).

1.9.3 Polymerase Gamma (POLG) Mutations

Pathogenic mutations occurring in the catalytic subunit of *POLG* are a major cause of human mitochondrial disease. To date over 200 *POLG* mutations have been reported and have been associated with an overlapping spectrum of disorders which differ in the age of onset, pattern of inheritance and clinical presentation (discussed in the subsequent section). Understanding the effects of *POLG* mutations on different domains and functions of the protein is crucial and may provide insight into the mechanisms accounting for phenotypic diversity.

Pathogenic mutations can be either autosomal recessive or autosomal dominant with the former mode of inheritance being the most frequently associated with disease. Dominant mutations are associated with adult-onset disease, while recessive mutations may occur throughout the life span (Saneto and Naviaux, 2010; Saneto *et al.*, 2013). *POLG* mutations identified are listed on The Human DNA Polymerase Gamma Database (Figure 1.13) (Copeland, n.d.).

Mutations located in the catalytic subunit of POLG are suggested to affect DNA-binding affinity, and reduce catalytic efficiency (Euro *et al.*, 2011). The function of the different POLG domains partially dictates the effect of the mutation. Mutations found in the AID destabilise POLG-DNA complex; while mutations found in the IP reduce processivity of the holoenzyme, DNA binding and polymerase activity (Chan *et al.*, 2006). *POLG* mutations harboured within the exonuclease region are believed to reduce the fidelity of the polymerase activity rather than diminishing exonuclease activity (Szczepanowska and Foury, 2010; Saneto *et al.*, 2013).

Mutations occur all throughout the domains of *POLG*. Three pathogenic mutations have been classified as the most common and result in a wide range of phenotypes ranging from severe early-onset disorders to milder adult-onset disorders. These mutations include: p.(Ala467Thr), p.(Trp748Ser) and p.(Gly848Ser) (Hakonen *et al.*, 2007).

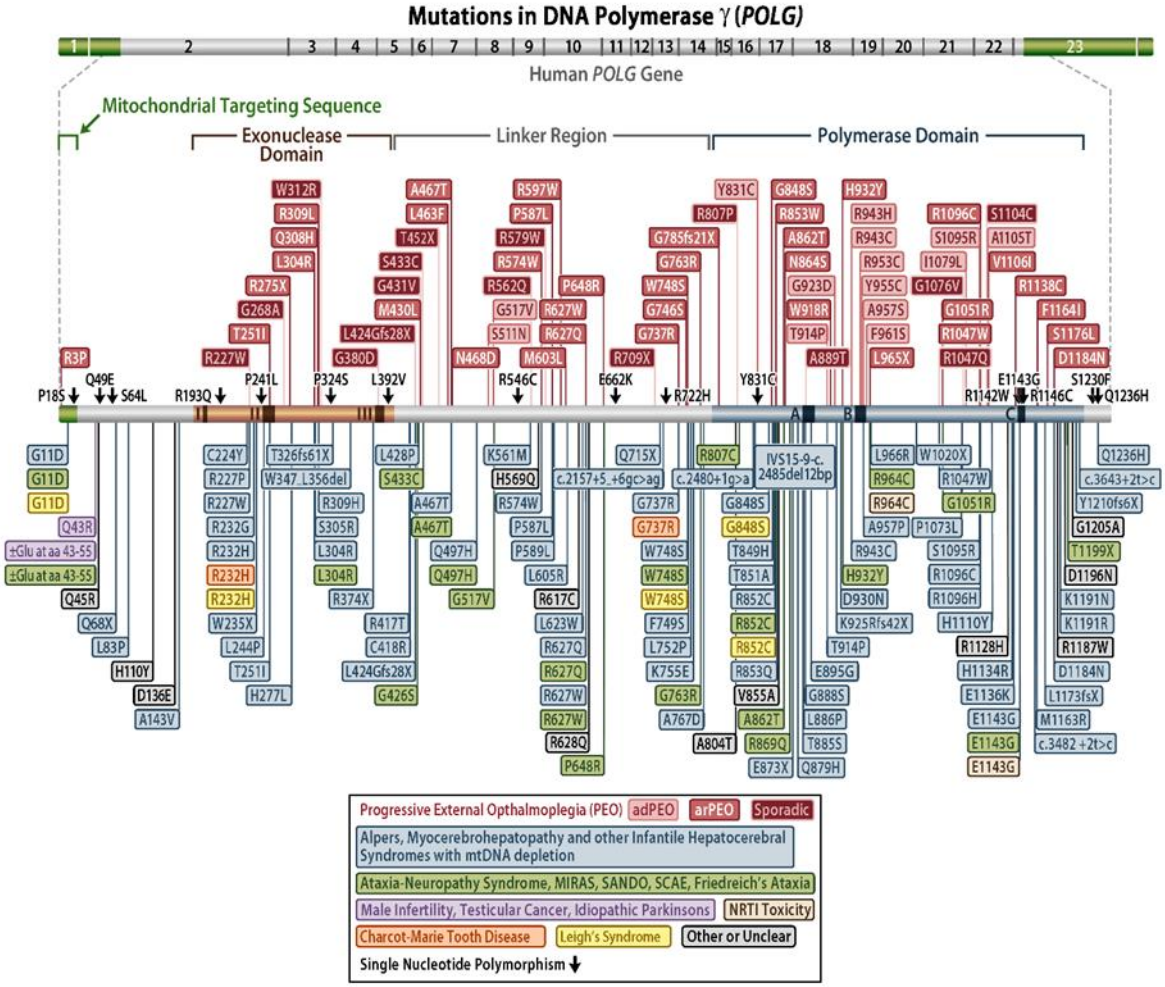

Figure 1.13: Mutations identified in *POLG*. A schematic representation of the mutations that have been reported to date, their location within *POLG* and associated syndromes. Most mutations are missense point mutations. Image taken from: The Human DNA Polymerase Gamma Mutation Database (Copeland, n.d.).

The incidence of p.(Ala467Thr) mutation has been estimated to be 0.6% in the Belgian population (Van Goethem *et al.*, 2001), 0.69% in the British population (Horvath *et al.*, 2006) and 1% in the Norwegian population (Winterthun *et al.*, 2005). In another study p.(Ala467Thr) has been reported as the most common in the paediatric population (Horvath *et al.*, 2006).

The p.(Ala467Thr) mutation is located in the linker domain of POLG, and disrupts the interaction with the proximal p55 subunit. Evidence stems from the observation that p.(Ala467Thr) resulted in less than 4% POLG activity compared to the wild-type POLG *in vitro.* Interestingly, the p.(Ala467Thr) mutation resulted in poor binding of the p140 subunit to the p55 subunit as shown by co-immunoprecipitation, processivity and primer extension studies (Chan *et al.*, 2005a). The p.(Ala467Thr) mutation is associated with a dramatic reduction in DNA polymerase activity,

however the exonuclease function is only reduced by a 2-fold (Chan *et al.*, 2005a). Based on structure-function studies, the location of the mutation in the hydrophobic centre of the thumb sub-domain suggests that the Thr467 hydroxyl group may disturb the hydrophobicity of the region (Euro *et al.*, 2011).

The p.(Trp748Ser) (c.2243G > C, Exon 13) mutation is the second most common mutation reported and has been found to occur with the p.(Glu1143Gly) mutation in 1:125 patients from Finland. The p.(Trp748Ser) mutation is the most common mutation reported in ataxia-neuropathy spectrum disorders and Alpers (Hakonen *et al.*, 2007).

The p.(Trp748Ser) mutation is located within the IP of the linker domain, and affects DNA-binding affinity. Biochemical characterisation of the p.(Trp748Ser) mutation alone revealed poor DNA-binding ability resulting in reduced processivity of mtDNA synthesis and primer extension. Interestingly, the interaction of p140 subunit with the p55 subunit remained intact; however, this failed to rescue the catalytic defect (Chan *et al.*, 2006). In contrast the activity of the POLG containing the p.(Glu1143Gly) mutation was found to be 1.4-fold higher than the wild-type. The p.(Glu1143Gly) mutations is believed to modulate the deleterious effects of p.(Trp748Ser) when found with the p.(Glu1143Gly) increased overall DNA binding, catalytic activity and fidelity of POLG (Chan *et al.*, 2006).

The p.(Gly848Ser) is is the third most common POLG mutation that has been associated with Alpers, MELAS, CPEO and LS in a recessive state. There has been very little data reported on the prevalence of this mutation. The p.(Gly848Ser) is located in the thumb region of the polymerase domain of the p140 catalytic subunit. It results in a 5-fold decrease in the DNA-binding affinity compared to the wild-type *in vitro*. Interestingly, the holoenzyme retained only 0.03% polymerase activity of the wild-type (Kasiviswanathan *et al.*, 2009); whereas POLG with mutations located in the palm sub-domain retained 50-70% of the polymerase activity. The p140-p55 interaction was not affected and the fidelity of the enzyme remained normal (Kasiviswanathan *et al.*, 2009). In agreement with the biochemical data Euro and colleagues demonstrated that the p.(Gly848Ser) variant affects the ‘RR loop’ of the p140 which interacts with the primer DNA template; thus leading to DNA-binding and polymerase activity defects (Euro *et al.*, 2011).

1.9.4 Polymerase Gamma 2 (POLG2) Mutations

Mutations in *POLG2*, encoding the p55 accessory subunits have rarely been reported and are not as well characterised as *POLG* mutations. The first *POLG2* mutation identified, c.1352G>A; p.(Gly451Glu) was reported in one patient with late-onset autosomal dominant progressive external ophthalmoplegia (adPEO) who had ptosis associated with mtDNA deletions in muscle. The p.(Gly451Glu) substitution is located in the region of p55 that interacts with p140 resulting in poor processivity of the holoenzyme due to disrupted interaction between p140 and p55 (Longley *et al.*, 2006).

More recently, a study performed in 112 patients, identified 8 heterozygous (7 novel) *POLG2* mutations in the absence of *POLG* mutations (Young *et al.*, 2011). These mutations were associated with decreased binding affinity to the catalytic subunit combined with reduced enzyme processivity. For example, p.(Arg369Gly), was reported in another patient with adPEO and multiple mtDNA deletions. Biochemical analysis of the recombinant mutant p55 revealed a reduced affinity for p55 binding to p140 (Craig *et al.*, 2012).

Analogously to POLG, POLG2 function is crucial for embryogenesis and mtDNA replication; as revealed from *POLG2* mouse knockouts. However, a single copy of wild-type *POLG2* is sufficient to sustain life (Humble *et al.*, 2013). A better understanding of structure-function relationships will provide more insight into the *POLG2*-related mitochondrial disease pathogenesis.

1.9.5 Polymerase Gamma (POLG) Related Disorders

POLG-related disorders refer to a continuum of heterogeneous but clinical overlapping phenotypes (Cohen, 2014). The onset of *POLG*-related disorders is variable, ranging from infancy to late adulthood. Disease associated with infancy and childhood is more severe when compared to cases presenting later in life, albeit the reasons behind this observation remain unclear.

POLG-related disorders include the following syndromes: Alpers, Myoclonic Epilepsy Sensory Ataxia (MEMSA), Ataxia Neuropathy Spectrum (ANS), Myocerebrohepatopathy Syndrome (MCHS) and adPEO or arPEO. Alpers is the most severe form of *POLG*-related disorders. A description of the *POLG*-related phenotypes is given in Table 1.2.

Disorder	Clinical features	Onset
Alpers	Seizures/epilepsy, psychomotor regression and liver dysfunction/failure.	Infancy/childhood or adolescence/early adulthood
MCHS	Developmental delay, early-onset dementia, lactic acidosis and myopathy with failure to thrive.	First months of life
ANS	Ataxia and neuropathy (seizures and ophthalmoplegia).	Early to late-onset
MEMSA	Epilepsy, myopathy and ataxia.	Early to teenage-onset
adPEO	Ophthalmoplegia, ptosis, generalised myopathy, depression, Parkinsonism, sensorineural hearing loss and ataxia.	Late-onset
arPEO	Ophthalmoplegia and ptosis.	Late-onset

Table 1.2: Clinical description of mitochondrial disorders. Key: MCHS=myocerebrohepatopathy spectrum; ANS=ataxia neuropathy spectrum; MEMSA=myoclonic epilepsy myopathy sensory ataxia; adPEO=autosomal dominant progressive external ophthalmoplegia; arPEO=autosomal recessive progressive external ophthalmoplegia.

POLG-related disorders are linked to faulty mtDNA maintenance and expression. Although the exact mechanisms remain unclear, *POLG* mutations result in mtDNA depletion and/or multiple deletions in affected tissues, leading to OXPHOS dysfunction and ATP depletion. MtDNA depletion ultimately results in reduced number of complexes of the ETC (as the mtDNA-encoded subunits become rate-limiting), thereby disrupting the ratio of complexes within the supercomplexes, and leading to reduced production of ATP (Saneto and Naviaux, 2010).

Biochemical assays may show mtDNA depletion and respiratory chain deficiencies involving complexes I-V in both adults and children; however biochemical tests in muscle may be normal; suggesting the effects of *POLG* mutations are tissue-specific. Thus, normal respiratory chain function and mtDNA content in any given tissue, should not exclude the possibility of a *POLG*-related disorder and the genetic confirmation of biallelic *POLG* variants should be the gold standard for the diagnosis of *POLG*-related disorders (Saneto and Naviaux, 2010; Cohen, 2014; Anagnostou *et al.*, 2016).

Recessive *POLG* mutations have been described in the form of homozygous or compound heterozygous. Although no clear genotype to phenotype correlations exist, compound heterozygous mutations are associated with more severe early-

onset phenotypes (Graziewicz *et al.*, 2006). On the contrary, homozygous mutations are associated with late-onset milder disease. Further, homozygous p.(Ala467Thr) and p.(Trp748Ser) mutations have been linked to longer survival compared to p.(Ala467Thr)/p.(Trp748Ser) compound heterozygotes (Tzoulis *et al.*, 2006). It is intriguing that both homozygous and compound heterozygous mutations occur in early-onset and late-onset *POLG*-related disease (Graziewicz *et al.*, 2006); thus making genotype to phenotype correlations difficult to establish. The reasons for such a genotypic/phenotypic variation within a single or multiple syndromes remain unclear (Saneto *et al.*, 2013).

1.9.6 Polymerase Gamma (POLG) Mouse Models

To date, many mouse models have been created to investigate mitochondrial disease. Models of nuclear gene modifications that alter mtDNA maintenance are currently being used. The *POLG* mutator mouse does not mimic the epileptic phenotype seen in human patients. In contrast, the *POLG* mutator mouse demonstrates a premature ageing phenotype.

To better understand genotype to phenotype relationships, mice harbouring mutations in *POLG* have been created. A homozygous *POLG* mouse model (lacking exon 3) resulted in embryonic lethality (Hance *et al.*, 2005); suggesting that POLG function is absolutely essential for survival. Another study performed on a mouse model with an insertion of a proof-reading-deficient version of POLG, resulted in a premature ageing phenotype with characteristic features including: weight and hair loss, kyphosis, osteoporosis, reduced fertility, cardiomyopathy and anaemia (Trifunovic *et al.*, 2004). Interestingly, these models showed increased mutation rates which accumulated with time, resulting in extensive respiratory chain deficiencies without any observable increase in ROS (Trifunovic *et al.*, 2005). However, despite the deficiency in the exonuclease activity of POLG, the mice remained viable.

Studies with mouse models succinctly described above may expand our understanding of disease progression and the effect of *POLG* mutations on the catalytic function; however, these are not applicable to study the pathomechanisms of *POLG*-related epilepsy, given that the mice do not develop seizures. The reason for which mice with defective proofreading activity (Trifunovic *et al.*, 2004) do not develop epilepsy despite accumulating mtDNA deletions and point mutations with age is unclear. However, mtDNA depletion has not been detected and it is therefore possible that mtDNA depletion is a key factor leading to downstream pathophysiological processes, which culminate in seizures. Therefore, despite the existence of mouse models with *POLG* mutations, the absence of a seizure phenotype, perhaps due to absence of mtDNA depletion leads to the conclusion that currently there is no mouse modelling for *POLG*-related epilepsy.

1.10 Alpers' Syndrome

1.10.1 Clinicopathological Description and History

Alpers' syndrome is an uncommon autosomal recessive cerebrohepatopathy with an estimated incidence of 1 in 100,000 births (Mangalat *et al.*, 2012). It is clinically

characterised by a classical triad of: seizures/epilepsy, psychomotor regression and liver dysfunction/failure. The majority of patients are healthy before disease onset and seizures are the heralding manifestation of the disease. Disease onset has a bimodal distribution with the first peak occurring in infancy/childhood (2-4 years, range: 3 months to 8 years) and a second peak in adolescence/early adulthood 17-24 years, range: 10 years to 27 years), albeit disease onset in infancy/childhood is most frequent (Saneto *et al.*, 2013).

Bernard Alpers was the first to describe a case of 'diffuse progressive neurodegeneration of the grey matter of the cerebrum' in a 4-month-old girl who presented with intractable seizures in the course of a one-month-illness (Alpers, 1931). The acronym Alpers has since been used to describe the neurological involvement of the disease. The first report by Alpers led to the description of other cases with this disorder (Morse, 1949; Ford *et al.*, 1951; Palinsky *et al.*, 1954). The first evidence of liver involvement was reported by Blackwood and colleagues in two siblings who presented with diffuse cerebral degeneration and liver cirrhosis (Blackwood *et al.*, 1963). It was only 10 years later that the first suggestion of dysfunctional neuronal mitochondria and autosomal recessive pattern of inheritance was made (Sandbank and Lerman, 1972). Autosomal recessive inheritance was confirmed by Peter Huttenlocher who also noted that hepatic involvement was not always present in previously described Alpers cases (Huttenlocher *et al.*, 1976). The term 'Huttenlocher' was then used to describe hepatic involvement. The terms 'Alpers and 'Alpers-Huttenlocher' (AHS) are considered synonymous (Harding, 1990). Alternative terms exist such as 'Alpers-like' and 'Alpers' syndrome type 1', however these are not commonly used.

The diagnosis of Alpers syndrome is based upon evidence from clinical assessment, and include EEG recordings, neuroimaging including Magnetic Resonance Imaging (MRI) and neuropathological investigations at post-mortem.

1.10.2 Early-onset Alpers

Alpers is hallmarked by seizures, which are believed to be the first presenting symptom in 50% of the cases (Anagnostou *et al.*, 2016). Once seizures occur the disease becomes rapidly progressive eventually leading to death within 4 years (Cohen, 2014). Seizures can be focal, primary generalised or myoclonic. Some patients may present with Epilepsia Partialis Continua (EPC) which may progress to status epilepticus (EPC) (Horvath *et al.*, 2006; Tzoulis *et al.*, 2006). Seizures may

initially be controlled through the use of anticonvulsive drugs, however some seizures may be refractory to treatment from the onset (Cohen, 2014).

Infants/children with Alpers develop normally over the first weeks/months and years of their life. Some patients demonstrate psychomotor regression prior to the seizure onset (Saneto *et al.*, 2013). A recent study demonstrated that anaemia is a common feature of patients with Alpers and MCHS harbouring *POLG* mutations. Interestingly, anaemia is present at disease onset in 35% of the cases (Hikmat *et al.*, 2017a).

Seizure onset is usually sudden and leads to death within a few months from the presentation, however some patients can survive up to four years. Seizures are accompanied by other features including: developmental delay, nausea, vomiting, jaundice, ataxia, neuropathy, headache, hemiparesis, cortical blindness and liver failure (Gordon, 2006). When liver dysfunction is present it will progress to end-stage liver failure unless disease progression is rapidly fatal (Stumpf *et al.*, 2013).

1.10.3 Late-onset Juvenile Alpers

The first signs of Juvenile Alpers are not as well-characterised as typical early-onset Alpers. Unlike early-onset Alpers cases, the majority of patients with Juvenile Alpers present with headache with or without visual impairment (Wiltshire *et al.*, 2008; Saneto *et al.*, 2013; Anagnostou *et al.*, 2016). As with early-onset Alpers, seizures become the predominant manifestation of Juvenile Alpers. Neurological deterioration following seizure onset in Juvenile Alpers cases is not as rapidly progressive as in early-onset Alpers, and patients have a longer survival (Tzoulis *et al.*, 2006). The reasons behind this observation remain unclear.

1.10.4 Alpers and POLG

POLG mutations constitute the underlying genetic defect in over 90% of Alpers cases. Alpers is an mtDNA maintenance syndrome and is considered to be the most severe phenotype of *POLG*-related disorders. Recessive *POLG* mutations are thought to cause POLG dysfunction, resulting in secondary mtDNA defects (including mtDNA depletion and rarely deletions), which eventually lead to respiratory chain dysfunction.

The first association between Alpers syndrome and POLG dysfunction was recognised in 1999 when Naviaux and colleagues reported a patient with Alpers and undetectable levels of POLG activity combined with mtDNA depletion in both skeletal muscle and liver (30% and 25% of normal controls respectively). In addition,

biochemical assays revealed a reduction in the activity of complexes I-IV (Naviaux *et al.*, 1999). The link between genetic aetiology and molecular pathophysiology was established in 2004 when *POLG* mutations were described as the cause of Alpers syndrome (Naviaux and Nguyen, 2004). To date over 60 recessive *POLG* mutations have been reported and associated with Alpers; highlighting the frequency and importance of *POLG* mutations in Alpers pathogenesis (Saneto *et al.*, 2013). As with other *POLG*-related syndromes, the most commonly identified mutations in Alpers are: p.(Ala467Thr), p.(Trp748Ser) and p.(Gly848Ser).

Given the heterogeneous nature of the clinical symptoms and the wide spectrum of *POLG* mutations, there are no clear genotype to phenotype correlations to date. The common mutations such as p.(Ala467Thr) may occur in various syndromes ranging from severe early-onset to milder late-onset disease.

One report identified a homozygous p.(Ala467Thr) mutation in a paediatric Alpers patient with a later disease onset (8 years of age) (Nguyen *et al.*, 2005). Another study revealed that compound heterozygous p.(Ala467Thr)/p.(Trp748Ser) mutations are associated with shorter survival and more severe disease when compared to homozygous p.(Ala467Thr) and p.(Trp748Ser) mutations (Tzoulis *et al.*, 2006). This finding is opposed to the previously mentioned study (Nguyen *et al.*, 2005), where the paediatric patient died within one year from the disease onset. Thus, homozygous mutations do not lead exclusively to milder phenotypes.

Another study, including 21 patients with Alpers, showed mtDNA depletion in the liver and/or muscle of patients with mutations in the polymerase and exonuclease domains of *POLG*. The patients exhibiting mtDNA depletion had a severe clinical phenotype with rapid progression. In contrast, patients harbouring two mutations in the linker domain did not exhibit mtDNA depletion and manifested a milder clinical phenotype with a later disease onset (childhood and adolescence). It is likely that defects in two different domains of POLG may further compromise POLG catalytic activity (Ashley *et al.*, 2008).

Overall, these findings imply that the location of the mutations within the catalytic subunit of *POLG* may modulate in part the clinical phenotype. It is generally accepted that homozygous mutations are associated with Juvenile onset and longer survival compared to compound heterozygous mutations. However, this hypothesis cannot explain why the same homozygous or compound heterozygous mutations can be found in severe early-onset Alpers and milder Juvenile Alpers or other *POLG*-related

disorders such as adPEO. A better understanding of the effects of these mutations on the clinical phenotypes is essential in order to understand the heterogeneity of *POLG*-related disorders.

1.10.5 Involvement of Other Genes than POLG in Alpers

Despite *POLG* mutations constituting the major cause of Alpers, there is increasing evidence supporting that other genes are implicated in Alpers-like epileptic encephalopathies. Mutations in the gene encoding TWNK (Twinkle helicase) have been reported in a 4-year old patient with status epilepticus and an Alpers-like phenotype in the absence of *POLG* mutations (Hunter *et al.*, 2011). More recently, defects in mitochondrial translation have emerged. Mutations in genes encoding tRNA synthetases including NARS2, FARS2, PARS2 and CARS2 have been identified as a cause of mitochondrial epileptic syndromes similar to Alpers (Coughlin *et al.*, 2015; Sofou *et al.*, 2015; Cho *et al.*, 2017). Biochemical investigations have shown that such mutations have been associated with respiratory chain deficiencies and mitochondrial dysfunction. More research is required to completely understand Alpers and other mitochondrial encephalopathies.

1.10.6 Affected Tissues

There is a general consensus that Alpers manifestations are tissue-specific. The most affected tissues include the brain and liver. The brain is largely affected as it requires a high ATP supply to function properly. When ATP production is compromised, neurons become particularly vulnerable as these are OXPHOS-dependent given their limited glycolytic capacity (Zsurka and Kunz, 2015).

Neuroimaging findings including MRI and Computerised Tomography (CT) from patients with Alpers reveal abnormalities such as generalised brain atrophy, oedema and inflammation (Flemming *et al.*, 2002; Saneto *et al.*, 2013). Generally, changes in the posterior brain areas (including the cerebellum and occipital lobes) are most prominent than in anterior areas. In some patients, neuroimaging findings can be normal, especially in early disease-stage. As the disease progresses degeneration and gliosis become evident (Saneto *et al.*, 2013).

Neuropathological investigations are in accordance with neuroimaging data showing a predilection for the occipital lobe and variable cerebellar involvement. Major abnormalities include: cortical neuron loss, astrogliosis, Purkinje cell loss and spongiform changes (reviewed in Chapter 3).

Liver dysfunction/failure is a characteristic feature of Alpers. Liver dysfunction can be variable among patients and can rapidly progress to liver failure, which can either occur before or after the seizure onset. Liver dysfunction can be a defining finding, taking into account following histological characteristics: microvesicular steatosis, bile duct proliferation, fibrosis, hepatic dropout, parenchymal disarray, regenerative nodules and collapse of liver plates (Nguyen *et al.*, 2006; Stumpf *et al.*, 2013).

Liver failure can be triggered by the use of sodium valproate (an anticonvulsant drug) within 6 months. Therefore, the use of sodium valproate is contraindicated in cases with Alpers. Interestingly, the neurological deterioration is the most important aspect of the disease as patients who received liver transplants due to liver failure, eventually died from neurological complications (Delarue *et al.*, 2000; Kayihan *et al.*, 2000).

MtDNA depletion is frequently reported in the liver and muscle from patients suffering from Alpers; although muscle findings are not consistent. It is important to note that early in the disease course, mtDNA copy number may appear normal and will decline with disease progression. MtDNA depletion is accompanied by respiratory chain deficiencies involving single or multiple complexes. As the scope of this thesis involves the pathophysiology of Alpers and *POLG*-related epileptic disorders, a detailed systematic review of the published molecular genetics, biochemistry, neuropathology and mitochondrial dysfunction is provided in Chapter 3.

1.10.7 Treatment of Alpers Manifestations

Currently, there are no existing therapies for Alpers and management is supportive. Supportive treatment strategies include: the use of anticonvulsant drugs, ketogenic diet and magnesium therapy. Anticonvulsants such as carbamazepine and levetiracetam can be used to treat seizures, however seizures often prove refractory to treatment and any early beneficial effects of treatment are usually not long-lasting.

Ketogenic diet is frequently used as part of the management in paediatric epilepsy. It involves a diet with high fat, moderate protein and low carbohydrate content and helps control seizures in some individuals.

The ketogenic diet mimics the state of starvation, in which fat is the major source of energy and undergoes mitochondrial β-oxidation of fatty acids in the liver, producing ketones. Ketones are then used by the brain instead of glucose as an energy source (Beth and Emily, 2008). The exact mechanisms by which ketogenic diet leads to

seizure inhibition are unclear, however several hypotheses have been proposed. Decanoic acid (C10), a component of the medium-chain fatty acid (MCT) diet has been found to down regulate transcription of genes involved in glucose metabolism and upregulate transcription of genes responsible for fatty acid metabolism (Paleologou *et al.*, 2017). C10 has also been associated with increased mitochondrial biogenesis and increased complex I activity in neuronal cells (Hughes *et al.*, 2014). Overall, since seizures are associated with ATP depletion, it is hypothesised that the ketogenic diet mediates anticonvulsant effects by increasing efficiency of ATP generation.

The beneficial effect of ketogenic diet in patients with Alpers is questionable. One study has revealed a significant improvement in EEG and a termination of seizures for 7 months in a young girl with Alpers (Joshi *et al.*, 2009). Another study performed in a larger cohort involving 32 infants with refractory epilepsy showed that ketogenic diet resulted in over 50% reduction in seizure frequency. However, these patients were not diagnosed with Alpers (Nordli *et al.*, 2001). In contrast, a patient with Juvenile Alpers showed no improvement after being placed on a ketogenic diet (Wiltshire *et al.*, 2008). Therefore, ketogenic diet may be beneficial for some patients, however more research is required to confirm whether ketogenic diet is effective in the management of Alpers.

Alpers is a progressive and life-threatening condition which is particularly devastating for families. The lack of effective treatments targeting the underlying mitochondrial dysfunction makes it a challenging condition to manage.

Although Alpers is fatal, some recent findings may provide hope for future therapy. A novel benzoquanine (EPI-743) drug modified disease progression in patients with mitochondrial disease including patients harbouring *POLG* mutations (Enns *et al.*, 2012). Another study performed in the mtDNA mutator mouse showed that endurance exercise (for 5 months) remarkably increased mitochondrial biogenesis, prevented mtDNA depletion and mutations, enhanced mitochondrial oxidative capacity and respiratory chain assembly and restored mitochondrial morphology (Safdar *et al.*, 2011). However, the effect of endurance exercise on humans remains unknown.

1.11 Aims and Objectives of Study

As demonstrated throughout this chapter, Alpers is a rare mitochondrial cerebrohepatopathy caused in the vast majority of the cases by recessive mutations in *POLG*, and is considered to be the most severe form of *POLG*-related disorders. Although *POLG* mutations are thought to cause mtDNA depletion with ultimate OXPHOS dysfunction, the exact mechanisms remain obscure. Alpers is hallmarked by the triad of seizures, psychomotor regression and liver failure; however, our understanding of Alpers pathophysiology remains incomplete. The limited understanding on how *POLG* mutations modulate disease phenotype combined with the severe seizure involvement and lack of treatment, makes Alpers a particularly challenging syndrome to investigate.

The focus of this project is to further understand the effect of *POLG* mutations on mitochondrial function in patients suffering from Alpers. This study aims to test the hypothesis that *POLG* mutations cause mitochondrial dysfunction leading to Alpers and *POLG*-related epilepsy. To this purpose, *POLG*-mutant fibroblasts will be assessed and post-mortem brain tissue from patients with clinically and/or genetically defined Alpers will be used in order to understand the mechanisms leading to the characteristic neurological deficits (especially epilepsy) seen in these patients. To this aim the specific objectives are:

1) To conduct a systematic review of the published literature to date, evaluating the effect of *POLG* mutations on the molecular and biochemical features of patients with Alpers and other *POLG*-related epileptic disorders.
2) To characterise the baseline mitochondrial function in *POLG*-mutant fibroblasts derived from patients with early and late-onset Alpers. The specific objectives to this aim were to:

- Assess bioenergetics and mitochondrial morphology/networks/nucleoids.
- Assess mitochondrial motility and membrane potential.
- Quantify mtDNA copy number using qPCR.
- Evaluate the expression of POLG.

3) Perform a detailed post-mortem neuropathological study in occipital, parietal and frontal lobe tissue from patients with clinically and/or genetically confirmed Alpers in order to investigate the mechanisms of mitochondrial epilepsy and

neurological deficits seen in these patients. The specific objectives to this aim were to:

- Assess densities of neuronal sub-populations (interneurons and pyramidal neurons) by quantitative immunohistochemical assays.
- Determine respiratory chain protein deficiency involving complexes I and IV in interneurons and pyramidal cells by quantitative immunofluorescence.
- Characterise the neuropathology of Alpers, using a semi-quantitative approach to evaluate grey matter and white matter abnormalities such as astrogliosis via immunohistochemistry.
- Achieve a genetic confirmation of *POLG*-mutations in patients where there was no available genetic diagnosis.
- Assess mtDNA abnormalities using qPCR.

Chapter 2 Materials and Methods

2.1 Equipment and Consumables

2.1.1 Equipment

ABI Gen Amp 9700 Thermal Cycler	Applied Biosystems
Antigen Retriever 2100	Aptum Biologics
AURA PCR UV Cabinet	Bio Air Instruments
Automated Plate Reader EIx800	Bio-Tek
Axiovert 200 Zeiss	Zeiss
Bench-Top Centrifuge 3-15	Sigma
Bench-Top Micro-Centrifuge 5418	Eppendorf
Bench-Top pH Meter 3510	Jenway
ChemiDoc MP Imaging System	Bio-Rad
Countess® Automated Cell Counter	Life Technologies
Dry Heat Block DB.3.A	Techne
Electrophoresis Power Supply	Cleaver Scientific Ltd
ErgoOne® Single & Multi-Channel Pipettes (2.5µl, 10µl, 20µl, 200µl, 1000µl)	Starlab
Grant JB Series Water Bath	Grant Instruments
IKA Magnetic Stirrer Hotplate RCT Basic	Fisher Scientific
InCu Safe TM CO_2 Incubator	Sanyo
Incubator (60^{o}C)	Genlab
Light Microscope	Leica
Mini-ProteanR® Tetra Cell System	Bio-Rad
Nanodrop ND-1000 Spectrophotometer	Labtech International

NANOpure II Water Purification System	Barnstead
Neubauer Improved Haemocytometer	Millipore
Nikon A1R Invert Imaging System	Nikon
Nikon A1R Scanning Confocal System	Nikon
OHAUS Adventurer® Balance	OHAUS
Olympus Microscope BHX51	Olympus
Seahorse Extracellular Analyser XF24	Agilent
SpectraMax M3 Plate Reader	Molecular Devices
StepOne Plus Real-Time PCR System	Applied Biosystems
Thermomixer C	Eppendorf
Vortex Genie 1 Touch Mixer	Wolf Laboratories
Vortex Genie 2	Scientific Industries

2.1.2 Software

ImageJ Processing and Analysis	National Instutes of Health (NIH)
ChemiDoc MP Imaging Software, Image Lab (version 4.1)	Bitplane
GraphPad Prism (version 5.0)	GraphPad
IMARIS Scientific 3D/4D Image Processing and Analysis Software (version 7.2)	Bitplane
Matlab 2015b	MathWorks
Minitab	Pennsylvania State University (PSU)
Nikon Imaging Sofware (NIS) Elements Viewer	Nikon
Seahorse XF24 Software	Agilent

SPSS (version 17)	International Business Machines (IBM)
StepOne Software (version 2.1)	Applied Biosystems
StereoInvestigator Software	MBF Bioscience
Volocity® 3D Image Analysis and Quantitation	Perkin Elmer

2.1.3 Consumables

Coverslips (22x20mm, 22x32mm, 22x40mm, 22x50mm)	VWR Internationals
0.2ml Thin-Walled PCR Tubes	Thermo Scientific
0.5ml PR Tubes	Thermo Scientific
96 Wel Optical Bottom Plates	NUNC
Cell Culture Plates (Plastic: 6-Well, 24-Well, 69-Well)	Greiner
Cellstar® Disposable Pipettes (5ml, 10ml, 25ml)	Greiner
Cellstar® Tissue Culture Flasks (25cm2 and 75cm2)	Greiner
Countess® Cell Counting Chamber Slides	Life Technologies
Cryotube Vials	NUNC
Falcon Tubes (15ml and 50ml)	BD Biosciences
iBIDI 35mm Glass Dishes	Thistle Scientific
Immobilon Transfer Membranes PVDF	Millipore
MILLEX Syringe-Driven Filters (0.22µm)	Millipore
PAP Pen Liquid Blocker-Super	Newcomer Supply

Pasteur Pipettes (Glass)	VWR Internationals
Pasteur Pipettes (Plastic)	Fisher Scientific
PCR Plate Seals (Real-Time PCR)	Starlabs
PCR Plates (Real-Time PCR)	Starlabs
Pipette Tips (Including Filter Tips: 10µl, 20µl, 200µl, 1000µl)	Starlabs
ProLongTM Gold Antifade Mountant	Life Technologies
QIAamp DNA FFPE Tissue Kit	Qiagen
QIAamp DNA Mini Kit	Qiagen
Seahorse XF24 Cell Culture Microplates	Agilent
Slide Racks	CellPath
Syringes	DB Plastipak
Weigh Boats	Fisher Scientific

2.2 Chemicals and Reagents

2.2.1 Solutions

0.5M Tris-HCl pH 6.8 (Stacking Buffer)	30.275g Trizma Base, 500ml dH_2O
1% Acid-Alcohol Solution	500ml Ethanol, 5ml HCl, 485ml dH_2O
10mM Tri-Sodium Citrate pH 6.0	2.941g Tri-Sodium Citrate, 1L dH_2O
1M Tris-HCl pH 8.0 (Separating Buffer)	60.55g Trizma Base, 500ml dH_2O
1mM EDTA pH 8.0	0.416g EDTA, 1L dH_2O
3% Hydrogen Peroxide	400ml dH2O, 12ml Hydrogen Peroxide
3% Sudan Black B	0.3g Sudan Black B, 100ml 70% Ethanol

5% Milk Solution in TBST	5g Skimmed Milk Powder, 100ml TBST
DNA Loading Buffer	0.25% (w/v) Bromophenol Blue, 0.25% (w/v) Xylene Cyanol, 30% (v/v) Glycerol
Electrophoresis Buffer	100ml 10x TAE, 900ml NANOpure Water, 80µl Ethidium Bromide
Lysis Buffer	100µl 0.5M Tris/HCl + 52µl 2.5M NaCl + 4µl 0.5M $MgCl_2$, 150µl 7x Roche Protease Inhibitors, 20µl Nonidet P-40, 674µl dH_2O
Phosphate-Buffered Saline (PBS)	prepared from Tablets, 1 Tablet in 100ml dH_2O
Running Buffer x5 (Westerns)	15g Trizma Base, 72g Glycine, 5g SDS
Sample Buffer (Westerns)	10ml Stacking Buffer, 4ml Glycerol
Scott's Tab Water	2g Sodium Bicarbonate, 20g Magnesium Sulphate, 1L Tap Water
Tris-Buffered Saline (TBS)	1.2g Trizma Base, 17g NaCl, 2L dH_2O
Tris-Buffered Saline-Tween (TBST) pH 7.4	1.2g Trizma Base, 17g NaCl, 2L dH_2O, 1ml Tween20

2.2.2 *Antibodies*

Anti-GAD56/67	Sigma-Aldrich
Anti-GFAP	DAKO
AlexaFluor® 405	Life Technologies
AlexaFluor® 647	Invitrogen
AlexaFluor® 647	Life Technologies
AlexaFluorTM 488	Invitrogen
AlexaFluorTM 546	Invitrogen
AlexaFluorTM 546	Life Technologies
Anti-Beta-Actin	Sigma
Anti-COX4l2	Abcam
Anti-MTCOI	Abcam
Anti-NDUFA13	Abcam
Anti-NDUFB8	Abcam
Anti-Neurofilament H (NF-H, SMI-32P)	BioLegend
Anti-Polg	Abcam
Anti-SDHA	Abcam
Anti-VDAC1	Abcam
Biotin-SP AffiniPure Fcγ Subclass 2b Specific	Jackson ImmunoResearch
Biotin-XX	Life Technologies
Streptavidin, AlexaFluor® 488 Conjugate	Life Technologies
Streptavidin, AlexaFluor® 546 Conjugate	Life Technologies

2.2.3 Histological Reagents

3,3' Diaminobenzidine Tetrahydrochloride (DAB)	Sigma
30% w/v Hydrogen Peroxide	Sigma
Anti-Mouse/Rabbit PolyVue HRP Labe	Diagnostic BioSystems
DPX™	Merck
Ethanol	Fisher Scientific
Ethylenediaminetetraacetic Acid, Disodium Salt, Dihydrate (EDTA)	Affymetrix
Histoclear™	National Diagnostics
Mayers haematoxylin	TCS Biosciences Ltd
Normal Goat Serum	Sigma
Polymer Penetration Enhancer	Diagnostic BioSystems
Sudan Black B	RAL Diagnostics
Tri-Sodium Citrate	VWR Internationals
Tween 20	Sigma

2.2.4 Tissue Culture Reagents

Accutase	Thermo Fisher Scientific
B27 Supplement (50x), Serum Free	Gibco
CHIR99021	Tocris
DMEM/F-12 GlutaMAXTM Supplement	Thermo Fisher Scientific
Foetal Calf Serum (FCS)	Gibco
Human Leukemia Inhibitory Factor (hLIF)	Cell Signalling
Laminin	Invitrogen
L-Glutamine (100mM)	Gibco
MEM Vitamins	Gibco
Modified Eagle Medium (MEM)	Gibco
N2 Supplement (100x)	Thermo Fisher Scientific
Neurobasal® Medium	Thermo Fisher Scientific
Non-Essential Amino Acids (NEAA)	Sigma
Paraformaldehyde Solution 4% in PBS	Santa Cruz Biotechnology
Penicillin and Streptomycin Solution	Gibco
Phospathe-Buffered Saline (PBS)	Gibco
PicoGreen	Invitrogen
ROCK Inhibitor	Sigma
SB431542	Stemgent Inc.
Sodium Pyruvate (100mM)	Sigma

Tetramethyl Rhodamine Methyl Ester (TMRM)	Invitrogen
TripLE	Gibco
Uridine	Sigma-Aldrich

2.2.5 Seahorse Reagents

Antimycin	Sigma
Oligomycin	Sigma
Rotenone	Sigma
Seahorse Assay Medium	Agilent
Trifluorocarbonylcyanide Phenylhydrazone (FCCP)	Sigma
XF Cell Mito Stress Kit	Agilent

2.2.6 Molecular Biology Reagents

1kb DNA Ladder	Norgen
5x GoTaq® PCR Buffer	Promega
Agarose MP	Roche
Bromophenol Blue	Sigma-Aldrich
Deoxynucleotide Triphosphates (dNTPs)	Rovalab
DEPC-Treated H_2O	Ambion
ECL-Plus Western Detection Kit	Amersham
Ethidium Bromide	Merck
GelRedTM Nucleic Acid Stain	Biotium
Glycerol	Sigma
GoTaq® Hot Start Polymerase	Promega
Immobilon-P Transfer Membrane	Millipore
Magnesium Chloride ($MgCl_2$)	Promega

Mouse anti-Rabbit HRP Conjugated	DakoCytomation
Pyro Gold Reagents	Qiagen
Rabbit anti-Mouse HRP conjugated	DakoCytomation
Skimmed Milk Powder	Marvel
TaqMan ND1/B2M Probes	Applied Biosystems
TaqMan Universal PCR Mastermix	Applied Biosystems
Tris-Acetate-EDTA (TAE 10x) Buffer	Sigma
Trizma Base	Sigma
Tween 20	Sigma
Xylene Cyanol	Sigma

2.3 Tissue Culture

2.3.1 Human Fibroblasts

Human fibroblasts were obtained from skin biopsies from patients and controls. Full consent was provided.

Case Code	Age at Biopsy	Gender	Phenotype	*POLG* Mutations	Location in *POLG* Gene
M0528-12	6 months	Male	Control	N/A	N/A
M0465-11	5 months	Male	Control	N/A	N/A
M1171-13	8 months	Male	Control	N/A	N/A
M0857-15	24 years	Male	Control	N/A	N/A
M0858-15	26 years	Male	Control	N/A	N/A
M0859-15	34 years	Male	Control	N/A	N/A
M1453-12	1 month	Male	Alpers	p.(Ala467Thr)/ p.(Thr914Pro)	Linker/Polymerase
M1059-10	1 year	Male	Alpers	p.(Leu428Pro)/ p.(Ala467Thr)	Exonuclease/ Linker
M1936-13	15 years	Female	Alpers	p.(Ala467Thr)/ p.(Ala467Thr)	Linker/Linker
M0174-17	16 years	Female	Alpers	p.(Trp748Ser)/ p.(Cys418Arg)	Linker/Linker

Table 2.1: Human Fibroblasts used in this study. Key: N/A=not applicable.

2.3.2 General Cell Growth and Maintenance

Cells were removed from liquid nitrogen stores or -80ºC freezer and thawed by trituration with 0.5ml pre-warmed medium (see Table 2.2). The aliquot containing the cells was re-suspended to 9.5ml of pre-warmed medium. The cells were spun at 124g for 4 minutes to release DMSO from the cells into the supernatant. The supernatant was discarded and the cells were re-suspended in 5-10ml fresh pre-warmed growth medium (depending on the number of flasks to be seeded). An appropriate volume (3-10ml) of medium was added in each flask. The flasks were placed in an incubator (37ºC, 5% CO_2) until they reached 70-80% confluency. For quiescence studies, when fibroblasts reached 80% confluency, medium was replaced by fibroblast growth medium containing 0.1% Fetal Calf Serum (FCS) for 7 days, before being harvested as described in the following section. Medium formulations are summarised below.

Fibroblast Growth Medium	Neuroinduction Medium	Freezing Medium
433ml MEM	12ml DMEM/F-12 Glutamax	4.5ml Growth Medium
50ml FCS	12ml Neurobasal Medium	500µl DMSO
5ml MEM-vits	500µl N-2 Supplement	
5ml NEAA	1ml B-27 Supplement	
5ml L-glutamine	3.75µl CHIR99021	
5ml Pen/Strep	5µl SB431542	
5ml Sodium Pyruvate	25µl hLIF	
1ml Uridine		

Table 2.2: Medium formulations. Key: FCS=foetal calf serum; vits=vitamins; NEAA=non-essential amino acids; pen/strep=penicillin/streptomycin; hLIF=human leukaemia inhibitory factor; DMSO=dimethyl sulfoxide; CHIR99021=GSK-3 inhibitor; SB431542=TGF-β inhibitor.

2.3.3 Harvesting Cells

When the cells reached the desired confluency the medium was discarded and cells were washed in 5ml Phosphate Buffered Saline (PBS) to remove all traces of FCS which inhibits trypsin. The PBS was aspirated and 2ml of trypsin were added in the flask ensuring coverage of the entire cell surface. The flask was incubated for 2-5 minutes at 37ºC with 5% CO_2 and then gently tapped to ensure cell detachment. A total of 8ml of pre-warmed medium was added into the flask to inhibit trypsin and contents were transferred to a universal. Cells were spun at 124g for 5 minutes and fully re-suspended prior to being collected or divided into the appropriate number of

flasks. For collection of cell pellets, cells were re-suspended in 1ml medium, spun at 124g for 5 minutes before the supernatant was discarded and pellets were snap-frozen in liquid nitrogen and stored at -80ºC. Flasks were incubated (37ºC, 5% CO_2) until confluent.

2.3.4 Freezing and Storage

To freeze cells, cells were harvested as described above. The 10ml medium containing cells were collected and spun at 124g for 5 minutes. The medium was aspirated and cells were re-suspended in freezing medium (see Table 2.2). Cells were then aliquoted into cryotubes (1ml/vial). Tubes were sealed and stored at -80ºC freezer. For longer storage cells were transferred to liquid nitrogen.

2.3.5 Conversion of POLG-Mutant Human Fibroblasts into induced Neuronal Progenitors (iNPC's)

The protocol used has been previously published (Lu *et al.*, 2013). A total of 10^4 cells were seeded into one well of a six-well plate. Cells were left in the incubator (37ºC, 5% CO_2) overnight to attach. On the following day 1ml of fibroblast growth medium containing 27.5µl of a mixture of Sendai virus (Thermo Fisher Scientific) containing the transgenes which express factors hKOS (polycistronic vector, 7.5µl), c-Myc (10µl) and hKlf4 (10µl) was applied to the cells. After transduction, these viral vectors will cause cells to express the aforementioned genes, resulting in reprogramming. Cells were incubated (37ºC, 5% CO_2) for 24 hours prior to being washed with 0.5ml neuroinduction medium (see Table 2.2). The washing step was repeated 3x before 1ml of neuroinduction medium was applied on the cells. Cells were then placed in an incubator at 39ºC with 5% CO_2 (higher temperature assists faster elimination of the virus from the cells). Cells were monitored daily and 1ml neuroinduction medium was replaced every 2 days. On day 7, cells were collected and re-plated into one well of a 6-well plate pre-coated (2 hours) with 50µg/ml laminin (Invitrogen). Firstly, cells were washed with 0.5ml PBS before application of 300µl accutase (Thermo Fisher Scientific). Cells were placed in the incubator (37ºC, 5% CO_2) for 1-2 minutes to ensure detachment of cells. To inhibit accutase 1ml of fresh neuroinduction medium was added before cells were centrifuged at 200g for 4 minutes. Cells were then re-suspended in 1ml fresh neuroinduction medium containing 10µM ROCK Inhibitor (Sigma). Cells were placed in one well of pre-coated laminin 6-well plate and returned to the incubator (39ºC, 5% CO_2). Medium containing ROCK inhibitor was replaced every 2 days. Once cells changed in shape and formed large sphere-like

structures (neurospheres), these were collected using a pipette and each neurosphere was then placed in one well of pre-coated laminin 48-well plate to expand and form colonies.

2.4 Live-Cell imaging

2.4.1 Growing Cells

Cells were seeded at a density 30,000-100,000 cells (depending on cell type) in iBIDI dishes (Thistle Scientific). Cells were maintained in 2ml normal growth medium and incubated (37^{o}C, 5% CO_2) for at least 24 hours prior to experimentation.

2.4.2 Live Cell Dyes

For PicoGreen (Invitrogen) staining, cells were incubated with 3µl of PicoGreen in 1ml normal growth medium for 45 minutes at 37^{o}C and 5% CO_2 prior to imaging. For Tetramethyl Rhodamine Methyl Ester (TMRM) (Invitrogen) staining, cells were incubated with 1ul 5nM TMRM in 2ml medium for 30 minutes. Cells were washed and left in normal growth medium prior to imaging.

2.4.3 Confocal Imaging

Live-cell imaging was undertaken on an inverted point scanning confocal microscope (Nikon, A1R), housed in a 37^{o}C and 5% CO_2 controlled chamber. The microscope is fully equipped with a heated environmental chamber with the ability to set, maintain and monitor temperature, humidity CO_2 and O_2 levels according to imaging conditions. Cells were monitored using a 60x oil immersion lens with a 3.09x further confocal zoom and Galvano scanning. Z-stacking was performed. The system is set up for achieving optical thickness of 0.17µm and at least 15 Z-stacks were captured prior to analysis.

2.4.4 Mitochondrial Network Analysis

Analysis of mitochondrial networks was carried out using ImageJ. Individual z-stacks obtained from confocal imaging were merged into a single image using a maximum projection technique. To smooth the image signal, a filter using deconvolution was applied. Images were then binarized to allow the automatic quantification of mitochondrial morphological parameters. These include: aspect ratio (AR; ratio between major and minor axes of an ellipse equivalent to a mitochondrion), which indicates mitochondrial length, perimeter (mitochondrial outline length) and area (area of mitochondrion). Using the aforementioned morphological characteristics,

form factor (FF, a measure of mitochondrial length and degree of branching) was calculated using the formula: perimeter^2/4pi x area. FF and AR from patient fibroblasts were compared to controls. Statistical analysis was carried out using Prism GraphPad software (version 5.0).

2.4.5 Nucleoid Analysis

Nucleoids were analysed by ImageJ. As with analysis of mitochondrial networks described above, z-stacks were merged into a single image using maximum projection method. A filter was applied, prior to binarization of images and the automatic quantification of morphological parameters. The number of nucleoids per cell analysed was taken into consideration. The number of nucleoids per cell in patient fibroblasts was compared to controls. Statistical analysis was performed using Prism GraphPad software (version 5.0).

2.4.6 Mitochondrial Membrane Potential and Motility Analysis.

Mitochondria were visualised by TMRM as described in section 2.4.2. Confocal imaging was performed every second for ten minutes. Movie files were analysed using Imaris (version 7.2, Bitplane). For mitochondrial tracking, mitochondria were defined as surfaces and using a touching components algorithm these were tracked through multiple time points. Mapping of individual mitochondria was facilitated by intensity and size parameters prior to tracking. Mitochondrial membrane potential quantification was based on TMRM intensity and motility analysis was based on information generated on bi-directionality, size, volume and distance travelled. All parameters were then assessed in controls compared to patient-derived fibroblasts. Statistics were carried out using Prism GraphPad software (version 5.0).

2.5 Bioenergetics

2.5.1 XF Extracellular Flux Analysis Experiments

Fibroblasts were seeded at an optimal density 30,000-50,000 cells/well in 20 wells of a 24-well seahorse plate, 24 hours prior to experimentation. Each well was filled with 100µl fibroblast growth medium. Four wells were left blank as background controls for each run. To allow the formation of a monolayer, fibroblasts were incubated for 3 hours (37^{o}C, 5% CO_2) prior to topping up with medium to a final volume of 250µl. Cells were then lest overnight in the incubator (37^{o}C, 5% CO_2). At this time the cartridge was rehydrated. Each well was filled with 1ml calibration buffer and left overnight at 37^{o}C without CO_2.

On the day of the run, experimentation medium was prepared by supplementing fibroblast growth medium with 1mg/ml glucose, 2% FCS and 1mM pyruvate. The pH of the medium was set to 7.4 and then was warmed to 37^{o}C prior to use. The wells of the seahorse plate were gradually replaced with experimentation medium by removing and replacing 200µl at a time to ensure adequate cell covering. The washing procedure was repeated three times with the final volume in each well topped up to 500µl. The plate was then left to equilibrate for 1 hour at 37^{o}C without CO_2. At this time, experimentation injections were prepared. Adjusted volumes of a total of 4 compounds were injected sequentially from ports A, B and C at appropriate concentrations according to manufacturer's instructions (Table 2.3). The injection cartridge was then removed from the incubator and 75µl of each compound was added in the appropriate port. The cartridge containing the injections was then placed in the Seahorse Extracellular Flux Analyser (Agilent Technologies) to calibrate (20 minutes). Following calibration, the experimentation plate containing the cells to be investigated was added and the selected protocol was run.

Port	Solution	Function	Concentration	Volume
A	Oligomycin	ATP Synthase Inhibitor	1µg/ml	75µl
B	FCCP	Respiratory Chain Uncoupler	2µM	75µl
C	Rotenone/ Antimycin	Complex I/III Inhibitor	0.5µM	75µl

Table 2.3: Compounds used in seahorse extracellular flux analyser. To assess different parameters of mitochondrial baseline function injections of oxidative phosphorylation (OXPHOS) inhibitors were used at appropriate concentrations. Key: FCCP=carbonyl-cyanide-p-trifluoromethoxyphenylhydrazone.

To control for variations in cell growth, after completion of the assay, each well was washed in PBS prior to fixation with 4% PFA for 10 minutes and storage in 500ml PBS at 4^{o}C. Cell nuclei were visualised through Hoescht staining (30 minutes; 1:200 dilution in dH_2O). Imaging was performed at 10x magnification using Axiovert 200M (Zeiss). The cell nuclei were then quantified using the Matlab software. All seahorse measurements were then normalised to cell number. Statistical analysis was performed using Prism GraphPad software (version 5.0).

2.6 Neurohistopathological Methods in FFPE Brain Tissue

2.6.1 Patient Cohort

The patients included in this study all had a clinical diagnosis of epileptic encephalopathy and were suspected to have Alpers' syndrome. Patients fulfilled the criteria of Alpers based on the presentation of defined clinical features. Patients included in this study were characterised by the presence of seizures based on the diagnosis given by the clinician noted on the medical notes. Patient material was obtained from multiple sources. The Institute of Neurology, University of Vienna (Austria) provided FFPE tissue for patients 1 and 2. The Newcastle Brain Tissue Resource (NBTR) provided formalin-fixed and paraffin-embedded (FFPE) tissue for patients 3 and 4. FFPE tissue for patients 5, 6 and 7 was provided by University of Bergen (Norway). The diagnosis of patients 3 and 4 was confirmed by the genetic identification of *POLG* mutations. Genetic diagnosis was not available for patients 1 and 2, therefore diagnosis of Alpers' syndrome was based upon the clinical characteristics and gross neuropathology findings. A summary of the clinical, genetic and neuropathological details of patients is provided in Table 2.4 (patient numbering is the same throughout the thesis for consistency). *POLG* mutations are specified where known. Newcastle and North Tyneside Local Research Ethics Committee (LREC/2002/205) approved this work, and full consent for brain tissue retention and research was obtained. Not all brain regions were available for each patient and control and this is indicated by Tables 2.4 and 2.5. The available clinical histories for the patients considered are detailed below. The clinical histories for patients 5-7 were limited. Information regarding patients 5-7 has been previously published (Tzoulis *et al.*, 2014).

Patient 1

Patient 1 was the second child of the family. A sister had previously died at 4 months of age after a similar clinical course. Patient 1 was born 14 days preterm and at birth he presented with a 20 minute bradycardia combined with apnoea, generalised cyanosis and required resuscitation. At the time, he was diagnosed with neonatal respiratory distress syndrome. Episodes of apnoea occurred and these were identified as a consequence of epileptic seizures.

At 2 months of age, he developed swallowing problems, cyanosis and epileptic seizures combined with apnoeic episodes. A CT scan showed symmetrical

hydrocephalus. At 5 months of age, he showed hypotonia, developmental regression and had no gaze fixation. He died at 5.5 months of age during an epileptic seizure due to heart and respiratory failure. Post-mortem macroscopic evaluation of the brain showed diffuse cerebellar and cerebral atrophy in the medio-basal and temporo-occipital lobes. Genetic diagnosis of *POLG* was not confirmed and there was no conclusive diagnosis.

Patient 2

Patient 2 was a boy born by caesarean section after a normal pregnancy. At 4 months, his parents noticed a poor interaction with various environmental stimuli with no interest in toys, rapid fatigue and difficulties with drinking. He showed a stereotypical mouth movement accompanied by spasms of the upper and lower extremities.

At 9 months, he showed variable muscle tone, he had no head or trunk control, no gripping and no lifting of the body. At 11 months, he developed strabismus with no gaze fixation, showed motor retardation and dyskinetic movements of the eyes (movement coordination of a 3-month old baby).

An EEG scan showed hypsarrhythmia. Adrenocorticotrophic hormone (ACTH) therapy was started at this time but this was withdrawn after 4 weeks due to development of tachycardia, high blood pressure and fever. An acute focal neurological deficit appeared and the patient experienced pneumonia. Penicillin and IV therapy was commenced, however the patient died at 13 months of age due to pneumonia, hydro pericardia and liver steatosis. Macroscopic evaluation of the brain showed medium diffuse atrophy with hydrocephalus internus as a consequence of white matter thinning. Histological findings revealed infantile spongio-neuronal dystrophy Alpers type.

Patient 3

Patient 3 was the first female child of healthy unrelated parents and was born at full term. Family history of epilepsy was noted on the mother’s side. The patient developed normally until 11 months of age, where she presented at hospital with continuous right focal seizures which were treated with sodium valproate (anticonvulsants). After a few months free of seizures, they recurred following her MMR (measles, mumps and rubella) vaccination and she developed regression and failure to thrive. At 13 months old, she showed drowsiness, irritation, weight loss and

became jaundiced. Epileptic episodes with intermittent vomiting continued. At 13 months of age, she became sleepy, irritable, lost weight and became jaundiced. The jaundice was accompanied by clinical evidence of the following: abnormal clotting (easy bruising and bleeding gums), hypoproteinaemia (oedema) and enterohepatic obstruction (dark urine and pale stools).

The patient was admitted to Newcastle General Hospital with encephalopathy and required ventilation. She developed hypoglycaemia and liver function tests were abnormal: bilirubin 113, alkaline phosphatase 243, alanine transaminase 189, albumin 31 and ammonia 70. In addition, she showed coagulopathy: prothrombin>200, partial thromboplastin>180, fibrinogen<0.1, platelets 60, haemoglobin 8.9 and white cell count 6.6. She was then referred to Birmingham Children's Liver Unit to be considered for liver transplant. A CT scan at this time showed mild generalised cerebral atrophy with a low attenuation area in the right frontal lobe. She was diagnosed with Alpers and transferred back to Newcastle General Hospital for terminal care. Molecular genetic investigations confirmed the patient was compound heterozygous for p.(Ala467Thr) and p.(Gly848Ser) *POLG* mutations. Biochemical investigations in the muscle showed 50% activity for complex I and 75% activity for other complexes compared to normal controls. Histochemistry showed 20% COX-negative fibres in the muscle.

Patient 4

Patient 4 was born at term following a normal pregnancy. He was the first child of the family and he had a clinically normal younger sister. He developed normally until 17 months of age when following a day of vomiting, fever and drowsiness he experienced Status Epilepticus (SE). A right hemiparesis resolved but hemianopia continued. An EEG scan was performed after a few months and this was normal. At 19 months of age he developed seizure combined with a convergent squint and left-sided neurological deficits. His speech and motor functions returned to normal but again hemianopia continued. A CT scan revealed atrophy in left occipital lobe and an EEG scan showed deterioration. One month later a similar readmission with visual loss was noticed. He was discharged on a ketogenic diet with anticonvulsants including sodium valproate. A few months later the patient showed evident feeding deterioration and drowsiness. The patient's condition continued to deteriorate as he became unable to walk, had poor vision and experienced seizures in the right upper limbs. A respiratory chain disorder was suspected and molecular investigations

confirmed the patient was compound heterozygous for p.(Ala467Thr) and p.(Thr914Pro) *POLG* mutations. The patient died at 27 months of age due to pulmonary haemorrhage and respiratory failure. A case report of this patient was published describing the clinical course, a partial COX-deficiency in muscle and reduced activity of this enzyme was below 30% of the normal controls (Morris *et al.*, 1996).

Patient 5

Patient 5 (AL-1A in the report by Tzoulis and colleagues) presented with epilepsy at 11 months of age. He developed Epilepsia Partialis Continua (EPC) and died in status epilepticus at 13 months of age. Liver enzymes were abnormal at death. Genetic testing revealed compound heterozygous p.(Ala467Thr)/p.(Gly303Arg) mutations (Tzoulis *et al.*, 2014).

Patient 6

Patient 6 (AL-2A in the report by Tzoulis and colleagues) was a 7-month old boy who presented with explosive epilepsy. He died in Status Epilepticus within 1 month from the onset. Liver function tests were abnormal terminally. Genetic testing confirmed the presence of compound heterozygous p.(Ala467Thr)/p.(Gly848Ser) (Tzoulis *et al.*, 2014).

Patient 7

Patient 7 (AL-1B in the report by Tzoulis and colleagues) presented at 2 years with failure to thrive, which was followed by epilepsy. He died at age of 8 years from terminal seizures after prolonged illness. Genetic testing confirmed the presence of compound heterozygous p.(Ala467Thr)/p.(Gly303Arg) mutations (Tzoulis *et al.*, 2014).

Code	Patient	Source	Age at Death	Sex	Fixation Length	PMI	Cause of Death	POLG Mutations	Brain Region
1977/0047	Patient 1	Vienna	5.5 months	Male	Unknown	Unknown	Cardiac and respiratory failure	Unknown	Parietal
1978/0171	Patient 2	Vienna	13 months	Male	Unknown	Unknown	Pneumonia	Unknown	Parietal
1993/0149	Patient 3	NBTR	14 months	Female	1 month	12h	Hepatic failure	p.(Ala467Thr)/ p.(Gly848Ser)	Parietal
1994/0014	Patient 4	NBTR	27 months	Male	5 weeks	12h	Pulmonary haemorrhage and respiratory failure	p.(Ala467Thr)/ p.(Thr914Pro)	Parietal
O-04/25	Patient 5	Bergen	13 months	Male	2 weeks	Unknown	SE	p.(Ala467hr)/p.(Gly303Arg)	Occipital (Tzoulis *et al.*, 2014)
O-134	Patient 6	Bergen	7.8 months	Male	2weeks	Unknown	SE	p.(Ala467Thr)/ p.(Gly848Ser)	Occipital, Frontal (Tzoulis *et al.*, 2014)
0-09/36	Patient 7	Bergen	8 years	Male	2 weeks	Unknown	SE	p.(Ala467Thr)/ p.(Gly303Arg)	Frontal (Tzoulis *et al.*, 2014)

Table 2.4: Patient details used in the neuropathology study. Key: SE=status epilepticus.

2.6.2 Control Tissue

To determine the extent of neuropathological changes in patients with Alpers, FFPE brain tissue from neurologically normal controls were used. Control sections were obtained from the Newcastle Brain Tissue Resource (NBTR) (Control 1), Edinburgh (Control 2, 3 and 8) and Bergen (Control 4, 5, 6 and 7). Neuropathological details for the controls are summarised in Table 2.5.

Code	Control	Source	Age	Sex	Fixation Length	PMI	Cause of Death	Brain region
1992-36	Control 1	NBTR	13 months	Female	2-4 weeks	72 hours	Occipital porencephaly	Parietal
SD020-07	Control 2	Edinburgh	22 years	Female	7 days	44 hours	Poisoning	Parietal
SD023-08	Control 3	Edinburgh	24 years	Female	7 days	47 hours	Suspension by ligature	Parietal
R25-12	Control 4	Bergen	4.5 months	Female	2 weeks	Unknown	SIDS	Occipital, Frontal
R28-12	Control 5	Bergen	1 month	Male	2 weeks	Unknown	SIDS	Occipital, Frontal
R266-11	Control 6	Bergen	8 years	Male	2 weeks	Unknown	Asphyxia	Frontal
R303-11	Control 7	Bergen	6y	Female	2 weeks	Unknown	Drowning	Frontal
SD001-06	Control 8	Edinburgh	16 years	Male	2 weeks	47 hours	Suspension by ligature	Frontal

Table 2.5: Neuropathological details of the controls used in this study. Key: PMI= post-mortem interval; SIDS= sudden infantile death syndrome; NBTR= Newcastle brain tissue resource.

2.6.3 Immunohistochemical Staining Protocol

FFPE tissue sections (5µm) were deparaffinised in a 60ºC incubator for 20 minutes followed by incubation in Histoclear™ (National Diagnostics) for 2x5 minutes. Sections were rehydrated through a series of graded ethanols (2x100%, 95% and 70%) for 5 minutes and finally washed thoroughly in distilled water for 10 minutes. To allow access to epitopes, antigen retrieval was performed. This involved either immersion of sections in Ethylenediaminetetraacetic Acid (EDTA; Affymetrix) (1mM; pH 8.0) and pressure cooking for 40 minutes or microwaving in boiling Tris-Sodium Citrate (10mM; pH 6.0) for 10 minutes depending on the primary antibody used. Endogenous peroxidase activity was blocked by incubating in 3% hydrogen peroxide solution for 20 minutes at RT. Sections were washed (3x5 minutes) with Tris-Buffered Saline with 0.1% Tween (TBST) prior to primary antibody application at the appropriate dilution (see Table 2.6) overnight at 4ºC. On the following day, sections were washed (3x5 minutes) with TBST prior to treatment with a Polymer Penetration Enhancer (Diagnostic Biosystems) for 30 minutes at RT. Sections were washed with TBST (3x5 minutes) prior to application of Anti-Mouse/Rabbit PolyVue Horseradish Peroxidase (HRP) (Diagnostic Biosystems) for 30 minutes at RT, followed by a thorough wash in distilled water. To detect antibody binding to the epitope of interest sections were incubated with 3,3'-Diaminobenzidine Tetrahydrochloride (DAB; Sigma-Aldrich) chromogen for 5 minutes at RT. Sections were then washed in running water and counterstained in Mayer's Haematoxylin (TCS Biosciences Ltd) for 15 minutes. To achieve 'blueing' of the nuclei samples were immersed in Scott's tab water for 30 seconds. Sections were finally dehydrated in a series of graded ethanols (70%, 95%, and 2x100%), cleared in Histoclear™ (National Diagnostics) and cover-slipped with Distyrene Plasticizer Xylene (DPX™, Merck).

Primary Antibody	Target	Dilution	Antigen Retrieval	Host and IgG Isotype	Manufacturer	Catalog No.
Anti- Glutamic Acid Decarboxylase 65-67 (GAD65-67)	GABAergic neurons-GAD 67 and Inhibitory axonal terminals GAD 65	1 in 6,000	Microwave, 10mmol tris-sodium citrate (pH 6) for 10 minutes	Rabbit Polyclonal IgG	Sigma	G5163
Purified anti-Neurofilament H (NF-H) Nonphosphorylated antibody (SMI-32-P)	Glutamatergic pyramidal neurons	1 in 6,000	Pressure cooker, 1mM EDTA (pH 8.0) for 40 minutes	Mouse Monoclonal IgG1	BioLegend	801701
Anti-Glial Fibrillary Acidic Protein (GFAP)	Astrocytes	1 in 15,000	Microwave, 10mM Tris-sodium citrate (pH 6.0) for 15 minutes	Rabbit Polyclonal IgG	DAKO	Z0334

Table 2.6: Primary antibodies used for immunohistochemistry.

2.6.4 Two-Dimensional Quantification of Neuronal Density

To assess the degree of neuronal loss in the occipital, parietal and frontal cortex tissue from patients with Alpers, 5µm FFPE patient and control tissue sections were subjected to a two-dimensional neuronal density protocol as previously described (Lax *et al.*, 2012a). Quantification was performed using a modified light microscope (Olympus BX51) with motorised stage for automatic sampling, CCD colour video and stereology software (StereoInvestigator, MBF Bioscience, Williston, VT). For each patient and control an area of at least 10mm^2 along the cortical ribbon was outlined, encompassing cellular layer I-VI at 4x magnification. Within this area GAD65-67-positive interneurons and SMI-32P-positive pyramidal neurons were counted at x20 magnification in three cortical areas spaced by at least 10mm^2. Positive neurons were detected by dark brown chromogen. Neuronal densities were calculated as number per mm^2. Patient mean neuronal densities were then compared to mean neuronal densities of controls. Statistical analysis was performed using Prism GraphPad software (version 5.0)

2.6.5 Immunofluorescent Identification of Respiratory Chain-Deficient Interneurons and Pyramidal Neurons

Immunofluorescent staining was performed on FFPE brain tissue sections (5µm). All patient and control sections were stained under the same conditions. Sections were dewaxed for 20 minutes in a 60^{o}C incubator and rehydrated through a series of graded ethanols (2x100%, 95% and 70%) for 5 minutes. Antigen retrieval was performed by immersion of the sections in 1mM EDTA pH 8.0 using the 2100 retriever unit (Electron Microscopy SciencesC, Hatfiled) and pressure cooked for 40 minutes. Following a thorough wash in distilled water, sections were blocked in TBST containing 10% goat serum for 1 hour at RT. Samples were washed with TBST (3x5 minutes). Mouse monoclonal and rabbit polyclonal primary antibodies were applied in appropriate dilutions overnight at 4^{o}C. Sections were washed 3x5 minutes in TBST prior to incubation with a biotinylated secondary antibody (where appropriate). Sections were washed 3x5 minutes in TBST prior to incubation with IgG subtype-specific secondary anti-mouse or anti-rabbit antibodies conjugates with Alexa Fluor 405, 488, 546 and 647 (Life Technologies), diluted 1:100 in TBST containing 10% goat serum for 2 hours at 4^{o}C, followed by a further 3x5 minutes washes in TBST. Sections were washed again 3x with TBST. To reduce autofluorescence (inherent in formalin-fixed brain tissue) and increase the signal-to-noise ratio, all sections were

subjected to 3% Sudan Black B solution (RAL Diagnostics) for 10 minutes at RT. This was followed by a final wash in running water. All sections were mounted in Prolong Gold (Life Technologies) and stored at -20^{o}C. To allow background correction, immunofluorescent staining was performed on positive controls (all antibodies) and no primary antibody (NPA). All primary and secondary antibodies used for this study are listed in Table 2.7.

Primary Antibody	Target	Host and Isotype	Dilution	Antigen Retrieval	Manufacturer	Catalog No.
Glutamic acid decarboxylase 65-67 (GAD65-67)	GABAergic neurons-GAD 67 and Inhibitory axonal terminals GAD 65	Rabbit polyclonal IgG	1:500	Pressure cooker, 1mM EDTA (pH 8.0) for 40 minutes in 2100 antigen retriever	Sigma	G5163
Purified anti-Neurofilament H (NF-H) Nonphosphorylated antibody (SMI-32-P)	Glutamatergic pyramidal neurons	Mouse Monoclonal IgG1	1:800	Pressure cooker, 1mM EDTA (pH 8.0) for 40 minutes in 2100 antigen retriever	Biolegend	801701
Complex I subunit NDUFA13	NDUFA13	Mouse monoclonal IgG2b	1:100	Pressure cooker, 1mM EDTA (pH 8.0) for 40 minutes in 2100 antigen retriever	Abcam	ab110240
Complex I subunit NDUFB8	NDUFB8	Mouse monoclonal IgG1	1:100	Pressure cooker, 1mM EDTA (pH 8.0) for 40 minutes in 2100 antigen retriever	Abcam	ab110242
Complex IV subunit I	COX1	Mouse monoclonal IgG2a	1:200	Pressure cooker, 1mM EDTA (pH 8.0) for 40 minutes in 2100 antigen retriever	Abcam	ab14705
Complex IV subunit IV	COX4+COX4L2	Mouse monoclonal IgG2a	1:200	Pressure cooker, 1mM EDTA (pH 8.0) for 40 minutes	Abcam	ab110261

Voltage-dependent anion channel 1 (VDAC1)	Outer mitochondrial membrane protein (VDAC1/Porin)	Mouse monoclonal IgG2b	1:200	Pressure cooker, 1mM EDTA (pH 8.0) for 40 minutes	Abcam	Ab14734
Secondary Antibody	**Target**	**Host**	**Dilution**	**Antigen Retrieval**	**Manufacturer**	**Catalog No.**
Biotin-XX	Mouse IgG1	Goat	1:100	N/A	Life Technologies	A10519
Biotin-SP Affini Pure Fcγ subclass 2b specific	Mouse IgG	Goat	1:100	N/A	Jackson ImmunoResea rch	115-065-207
AlexaFluor® 647	Mouse IgG1	Goat	1:100	N/A	Life Technologies	A21240
Alexa Fluor™ 488	Mouse IgG2a	Goat	1:100	N/A	Invitrogen	A21131
Alexa Fluor™ 546	Mouse IgG2b	Goat	1:100	N/A	Invitrogen	A21143
Streptavidin, Alexa Fluor® 488 Conjugate	Biotin	N/A	1:100	N/A	Life technologies	S11223

Alexa Fluor™ 546	Mouse IgG2a	Goat	1:100	N/A	Life technlogies	A21133
Alexa Fluor® 405	Rabbit IgG	Goat	1:100	N/A	Life Technologies	A31556
Streptavidin, Alexa Fluor® 546 Conjugate	Biotin	N/A	1:100	N/A	Life Technologies	S11225
Alexa Fluor® 647	Mouse IgG2b	Goat	1:100	N/A	Life Technologies	A21242

Table 2.7: Primary and secondary antibodies used for immunofluorescence staining.

2.6.6 Confocal Microscopy and Image Processing

Immunofluorescently stained sections from patients and controls were imaged using a confocal system (Nikon A1R). The system is equipped with a fully motorised inverted point scanning confocal microscope (Nikon), four spectrally unmixed lasers (405nm, 488nm, 561nm and 647nm), six objectives (air and oil) and the NIS-Elements software (version 4.2, Nikon). Neurons were detected using an immersion oil 60x objective with numerical aperture 1.2 by their GAD65-67 or SMI-32P positive signal. At least 40 interneurons and 35 pyramidal neurons were identified and images were captured using 4x line averaging and 3.09x electronic zoom. Microscope and laser settings were kept constant throughout each experiment. The resonant scanning mode was selected as this enabled fast scanning at high resolution (512x512 frames). The background signal for all antibodies was detected using a no primary antibody tissue section. To allow quantification of respiratory chain protein expression within GAD65-67-positive interneurons and SMI-32P-positive pyramidal neurons, Volocity software (PerkinElmer) was used. Neurons were outlined manually according to their GAD65-67-positive 405nm (interneurons) or SMI-32P-positive 647nm signal (pyramidal neurons). These were selected as 'regions of interest' (ROI). A protocol was then applied to recognise mitochondria within this ROI as determined by Porin or COX4 signal. The mean intensities for each fluorophore within the mitochondria were recorded and background corrected.

2.6.7 Statistics

The background corrected mean intensities obtained from the quantification of respiratory chain proteins were not normally distributed therefore the data were normalised using natural log transformation. Linear regression of transformed NDUFB8 data against transformed Porin data, transformed NDUFA13 data against transformed COX4 data and transformed COX1 data against transformed Porin data were performed to ensure the residuals of the regression were normally distributed. NDUFA13, NDUFB8 and COX1 were corrected for mitochondrial mass by dividing the values by those obtained from the mitochondrial mass marker they were used in conjunction with (Porin or COX4). For each interneuron and pyramidal neuron, the z-score for the mitochondrial mass-corrected NDUFA13 ($NDUFA13^Z$), NDUFB8 ($NDUFB8^Z$) and COX1 ($COX1^Z$) values were calculated. Finally, interneurons and pyramidal neurons were classified based on standard deviation (SD) limits (for $NDUFA13^Z$, $NDUFB8^Z$ or $COX1^Z$: overexpression if z >2SD, normal if z >-2SD, low

if z <-2SD, deficiency if z <-3SD and severe deficiency if z <-4SD). All statistical analyses were carried out using Prism GraphPad software (version 5.0).

2.7 Molecular Methods

2.7.1 Preparation of Whole Cell Lysate

Cells were harvested and pellets were re-suspended in 80-100µl lysis buffer. Lysis buffer was prepared with 50mM Tris/HCl pH 7.4, 130mM NaCl, 2mM $MgCl_2$, 1mM PMSF and 1% Nonidet P-40 and one EDTA-free protease inhibitor cocktail tablet (Pierce) in 10ml final volume and was stored at -20^{o}C. Samples were vortexed for 30 seconds and centrifuged at 1,000g for 2 minutes at 4^{o}C to remove nuclei and unbroken cells. The supernatant was then transferred to a fresh pre-chilled micro-centrifuge tube, snap-frozen in liquid nitrogen and stored at -80^{o}C.

2.7.2 Bradford Assay

Quantification of protein concentration was performed using the Bradford assay. Samples were added to a final volume of 800µl dH_2O (1µl of cell lysate) before the addition of 200µl of Bradford reagents (Bio-Rad) to the cell lysate or BSA standard curve samples (0, 2µg, 5µg, 15µg and 20µg). The samples were thoroughly mixed, then incubated for 5 minutes at RT, followed by the addition of 200µl aliquots of each sample into a 96-well plate. Samples were prepared in duplicates. The absorbance for each sample was measured at 595nm using an EIx800 automated plate reader (BioTek). The optical density and the BSA standard curve were used to calculate the average protein concentration in the samples.

2.7.3 SDS-PAGE

SDS-PAGE was used to separate proteins according to their molecular weight. Resolving gels were prepared with 12% polyacrylamide (see Table 2.8) before a water layer above the resolving matrix was added allowing a smooth meniscus to form. This was removed after polymerisation was reached and a 3.75% stacking gel was prepared (see Table 2.8) and added on top. At this time samples were incubated with dissociation buffer (final concentrations: 6.25mM Tris/HCl pH 6.8, 2% SDS, 10% Glycerol, 0.01% bromophenol blue and 10mM DTT) and incubated at either 95^{o}C for 5 minutes or at 37^{o}C for 20 minutes depending on the antibody to be used. Samples were then loaded in appropriate volumes. Protein ladder (5µl) was also loaded in each gel. Protein separation was then performed by SDS-PAGE in 1x running buffer

(192mM glycine, 0.1% SDS and 25mM Tris) at 200V using the Mini-PoteanR®Tetra Cell system (Bio-Rad).

	12% Resolving gel	3.75% Stacking Gel
30% Acryl/Bisacrylamide (29:1)	2ml	0.625ml
3.75M Tris/HCl pH 8.5	0.5ml	-
0.5M Tris/HCl pH 6.8	-	1.25ml
dH_2O	2.395ml	3.02ml
10% SDS	50µl	50µl
TEMED	5µl	5µl
10% APS	50µl	50µl
Final volume	5ml	5ml

Table 2.8: Reagents and volumes used for SDS-PAGE.

2.7.4 Western Blotting and Immunodetection

To facilitate immunodetection the proteins separated by SDS-PAGE were transferred from the polyacrylamide gel to a PVDF membrane (Immobilon-P, Milipore). The gel was incubated in transfer buffer (192mM glycine, 25mM Tris, 0.02% SDS and 15% methanol) to equilibrate. The PVDF membrane was firstly activated in 100% methanol for 15 seconds before washing with dH_2O and then placed in transfer buffer. The gel and membrane was placed between double thickness filter paper (8.5cm x 5.5cm) and sponges pre-soaked in transfer buffer in a cassette. The cassette was placed in the transfer tank (Mini Trans-Blot^{TM}, Bio-Rad) and filled with transfer buffer. The transfer of proteins from the gel to the PVDF membrane was performed at 100V for 1 hour at 4^{o}C with the Bio-Rad System. To block non-specific antibody binding, the PVDF membrane was incubated in 5% milk/TBST (Tris-buffered saline with Tween 20: 50mM Tris, 150mM NaCl, 0.05% Tween 20) for 1 hour at RT with gentle agitation. The membrane was then incubated overnight at 4^{o}C with primary antibodies diluted in 5% milk-TBST (see Table 2.9 for antibody dilutions). The membrane was washed 3x in TBST for 10 minutes with gentle agitation at RT. Following washing, the membrane was incubated with the appropriate HRP-conjugated secondary antibody (Dako Cytomation) for 1 hour at RT. The membrane was then washed 5x in TBST for 5 minutes at RT with gentle agitation prior to detection using the WesternC^{TM} kit (Bio-Rad) according to

manufacturer's instructions. Chemiluminescent signals were visualised using the Chemi-Doc^{TM} MP system (Bio-Rad).

Antibody	Type	Dilution	Manufacturer
Anti-Beta-actin	Mouse Monoclonal	1:10,000	Sigma; A1978
Anti-Polg	Rabbit Monoclonal	1:2,000	Abcam; ab128899

Table 2.9: Primary antibodies used for immunodetection.

2.7.5 DNA Extraction from Human Fibroblasts

Fibroblasts from T75 flasks were harvested as described in section 2.3.3. DNA extraction from fibroblasts was performed using a silica column-based QIAmp DNA Mini Kit (QIAGEN) following the manufacturer's specifications. In brief: Cell pellets in 1.5ml micro-centrifuge tubes were washed in PBS before re-suspending in a final volume of 200µl PBS. A volume of 20µl of QIAGEN Proteinase K was added. 200µl of Buffer AL were added followed by pulse-vortexing for 15 seconds. Samples were then incubated for 10 minutes at 56^{o}C. Samples were briefly centrifuged to remove drops from the inside of the lid. 200µl of 100% ethanol was added to the sample, followed by vortexing for 15 seconds and brief centrifugation. The mixture from each sample was transferred carefully to the QIAamp Mini spin column (in a 2ml collection tube) without wetting the rim. Centrifugation at 6,000g for 1 minute followed. The tube collecting the filtrate was discarded and the QIAamp Mini spin column was placed in a clean 2ml collection tube. A total volume of 500µl of Buffer AW1 was carefully added in the column, centrifuged at 6,000g for 1 minute. The tube containing the filtrate was discarded and the spin column was added in a clean 2ml collection tube. This step was followed by the careful addition of Buffer AW2. The columns were centrifuged at full speed (20,000g) for 3 minutes. The collection tube was discarded and replaced by a clean 2ml collection tube. Samples were then centrifuged at 20,000g for 1 minute. The columns were then placed in clean micro-centrifuge tubes. To collect the extracted DNA, 50µl of distilled water was added to the columns, incubated for 1 minute at RT and centrifuged at 6,000g for 1 minute. DNA concentrations were measured using the nanodrop ND-1000 spectrophotometer (Labtech International). DNA samples were then stored in 10µl aliquots at -20^{o}C.

2.7.6 DNA Extraction from FFPE Brain Tissue

DNA was extracted from FFPE tissue in patients where a *POLG* diagnosis had not been confirmed. A silica-column based QIAamp DNA FFPE Tissue Kit (QIAGEN) was used. Tissue sections of 20µm thickness were placed in 1.5ml micro-centrifuge tubes. 1 ml of Histoclear™ was added to each sample and vortexed vigorously for 10 seconds. Samples were centrifuged at full speed (20,000g) for 2 minutes at RT and the supernatant was discarded. To remove residual Hstoclear™, 1ml of 100% ethanol was added to the pellet prior to vortexing for 10 seconds. Samples were centrifuged at full speed (20,000g) for 2 minutes at RT. The supernatant was then discarded and the tubes were incubated at 37ºC with the lid open for 10 minutes to ensure complete evaporation of residual ethanol. The pellets were then re-suspended in 180µl Buffer ATL. 20µl proteinase K were added, followed by vigorous vortexing. To ensure complete lysis of the samples, tubes were incubated for 1 hour at 56ºC. Samples were then incubated at 90ºC for 1 hour. Micro-centrifuge tubes were briefly centrifuged to remove the drops from inside of the lid. 200µl of Buffer AL were added to each sample followed by vigorous vortexing. Then 200µl 100% ethanol were added followed again by vigorous vortexing prior to brief centrifugation. The lysates were carefully transferred to QIAamp MinElute columns (in 2ml collection tubes) without wetting the rim. Samples were centrifuged at 6,000g for 1 minute. The tube was discarded and replaced by a clean 2ml collection tube. 500µl Buffer AW1 were carefully added in the columns prior to centrifugation at 6,000g for 1 minute. The collection was again discarded and replace by a clean tube. A total volume of 500µl Buffer AW2 was carefully added to the column, centrifuged at 6,000g for 1 minute before the tube containing the filtrate was discarded. To dry the membrane completely centrifugation at full speed (20,000g) for 3 minutes followed. The QIAamp MinElute columns were added in clean 1.5ml eppendorf tubes and 50µl Buffer ATE were applied to the centre of the membrane. Samples were incubated for 1 minute at RT before centrifugation at full speed (20,000g). To check DNA concentrations, the DNA samples were tested on the nanodrop ND-1000 spectrophotometer (Labtech International). The DNA samples were then stored at -20ºC.

2.7.7 DNA Extraction from Frozen Brain Homogenate Tissue

20µm sections of frozen tissue were lysed in Tris-Tween-Proteinase K lysis buffer (0.5M Tris-HCl, 0.5% Tween 20, 1% Proteinase K, pH 8.5). Tissue was homogenised in 50µl of lysis buffer, vortexed, centrifuged briefly and incubated at 55ºC for 3 hours,

followed by deactivation of proteinase K at 95^{o}C for 10 minutes in Thermomixer C (Eppendorf). Details regarding patients and controls from whom frozen tissue was examined is summarised in Table 2.10.

Patient/Control	Patient Code	Age at Death	Gender	Clinical Phenotype	Genetic Diagnosis	Available Brain Region
Patient 8	2001/0017	24 years	Female	Alpers	*POLG* p.(Ala467Thr)/p.(Trp748Ser)	Occipital, Parietal, Frontal (Lax et al., 2016)
Patient 9	1997/0064	6 years	Male	Encephalopathy similar to Alpers with liver failure	*IDH3A* (p.(Arg178His)/p.(Ala330Val))	Occipital, Parietal
Patient 10	4217	45 years	Female	PEO and Epilepsy	*POLG* p.(Ala467Thr)/p.(Trp748Ser)	Frontal
Patient 11	110-05	59 years	Male	Parkinsonism	*POLG* p.(Ser1104Cys)/p.(Gly848Ser)	Occipital (Betts-Henderson et al., 2009)
Patient 12	141-97	50 years	Male	CPEO	*POLG* p.(Ala467Thr) and p.(X1240Gln)	Occipital (Lax et al., 2012b)
Patient 13	958-10	79 years	Male	CPEO, Ataxia	*POLG* p.(Thr251Ile)/p.(Pro587Leu) and p.(Ala467Thr)	Occipital (Lax et al., 2016)
Patient 14	224-11	55 years	Male	CPEO, Epilepsy and Ataxia	*POLG* p.(Trp748Ser)/p.(Arg1096Cys) and p.(Glu1143Gly)	Occipital (Lax et al., 2016)
Control 9	1985-647	6 years	Female	N/A	N/A	Occipital, Parietal
Control 10	729-10	70 years	Male	N/A	N/A	Occipital

Control 11	118-09	55 years	Male	N/A	N/A	Occipital
Control 12	891-11	81 years	Male	N/A	N/A	Occipital
Control 13	1993-173	19 years	Male	N/A	N/A	Parietal, Frontal
Control 14	1993-179	27 years	Male	N/A	N/A	Parietal, Frontal

Table 2.10: Details of patients and controls used in the study of mtDNA damage. Key: N/A=not applicable.

2.7.8 Polymerase chain reaction (PCR)

Pyrosequencing PCR was performed on DNA extracted samples from human FFPE brain tissue. All reactions were set under a UV hood (Applied Biosystems). DEPC-treated H_2O and pipettes that had been left for 30 minutes in the UV hood prior to experimentation were used. A master mix for each assay (50µl volume) was prepared as follows: 10µl 5x reaction buffer, 5µl 2mM dNTPs (dATP, dTTP, dCTP, dGTP), 6µl 25mM $MgCl_2$, 2.5µl 10µM forward primer, 2.5µl 10µM reverse primer, 0.2µl 10/U/µl Hotstart GoTaq G2 polymerase and 21.6µl DEPC-treated H_2O. The primers are listed in Table 2.11. The mastermix was vortexed for 15 seconds. The master mix was aliquoted to each well of the PCR plate, before 2µl of DNA were added to each well according to the plate layout. DNA from a wild-type control was used. A negative control was also used. This sample contained 2µl DEPC-treated H_2O instead of DNA. The plates were then sealed, briefly vortexed and centrifuged. PCR reactions were performed on a thermal cycler (GeneAmp® PCR System 9600) under the following conditions: 95ºC for 10 minutes then 32 cycles of 95ºC for 30 seconds, 62°C for 30 seconds and 72°C for 30 seconds. The final extension was at 72ºC for 10 minutes. In order to obtain more DNA to enable subsequent genotyping by pyrosequencing, another PCR reaction on the product obtained from the first PCR round was preformed using a biotinylated primer for each pair of primers under the PCR conditions stated above (primers listed in Table 2.12).

***POLG* Mutation Primers**	**Primer Sequence**
Exon7 p.(Ala467Thr)	Forward: 5'-TGTAAAACGACGGCCAGTATGGGATGATATTGTTCCCATTT-3'
	Reverse: 5'-CAGGAAACAGCTATGACCAGTCCACTAGGGCAGGGCTA-3'
Exon 13 p.(Trp748Ser)	Forward: 5'-TGTAAAACGACGGCCAGTACAGTTTCAGGCCCTTTTCC-3'
	Reverse 5'-CAGGAAACAGCTATGACCTGTGCCTGAAATCACACTCTG-3'
Exons 15+16 p.(Gly848Ser)	Forward: 5'-TGTAAAACGACGGCCAGTAGTGAGGCTGGGTAATGGAG-3'
	Reverse: 5'-CAGGAAACAGCTATGACCCAGGGTCCTTTTCATGATCC-3'

Table 2.11: Primer sequences used to amplify the nuclear DNA regions spanning the sites containing the individual point mutations in the *POLG* gene.

***POLG* Mutation Primers**	**Primer Sequence**	**Expected Product Size**
c.1399G>A p.(Ala467Thr)	Forward (Biotynylated): 5'-CCAGCGGGAGATGAAGAA-3'	171bp
	Reverse: 5'-TACAGAGCCAGTCCACTAGGG-3'	
c.2243G>C p.(Tr748Ser)	Forward: 5'-CTCACAGACTGCCCGTGGT-3'	142bp
	Reverse (Biotinylated): 5'-CAGGACAGGCCATGACCC-3'	
c.2542G>A p.(Gly848Ser)	Forward: 5'-CTGCCCCAAGTGGTGACT-3'	106bp
	Reverse (Biotinylated): 5'-AGGGGCCAGAGGTACAGAG-3'	

Table 2.12: Primer sequences used to amplify the previous PCR product. The forward or reverse primer was biotinylated which resulted in a biotinylated PCR product in one direction, which would enable genotyping of single base pair changes by pyrosequencing.

2.7.9 Gel Electrophoresis

Following amplification, PCR products were run through a 1.5% agarose gel (1.5g agarose in 100ml TAE). The agarose was heated in a microwave, before 2µl of ethidium bromide were added. The gel was prepared and allowed to cool. After cooling, 2µl of each sample was loaded into each well with the addition of 0.5µl loading buffer (0.25% (w/v) bromophenol blue, 0.25% (w/v) glycerol). To confirm fragment size 2µl of 100bp DNA ladder (New England Biolabs) was loaded on the gel. The gel was ran in TAE buffer at 75V to separate products. Visualisation of the bands was performed using the UV gel documentation system after intercalation of ethidium bromide into the DNA.

2.7.10 Assessment of mtDNA Copy Number and Deletions

Relative levels of mtDNA copy number in fibroblasts were determined by real-time PCR using singleplex Taqman assays designed to target the mitochondrial *MT-ND1* gene (rarely deleted) and the nuclear *B2M* gene (GenBank accession number: NG_012920) as previously described (Grady *et al.*, 2014). Primers and probes are listed in Tables 2.13 and 2.14 respectively. The reaction mixture consisted of 10µl TaqMan Universal PCR Mastermix (Applied Biosystems), 0.6µl 10µM B2M/ND1 forward primer, 0.6µl 10µM B2M/ND1 reverse primer, 0.4µl 5µM B2M/ND1 fluorgenic probe and 2.2µl DETC-treated H_2O. Each 20µl B2M reaction was supplemented with 3mM $MgCl_2$. Each reaction was completed in triplicate (final DNA concentrations: 10ng/µl) and performed using the ABI PRISM 7000 Sequence Detection System (Applied Biosystems). Amplification conditions were: 50°C for 2 minutes, 95°C for 10 minutes, followed by 40 cycles of 95°C for 15 seconds and 60°C for 1 minute. Standard curves were included for analysis of data. *MT-ND1* and *B2M*. Taqman assays were analysed sequentially on the same real time machine. To minimise well-to-well error, samples were located in the same wells on paired plates. The *MT-ND1*/*B2M* copy number ratio was calculated for each sample well on each plate.

For determination of mtDNA copy number and levels of deletions in brain homogenates a multiplex Taqman assay designed to target mitochondrial *MT-ND1* (rarely deleted) and *MT-ND4* (commonly deleted) genes and a singleplex Taqman assay designed to target the nuclear *B2M* gene were performed. Primers and probes are summarised in Tables 2.13 and 2.14 respectively. The reaction mixture preparation and amplification conditions were the same as described above.

The mtDNA copy number and deletions were compared to controls and statistical analysis was carried out using Prism GraphPad (version 5.0).

Primer pair	Primer	Sequence	Location
B2M	*B2M* forward	5'-CCAGCAGAATGGAAAGTGGAAAGTCAA-3'	n.8969-8990
	B2M reverse	5'-TCTCTCTCCATTCTTCAGTAAGTCAACT-3'	n.9064-9037
MT-ND1	*MT-ND1* forward	5'-CCCGCCACTACATCTCCCACTACC-3'	chrM: 3485-3504
	MT-ND1 reverse	5'-GAGCGATGGTGAGAGCTAAGGT-3'	chrM:3532-3553
MT-ND4	*MT-ND4* forward	5'-CCATTCTCCTCCTATCCCTCAAC-3'	chrM: 12087-12109
	MT-ND4 reverse	5'-CACAATCTGATGTTTTGGTTAAACTATATTT-3'	chrM: 12170-12140

Table 2.13: Primer locations and sequences used for real-time PCR. All primer sequences are based on the revised Cambridge reference sequence (NC_012920.1).

Probe	Sequence	Location
B2M	FAM 5'-ATGTGTCTGGGTTTCATCCATCCGACA-3'MGB	n.9006-9032
MT-ND1	VIC 5'-CCATCACCCTCTACATCACCGCCC-3' MGB	chrM: 3506-3529
MT-ND4	FAM 5'-CCGACATCATTCCGGGTTTTCCTCTTG-3' MGB	chrM: 12111-12138

Table 2.14: Probe locations and sequences used for real-time PCR. Primer sequences are based on the revised Cambridge reference sequence (NC_012929.1).

Chapter 3 Epilepsy due to Mutations in the Mitochondrial Polymerase Gamma (*POLG*) Gene: A Systematic Review

3.1 Introduction

Mutations in the *POLG* gene result in a heterogeneous group of mitochondrial disorders known as *POLG*-related disorders, which are characterised by overlapping clinical features.

POLG-related disorders have been shown to display both autosomal dominant and autosomal recessive inheritance. Autosomal dominant disorders present in adulthood, whereas autosomal recessive disorders can present at any age and encompass the predominant phenotypes of *POLG*-related disorders (Cohen, 2014).

Alpers' syndrome is an autosomal recessive neurodegenerative disease, is believed to be the most severe phenotype of the *POLG*-related disorders spectrum (Cohen, 2014), and it is classified as an mtDNA depletion syndrome arising from disrupted mtDNA replication.

The clinical hallmarks of Alpers comprise the triad of refractory seizures, psychomotor regression and hepatic dysfunction with or without hepatic failure. Hepatic failure most often occurs in the terminal phase of the disease rather than as a presenting feature (Saneto *et al.*, 2013).

Seizures, refractory to treatment are the heralding feature of Alpers. With regards to seizure type, these are most often myoclonic or focal motor and progress into Epilepsia Partialis Continua (EPC). The disease onset is bimodal with a typical peak at 2-4 years (range 3 months 8 years). Usually, development is normal after birth until the disease onset (ranging from a few months after birth to years). In some cases, psychomotor regression may occur before the clinical signs appear, however it is unclear whether this is specific to the effect exerted by *POLG* mutations (Saneto *et al.*, 2013; Cohen, 2014).

A second disease peak occurs at 17-24 years (range 10-27 years) and this is termed Juvenile Alpers. As with infant/childhood onset, young adults develop normally at birth until the clinical signs occur. Clinical features of Juvenile onset Alpers involve seizures/epilepsy, visual defects and migraine-like headaches with seizures/epilepsy being the heralding manifestation. Patients with Juvenile Alpers survive longer

compared to those presenting in infancy/childhood, who have a poorer prognosis, with few children surviving into their teens (Saneto and Naviaux, 2010; Cohen, 2014). Pathological features of Alpers have been described in post-mortem brain and liver tissue.

Myocerebrohepatopathy Spectrum (MCHS), which is the rarest of *POLG*-related syndromes and has overlapping features with Alpers including encephalopathy and liver dysfunction. However, disease onset in MCHS tends to occur earlier (median of 1 year) with seizure activity being milder and liver failure more devastating when compared to Alpers (Saneto *et al.*, 2013; Cohen, 2014).

Other *POLG*-related syndromes include Myoclonic Epilepsy Sensory Ataxia (MEMSA), Ataxia Neuropathy Spectrum (ANS) and Autosomal recessive or dominant progressive External Opthalmoplegia (arPEO, adPEO). Despite the clinical variability of those phenotypes, these are caused by the same spectrum of *POLG* mutations which are associated with Alpers.

POLG mutations result in disrupted mtDNA replication, through yet undefined mechanisms. However, it has been shown that POLG dysfunction results in mtDNA depletion ultimately leading to OXPHOS impairment and subsequent cellular failure.

To date over 200 mutations have been identified as a cause of *POLG*-related disorders. The pathogenic variants p.(Ala467Thr) and p.(Trp748Ser) have been classified as the most common in Caucasians (0.5-1% prevalence) (Hakonen *et al.*, 2007). The p.(Ala467Thr) mutation has been also found as the most common in the paediatric population (Horvath *et al.*, 2006).

To date, over 60 *POLG* mutations have been described to be causative of Alpers, which can exist in either homozygous or compound heterozygous states. Research has provided some insight into genotype to phenotype correlations, although these remain poor. For example, homozygous p.(Ala467Thr) and p.(Trp748Ser) mutations have been associated with later onset and better survival when compared to compound heterozygous p.(Ala467Thr)/p.(Trp748Ser) mutations (Tzoulis *et al.*, 2006). The reasons behind this observation are unclear as homozygous mutations may also be present in patients with Alpers who present early and are severely affected by the disease (Horvath *et al.*, 2006).

In contrast, compound heterozygous mutations have been linked to more severe disease and worse prognosis. However, it is not understood how identical compound

heterozygous mutations can lead to mild phenotype in one patient but severe disease in another. It is believed that the location of the mutation within the domains of *POLG* may partly dictate the phenotype; however other unknown mechanisms are also involved. As such genotype to phenotype correlations are still lacking. Understanding the genotypic and phenotypic variability of *POLG*-related disorders remains challenging.

3.2 Aims and Objectives

This chapter systematically reviews the tissue-specific effects of *POLG*-mutations in patients with clinically and genetically confirmed (autosomal recessive *POLG* mutations) defined Alpers or similar encephalopathies with or without hepatopathy reported in the literature.

The aim of this work is to better understand the molecular pathophysiology of Alpers and *POLG*-related epilepsy; through the evaluation of the genetic, histopathological and molecular characteristics of the disease.

The systematic review was performed by myself and Dr. Yi Ng. Part of this work has been published in a peer-reviewed journal (Anagnostou *et al.*, 2016). The article can be found in Appendix A. The specific objectives of this study are summarised below.

1) Identify patients in the literature with Alpers or other *POLG*-related epilepsy syndromes with confirmed genetic diagnosis of *POLG* mutations.
2) Review the *POLG* pathogenic variants identified.
3) Summarise the macroscopic and microscopic findings of affected tissues (brain, liver and muscle).
4) Evaluate and compare the effect of *POLG* mutations on mtDNA content and OXPHOS proteins on different tissue types (brain, muscle, liver, blood and fibroblasts).
5) Compare childhood disease to Juvenile/adult disease.
6) Identify any genotype to phenotype correlations.

3.3 Methods

3.3.1 Search strategy

An electronic search using Ovid Medline and Scopus databases was performed. Search terms were 'POLG', 'polymerase gamma', 'POLG', 'Alpers' syndrome' and 'Alpers- Huttenlocher syndrome'. The literature search was limited to studies published from January 2000 to January 2015 involving humans and written in English. A manual search on studies published from January 2015 to August 2017 was also performed. Articles were selected if the title and/or abstract included one of the following terms: Alpers syndrome, hepatocerebral syndrome/disease, encephalopathy, seizures, epilepsy, status epilepticus or hepatic/liver dysfunction/failure. Only patients with recessive homozygous or compound heterozygous *POLG* mutations were considered. To confirm the pathogenicity of any given rare allelic variant the Human DNA Polymerase Gamma (POLG) Mutation Database webpage (Copeland, n.d.) was used for cross-reference. Patients with clinically diagnosed adPEO, PEO and/or Parkinsonism harbouring a single *POLG* variant in a heterozygous state were excluded from the study.

3.3.2 Data extraction and statistics

Articles were screened for the following information: number of patients, clinical details (age of onset, age of death, gender), *POLG* variants, histopathology, mtDNA content and OXPHOS biochemistry in various tissue types where available. Statistical analysis was carried out using the statistical software Minitab version 17, SPSS version 23.0 and GraphPad Prism version 5.0. Descriptive statistics were used for summative information of data. Data were presented as mean ± standard deviation (SD). Kaplan-Meier survival analysis was also performed. Statistical significance level was considered when $p<0.05$.

3.4 Results

3.4.1 Systematic search results

The initial search resulted in 64,272 articles from combined databases (Ovid=22,721 and Scopus=41,551). A total of 278 articles met the inclusion criteria and were used for further analysis. After removing the duplicates and only including cases with two pathogenic variants in *POLG* gene, 372 patients from 72 articles were selected for evaluation. (see Figure 3.1). An additional 5 patients were selected from a manual search from two publications, therefore a total of 377 patients from 74 articles were

selected for further evaluation. A complete list of the patients included in the analysis of *POLG* pathogenic variants can be found in Appendix B.

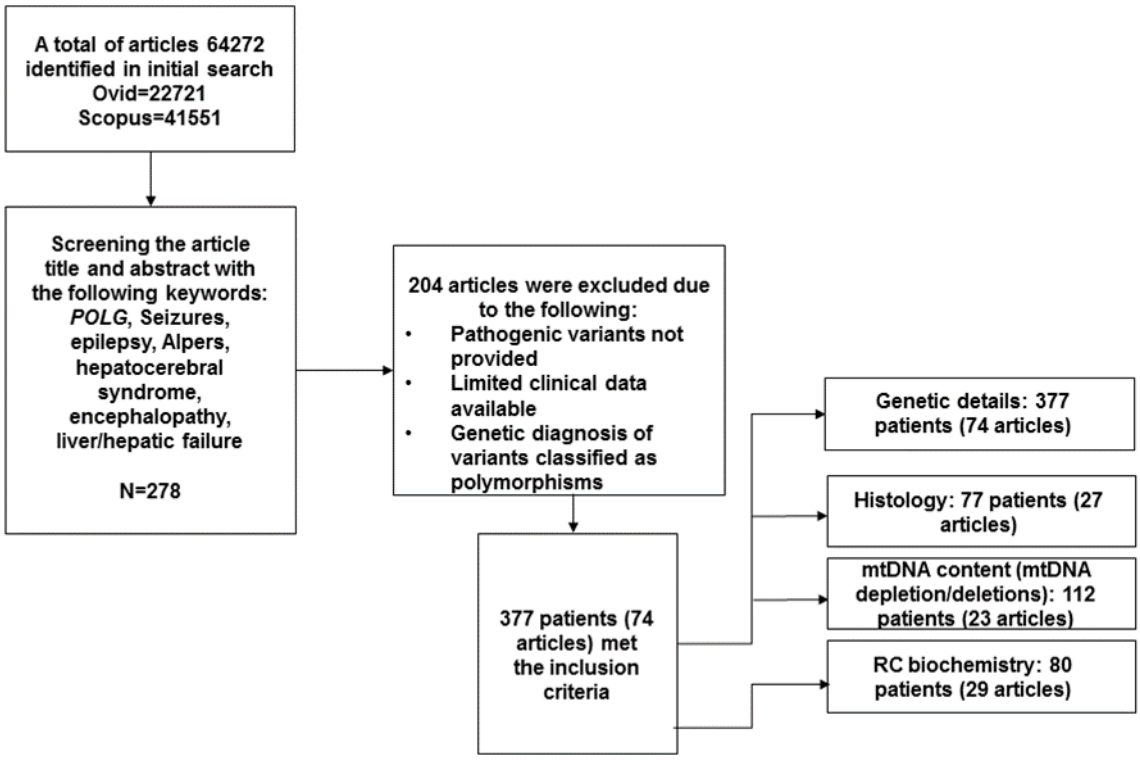

Figure 3.1: Flow chart of literature search and selection.

3.4.2 Summary of clinical findings

The age of onset ranged from infancy to late adulthood (<30 days to 64 years, n=270). The median age was 2 years. From the patients analysed 51% of the cases presented with seizures (n=191). With regards to the paediatric patients (n=281), 26% of the cases (n=73) presented with the following features: hypotonia, developmental regression or failure to thrive. These features were evident prior to seizure presentation. Liver involvement was rarely reported as a presenting manifestation (5% of cases) and was usually associated with pre-terminal phase. From the patients considered, 48% (n=181) of the cases were reported as Alpers or encephalopathy fulfilling some of the diagnostic criteria of Alpers, including seizure and liver involvement.

3.4.3 POLG Genetics

A total of 128 *POLG* pathogenic variants were identified in the patients considered. The 10 most common pathogenic variants with their frequencies and their location within the *POLG* gene are illustrated in Figure 3.2. The three most common *POLG*

variants identified were the p.(Ala467Thr), p.(Trp748Ser) and the p.(Gly848Ser). The frequency of the reported genotypes is depicted in Figure 3.3.

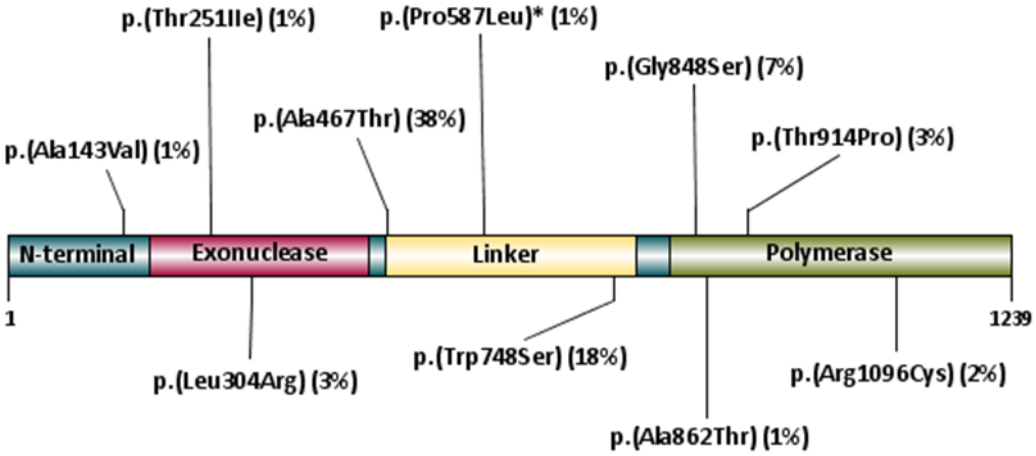

Figure 3.2: The ten most common *POLG* pathogenic variants identified in literature and their location within *POLG* domains. Domains include: exonuclease (pink), linker (yellow) and polymerase (green). N-terminal (blue). The three most common mutations are linker p.(Ala467Thr) (38%) and p.(Trp748Ser) (18%) followed by polymerase p.(Gly848Ser). (7%). Exonuclease p.(Thr251Ile)* (1%) and p.(Pro587Leu)* (1%) are commonly present in the same allele. Figure adapted from (Anagnostou *et al.*, 2016).

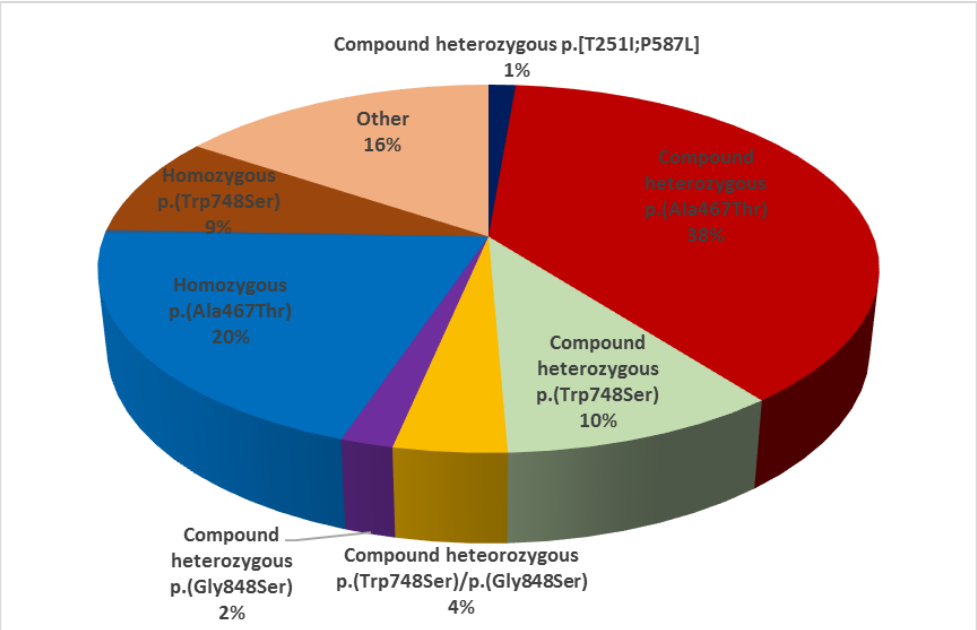

Figure 3.3: Pie chart demonstrating the frequencies (%) of pathogenic *POLG* recessive mutations identified in the literature. Homozygous and compound heterozygous p.(Ala467Thr) mutations are the most commonly reported (58%). Homozygous and compound heterozygous p.(Trp748Ser) account for 19% of the reported cases. Compound heterozygous p.(Gly848Ser) are infrequently reported (2%). Compound heterozygous p.(Trp748Ser)/p.(Gly848Ser) are uncommon (4%). Other pathogenic recessive *POLG* mutations account for only 16% of the cases considered. Modified from (Anagnostou *et al.*, 2016).

3.4.4 Histopathology

A. Brain

Neuropathological information for 30 patients was extracted, of whom 26 were post-mortem (Van Goethem *et al.*, 2004; Kollberg *et al.*, 2006; Uusimaa *et al.*, 2008; Boes *et al.*, 2009; Hunter *et al.*, 2011; Scalais *et al.*, 2012; Sofou *et al.*, 2012; Tzoulis *et al.*, 2014; Montassir *et al.*, 2015; Rajakulendran *et al.*, 2016) and four were biopsies (Bao *et al.*, 2008; Wiltshire *et al.*, 2008; Nolte *et al.*, 2013; Rajakulendran *et al.*, 2016). From the 30 patients identified, 22 were infants/children at disease onset (0-9 years) and eight were adolescents/adults (12-39 years). The majority of the patients considered (n=24, 80%) had Alpers.

Macroscopic findings from post-mortem brain of 12 patients were identified. Seven were infants/children (age of death: 0.67-5.5 years), three adolescents (age of death: 14-17 years) and two adults (20 and 39 years) (Kollberg *et al.*, 2006; Uusimaa *et al.*, 2008; Sofou *et al.*, 2012; Montassir *et al.*, 2015). The younger group exhibited a reduction in the cortical thickness with focal softening in the occipital lobes (Kollberg *et al.*, 2006; Sofou *et al.*, 2012). The brain of one infant demonstrated massive oedema with caudal necrosis (Montassir *et al.*, 2015). The macroscopic examination from a 5.5-year old patient was unremarkable (Rajakulendran *et al.*, 2016).

The adolescent group demonstrated a decrease in cortical thickness with cortical softening in occipital and parietal lobes (Kollberg *et al.*, 2006; Sofou *et al.*, 2012). The hippocampus, basal ganglia and thalami were well preserved in one patient (Van Goethem *et al.*, 2004) while in another, ischaemia of the thalamus was evident (Uusimaa *et al.*, 2008). The brain of a 20-year old patient with Alpers revealed mild atrophy of the cerebellar vermis (Uusimaa *et al.*, 2008), while the cerebellar and cerebral hemispheres in a 39-year old patient with other *POLG*-related epilepsy syndrome were preserved (Van Goethem *et al.*, 2004).

Microscopically, the posterior parts of the brain were most frequently affected comparatively to anterior brain areas. The majority of the patients demonstrated histologic changes in the brain cortex (n=22) (Kollberg *et al.*, 2006; Bao *et al.*, 2008; Uusimaa *et al.*, 2008; Wiltshire *et al.*, 2008; Boes *et al.*, 2009; Hunter *et al.*, 2011; Scalais *et al.*, 2012; Sofou *et al.*, 2012). Changes include: neuronal loss (specific neuronal subtype not provided), spongiosis (as a consequence of end-stage disease) and astrogliosis; which were reported to be most prominent in the occipital lobes

(n=8) (Kollberg *et al.*, 2006; Bao *et al.*, 2008; Hunter *et al.*, 2011; Scalais *et al.*, 2012; Sofou *et al.*, 2012).

Similar changes have been observed in the parietal lobes of three paediatric Alpers patients (Hunter *et al.*, 2011; Sofou *et al.*, 2012; Rajakulendran *et al.*, 2016) and in the frontal lobes of an adolescent patient with Alpers (Kollberg *et al.*, 2006); however to a lesser extent. White matter changes such as gliosis and swollen astrocytes known as Alzheimer Type II glia and spongiosis have also been reported (n=7) (Kollberg *et al.*, 2006; Bao *et al.*, 2008; Montassir *et al.*, 2015; Sofou *et al.*, 2015). Alzheimer Type II astrocytes are reactive astrocytes characterised by pale nuclei with a rim of chromatin, enlarged cytoplasm and decreased GFAP immunostaining (Aldridge *et al.*, 2015). Alzheimer Type II astocytes have been reported in other diseases including hepatic encephalopathy (Norenberg, 1987) and Wilson's disease (Bertrand *et al.*, 2001).

The hippocampus was well preserved in one patient with Alpers (Scalais *et al.*, 2012), however neuronal loss in CA1 was evident in three patients, all diagnosed with Alpers (Kollberg *et al.*, 2006; Sofou *et al.*, 2015; Rajakulendran *et al.*, 2016). In addition, one of the patients exhibited gliosis of CA1 and a less severe neuronal loss in CA2, CA3 and CA4 (Rajakulendran *et al.*, 2016).

Histologic abnormalities of the cerebellum were commonly identified (n=19) (Van Goethem *et al.*, 2004; Kollberg *et al.*, 2006; Uusimaa *et al.*, 2008; Hunter *et al.*, 2011; Scalais *et al.*, 2012; Sofou *et al.*, 2012; Tzoulis *et al.*, 2014; Montassir *et al.*, 2015). These consist of: mild to severe Purkinje cell loss, spongiosis, proliferation of Bergmann glia, loss of granular cells and neuronal loss and gliosis of dentate and olivary nuclei. These changes were variable in terms of severity among patients. Spongiosis in the white matter of the cerebellar cortex was observed in two patients with Alpers (Boes *et al.*, 2009; Sofou *et al.*, 2012).

Microscopic abnormalities of the thalamus and basal ganglia (substantia nigra and globus pallidus) have been commonly reported (n=11). These changes are milder compared to brain cortex and consist of: neuronal loss, spongiosis, gliosis, capillary proliferation and Type II Alzheimer astrocytes/glia. One patient demonstrated linear necrosis of the caudate nucleus. Normal histology of the basal ganglia is infrequently reported (n=3).

Changes in the brainstem have rarely been reported (n=2) (Wiltshire *et al.*, 2008; Boes *et al.*, 2009). However, these severe neuronal loss and bleeding have been detected in two Alpers patients 17.5 and 17.75 years old respectively. Interestingly the brainstem of a 5.5-year old patient with Alpers was unremarkable (Rajakulendran *et al.*, 2016), suggesting that pathology of the brainstem may be a characteristic of older patients.

Ultrastructural analysis by electron microscopy (EM) revealed evidence of mitochondrial dysfunction. Characteristic morphological alterations comprise increased number of mitochondria with atypically short, curved cristae with deep invaginations of the outer membranes. However, these features were detected in only one brain biopsy from a 17-year old patient with *POLG*-related epilepsy (Nolte *et al.*, 2013). In addition, immunohistochemistry revealed complex I and IV deficiencies (n=5) in different brain areas, however deficiencies were more severe in the substantia nigra, dentate nucleus, hippocampus and cerebellum (Tzoulis *et al.*, 2014). The histological abnormalities found in patients with *POLG*-related epilepsy are summarised in Table 3.1.

Cerebral cortex	Cerebellum	Basal ganglia	Thalamus	Brainstem	Hippocampus
Neuronal loss, spongiosis and astrogliosis. Changes most prominent in occipital lobes (n=8). Parietal lobes affected to a lesser extent (n=3).	Changes (n=19) including: Purkinje cell loss, spongiosis, proliferation of Bergmann glia, loss of granular cells	Normal (n=3) Neuronal loss, spongiosis, gliosis, capillary proliferation. All these changes to a lesser extent compared to the cerebral cortex (n=6).	Vacuolisation, neuronal loss, astrocytosis and astrogliosis (n=5).	Normal (n=1) Severe neuronal loss and bleeding (n=2).	Severe neuronal loss (n=3) and gliosis (n=1) in CA1. Moderate neuronal loss in CA2, CA3 and CA4 (n=1).

Table 3.1: Summary of histological abnormalities identified in different brain regions (including cerebral cortex, cerebellum, basal ganglia, thalamus, brainstem and hippocampus) from patients with Alpers and *POLG*-related epilepsy. Key: n=number of patients.

B. Liver

Histological data from the liver of a total of 31 patients (11 biopsies and three post-mortem) was available for review. The tissue source for 17 patients was not specified in the literature (Davidzon *et al.*, 2005; Kollberg *et al.*, 2006; Boes *et al.*, 2009; Roels *et al.*, 2009; Stewart *et al.*, 2009; Hunter *et al.*, 2011; Mangalat *et al.*, 2012; Uusimaa *et al.*, 2013; Simon *et al.*, 2014; Montassir *et al.*, 2015). Of the patients considered, 29 were infants/children (0-8.5 years) with Alpers, one 12-year adolescent and one 39-year old adult (Stewart *et al.*, 2009).

Only macroscopic analysis of the liver from 1 patient was available. Examination showed an atrophic liver (200g) with a hard, irregular surface (Montassir *et al.*, 2015). Microscopically, prominent liver abnormalities were detected in 29 patients. These include: microvesicular fatty changes, microvesicular steatosis and fibrosis (Davidzon *et al.*, 2005; Nguyen *et al.*, 2005; Roels *et al.*, 2009; Hunter *et al.*, 2011; Uusimaa *et al.*, 2013; Montassir *et al.*, 2015). Other changes such as necrosis, bile duct proliferation, oncocytosis, cytoplasmic vacuolization and metaplasia of parenchyma were less frequently reported (Nguyen *et al.*, 2005; Hunter *et al.*, 2011; Uusimaa *et al.*, 2013; Simon *et al.*, 2014). Two paediatric patients with Alpers (aged 1.25 years and 10 years respectively) demonstrated normal liver histology (Stewart *et al.*, 2009; Hunter *et al.*, 2011).

Immunohistochemistry revealed a mosaic of cytochrome c (COX) activity in the liver of 6 infants (0-5 years) and two older patients, 12 and 39 years old, respectively (Kollberg *et al.*, 2006; Boes *et al.*, 2009; Roels *et al.*, 2009; Stewart *et al.*, 2009). ‘Ragged-red’ changes (which are a consequence of increased mitochondrial density accumulating at the periphery of hepatocytes) were only observed in the two older patients indicating that these features may be uncommon in the younger population (Stewart *et al.*, 2009).

Moreover, hepatic-specific ultrastructural abnormalities of the mitochondria in eight patients with early-onset Alpers (0-3 years) were observed by electron microscopy. These changes involved in all cases densely packed, enlarged and abnormally shaped mitochondria accompanied by pale matrix and displacement/absence of cristae (Roels *et al.*, 2009; Hunter *et al.*, 2011; Mangalat *et al.*, 2012). The abnormalities in the liver of patients are summarised in Table 3.2.

C. Muscle

In terms of muscle histology, a total of 41 biopsies or post-mortem tissue were considered, of whom 29 (74%) suffered from Alpers syndrome. The majority of the patients identified had early onset (0-6 years), while eight patients had later onset (11-64 years). Normal histological findings were detected in nine patients, of whom all were infants (0-2 years) except one Juvenile case (17 years) (McFarland *et al.*, 2009; Hunter *et al.*, 2011; Isohanni *et al.*, 2011; McCoy *et al.*, 2011; Sofou *et al.*, 2012; Uusimaa *et al.*, 2013; Rouzier *et al.*, 2014). Interestingly, two patients with Alpers with severe histological abnormalities in the liver had normal muscle histology (Hunter *et al.*, 2011; Uusimaa *et al.*, 2013a).

Microscopic, non-specific changes were detected in 29 patients including: mild to moderate lipid accumulation, myopathy, type II atrophy, increased glycogen, fibre necrosis and microvesicular steatosis. Mitochondrial abnormalities similar to those observed in the liver were also evident; as revealed by EM (n=5) (Van Goethem *et al.*, 2004; Kollberg *et al.*, 2006; Uusimaa *et al.*, 2008; Stewart *et al.*, 2009; Cardenas and Amato, 2010; Hunter *et al.*, 2011; Isohanni *et al.*, 2011; Cheldi *et al.*, 2013; Nolte *et al.*, 2013; Uusimaa *et al.*, 2013; Rouzier *et al.*, 2014; Simon *et al.*, 2014). Histochemical investigations showed mosaic COX-negative fibres (n=11) and ‘ragged-red’ fibres (n=8) (Kollberg *et al.*, 2006; Stewart *et al.*, 2009; Hunter *et al.*, 2011; Sofou *et al.*, 2012; Cheldi *et al.*, 2013; Uusimaa *et al.*, 2013; Woodbridge *et al.*, 2013; Simon *et al.*, 2014). The aforementioned histological abnormalities in muscle were observed in the presence of liver abnormalities (n=7) (Kollberg *et al.*, 2006; Stewart *et al.*, 2009; Hunter *et al.*, 2011; Uusimaa *et al.*, 2013; Simon *et al.*, 2014). Of interest, the presence of fibre necrosis, COX-deficient fibres and ‘ragged-red’ fibres in a patient with MELAS-like phenotype (64 years); suggests that such histological features in the muscle are not specific to Alpers (Cheldi *et al.*, 2013). All histological abnormalities found in the muscle of the patients considered are summarised in Table 3.2.

Brain	Liver	Muscle
Histopathology: (n=22), neuronal loss, gliosis, spongiosis, astrocytosis (most prominent in occipital lobes and cerebellum), substantia nigra, thalamus, brainstem, degeneration of spinal cord and variable CI and CIV deficiencies. EM microscopy: (n=1), enlarged mitochondria with short cristae with deep invavigations of the outer membrane.	Normal Histology : (n=2) Microscopic Abnormalities: (n=29), macro/micro-vesicular steatosis, fibrosis, cirrhosis, necrosis, bile duct proliferation. Histochemistry: mosaic COX-deficient fibres (n=8), ragged-red fibre-like structures (n=2)	Normal Histology: (n=9) Microscopic Abnormalities: (n=29), mild to moderate lipid accumulation, type II atrophy, myopathy, elevated lipofuscin/glycogen, fibre necrosis, microvesicular steatosis. Histochemistry: COX-negative fibres (n=11) and ragged-red fibres (n=8). EM microscopy: (n=5), enlarged mitochondria with abnormal shape, cristae displacement and abnormal mitochondrial clustering.

Table 3.2: Summary of histopathological findings in brain, liver and muscle from patients with Alpers and *POLG*-related epilepsy. Key: EM=electron microscopy; CI= complex I; CIV= complex IV; COX=cytochrome *c* oxidase; n=number of patients.

3.4.5 MtDNA Copy Number

A. Brain

The mtDNA copy number from brain biopsies has not been reported to date. Post-mortem analysis from the frontal cortex of a single patient with Alpers revealed a 30% mtDNA copy number reduction (Ferrari et al., 2005). Interestingly this patient was homozygous for p.(Ala467Thr) with disease-onset at 7 years of age and died at the age of 19. Another study performed on grey matter tissue homogenates and micro-dissected neurons from multiple brain areas (including: frontal, hippocampus and cerebellum) showed marked mtDNA depletion (20-30% of age-matched control mean). There was no difference detected in the mtDNA depletion among different brain regions (Tzoulis *et al.*, 2014).

B. Liver

The findings of mtDNA copy number in liver tissue were reviewed for a total of 40 patients (age of onset: 0-12 years), of whom 34 (85%) had Alpers. Liver samples examined were biopsies or taken at post-mortem.

The mtDNA copy number was severely reduced in all cases. Depletion of mtDNA copy number (3-29% of control mean) was remarkable in 37 cases (92.5%) (Davidzon et al., 2005; Sarzi et al., 2007; Ashley et al., 2008; Wiltshire et al., 2008; Boes et al., 2009; Lutz et al., 2009; Taanman et al., 2009; Hunter et al., 2011; Schaller et al., 2011; Tang et al., 2011; Scalais et al., 2012; Montassir et al., 2015) and interestingly three patients with Alpers showed significant mtDNA copy number loss (30-36% of control mean) (Ashley et al., 2008; Rouzier et al., 2014). It is intriguing that the mtDNA copy number in one patient was 55% of control mean at the initial biopsy and dramatically depleted at post-mortem (10% of control mean). This patient with Alpers survived with the condition 12.5 years and was homozygous for p.(Ala467Thr) mutation (Boes et al., 2009). A significant correlation between early age of death and lower mtDNA copy number in liver was found (Spearman r=0.43, p=0.04, Figure 3.4A). In addition, a trend of positive correlation between short disease duration and reduced mtDNA copy number was observed, although it failed to reach significance (Spearman r=0.39, p=0.06, Figure 3.4B).

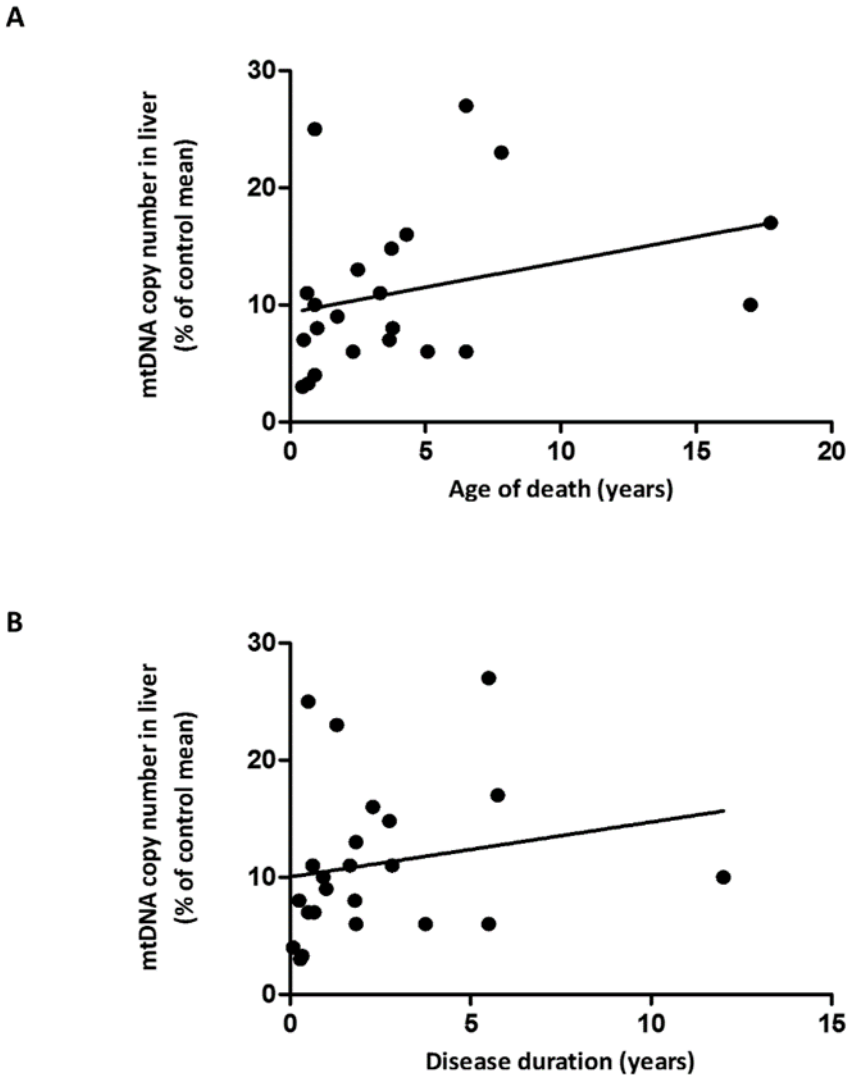

Figure 3.4: Correlation between mtDNA copy number in the liver and age of death/disease duration in patients with Alpers and *POLG*-related epilepsy reported in the literature. (A) Scatter plot showing a significant correlation between mtDNA depletion and early death (Spearman r=0.43, p=0.04). (B) Scatter plot showing a trend (albeit not significant) of decreased mtDNA copy number in liver with short disease course (Spearman r=0.39, p=0.06).

C. Muscle

The mtDNA copy number was reported in muscle samples of 41 patients, of whom 26 (63%) were paediatric (0-9 years) diagnosed with Alpers. The findings of mtDNA copy number in the muscle of the patients considered was highly variable. Only four samples, taken from patients with Alpers were within the normal mtDNA copy number range (70-93% of control mean) (Kollberg *et al.*, 2006; Bao *et al.*, 2008; Schaller *et al.*, 2011; Tang *et al.*, 2011). A total of 14 patients showed mild to moderate mtDNA reduction (32-62% of control mean) (Ashley *et al.*, 2008; Tang *et al.*, 2011; Rouzier *et al.*, 2014; Rajakulendran *et al.*, 2016); whereas 18 (44%) samples demonstrated

depletion of mtDNA (3-29% of control mean) (Kollberg *et al.*, 2006; Sarzi *et al.*, 2007; Ashley *et al.*, 2008; Taanman *et al.*, 2009; Tang *et al.*, 2011; Navarro-Sastre *et al.*, 2012; Scalais *et al.*, 2012; Rouzier *et al.*, 2014). Interestingly, an mtDNA copy number increase was detected in five patients (Kollberg *et al.*, 2006; Ashley *et al.*, 2008; Tang *et al.*, 2011). The mtDNA copy number in muscle of 14 patients was significantly higher compared to liver (paired t-test, p=0.0321; Figure 3.5). It is intriguing that mtDNA copy number from a muscle biopsy of one patient with Alpers taken late in the disease course was within the normal range (93% of control mean) (Boes *et al.*, 2009). In contrast, an early muscle biopsy from another patient with Alpers demonstrated severe mtDNA depletion (7% of control mean) (Kollberg *et al.*, 2006). Statistical analysis did not reveal significant correlation between age of death and mtDNA copy number (Spearman r=0.18, p=0.57) in muscle. Similarly, there was no correlation between disease duration and mtDNA copy number (Spearman r=0.29, p=0.36).

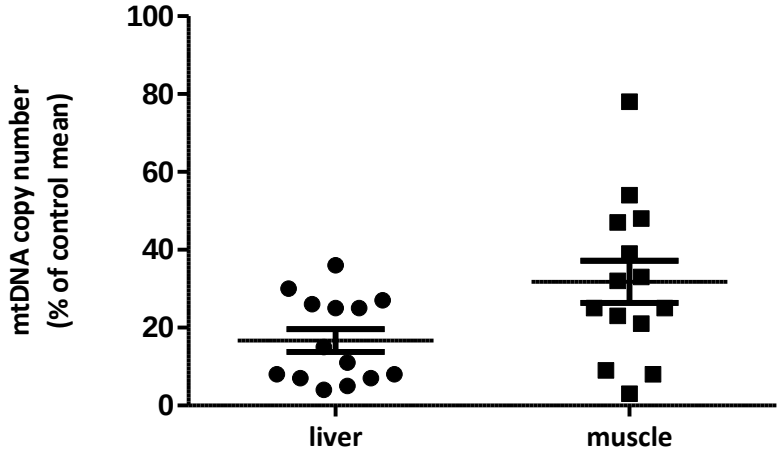

Figure 3.5: Comparison of mtDNA copy number (% of control mean) in liver and muscle from patients with Alpers and *POLG*-related epilepsy patients. Plot showing the mtDNA copy number in liver is significantly lower than in the muscle of the same patients (Student's paired t-test; p=0.0321).

D. Blood and Fibroblasts

The mtDNA copy number findings in blood samples from 49 patients were available (Tang *et al.*, 2011; Khan *et al.*, 2012) and, in the samples analysed, mtDNA copy number was highly variable.

A total of 23 patients (49%) exhibited a reduction in the mtDNA copy number; whereas depletion was uncommon as this was detected in the blood of only five patients (mtDNA 15-27% of control mean). A total of 13 samples were found to be

within the normal range (70-100% of control mean). As with the results reported in muscle, a total of eight patients showed an increase in mtDNA copy number (101-167% of control mean), although the tissues analysed were not patient-matched.

MtDNA copy number in fibroblasts has been rarely assessed. However, it has been reported in five paediatric patients with Alpers (Ashley *et al.*, 2008; Schaller *et al.*, 2011). From the patients considered, three showed a decrease in the mtDNA copy number (37-62% of control mean), while the remaining two patients demonstrated normal mtDNA copy number (82-98% of control mean). One paediatric patient exhibited normal mtDNA copy number in fibroblasts; whereas in the liver, mtDNA copy number was severely depleted (Schaller *et al.*, 2011). Overall, the mtDNA copy number findings in blood and fibroblasts were less consistent compared to muscle. Descriptive statistics and a summary of mtDNA copy number (% of control mean) in the aforementioned tissues can be found in Tables 3.3 and 3.4 respectively.

Tissue	Number of Cases (n)	Mean mtDNA (% of control)	SD mtDNA	Median mtDNA	Number of References
Liver	40	13.13	9.21	10.00	14
Muscle	41	47.85	41.70	37.00	12
Blood	49	67.67	31.93	63.00	2
Fibroblasts	5	63.9	27.4	62.00	2

Table 3.3: Descriptive statistics for mtDNA copy number from liver, muscle, blood and fibroblasts from patients with Alpers and *POLG*-related epilepsy reported in the literature.

MtDNA (%of control)	Liver	Muscle	Blood	Fibroblasts
<30 (depletion)	N=37 (92.5%)	N=18 (44%)	N=5 (10.2%)	N=0
30-50	N=3 (7.5%)	N=6 (14.6%)	N=12 (24.5%)	N=2 (40%)
51-69	N=0	N=8 (19.5)	N=11 (22.4%)	N=1 (20%)
>70 (normal or increased)	N=0	N=9 (21.95%)	N=21 (42.9%)	N=2 (40%)

Table 3.4: MtDNA copy number in liver, muscle, blood and fibroblasts from patients with Alpers and *POLG*-related epilepsy. The mean mtDNA copy number is divided into four groups: <30% (depletion), 30-50%, 51-69% and >70% (normal or increased). N=number of cases.

3.4.6 MtDNA Deletions/Rearrangements

Multiple deletions were detected by Southern blotting or long-range PCR in muscle samples of 12 patients, of whom six were paediatric cases (0-5 years), three adolescents (1-15 years) and three adults (20-48 years) (Van Goethem *et al.*, 2003; Kollberg *et al.*, 2006; Naimi *et al.*, 2006; Boes *et al.*, 2009; Stewart *et al.*, 2009; Hansen *et al.*, 2012; Sofou *et al.*, 2012).

From the paediatric patients, five had Alpers of whom only three cases had mtDNA depletion in the presence of deletions (Kollberg *et al.*, 2006; Boes *et al.*, 2009; Sofou *et al.*, 2012). Interestingly, from the aforementioned patients, two showed depletion, early in the disease course (Kollberg *et al.*, 2006; Boes *et al.*, 2009). Deletions/rearrangements in fast-dividing tissues (liver, blood and fibroblasts) of patients with Alpers or other *POLG*-related epilepsy have not been reported to date. Similarly, deletions/point mutations were not detected in the brain tissue of the patients considered.

3.4.7 Respiratory Chain (RC) Biochemistry

To better understand the effect of *POLG* mutations on the OXPHOS machinery, RC and complex V biochemical data were evaluated from a total of 63 patients. Findings from liver (n=17), muscle (n=63), brain (n=1) and cultured fibroblasts (n=16) were considered. The RC activity was highly variable among different tissue types.

With regards to liver samples, normal RC activity was rarely detected (n=3) (Nguyen *et al.*, 2005; de Vries *et al.*, 2008). RC deficiencies were identified (n=17), multi-complex in the majority of the patients (n=9, involving complex I-IV) (Sarzi *et al.*, 2007; Wiltshire *et al.*, 2008; Blok *et al.*, 2009; Kurt *et al.*, 2010; Mousson de Camaret *et al.*, 2011; Schaller *et al.*, 2011; Rouzier *et al.*, 2014) and isolated complex I (n=1) or complex IV (n=3) (Nguyen *et al.*, 2005; Lutz *et al.*, 2009; Scalais *et al.*, 2012). Isolated complex V deficiency was detected in the sample of a single patient (Sarzi *et al.*, 2007). From the patients included, a total of nine patients (53%) showed mtDNA copy number reduction (mean mtDNA copy number range: 3-36% of control mean) when an OXPHOS defect was present (Sarzi *et al.*, 2007; Wiltshire *et al.*, 2008; Lutz *et al.*, 2009; Schaller *et al.*, 2011; Scalais *et al.*, 2012; Rouzier *et al.*, 2014).

Conversely, the OXPHOS activity was normal in the majority (60.3%) of muscle samples (n=38) (Nguyen *et al.*, 2006; de Vries *et al.*, 2008; Uusimaa *et al.*, 2008; Wiltshire *et al.*, 2008; Blok *et al.*, 2009; Lutz *et al.*, 2009; McFarland *et al.*, 2009;

Taanman *et al.*, 2009; Hasselmann *et al.*, 2010; Kurt *et al.*, 2010; Isohanni *et al.*, 2011; Mousson de Camaret *et al.*, 2011; Scalais *et al.*, 2012; Sofou *et al.*, 2012; Uusimaa *et al.*, 2013; Rouzier *et al.*, 2014; London *et al.*, 2017). Multi-complex deficiencies were found in 18 muscle biopsies (de Vries *et al.*, 2007; Roels *et al.*, 2009; Witters *et al.*, 2010; Mousson de Camaret *et al.*, 2011; Khan *et al.*, 2012; Navarro-Sastre *et al.*, 2012; Sofou *et al.*, 2012; Horst *et al.*, 2014; Rouzier *et al.*, 2014; Rajakulendran *et al.*, 2016). Isolated complex I (n=2), complex III (n=1), complex IV (n=3) and complex V (n=1) were also detected (de Vries *et al.*, 2007; Ferreira *et al.*, 2011; Schaller *et al.*, 2011; Sofou *et al.*, 2012; Uusimaa *et al.*, 2013). One patient showed normal RC activity in the muscle late in the disease course, in the presence of mtDNA depletion. In contrast another patient exhibited both mtDNA depletion and reduced RC activity late in the disease course (Kollberg *et al.*, 2006).

The muscle biopsies from 11 patients showed normal RC activity when deficiencies were detected in the liver of the same patients (Nguyen *et al.*, 2005; Sarzi *et al.*, 2007; Wiltshire *et al.*, 2008; Lutz *et al.*, 2009; Kurt *et al.*, 2010; Scalais *et al.*, 2012; Rouzier *et al.*, 2014). In contrast, only five patients showed low RC enzymes in both muscle and liver (Sarzi *et al.*, 2007; Lutz *et al.*, 2009; Mousson de Camaret *et al.*, 2011; Schaller *et al.*, 2011; Rouzier *et al.*, 2014).

In addition, two patients exhibited OXPHOS deficiency when mtDNA copy number was depleted (mean mtDNA copy number: 3% and 25% respectively) (Sarzi *et al.*, 2007); however, three patients demonstrated normal RC enzymology when mtDNA was reduced (mean mtDNA: 21-39% of control mean) (Sarzi *et al.*, 2007; Scalais *et al.*, 2012; Rouzier *et al.*, 2014). It is intriguing that the OXPHOS machinery was defective in a single patient with normal mtDNA copy number (78% levels when compared to controls) in muscle (Schaller *et al.*, 2011). With regards to fibroblasts, the RC enzymology was normal except in one patient who showed complex III deficiency (Horst *et al.*, 2014). Similarly, complex III deficiency was reported in tissue from a single brain biopsy (Blok *et al.*, 2009).

3.4.8 Genotype to Phenotype Correlations

Homozygous p.(Ala467Thr) and p.(Trp748Ser) and compound heterozygous p.(Ala467Thr)/p.(Trp748Ser) mutations are associated with significantly longer survival when compared to other compound heterozygous mutations (p<0.001) (Figure 3.6). In addition, the presence of both pathogenic variants located in the exonuclease domain have rarely been reported (n=15, 3% of cases).

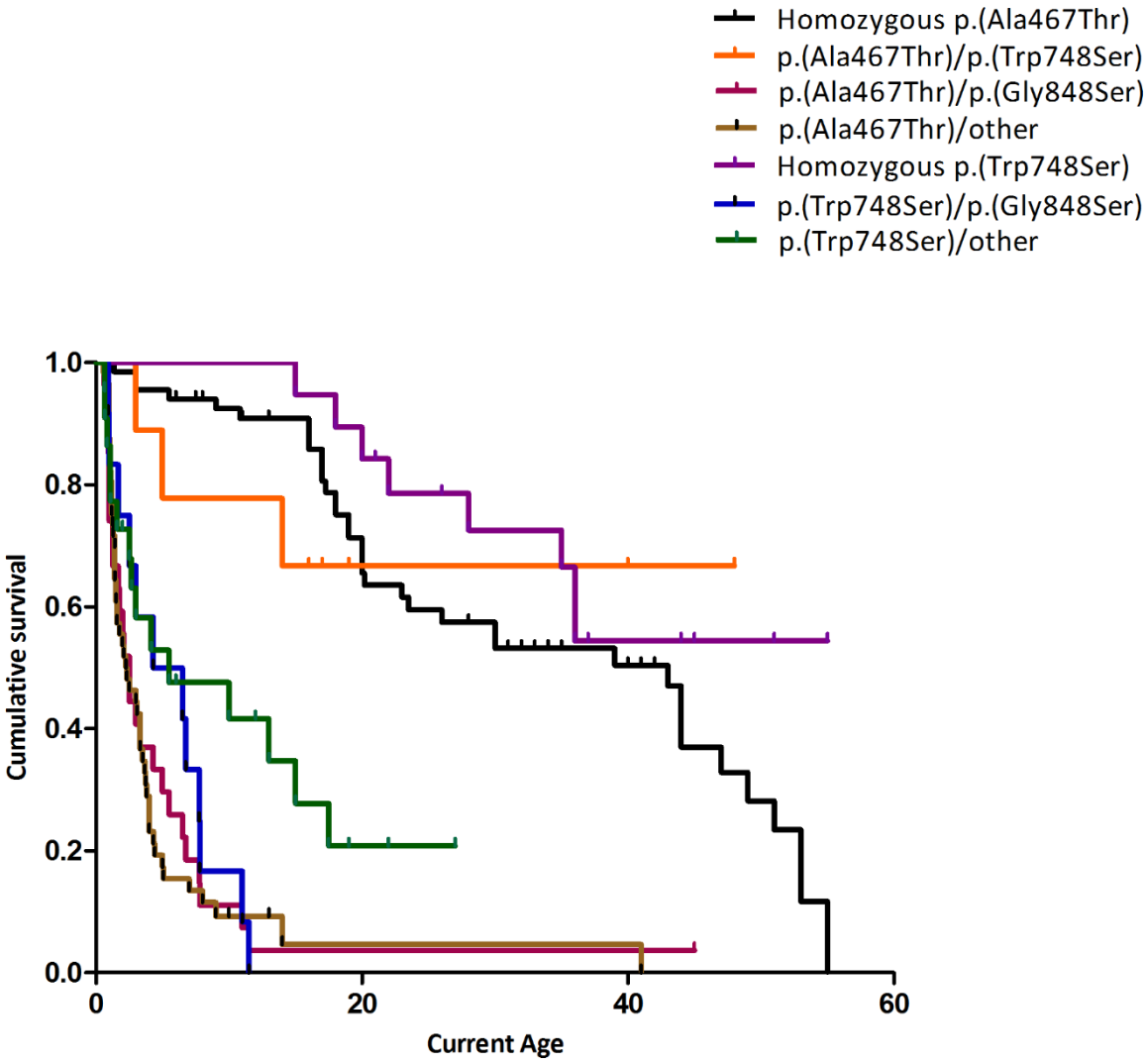

Figure 3.6: Kaplan-Meier survival curves based on the different genotypes. Censored data (patients that have been reported as alive) are represented as black vertical lines.

3.5 Discussion

In this chapter, the clinical manifestations, genetics, histopathology and molecular features of patients with Alpers and *POLG*-related epilepsy were reviewed and analysed. A total of 377 patients and 128 disease-causing variants located in the *POLG* gene were identified in the literature. The variants identified were associated with seizures/epilepsy, however these findings were based upon single case reports or small number of pedigrees.

Over 80% of patients with *POLG*-related epilepsy, harboured at least one of the three most common pathogenic variants, including p.(Ala467Thr), p.(Trp748Ser) and p.(Gly848Ser). In agreement with previous reports, homozygous mutations located in the linker domain of *POLG* are associated with later disease onset and longer survival (Tzoulis *et al.*, 2006; Farnum *et al.*, 2014).

The milder phenotype exhibited in patients homozygous for p.(Ala467Thr) or p.(Trp748Ser) mutations is not well understood. It is likely that the location of the mutation within the *POLG* gene partly dictates phenotype; although this warrants further investigation.

Functional studies have been reported suggesting that p.(Ala467Thr) and p.(Trp748Ser) mutations are associated with decreased catalytic efficiency of POLG. The p.(Ala467Thr)-mutant POLG retains only 4% of the wild-type activity *in vitro* and fails to bind efficiently to the p55 accessory subunit (Chan *et al.*, 2005b). Similarly, the p.(Trp748Ser)-mutant POLG exhibited a severe catalytic defect, resulting in poor primer extension and defective DNA synthesis (Luoma *et al.*, 2005).

The reduced catalytic activity, combined with compromised interaction with the p55 accessory subunits results in stalling of mtDNA replication in mutant POLG. However, DNA synthesis is enough to sustain life prior to and after the disease onset. Therefore, it has been suggested that in compound heterozygous patients, the mutation on the other allele determines the severity of the phenotype. In the case of homozygous p.(Ala467Thr) or p.(Trp748Ser) patients, POLG activity is inadequate to maintain functional mtDNA as the patient ages (Chan *et al.*, 2005a; Chan *et al.*, 2005b; Luoma *et al.*, 2005). Nevertheless, these hypotheses cannot explain the severe phenotype and early disease onset exhibited by patients homozygous for p.(Ala467Thr) or p.(Trp748Ser).

In addition, this work showed that mutations located in the exonuclease domain of *POLG* are uncommonly reported (3%). This observation could suggest that mutations associated with the exonuclease domain are embryonically lethal. This hypothesis is not supported by animal studies, given that mice with exonuclease-deficient POLG are viable (Trifuvonik 2004, Kujoth 2005). However, the *POLG*-mutator mouse exhibits a premature ageing phenotype and does not demonstrate epilepsy, therefore the *POLG*-mutator mouse model cannot be applied when considering human *POLG*-related epilepsy.

The findings of the current review are consistent with previous observations of a predisposition for occipital lobe involvement in *POLG*-related seizure disorders, in terms of clinical, radiological and histopathological findings, although this preferential involvement remains enigmatic (Engelsen *et al.*, 2008; Janssen *et al.*, 2015).

Seizures increase neuronal energy demand thus accounting for the lesions observed in metabolically active areas such as occipital lobes, hippocampus and brainstem. In addition, the cerebellar lesions may be secondary to high epileptic activity of other cortical regions, however this remains controversial (Tzoulis *et al.*, 2014). The stroke-like lesions in *POLG*-related epilepsy appear to overlap with those observed in Mitochondrial Encephalomyopathy, Lactic Acidosis and Stroke-like episodes (MELAS) caused by the m.3243A>G mutation and other primary mtDNA mutations (Deschauer *et al.*, 2007; Tzoulis *et al.*, 2010; Brinjikji *et al.*, 2011).

The findings of this work support the hypothesis of a tissue-specific predisposition associated with *POLG*-related epilepsy. Abnormalities including microscopic changes, mtDNA depletion and consequent OXPHOS dysfunction, are indeed molecular features characterising Alpers and *POLG*-related epilepsy. These abnormalities differ amongst tissue types.

With regards to the brain, microscopic abnormalities such as neuron loss, spongiosis, and astrogliosis have all been frequently reported at varying degrees in different brain regions. Changes in the occipital lobe and the cerebellum have been the most frequently reported. Other brain regions have been rarely studied, most likely due to the scarcity of post-mortem brain tissue. Studies of the mtDNA content and OXPHOS activity are lacking. However, a study by Tzoulis and colleagues, has shown mtDNA depletion in young patients remained unchanged with disease progression. The lowest mtDNA copy number was detected in an infant, suggesting that *POLG*

mutations resulting in defective mtDNA synthesis is an early developmental feature (Tzoulis *et al.*, 2014).

Deletions and point mutations were not detected in the younger population but only in older patients; suggesting an age-dependent process. Although deletions were detectable in multiple brain regions, these were most predominantly observed in substantia nigra. This is not surprising as it has been reported that substantia nigra neurons accumulate deletions with ageing and neurodegenerative disorders. The point mutations combined with the pre-existing mtDNA depletion/deletions identified may further decrease the number of wt-mtDNA copies, thereby contributing to respiratory chain deficiency. Whether deletions/point mutations are secondary to depletion is a matter for further investigation. Indeed, these finding are based on post-mortem brain tissue; thus representative of the most severe features of the disease (Tzoulis *et al.*, 2014).

Liver dysfunction rarely occurs as a presenting feature and tends to precede the terminal disease stage. Liver dysfunction is accelerated by valproate (VPA)-exposure which frequently results in liver failure. Severe mtDNA depletion and OXPHOS dysfunction, coupled with microscopic abnormalities indicative of liver failure and Alpers, characterise *POLG*-related epilepsy (Nguyen *et al.*, 2005). Interestingly, mtDNA depletion correlated with early age of death, suggesting that mtDNA depletion caused by *POLG* mutations is the mechanism underlying Alpers and *POLG*-related encephalohepatopathies. However, in the majority of the cases the biopsies were taken late in the disease or tissue was harvested at post-mortem, thus these findings may reflect the bias of severe liver involvement.

Myopathy is not frequently involved in *POLG*-related epilepsy. In agreement with this observation, the histological appearances of muscle from many paediatric patients may appear normal. The mtDNA copy number and RC biochemistry in muscle samples can be variable, therefore these findings should be interpreted with caution when considering Alpers and *POLG*-related epilepsy. Moreover, mtDNA copy number in muscle is significantly higher than in liver of patients. It is intriguing that histological appearances of muscle tissue can be normal even at late disease stages.

MtDNA reduction in muscle may characterise disease progression as the mtDNA copy number was 55% of the control mean in the initial biopsy of a p.(Ala467Thr) homozygous patient. However, this was reduced to 16% of residual mtDNA twelve years later, at post-mortem examination (Boes *et al.*, 2009). Taken together these

findings highlight that changes in muscle tissue may be unreliable, especially in early disease stages. Therefore, *POLG* genetic testing should be the gold standard diagnostic test for Alpers and *POLG*-related epilepsy, and assessing muscle tissue either by histological analysis, RC enzymology or mtDNA copy number should not be used for diagnostic purposes.

MtDNA abnormalities in blood and cultured fibroblasts were less consistent. Fibroblasts are characterised by high mitotic rate, which may mask any mtDNA abnormalities; thus mtDNA abnormalities may not be evident fibroblasts. Although it is still unclear, a possible explanation would involve a process of negative selection which may favour replication of cells with higher levels of mtDNA (van den Heuvel *et al.*, 2004). In agreement with this hypothesis, fibroblasts did not mimic the biochemical phenotype even when the liver was severely affected (Schaller *et al.*, 2011).

In summary, *POLG* mutations cause POLG dysfunction, resulting in mtDNA depletion with consequent OXPHOS dysfunction which is most predominant in the affected tissues. Epilepsy is a major manifestation of Alpers.

Currently, the mechanisms of mitochondrial epileptogenesis are not well understood due to the lack of neuropathological studies and scarcity of post-mortem brain tissue. However, several hypotheses have been proposed to explain seizure generation in mitochondrial disease and these involve: defects in calcium uptake, ROS-induced oxidation of ion channels, defective neurotransmitter transport (causing increased synaptic glutamate concentration) and reduced inhibitory neurotransmission, which may contribute to increased excitability (Bindoff and Engelsen, 2012; Zsurka and Kunz, 2015).

Furthermore, a recent post-mortem neuropathological study of adult patients with mitochondrial epilepsy demonstrated loss of GABAergic interneurons combined with severe mitochondrial respiratory chain deficiencies, resulting in impaired neuronal oscillations and an imbalance between inhibition and excitation, which may significantly contribute towards seizure development (Lax *et al.*, 2016).

The recent development of induced-pluripotent stem cell (iPSC) technology enables the conversion of human fibroblasts into pluripotent stem cells with the use of four transcription factors. These can be subsequently differentiated into neurons and glial

cells and used for further investigations aimed at unravelling molecular mechanisms and inform novel therapies.

Whilst recent advances have shed light on our understanding of the effects of *POLG* mutations on mitochondrial disease, the mechanisms underlying neurodegeneration, tissue specific dysfunction and genotype to phenotype correlations remain challenging.

3.5.1 Limitations

This study was based mostly on single case reports or small number of pedigrees. In addition, the tissue considered was not patient-matched in most of the cases and the available information regarding age/gender-matched controls was limited. Due to the limited data availability, cox-regression analysis for the identification of prognostic factors associated with differences in survival between different genotypes could not be performed.

3.5.2 Conclusions

This work provided evidence that 128 pathogenic *POLG* variants are associated with *POLG*-related epilepsy. The p.(Ala467Thr) mutations is the most frequently reported and compound homozygous mutations located within the linker domain of *POLG* are associated with longer survival compared to compound heterozygous.

Molecular and biochemical features vary amongst tissues, suggesting tissue-specific effects exerted by *POLG* mutations. Therefore, diagnosis should be based on *POLG* genetic testing.

Chapter 4 Characterisation of Human *POLG*-mutant Fibroblasts from Patients with Alpers

4.1 Introduction

Alpers is the most severe form of *POLG*-related disorders and occurs as a result of homozygous or compound heterozygous *POLG* mutations. Although the mechanisms remain unclear, *POLG* mutations result in POLG dysfunction, leading to reduced mtDNA replication and consequent reduction in the mtDNA copy number and/or deletions. When defects in the mtDNA reach a critical point, OXPHOS defects occur ultimately resulting in compromised ATP production. As a consequence, phenotypic manifestations become evident, especially in the affected tissues such as liver and brain (Saneto and Naviaux, 2010).

To date, there are no precise genotype to phenotype correlations, although compound heterozygous mutations are associated with poorer prognosis compared to homozygous mutations which correlate with later onset and longer survival (Tzoulis *et al.*, 2006). Increasing evidence suggests that the location of mutations within the catalytic subunit of POLG may play a role in the expression of the phenotype (Euro *et al.*, 2011). However, the factors and underlying mechanisms modifying the phenotype within the same or other *POLG*-related syndrome remain elusive.

The relentless progression of Alpers and the lack of treatment, makes it a challenging area to investigate. The scarcity of post-mortem brain tissue makes it difficult to proceed into further molecular studies; while patient cells from the affected tissues (brain and liver) are difficult to obtain and culture.

Skin fibroblasts are neural crest-derived, generated from the ectoderm, the same germ layer which gives rise to neurons. Fibroblasts are easily accessible through skin biopsies, a minimally invasive procedure, are easily grown in culture, and stored, thus constituting a useful tool for molecular investigations.

With regards to mitochondrial disease, the biochemical defects secondary to mtDNA mutations are often variable in fibroblasts, due to the differences in the heteroplasmy of mtDNA mutations, which are cell/tissue-specific (Rodenburg, 2011).

When the underlying mutation resides in nuclear-encoded genes, patient fibroblasts have been reported to show biochemical defects, as exemplified by fibroblasts from paediatric patients harbouring mutations in nuclear-encoded complex I genes, which demonstrate mitochondrial abnormalities. These abnormalities include: reduced complex I expression, increased ROS production, defects in mitochondrial morphology and depolarised membrane potential (Distelmaier *et al.*, 2009; Koopman *et al.*, 2012; Roestenberg *et al.*, 2012). As mitochondrial network formation is crucial for mitochondrial homeostasis, a disruption in mitochondrial networks may lead to impaired mtDNA integrity and thus affect mitochondrial functions, such as respiratory chain activity.

Similarly, fibroblasts from patients with mutations in the orphan F-box protein FBXL4, which have been found to cause mtDNA depletion syndromes, display abnormalities including: severe shortening of mitochondria and mitochondrial network fragmentation, aberrant distribution of nucleoids coupled with combined respiratory chain deficiencies, secondary to mtDNA depletion, thus implying a role of *FBXL4* in modulation of mitochondrial dynamics (Bonnen *et al.*, 2013; Gai *et al.*, 2013).

When considering *POLG* mutations, fibroblast findings are inconsistent and, in the majority of cases, they do not reveal biochemical abnormalities representative of the disease phenotype (reviewed in Chapter 3). Consistent with these observations fibroblasts with mutations in other nuclear genes such as *DGUOK* and *MPV17*, which also cause mtDNA depletion syndromes characterised by encephalopathy, often show normal enzyme activities (Mandel *et al.*, 2001; Spinazzola *et al.*, 2006).

Furthermore, fibroblasts from patients with early-onset encephalopathy, characterised by intractable epilepsy due to mutations in the gene encoding tRNA synthetase FARS2, do not express a biochemical defect. However, biochemical defects were detected in the muscle of the same patient (Almalki *et al.*, 2014).

In contrast, one study performed in fibroblasts from four paediatric patients with Alpers syndrome, revealed mosaic mtDNA depletion associated with reduced COX activity and decreased membrane potential (Ashley *et al.*, 2008). These findings may reflect disease stage and severity and location of the mutations, although it warrants further investigation.

4.2 Aims and Objectives

This chapter will explore fibroblasts derived from patients with clinically defined early and late-onset Alpers with confirmed diagnosis of *POLG* mutations. The scope of this work is to characterise the baseline mitochondrial function of *POLG*-mutant fibroblasts from patients with Alpers and test whether they mimic the biochemical defects of the disease phenotype. If the fibroblasts express biochemical defects, then these can be used as a model for investigating the underlying mechanisms of *POLG*-induced Alpers. To this aim my specific objectives are to:

1) Investigate and analyse nucleoid morphology, dynamic mitochondrial networks, motility and membrane potential by live-cell imaging.
2) Define bioenergetics by microscale oxygraphy.
3) Assess mtDNA copy number using a qPCR assay.
4) Assess steady-state levels of POLG by western blotting.

4.3 Results

For the purposes of fibroblast characterisation, two patients with early-onset and two patients with late-onset Alpers harbouring *POLG* mutations in a compound heterozygous or homozygous state and controls were considered (Table 4.1). Three patients harbour the most common p.(Ala467Thr) mutation and one patient harbours the second most common mutations, p.(Trp748Ser). Fibroblasts were obtained from skin biopsies and the patients or legal guardians, all consented for the cells to be used for biomedical research (consented by Professor McFarland and his clinical team)-reference number 16/NE/0267 (favourable opinion given 14 Nov 2016 by NRES Committee North East – Newcastle & North Tyneside 1). The cells were kept and made available by the Newcastle Mitochondrial Diagnostic Service.

Cases	Case code	Age at biopsy	Gender	*POLG* mutations	Location	Status
Patient 1	M1453-12	1 month	Male	p.(Ala467Thr)/p.(Thr914Pro)	Linker/Polymerase	Compound heterozygous
Patient 2	M1059-10	1 year	Male	p.(Leu428Pro)/p.(Ala467Thr)	Linker/Linker	Compound heterozygous
Patient 3	M1936-13	15 years	Female	p.(Ala467Thr)/p.(Ala467Thr)	Linker/Linker	Homozygous
Patient 4	M0174-17	16 years	Female	p.(Cys418Arg)/p.(Trp748Ser)	Linker/Linker	Compound heterozygous
Control 1	M0528-12	6 months	Male	N/A	N/A	N/A
Control 2	M1171-13	8 months	Male	N/A	N/A	N/A
Control 3	M0465-11	5 months	Male	N/A	N/A	N/A
Control 4	M0857-15	24 years	Unknown	N/A	N/A	N/A
Control 5	M0858-15	26 years	Unknown	N/A	N/A	N/A
Control 6	M0859-15	34 years	Unknown	N/A	N/A	N/A

Table 4.1: Characteristics of patient and control fibroblasts used in this study. Key: N/A=not applicable**.**

4.3.1 Investigation of Mitochondrial Morphology and Dynamic Networks in POLG-mutant Fibroblasts from Patients with Alpers

To test the hypothesis that *POLG* mutations disrupt mitochondrial morphology as reported in other mtDNA disorders, the dynamic mitochondrial networks were assessed in patient fibroblasts and appropriate controls. Mitochondrial networks were visualised by incubation of cells with Tetramethylrhodamine Methyl Ester (TMRM), a cell-permeant cationic dye which accumulates into mitochondria in a membrane potential-dependent manner. Specifically, TMRM accumulates in healthy mitochondria with high membrane potential, resulting in strong fluorescent signal. When the membrane potential drops, TMRM leaks from the mitochondria resulting in less fluorescence.

Imaging was performed using an inverted point scanning confocal microscope (Nikon A1R). Images were processed and analysed using ImageJ as described in section 2.4.4.

Patients 1 (p.(Ala467Thr)/p.(Thr914Pro)) and 2 (p.(Leu428Pro)/p.(Ala467Thr)) with early onset were compared to gender matched controls 1 and 2. Controls showed normal mitochondrial morphology, characterised by complex reticular networks. Fibroblasts from patients 1 (p.(Ala467Thr)/p.(Thr914Pro)) and 2 (p.(Leu428Pro)/p.(Ala467Thr)) did not display any differences in mitochondrial morphology when compared to the controls (see Figure 4.1A). Quantitative analysis of the aspect ratio (AR, measure of mitochondrial length) and form factor (FF, measure of mitochondrial network complexity) did not reveal significant differences in any of the patients when compared to controls (p=0.1430 and p=0.3364, respectively as revealed by One-Way ANOVA), as shown in Figures 4.1B and C.

To investigate the effect of *POLG* mutations on mitochondrial membrane potential, TMRM intensity was measured using IMARIS as described in section 2.4.6. Statistical analysis did not reveal any significant alterations in mitochondrial membrane potential in fibroblasts from both patients relative to the control mean (p=0.1133, Kruskal-Wallis), as illustrated in Figure 4.1D.

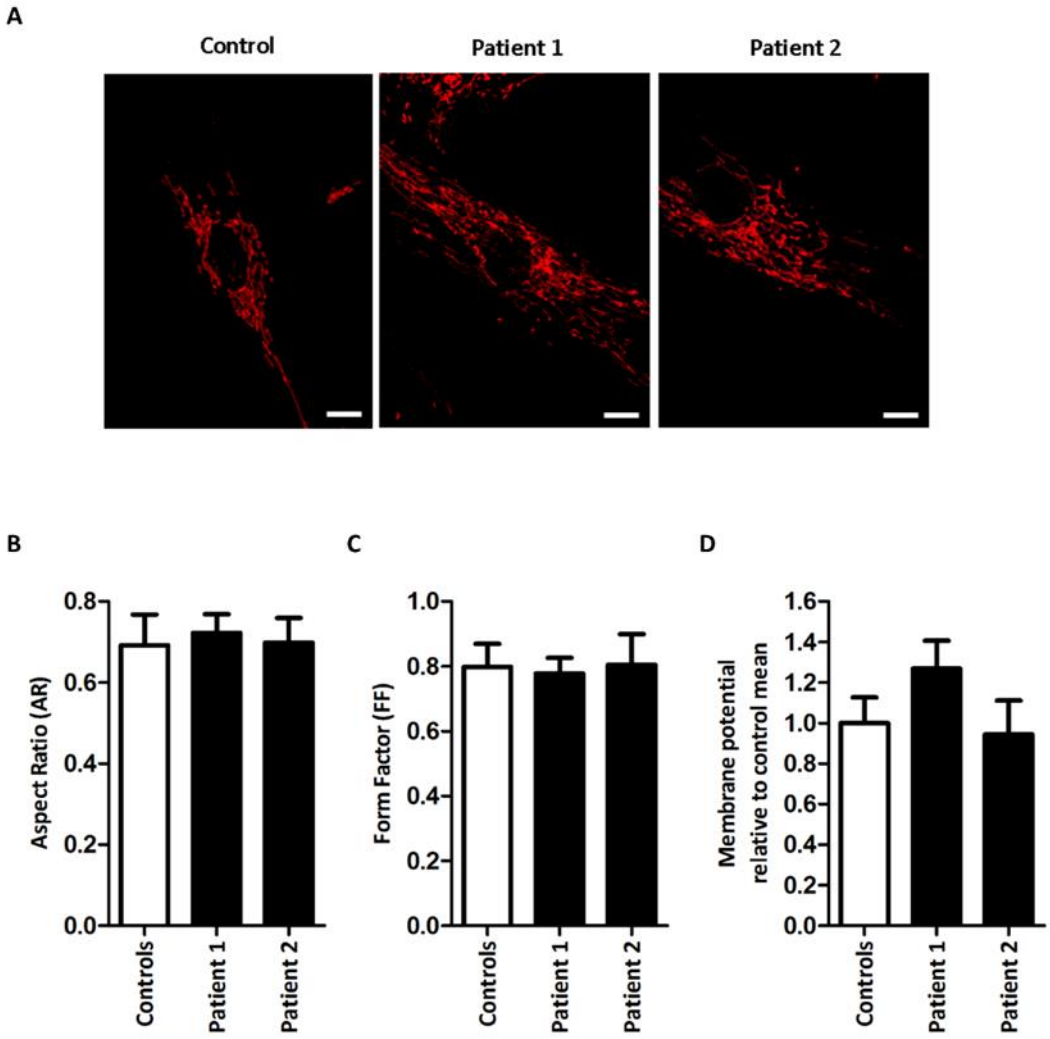

Figure 4.1: Mitochondrial networks and membrane potential in POLG-mutant fibroblasts from paediatric individuals withAlpers.(A) Representative images of TMRM staining in control (left), patient 1 (p.(Ala467Thr)/p.(Thr914Pro)) (middle) and patient 2 (p.(Leu428Pro)/p.(Ala467Thr)) (right), showing a well-connected tubular mitochondria network in both patients compared to control 1. Images captured at 63x magnification. Scale bar=10µm. Quantitative analysis did not reveal significant differences in (B) aspect ratio (AR, p=0.1430) and (C) form factor (FF, p=0.3364) as shown by One-way ANOVA. Data are represented as mean ± SD for n=30, obtained from triplicate experiments. (D) Statistical analysis using Kruskal-Wallis test did not reveal significant differences (p=0.1133) in the relative membrane potential in fibroblasts from both patients 1 (p.(Ala467Thr)/p.(Thr914Pro)) and 2 (p.(Leu428Pro)/p.(Ala467Thr)) compared to the control mean. Membrane potential data are represented as mean ± SD from n=2.

To confirm that *POLG* mutations do not interfere with mitochondrial networks in fibroblasts, *POLG*-mutant fibroblasts were compared to fibroblasts from an 8-month old patient with encephalopathy, psychomotor regression and lactic acidosis, resembling features of Alpers and genetic diagnosis of *FBXL4* mutations. Mutations in *FBXL4* have been previously been associated with impaired mitochondrial networks, suggesting a role of FBXL4 in the modulation of mitochondrial dynamics. (Bonnen *et al.*, 2013). Therefore, *FBXL4*-mutant fibroblasts were selected as a

disease control when investigating the impact of *POLG* mutations on dynamic mitochondrial networks in fibroblasts from patients with Alpers.

In contrast to *POLG*-mutant fibroblasts, *FBXL4*-mutant fibroblasts displayed marked differences in mitochondrial morphology (see Figure 4.2A). Analysis of the AR revealed significant mitochondrial shortening of *FBXL4*-mutant fibroblast networks when compared to controls ($p<0.05$, One-way ANOVA) and *POLG*-mutant fibroblasts from both patients ($p<0.0001$, One-way ANOVA) as seen in Figure 4.2B. Similarly, FF revealed significant hyper-fragmentation of mitochondrial networks in *FBXL4*-mutant fibroblasts when compared to controls and *POLG*-mutant fibroblasts ($p<0.001$, One-way ANOVA) as presented in Figure 4.2C. There was no significant difference between *POLG*-mutant fibroblasts and controls ($p=0.3763$, One-way ANOVA).

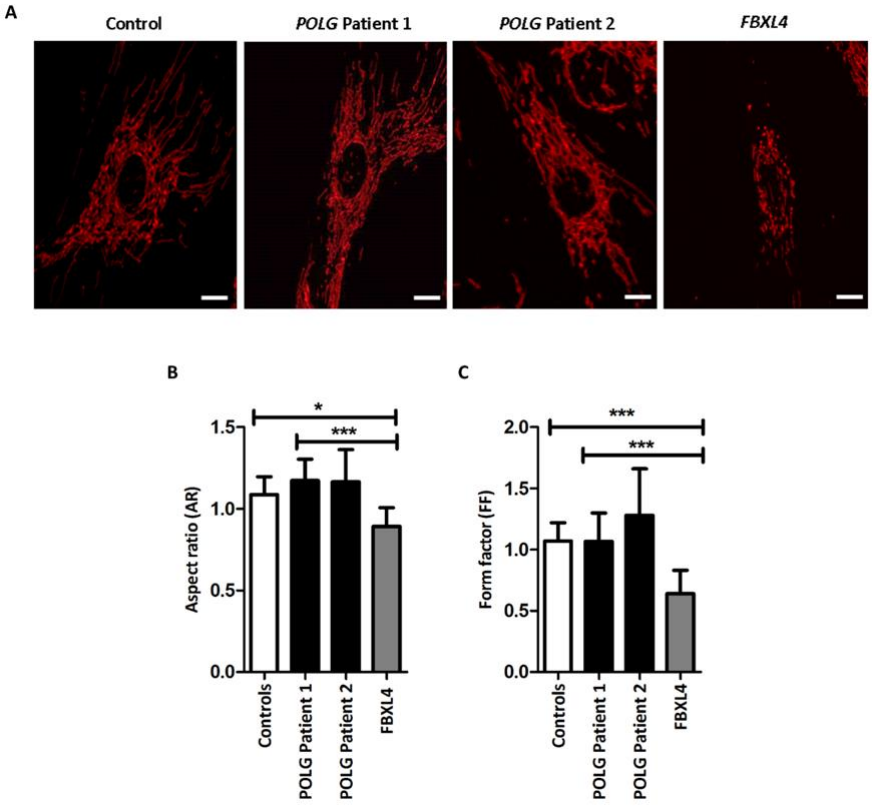

Figure 4.2: Mitochondrial morphology and networks in paediatric *POLG* and *FBXL4*-mutant fibroblasts. (A) Representative images of TMRM staining in control (left), patient 1 (p.(Ala467Thr)/p.(Thr914Pro)) (middle left), patient 2 (p.(Leu428Pro)/p.(Ala467Thr)) (middle right) and *FBXL4* patient (right) displaying a well-connected tubular mitochondrial network in both patients compared to control. Images captured at 63x magnification. Scale bar=10µm. One-way ANOVA revealed significant changes in (B) aspect ratio (AR) and (C) form factor (FF) in F*BXL4*-mutant fibroblasts compared to *POLG*-mutant fibroblasts and controls but not between *POLG*-mutant fibroblasts and controls ($p=0.3763$). All data are represented as mean ± SD for n=30, obtained from duplicate experiments. * =$p<0.05$, ***=$p<0.001$.

Similarly, in the older group results failed to reveal alteration in the dynamic mitochondrial in both adolescent patients with Alpers when compared to controls (see Figure 4.3A). Statistical analysis using One-way ANOVA confirmed no significant differences in AR (p=0.1331) and FF (p=0.0661) when compared to controls (see Figure 4.3B and C). Similarly, TMRM intensity was not different to controls (p=0.1017, Kruskal-Wallis), as shown by quantitative analysis in Figure 4.3D.

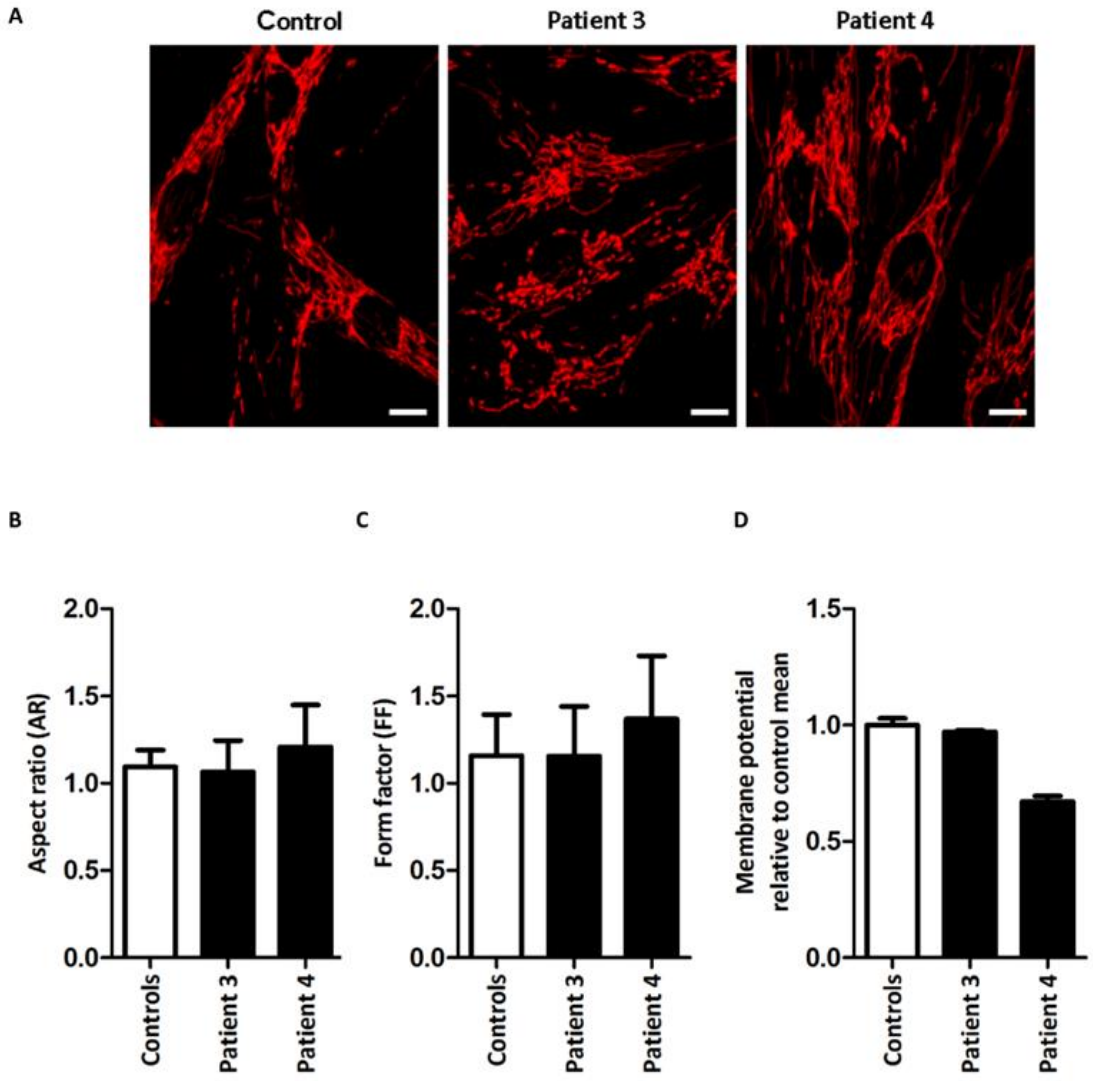

Figure 4.3: Mitochondrial networks and membrane potential in *POLG*-mutant fibroblasts from adolescent individuals with Alpers. (A) Representative images of TMRM staining in control (left), patient 3 (p.(Ala467Thr)/p.(Ala467Thr)) (middle) and patient 4 (p.(Trp748Ser)/p.(Cys418Arg)) (right), showing a well-connected tubular mitochondria network in both patients compared to control. Images captured at 63x magnification. Scale bar=10µm. Quantitative analysis did not reveal significant differences in (B) aspect ratio (AR, p=0.1331) and (C) form factor (FF, p=0.0661) as shown by One-way ANOVA. Data are represented as mean ± SD for n=30, obtained from triplicate experiments. (D) Quantitative analysis did not reveal significant differences (p=0.1017, Kruskal-Wallis) in the relative membrane potential in fibroblasts from both patients 3 (p.(Ala467Thr)/p.(Ala467Thr)) and 4 (p.(Trp748Ser)/p.(Cys418Arg)) compared to the control mean. Membrane potential data are represented as mean ± SD from n=2.

4.3.2 Analysis of Mitochondrial Nucleoids in POLG-Mutant Fibroblasts from patients with Alpers

To investigate the effect of *POLG* mutations on nucleoid morphology cells were incubated with Picogreen (see section 2.4.2). The controls displayed small nucleoids which were evenly spread across the cells. *POLG*-mutant fibroblasts from young and older patients showed no difference in nucleoid morphology compared to the controls (see Figures 4.4 and 4.5).

In contrast the fibroblasts from patient with *FBXL4* mutations showed enlarged nucleoids characterised by perinuclear clustering when compared to controls (see Figure 4.4). Quantitative analysis of nucleoid number (method described in section 2.4.5) revealed no difference in the *POLG*-mutant fibroblasts compared to the controls in both the younger group ($p=0.6727$) and older group ($p=0.1522$), however the nucleoid number was significantly lower in *FBXL4* mutant cells compared to controls ($p<0.0001$), as shown in Figures 4.6A and B).

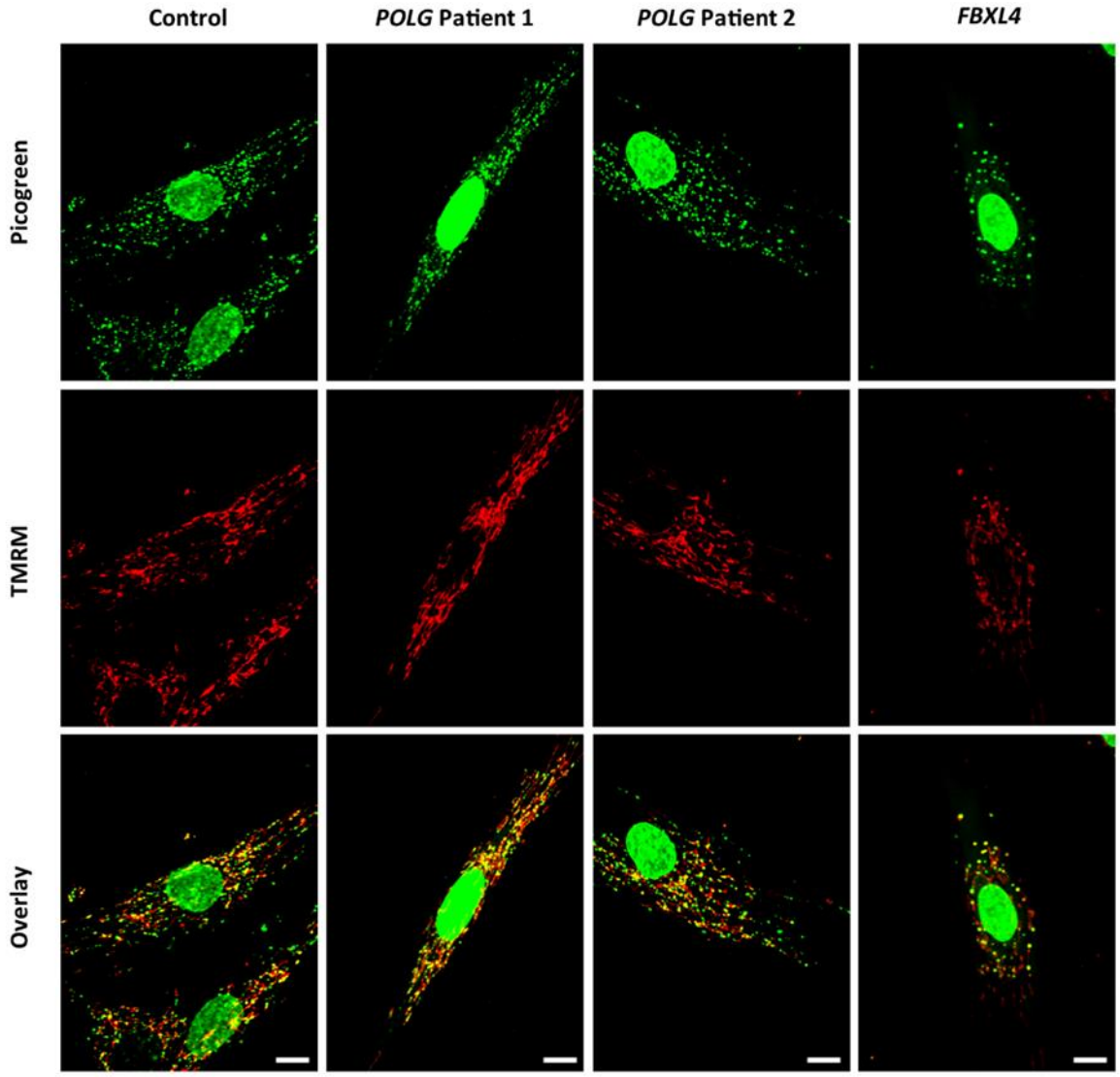

Figure 4.4: Nucleoid morphology and distribution in *POLG* and *FBXL4*-mutant fibroblasts derived from patients with early-onset Alpers. The upper panels show representative images of Picogreen staining of control (left), *POLG* patient 1 (p.(Ala467Thr)/p.(Thr914Pro)) (middle left), *POLG* patient 2 (p.(Leu428Pro)/p.(Ala467Thr)) (middle right) and patient with *FBXL4* mutations (right). Fewer, enlarged, with perinuclear clustering nucleoids are noted in the patient harbouring *FBXL4* mutations. *POLG* patients show similar numbers and distribution of nucleoids across the cell. The middle panels show TMRM staining, revealing mitochondrial shortening and fragmentation only in the patient with *FBXL4* mutations. The lower panels show representative merged images. Images were captured at 63x magnification. Scale bar=10µm.

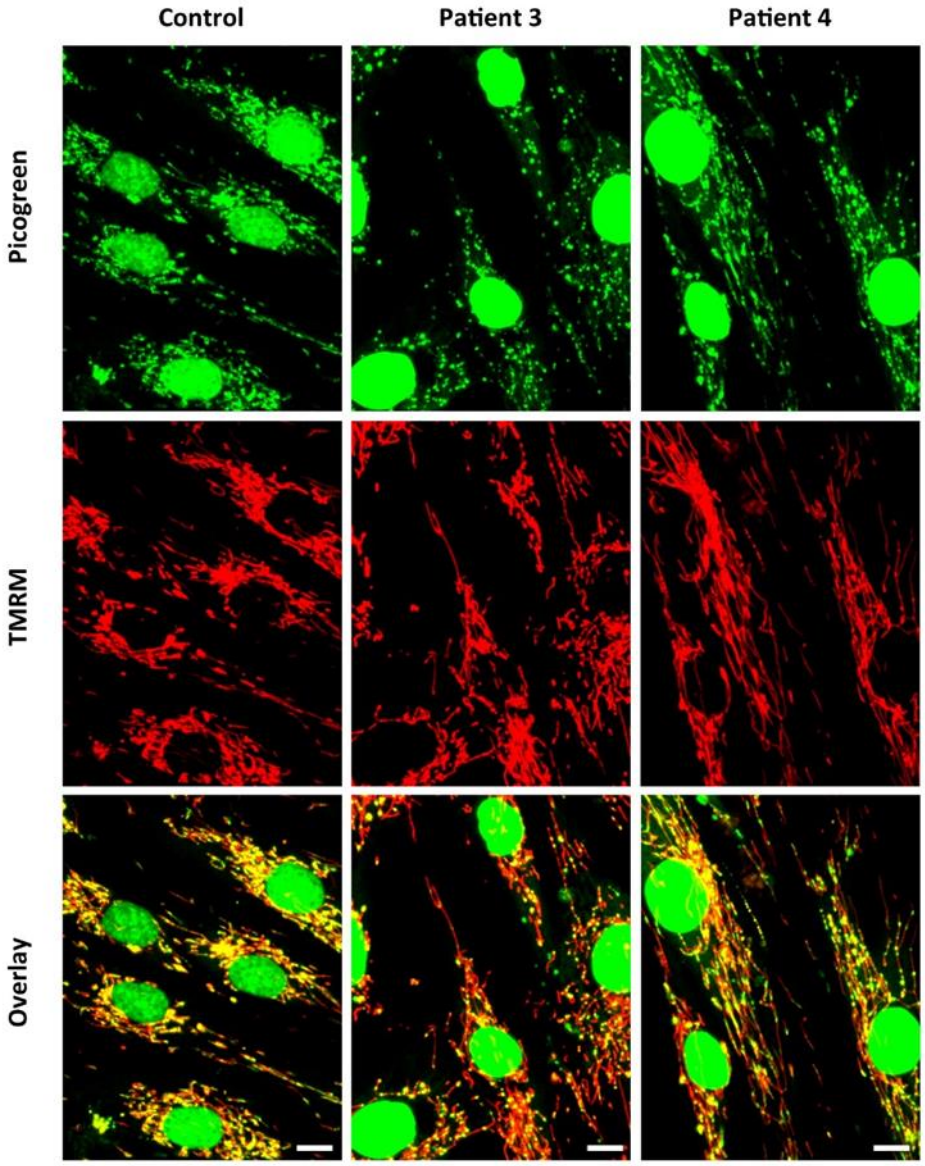

Figure 4.5: Nucleoid morphology and distribution in *POLG*-mutant fibroblasts from patients with late-onset Alpers. The upper panels show representative images of Picogreen staining of control (left), *POLG* patient 3 (p.(Ala467Thr)/p.(Ala467Thr)) (middle), *POLG* patient 4 (p.(Trp748Ser)/p.(Cys418Arg)) (right). Controls show normal morphology and distribution of nucleoids. *POLG* patients show similar numbers and distribution of nucleoids across the cell. The middle panels show TMRM staining, revealing normal mitochondrial networks in both *POLG* patients and controls. The lower panels show representative merged images. Images were captured at 63x magnification. Scale bar=10µm.

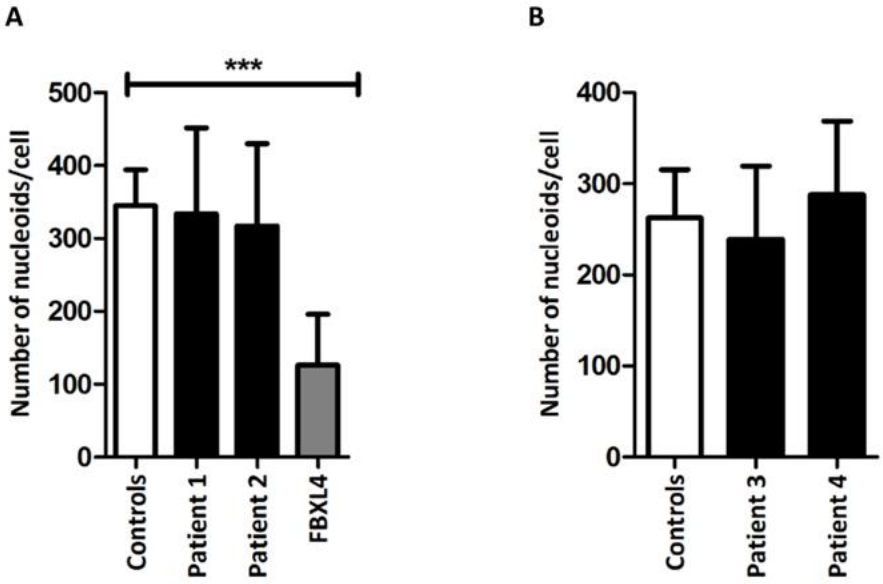

Figure 4.6: Quantitative analysis of number of nucleoids in early and late-onset *POLG*-mutant and early-onset *FBXL4*-mutant fibroblasts. Data are representative of mean nucleoid number per cell ± SD. (A) In the younger patient group there is no significant difference in the number of nucleoids between *POLG*-mutant fibroblasts and controls (p=0.6727). However, *FBXL4*-mutant fibroblasts have significantly fewer nucleoids per cell compared to controls and *POLG*-mutant fibroblasts as revealed by One-way ANOVA and Bonferroni correction test. ***=p<0.0001. (B) There is no significant difference in the number of nucleoids in *POLG*-mutant fibroblasts from late-onset patients with Alpers (p=0.1522, One-Way ANOVA and Bonferroni correction test). The number of nucleoids per cell was determined on unprocessed images using ImageJ. Data are represented as mean ± SD for n=20, from 2 biological repeats.

4.3.3 Motility Analysis of POLG-Mutant Fibroblasts derived from Patients with Alpers

Individual mitochondria from *POLG*-mutant fibroblasts were tracked by TMRM, videos were acquired on a confocal scanning point (NikonA1R) and motility parameters were calculated by IMARIS, as described in section 2.4.6. Motility tracking did not reveal any significant differences between patients and controls.

Mitochondria tracked in the *POLG*-mutant fibroblasts from patients 1 (p.(Ala467Thr)/p.(Thr914Pro)) and 2 (p.(Leu428Pro)/p.(Ala467Thr)) did not show any significant difference in speed compared to controls (p=0.1133, Kruskal- Wallis, Figure 4.7A). The average speed of the mitochondria tracked in patient 1 (p.(Ala467Thr)/p.(Thr914Pro)) was 1.70 µm/sec, in patient 2, 1.28 µm/sec, and in controls, 1.83 µm/sec. Similarly, there was no significant difference in mitochondrial track length (movement from point of origin) (p=0.3292, Kruskal-Wallis, Figure 4.7B) and in the volume occupied by mitochondria (p=0.1737, Kruskal-Wallis, Figure 4.7C) in both patients when compared to controls.

Motility analysis in the adolescent group did not reveal evidence of a difference in the speed (p=0.3679, Kruskal-Wallis, Figure 4.7D), mitochondrial track length (p=0.1561, Kruskal-Wallis, Figure 4.7E) and mitochondrial volume (p=1.0000, Kruskal-Wallis, Figure 4.7F).

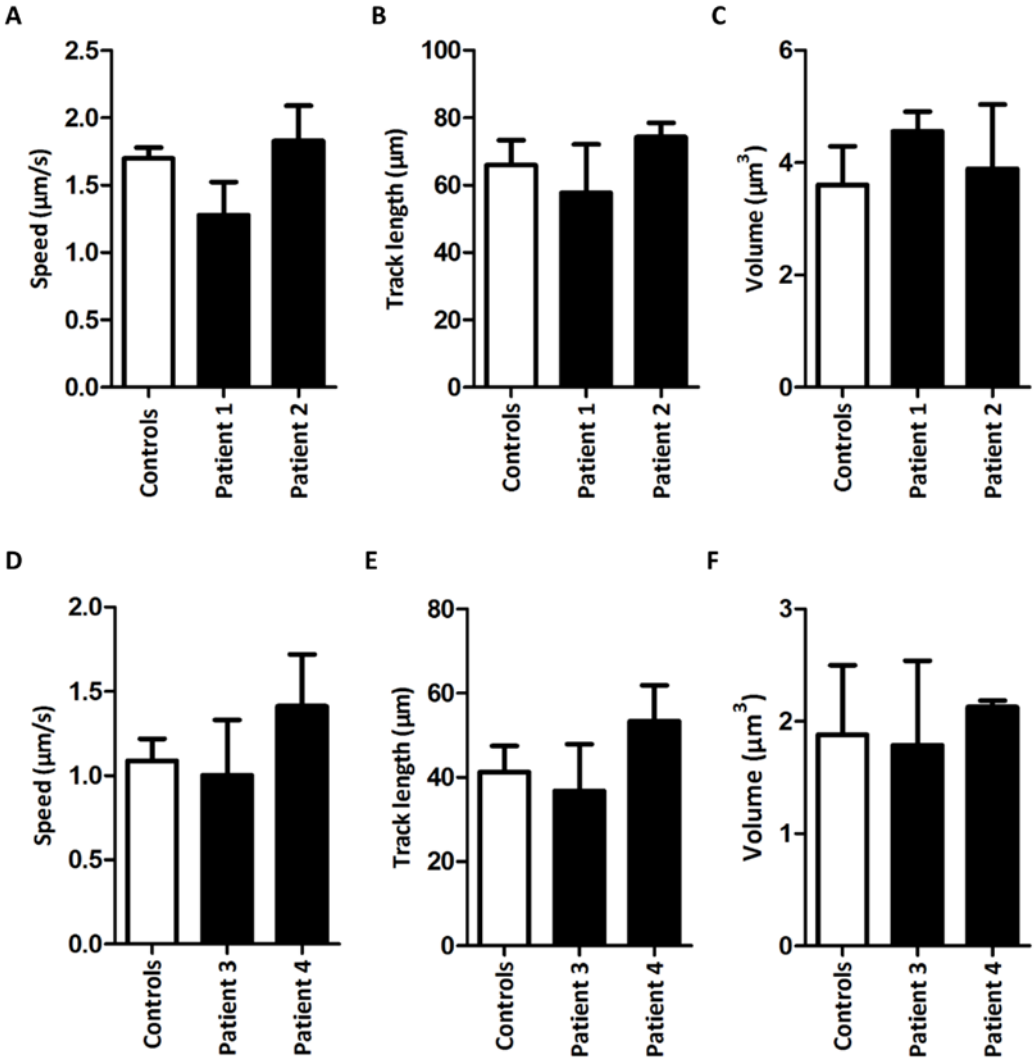

Figure 4.7: Quantification of mitochondrial motility in *POLG*-mutant fibroblasts derived from patients with Alpers. Tracks generated from videos of mitochondria within fibroblasts revealed no differences in (A and D) speed of mitochondria, (B and E) track length and (C and F) mitochondrial volume in all patients compared to controls as revealed by Kruskal-Wallis statistical test. All data are represented as mean ± SD from n=3.

4.3.4 Quantification of mtDNA Copy Number in POLG-mutant Fibroblasts from Patients with Alpers

To test the hypothesis that *POLG* mutations result in mtDNA depletion in Alpers, a previously described QPCR assay using an mtDNA target *Mitochondrially Encoded NADH Dehydrogenase 1* (*MT-ND1*) and the nuclear gene *Beta-2-microglobulin* (*B2M*) was performed in patient-derived fibroblasts as described in section 2.7.10.

Analysis was firstly performed on serum-fed (10% FCS) conditions in patients and controls. The mtDNA copy number was found to be similar to age-matched controls in both young (p=0.1479) and older (p=0.2521) patients, without any evidence of mtDNA depletion (as revealed by Kruskal-Wallis test, Figure 4.8A and C). The mtDNA copy number of patients 1 (p.(Ala467Thr)/p.(Thr914Pro)) and 2 (p.(Leu428Pro)/p.(Ala467Thr)) was 74% and 89% of the control mean respectively.

In the older group mtDNA copy number of patients 3 (p.(Ala467Thr)/p.(Ala467Thr)) and 4 (p.(Trp748Ser)/p.(Cys418Arg)) was found to be 88% and 106% of the control mean, respectively (see Table 4.2).

To overcome the limitation that the high mitotic rate of fibroblasts could mask any defects in the mtDNA, fibroblasts in serum-starved (0.1% FCS, 7 days) conditions were also analysed. Serum deprivation induces quiescence, therefore fibroblasts stop dividing and any defects may be unmasked.

Although mtDNA copy number in both patient fibroblasts and age-matched controls appeared to be lowered compared to serum-fed conditions, there was no significant difference in the mtDNA copy number of young (p=0.1931) and older (p=0.0608) patients when compared to controls (as shown by Kruskal-Wallis test, Figure 4.8B and D). Patients from both groups exhibited mtDNA copy number within the normal control range. Patient 1 (p.(Ala467Thr)/p.(Thr914Pro)) showed 84%, patient 2 (p.(Leu428Pro)/p.(Ala467Thr)) had 98% and patients 3 (p.(Ala467Thr))/p.(Ala467Thr)) and 4 (p.(Trp748Ser)/p.(Cys418Arg)) exhibited mtDNA copy number of 71% and 76% of the control mean respectively, as summarised in Table 4.2.

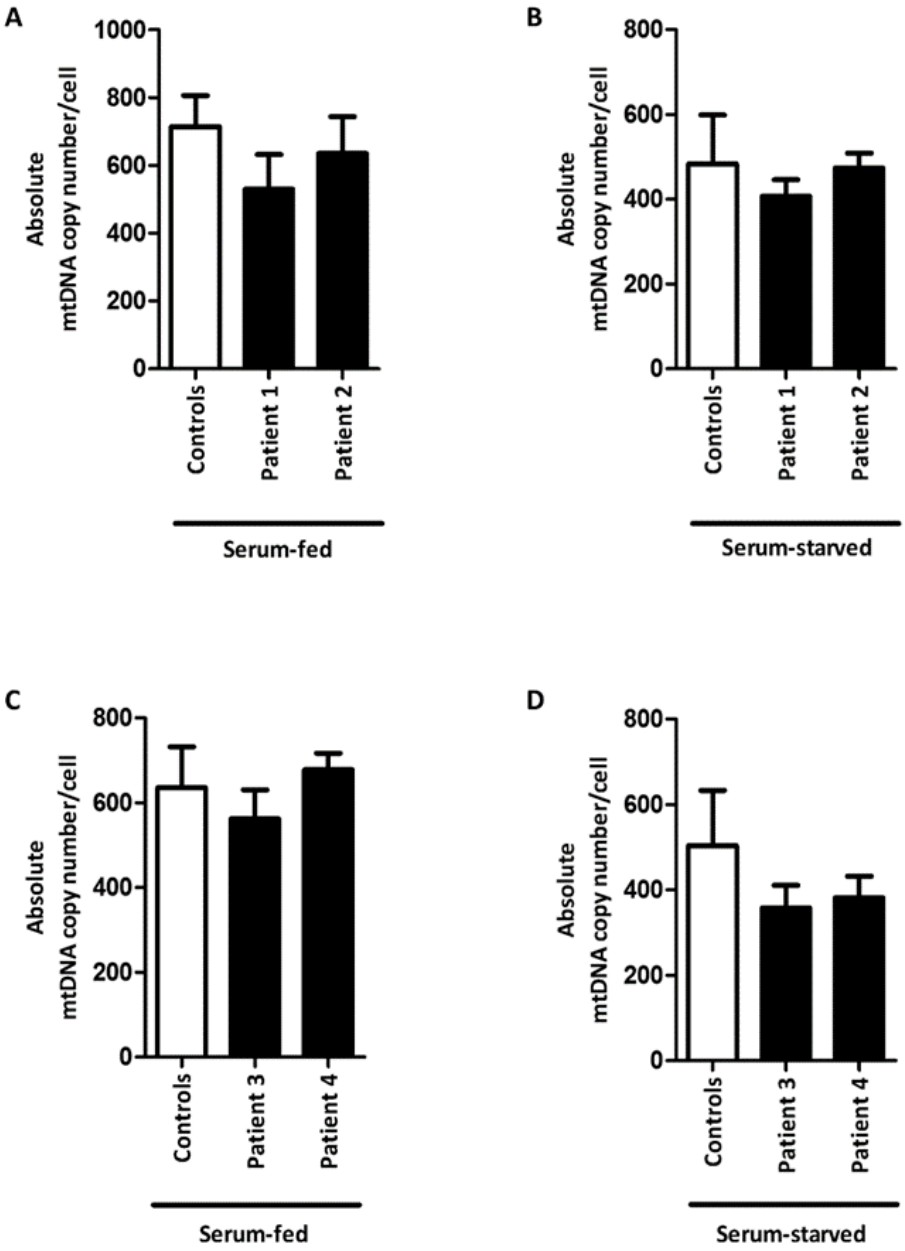

Figure 4.8: Quantification of mtDNA copy number in *POLG*-mutant fibroblasts from Alpers patients. Quantitative analysis did not reveal a significant difference in the mtDNA copy number of fibrobasts from (A) young patients 1 (p.(Ala467Thr)/p.(Thr914Pro)) and 2 (p.(Leu428Pro)/p.(Ala467thr)) in serum-fed conditions (10% FCS) compared to gender and age-matched controls (p=0.1479), (B) young patients 1 (p.(Ala467Thr)/p.(Thr914Pro)) and 2 (p.(Leu428Pro)/p.(Ala467Thr)) in serum-starved conditions (0.1% FCS) (p=0.1931). (C) Older patients 3 (p.(Ala467Thr)/p.(Ala467Thr)) and 4 (p.(Trp748Ser)/p.(Cys418Arg)) in serum-fed conditions (10% FCS, p=0.2521) compared to age-matched controls and (D) older patients 3 (p.(Ala467Thr)/p.(Ala467Thr)) and 4 (p.(Trp748Ser)/p.(Cys418Arg)) in serum-starved conditions (0.1% FCS, p=0.0608), as revealed by Kruskal-Wallis test. Data are represented as bars of mean absolute mtDNA copy number per cell ± SD from n=3.

mtDNA copy number (% of control mean)		
Patients	**Serum-Fed**	**Serum-Starved**
Patient 1	74 ± 14.34	84 ± 8.18
Patient 2	89 ± 15.14	98 ± 7.15
Patient 3	88 ± 10.83	71 ± 10.48
Patient 4	106 ± 6.13	76 ± 9.99

Table 4.2: Summary of mtDNA copy number (% of control mean) in *POLG*-mutant fibroblasts. Table showing mtDNA copy number of *POLG*-mutant fibroblasts as a percentage of the control mean ± SD from 3 biological repeats.

4.3.5 Bioenergetics of POLG-mutant Fibroblasts with Alpers

Mitochondrial bioenergetics was measured using the Extracellular Flux XF24 Seahorse Analyser (Agilent Technologies). Results did not reveal major changes in basal and maximal measurements between patients and controls (see Figures 4.9A and 4.10A).

In the younger group there was no significant difference in the basal oxygen consumption rate (OCR, p=0.1146, Kruskal-Wallis, Figure 4.9,), maximal OCR (p=0.5213, Kruskal-Wallis, Figure 4.9C) and ATP production by OXPHOS (p=0.3049, Kruskal-Wallis, Figure 4.9D) when compared to paediatric controls. Similarly, the spare respiratory capacity of *POLG*-mutant fibroblasts from patients 1 (p.(Ala467Thr)/p.(Thr914Pro)) and 2 (p.(Leu428Pro)/p.(Ala467Thr)) was not significantly different when compared to controls (SRC, p=0.7499, Kruskal-Wallis, Figure 4.9E).

Likewise, the fibroblasts from older patient 3 (p.(Ala467thr)/p.(Ala467Thr)) did not reveal any significant differences in basal OCR (0.3355, unpaired Student's t-test, Figure 4.10B), maximal OCR (p=0.8170, unpaired Student's t-test, Figure 4.10C), SRC (p=0.1291, unpaired Student's t-test, Figure 4.10D) and ATP production by OXPHOS (p=0.6629, unpaired Student's t-test, 4.10F) when compared to adult controls. A summary of the findings can be seen in Table 4.3.

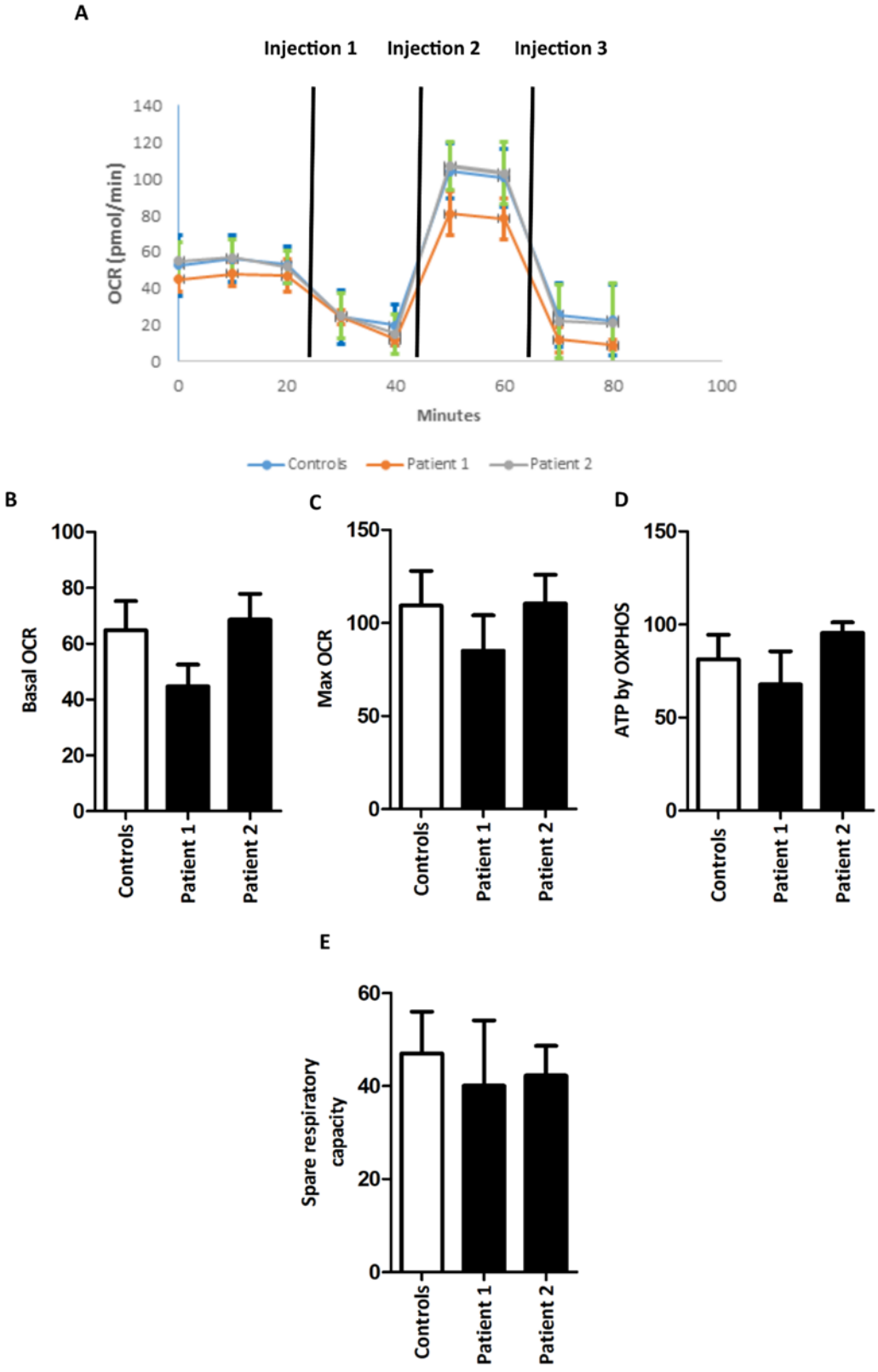

Figure 4.9: Bioenergetics of *POLG*-mutant fibroblasts derived from patients with early-onset Alpers. (A) Oxygen consumption rates (OCR) generated by the Seahorse XF24 Analyser. Injection 1=Oligomycin, Injection 2: FCCP, Injection 3: Rotenone/Antimycin. There is no significant difference in (B) Basal OCR (p=0.1146, Kruskal-Wallis), (C) Maximal OCR (p=0.5213, Kruskal-Wallis), (D) ATP produced by OXPHOS (p=0.3049, Kruskal-Wallis) and (E) SRC (p=0.7499, Kruskal-Wallis) between patient with early-onset Alpers and paediatric controls. Data are represented as mean ± SD from n=4. Key: OCR=oxygen consumption rate; SRC=spare respiratory capacity.

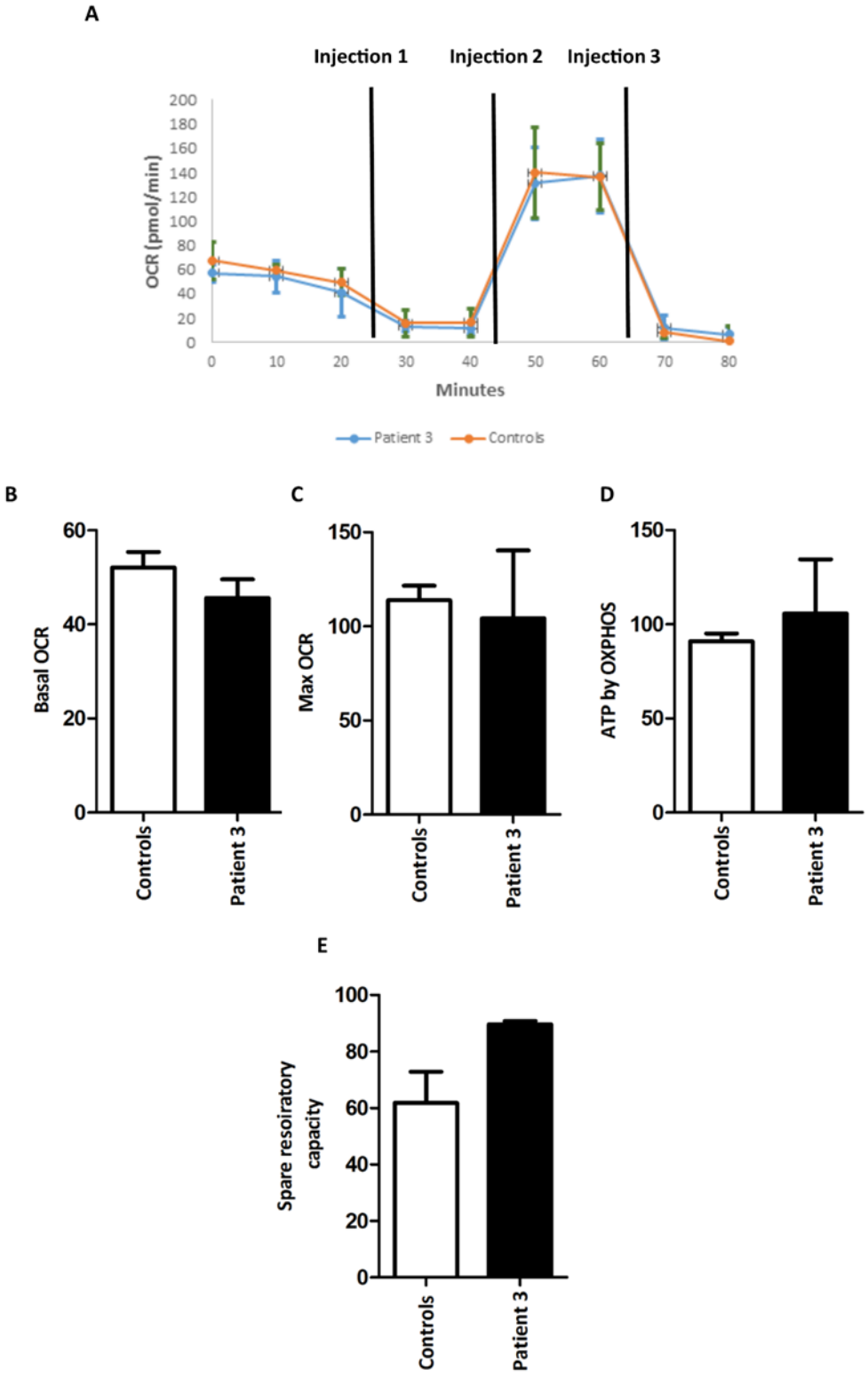

Figure 4.10: Bioenergetics of *POLG*-mutant fibroblasts derived from a patients with later-onset Alpers. (A) Oxygen consumption rates (OCR) generated by the Seahorse XF24 Analyser. Injection 1=Oligomycin, Injection 2: FCCP, Injection 3: Rotenone/Antimycin. There is no significant difference in (B) Basal OCR (p=0.335, unpaired Student's t-test), (C) Maximal OCR (p=0.8117, unpaired Student's t-test), (D) ATP produced by OXPHOS (p=0.6629, unpaired Student's t-test) and (E) SRC (p=0.1291, unpaired Student's t-test) between patient with later-onset Alpers and adult controls. Data are represented as mean ± SD from n=2.

Bioenergetic capacity (% of controls)				
Patients	**Basal OCR**	**Maximal OCR**	**SRC**	**ATP by OXPHOS**
Patient 1	68 ± 29.47	78 ± 34.68	85 ± 59.69	83 ± 49.21
Patient 2	105 ± 20.25	100 ± 28.25	90 ± 27.40	117 ± 12.82
Patient 3	88 ± 10.77	91 ± 44.90	145 ± 2.69	116 ± 44.81

Table 4.3: Bioenergetic capacity of *POLG*-mutant fibroblasts. Table illustrates OCR's as mean percentages of the control mean ± SD. Key: OCR=oxygen consumption rate; SRC=spare respiratory capacity.

4.3.6 Assessment of steady-state levels of POLG

To characterise the nature of *POLG* mutations on protein levels, protein extracts from control and patient-derived fibroblasts were analysed by western blotting. Qualitative assessment revealed similar levels of steady-state POLG (adjusted to loading control GAPDH) in both patient-derived and control fibroblasts (see Figure 4.11).

In lanes corresponding to controls 2 and 3 there is an impression of an additional band appearing on top of POLG, which could possibly suggest an additional isoform or that POLG is running as a doublet in the gel. However, the absence of such band in any other samples together with the fact that the two lanes referring to controls 2 and 3 are smudged, make it more probable that this is an artefact associated with the electrophoresis in these lanes, particularly as it is obvious from SDHA and GAPDH that they have very large amounts of protein. Whilst it may warrant further investigation, it is also relevant to mention that in the Ensembl Genome Browser (https://www.ensembl.org/Homo_sapiens/Gene/Summary?db=core;g=ENSG00000140521;r=15:89305198-89334861) no protein isoform has been described with a higher molecular weight than 140kDa, which reinforces the concept of the apparent higher band being an artefact.

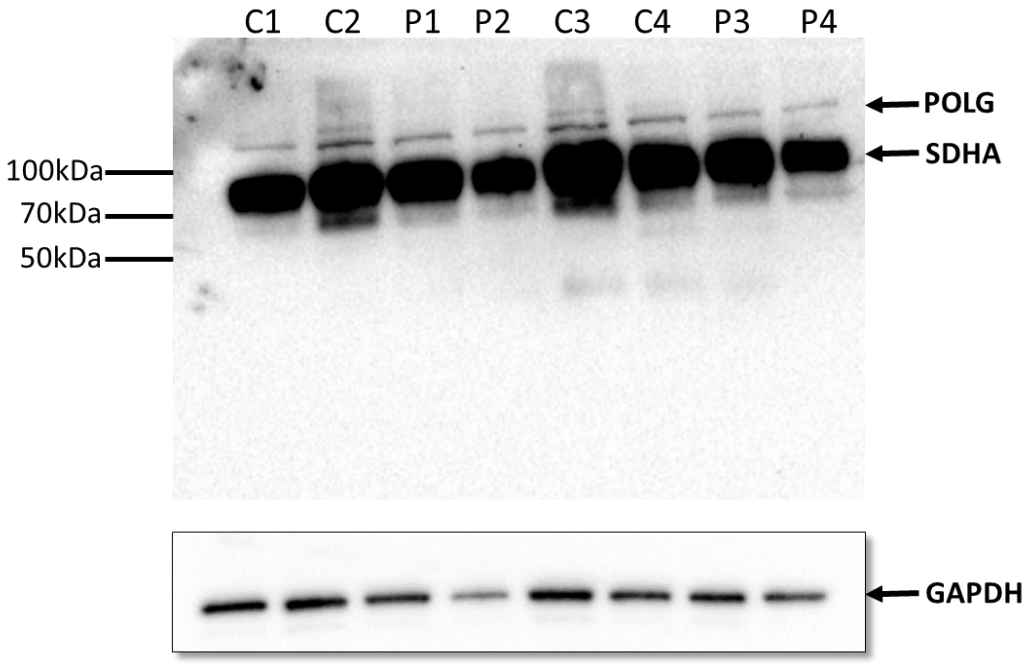

Figure 4.11: Characterisation of POLG steady-state levels in fibroblast from patients with Alpers. Western blot analysis of steady-state levels of POLG in fibroblast protein extracts (25µg) isolated from paediatric controls (C1, C2), adult controls (C3 and C4), early-onset patients with Alpers (P2, P3) and adolescent patients with Alpers (P3, P4). POLG bands corresponding to POLG, SDHA and GAPDH are marked by arrows. SDHA is a marker for mitochondrial respiratory chain complex II. GAPDH served as a loading control.

4.4 Discussion

Disorders of mitochondrial DNA (mtDNA) maintenance have emerged as major causes of mitochondrial disease. The commonest genetic defects responsible for autosomal recessive mtDNA depletion syndromes are considered to be mutations in the catalytic subunit of *POLG*, which lead to hepatocerebral and myopathic forms of disease (Cohen, 2014).

To date, over 200 *POLG* mutations have been reported and these are located all throughout the *POLG* domains which exert distinct function, including: exonuclease, linker and polymerase domains. Genotype to phenotype correlations have not been well established so far, while the exponential growth of the newly identified *POLG* mutations makes functional consequences of these substitutions challenging to investigate (Saneto and Naviaux, 2010; Saneto *et al.*, 2013).

Alpers' syndrome, is hallmarked by progressive deterioration and is considered to be the most severe form of mtDNA depletion, which is differentially expressed amongst tissues. The molecular mechanisms responsible for mtDNA depletion have not yet been identified. To date, most studies have focussed on post-mortem tissue from brain, liver and muscle biopsies from patients with *POLG*-related disease.

Several animal models have been created (Trifunovic *et al.*, 2004; Trifunovic *et al.*, 2005) to study the molecular effects of *POLG* mutations, however these models are limited as they do not recapitulate the epileptic phenotype seen in patients with Alpers and cannot explain the clinical heterogeneity caused by *POLG* mutations.

Fibroblasts derived from patients with *POLG* mutations are more easily available and may be useful to study the molecular defects of Alpers and *POLG*-related disease *in vitro*. Most studies on *POLG*-mutant fibroblasts have been limited to date (Ashley *et al.*, 2008; Schaller *et al.*, 2011; Stewart *et al.*, 2011), however there is some evidence supporting that the biochemical defects of *POLG* may be recapitulated in fibroblasts from some patients with Alpers (Ashley *et al.*, 2008; Horst *et al.*, 2014; Rouzier *et al.*, 2014).

This chapter sought to answer whether fibroblasts from patients with early and late-onset Alpers harbouring at least one of the most common *POLG* mutations in a homozygous or compound heterozygous state, express mitochondrial dysfunction. Investigation of the baseline mitochondrial function in all fibroblasts examined, did not

provide evidence of mitochondrial defects, hence supporting the hypothesis that *POLG* mutations lead to a phenotype through tissue-specific effects.

Mutations in nuclear-encoded genes involved in mtDNA maintenance have been shown to affect patient fibroblasts. Specifically, such mutations have been shown to impact on the dynamic mitochondrial networks, membrane potential, nucleoid distribution and OXPHOS machinery, secondary to mtDNA depletion (Bonnen *et al.*, 2013). Studies on *POLG*-mutant fibroblasts have not been frequently reported, however it has been demonstrated that fibroblasts do not express biochemical defects representative of the disease phenotype (Schaller *et al.*, 2011). In agreement with these observation, my findings did not reveal any evidence of mitochondrial dysfunction in *POLG*-mutant fibroblasts derived from patients with Alpers.

Ashley et al., reported mosaic mtDNA depletion, reduced COXI expression and reduced membrane potential in fibroblasts from four paediatric patients with early-onset Alpers (before 1 year of age) (Ashley *et al.*, 2008). My findings are in disagreement with these observations as I found no evidence of disturbed mitochondrial dynamics, nucleoid number/morphology and mtDNA depletion. However, fibroblasts in Ashley et al., did not harbour any of the common mutations present in the patients included in this study, while mtDNA depletion was evident in the fibroblasts from patients who were most severely affected by the disease and died by the age of 16 months (Ashley *et al.*, 2008).

Although genotype to phenotype correlations are poor, it has been demonstrated that patients who harbour both mutations in the linker region are associated with later onset and milder disease (Horvath *et al.*, 2006). Similarly, homozygous p.(Ala467Thr) mutations have been associated with later onset and longer survival (Tzoulis *et al.*, 2006; Ashley *et al.*, 2008; Anagnostou *et al.*, 2016).

In agreement with my findings there was no evidence of mtDNA depletion in the fibroblasts of an Alpers patient harbouring the p.(Ala467Thr) mutation, although mtDNA depletion was found in liver and muscle tissue (Schaller *et al.*, 2011). However, fibroblasts from a patient with a severe Alpers phenotype, harbouring the linker p.(Ala467Thr) mutation and the polymerase p.(Ser1095Arg) mutation in a compound heterozygous state, displayed CIII deficiency. This patient died at 7 years of age (Horst *et al.*, 2014). The variability of the findings described suggest that there are several factors which may influence the expression of the cellular phenotype. These include: location of the mutations within *POLG* and severity of the disease,

which may influence the expression of the cellular phenotype. However, the mechanisms leading to the cellular phenotype remain unidentified.

Further supporting the concept that fibroblasts are not always informative, mutations in other genes such as *FARS2* which also cause an early onset encephalopathy resembling Alpers, did not express any biochemical defects in fibroblasts (Almalki *et al.*, 2014). Interestingly, my findings showed that the steady state-levels of POLG in patient fibroblasts considered were not altered, suggesting that POLG is sufficiently expressed in fibroblasts. Although unclear, the different energy requirements in different tissue types may contribute to the tissue-specific effect.

In addition, my findings did not reveal any evidence of significant mtDNA copy number reduction or depletion in *POLG*-mutant patient-derived fibroblasts, even when the fibroblasts were examined in a quiescent state. These results suggest that mtDNA turnover is not compromised in fibroblasts by *POLG* mutations. Consistent with this finding, the mtDNA copy number in quiescent fibroblasts from a patient harbouring the common p.(Trp748Ser) mutation was similar to controls (Stewart *et al.*, 2011). Overall my findings suggest that *POLG* mutations do not mimic the biochemical phenotype of Alpers' syndrome, are not suitable for diagnostic purposes and are of limited value when characterising mitochondrial defects, secondary to *POLG* mutations.

Currently, it is not understood how *POLG* mutations exert a tissue-specific effect. The lack of biochemical phenotype in *POLG*-mutant fibroblasts could be explained by their fast-dividing nature, which may mask any mtDNA abnormalities. There are suggestions of a negative selection process occurring in fibroblasts, which tends to allow cells with high mtDNA copy number to divide, while the cells with the lowest levels do not survive (van den Heuvel *et al.*, 2004).

4.4.1 Limitations

A significant limitation of this work is the use of controls. These controls are disease-controls as they had been submitted to the Diagnostics Service due to suspicion of mitochondrial disease, even though metabolic defects were not detected in these cases. Normal controls are not easily accessible, especially when considering young infants, as biopsy is an unpleasant procedure for the patient. In addition, the controls were not age-matched, which makes results from control and experimental samples more challenging.

Another limitation of this study, is the use of TMRM for the analysis of mitochondrial networks. TMRM localises to the mitochondria in a membrane potential-dependent way. Therefore, any mitochondria with low membrane potential will be missed out from the analysis due to low/absent fluorescent signal. As such, the results of the present study may underestimate mitochondrial shortening/fragmentation in the case of a mitochondrial defect due to *POLG* mutations.

POLG levels assessed qualitatively by western blot in fibroblasts, did not show significant differences between patients and controls. However, it is noted that the blots were suboptimal with POLG appearing as a faint band at the expected molecular size (140kDa), and in addition in two lanes, there is a suggestion of an additional band higher than 140kDa. Whilst it is likely that POLG levels are similar in patients and controls, and that the additional band is due to artefact, further investigation is necessary in order to achieve a firm conclusion.

To address the limitations of the western blots presented, these could be repeated both with the same antibody and additional commercially available POLG antibodies (e.g. Polyclonal POLG antibody from Invitrogen; PA1-21791). If after repeating the experiments doubts subsisted regarding additional bands these could be assessed by cutting the band from the acrylamide gel and perform mass spectrometry, to determine whether this is likely to be the POLG peptide.

In summary, I report that *POLG* mutations do not cause significant alterations in POLG expression or significant mtDNA depletion. Therefore, mutant POLG is capable of synthesizing sufficient mtDNA in the fibroblasts from patients with Alpers harbouring the most common p.(Ala467Thr) or p.(Trp748Ser) mutations. As such, OXPHOS function is not impaired and energy production is sufficient to maintain mitochondrial networks. Consequently, fibroblasts are not a reliable model when investigating mitochondrial dysfunction seen in patients with Alpers. Considering using affected tissues may reveal biochemical defects, secondary to deleterious effects of *POLG* mutations.

4.4.2 Future Work

The current study investigated fibroblasts at baseline level, showing that *POLG*-mutant fibroblasts do not recapitulate the disease phenotype in the conditions described. Given the glycolytic nature of fibroblasts, galactose-medium has been established as a carbon source which forces cells to rely on OXPHOS rather than

glycolysis (Aguer *et al.*, 2011). Interestingly fibroblasts from patients with chronic progressive external ophthalmoplegia (CPEO), encephalopathy and parkinsonism harbouring mutations in the *OPA1* gene, showed increased mitochondrial fragmentation after 48 hours of incubation in galactose medium compared to controls (Carelli *et al.*, 2015). This would be a possible strategy to see whether *POLG*-mutant fibroblasts demonstrate mitochondrial defects when cultured in galactose-medium.

To verify the findings on mitochondrial networks, MitoTracker Green, a dye which localises into the mitochondria in a membrane potential-independent manner could be used in combination or as an alternative approach to TMRM. In this case, mitochondria regardless of membrane potential would be considered for mitochondrial network analysis giving a more accurate picture of the effect of *POLG* mutations on mitochondrial networks.

To verify the findings on mitochondrial networks, MitoTracker Green, a dye which localises into the mitochondria in a membrane potential-independent manner could be used in combination or as an alternative approach to TMRM. In this case, mitochondria regardless of membrane potential would be considered for mitochondrial network analysis giving a more accurate picture of the effect of *POLG* mutations on mitochondrial networks.

Although *POLG*-mutant fibroblasts are not suitable for understanding the tissue-specific pathogenesis of Alpers, they can be converted into other cell lineage such as neurons and hepatocytes through induced pluripotent stem cell technologies (Li *et al.*, 2015; Zurita *et al.*, 2016) or direct differentiation methods (Huang *et al.*, 2014; Meyer *et al.*, 2014), which are discussed in more detail in the next chapter. Using this approach, the effect of *POLG* mutations on specific cell types can be investigated and provide insight into the molecular pathogenesis of Alpers.

4.4.3 Conclusions

In this study the phenotypic characterisation of baseline mitochondrial function in *POLG*-mutant fibroblasts derived from patients with Alpers harbouring the common p.(Ala467Thr) or p.(Trp748Ser) mutation was performed. This is the only detailed study to date that investigated mitochondrial function in fibroblasts including OXPHOS activity, mtDNA depletion, mitochondrial morphology and POLG function. Collectively I report no evidence of significant mitochondrial dysfunction in *POLG*-mutant fibroblasts from early and late-onset Alpers patients. I suggest that *POLG*

mutations do not cause mtDNA depletion in fibroblasts, therefore ATP is sufficiently produced, maintaining normal mitochondrial networks. These findings further support the idea that fibroblasts do not recapitulate *POLG*-disease and therefore are not suitable when investigating the molecular pathogenesis of *POLG*-related disease at least under the experimental conditions described.

Chapter 5 Conversion of *POLG*-mutant Fibroblasts derived from Patients with Alpers into Induced Neuronal Progenitor Cells (iNPC's)

5.1 Introduction

The pathogenesis of mitochondrial disease and neurological disorders is particularly challenging to elucidate due to the scarcity of brain tissue and relevant cell types. The urgent need to understand pathological processes has led to the discovery of somatic cell reprogramming through various technologies (Takahashi *et al.*, 2007; Yu *et al.*, 2007; Vierbuchen *et al.*, 2010). These discoveries, have allowed the development of *in vitro* disease models, which serve to elucidate specific functions of the Central Nervous System (CNS) (Mertens *et al.*, 2016).

A decade ago, Takahashi and Yamanaka developed the technology of induced pluripotent stem cells (iPSC's), which enables the induction of pluripotency by the expression of specific transcription factors (Takahashi *et al.*, 2007), thus creating new opportunities in disease modelling and regenerative medicine (Takahashi and Yamanaka, 2013).

Direct conversion technologies (Lu *et al.*, 2013; Meyer *et al.*, 2014), are an extension to the iPSC reprogramming, however these involve the overexpression of transcription factors, which direct cellular identity towards specific cell lineages, bypassing the pluripotency state and most developmental stages (Takahashi and Yamanaka, 2013). Such techniques have been useful in elucidating disease mechanisms, nevertheless they have their own limitations such as the use of viral vectors, which are associated with tumourigenicity, limited proliferation capacity and limited cell type differentiation. (Lu *et al.*, 2013; Kelaini *et al.*, 2014).

Direct conversion into induced neuronal progenitors (iNPC's) is achieved using fibroblasts, which are neural-crest derived cells. iNPC's can further be differentiated into neurons, oligodendrocytes and astrocytes, enabling the investigation of neural activity.

To date, *in vitro* neuronal models of *POLG*-related disease do not exist; while animal models are limited in recapitulating the encephalopathic phenotype observed in patients. As such, *in vitro* models are useful in understanding the effects of *POLG* mutations on neuronal function.

5.2 Aims and Objectives

Given that *POLG*-mutant fibroblasts (discussed in Chapter 4) did not demonstrate evidence of mitochondrial dysfunction, it was hypothesised that the effect of *POLG* mutations may be exacerbated in neurons and mutant neurons could recapitulate the disease phenotype. To test this hypothesis and create patient-specific *in vitro* models of Alpers secondary to *POLG* mutations, conversion of *POLG*-mutant fibroblasts into iNPC's was attempted using direct conversion methodology.

5.3 Results

5.3.1 Conversion of Human Patient-derived Fibroblasts into iNPC's using Retroviral and Sendai Virus Treatment

In order to convert fibroblasts into iNPC's a collaboration was established with Professor Rita Horvath and Dr. Veronika Boczonadi (Institute of Genetic Medicine, Centre for Life, Newcastle upon Tyne).

Direct conversion was performed using retroviral treatment of vectors for the transcription factors OCT3, SOX2, KLF4 and c-MYC, following growth in neuronal progenitor medium containing Fibroblast Growth Factor 2 (FGF-2) and Epidermal Growth Factor (EGF) as previously described (Meyer *et al.*, 2014). The retrovirus used was custom-made and a generous gift from Dr. Meyer's lab at Nationwide Children's Hospital (Columbus, Ohio) to Professor Horvath's group. The details of the retrovirus have not been included in this thesis as they are at present confidential. The conversion of cells from two paediatric controls and two early-onset patients with Alpers (see Table 5.1) was performed by Dr. Veronika Boczonadi.

Case	Age at Skin Biopsy	*POLG* Mutations	Location	Status
Patient 1	1 month	p.(Ala467Thr)/ p.(Thr914Pro)	Linker/Polymerase	Compound heterozygous
Patient 2	1 year	p.(Leu428Pro)/ p.(Ala467Thr)	Linker/Linker	Compound heterozygous
Control 1	6 months	N/A	N/A	N/A
Control 2	8 months	N/A	N/A	N/A

Table 5.1:Characteristics of patient and control fibroblasts used in this study. Key: N/A=not applicable.

Briefly, the protocol involved the seeding of 1 x 10^4 fibroblasts into a well of six-well plate for one day. On the following day, a mixture containing the retroviral vectors was applied and cells were incubated overnight. On day 3, cells were washed with Phosphate Buffered Saline (PBS) and treated with regular fibroblast medium (DMEM+10% Fetal Bovine Serum (FBS)) to recover for three days. Cells were washed with (PBS) before the fibroblast medium was replaced by Neuronal Progenitor Cell (NPC) medium (DMEM/F12, 1% N2, 1% B27, 20 ng/mL FGF-2, 20

ng/ml EGF, and heparin (5 µg/mL)) on a daily basis. The cells were monitored and once sphere-like structures appeared, the cell culture was lifted with accutase, centrifuged and re-suspended in NPC conversion medium and re-plated in two wells pre-coated with fibronectin. Once the NPC culture was established (Day 10), the cells were cultured by myself in NPC medium containing DMEM/F12, 1% N2, 1% B27, and FGF-2 (40 ng/ml) only.

Only fibroblasts from control 1 and patient 1 (p.(Ala467Thr)/p.(Thr914Pro)) underwent morphological changes as shown in Figure 5.1. On day 10, appeared neurosphere-like structures appeared, however these structures were lost later, on day 15 with eventual death of cells. Fibroblasts from control 2 and patient 2 (p.(Leu428Pro)/p.(Ala467Thr)) did not form neurospheres, despite morphological changes being evident (day 8-10) as shown in Figure 5.1.

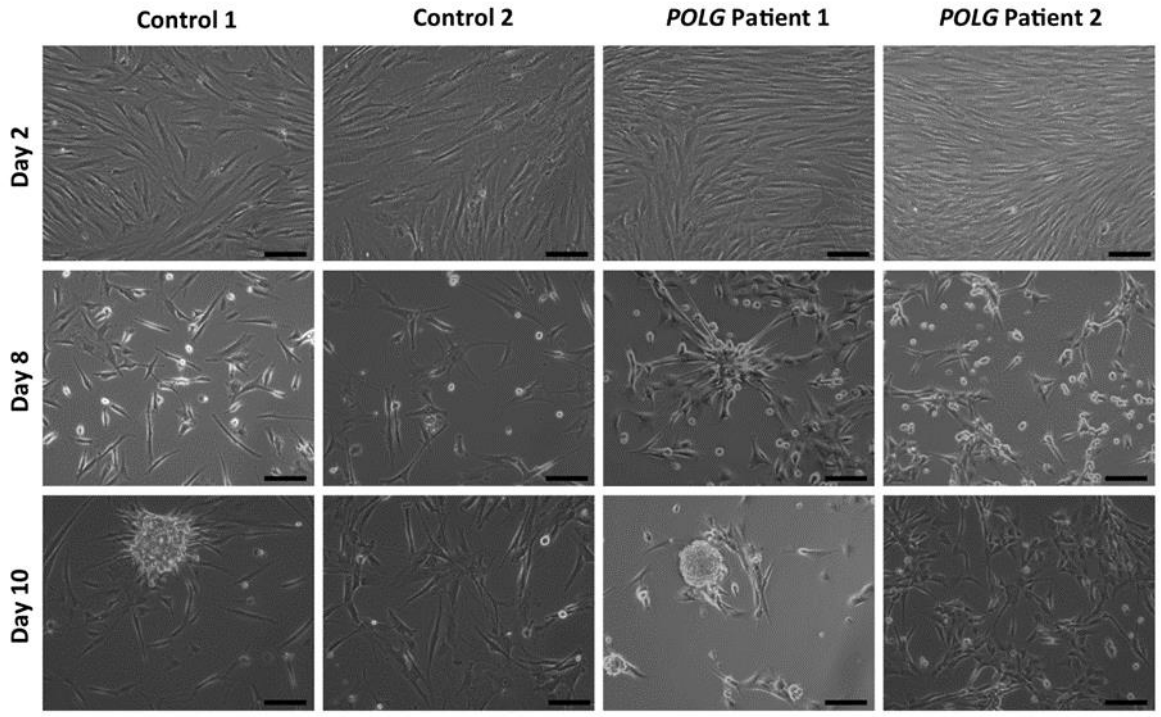

Figure 5.1: Conversion of *POLG*-mutant fibroblasts into iNPC's using retroviral treatment. Representative images of cells from controls and patients with *POLG* mutations and early-onset Alpers undergoing conversion from fibroblasts into iNPC's. On day 2 post- transfection, control and *POLG*-mutant fibroblasts displayed typical fibroblast morphology. On day 8 morphological changes are evident in all fibroblasts. Neurosphere-like structures started forming in patient 1 (p.(Ala467Thr)/p.(Thr914Pro)) and patient 2 (p.(Leu428Pro)/p.(Ala467Thr)). On day 10, neurospheres were formed in control 1 and patient 1. Fibroblasts from control 2 and patient 2 did not reach the state of neurosphere formation. Images were captured at 10x magnification using brightfield microscope (Axiovert 200 Zeiss). Scale bar=50µm.

A second attempt by Dr. Veronika Boczonadi involved conversion of another batch of *POLG*-mutant cells using twice the amount of retroviral vectors; however morphological changes did not appear and iNPC's were not formed (data not shown).

Given the unsuccessful conversions as described above, further attempts were performed by Dr. Veronika Boczonadi which involved replacing the retrovirus with the commercially available Sendai virus (ThermoFisher Scientific; AB34546). Sendai virus is a parainfluenza virus type I, 150-250nm in diameter, consisting of a single 15,384 bases long chain of RNA.

POLG-mutant fibroblasts successfully formed neurospheres on day 10 only for patient 1(p.(Ala467Thr)/p.(Thr914Pro)) (see Figure 5.2). Fibroblasts from patient 2 (p.(Leu428Pro)/p.(Ala467Thr)) failed to form neurospheres. In the case of patient 1 (p.(Ala467Thr)/p.(Thr914Pro)), although the culture was established and neurospheres were formed on day 10, the neurospheres failed to expand, started shrinking in size from day 15 and lost neurosphere-like morphology on day 20, eventually dying. Controls were not used at this attempt; as only late passage cells were available.

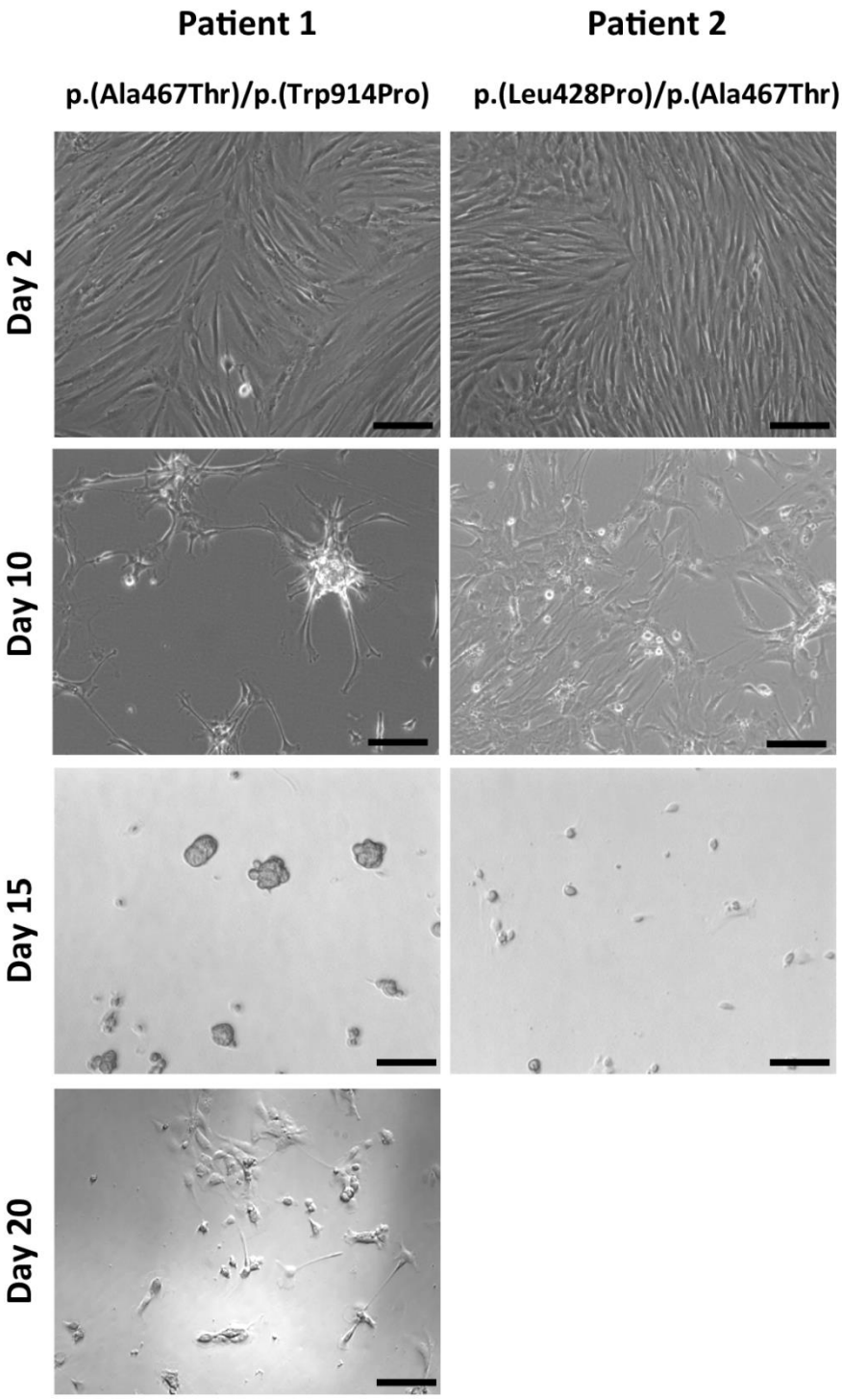

Figure 5.2: Conversion of *POLG*-mutant fibroblasts using Sendai virus. Representative images of conversion of *POLG*-mutant fibroblasts from patients with early-onset Alpers into iNPC's using Sendai virus. On day 2 post-treatment with Sendai virus, fibroblasts from both patients displayed fibroblast-like morphology. On day 10, neurospheres were formed in fibroblasts from patient 1. Patient 2 showed some morphological changes although neurospheres were not evident. On day 15, neurospheres from patient 1 started shrinking and cells from patient 2 were lost. On day 20, cells from patient 1 lost neurosphere-like morphology and eventually died. Images were captured at 10x magnification using brightfield microscope (Axiovert 200 Zeiss). Scale bar=50µm.

5.3.2 Conversion of POLG-mutant Fibroblasts into iNPC's using Sendai Virus

Given that the protocol discussed above failed to establish iNPC's, an alternative protocol was used as previously published (Lu *et al.*, 2013). In order to test whether the nature of the *POLG* mutations could be responsible for the unsuccessful conversion, fibroblasts from an adolescent patient with Alpers harbouring homozygous p.(Ala467Thr) mutations were selected for conversion. These fibroblasts were selected based on evidence that homozygous p.(Ala467Thr) mutations are associated with later disease onset and longer survival (Tzoulis *et al.*, 2006; Anagnostou *et al.*, 2016). The treatment with Sendai virus was performed by myself under the supervision of Dr. Veronica Boczonadi. The protocol is detailed in section 2.3.5. Controls were not suitable for conversion due to late passage.

Fibroblasts underwent morphological changes from day 1-7 post-transfection. On day 9 neurospheres started forming as illustrated in Figure 5.3. On day 15, neurospheres were large enough to be selected using a pipette and transferred into wells pre-coated with laminin for further expansion. However, the neurospheres did not attach to the wells, even when the concentration of laminin was increased (100µg/ml). The remaining neurospheres in iNPC culture started losing neurosphere morphology (day 20), resembling fibroblasts and showing signs of cell death (Figure 5.3).

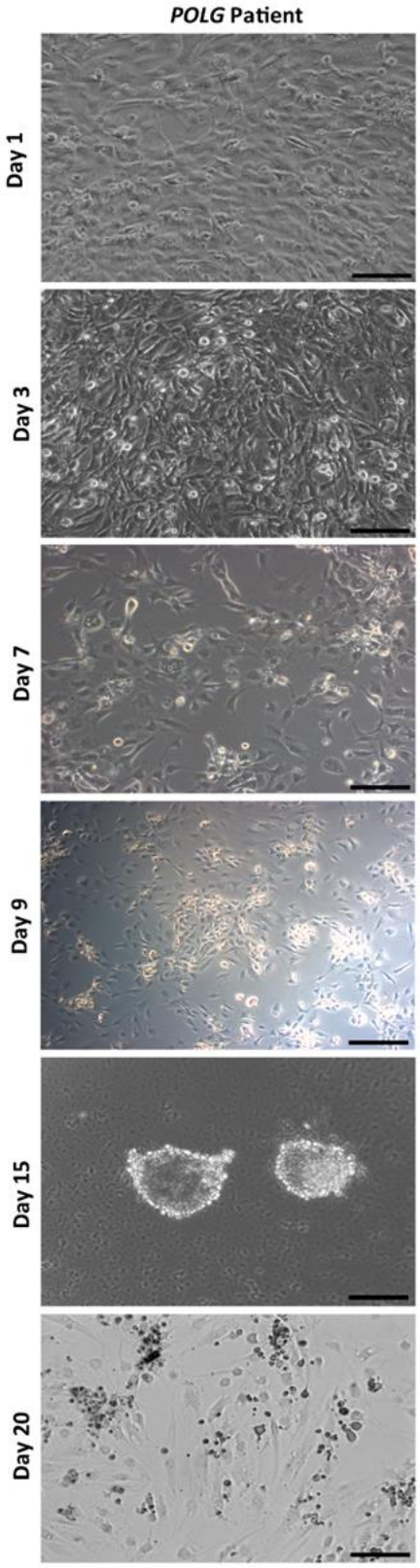

Figure 5.3: Timeline of conversion of fibroblasts with the homozygous p.(Ala467Thr) mutations from an adolescent patient with Alpers into iNPC's using Sendai virus. Representative images of fibroblast conversion into iNPC's. Fibroblasts underwent morphological changes from day 1-7 post-transfection. On day 9 post-transfection, neurospheres started forming. On day 15, neurospheres were large enough to be selected and expanded. However, neurospheres did not attach to the wells and the remaining neurospheres in iNPC culture converted back into fibroblasts and eventually died. Images were captured at 10x magnification using brightfield microscope (Axiovert 200 Zeiss). Scale bar=50µm.

5.4 Discussion

This chapter focussed on the attempt to directly convert *POLG*-mutant fibroblasts into induced neuronal progenitor cells (iNPC's). Two different protocols were selected for direct conversion; however, these did not yield in iNPC colonies.

Direct conversion has been shown to be an efficient and rapid technique in converting fibroblasts into specific cellular types including cardiomyocytes, hepatocytes and neurons. Direct conversion involves either the ectopic expression of lineage-specific transcription factors or micro-RNA's (Vierbuchen *et al.*, 2010; Pang *et al.*, 2011; Xue *et al.*, 2013).

In this work, neurospheres were formed using both protocols, however failed to expand into iNPC colonies. Using the protocol by Meyer et al., where iNPCs' were created with the potential of differentiating into neurons, astrocytes and oligodendrocytes (Meyer *et al.*, 2014), fibroblasts underwent morphological changes and formed neurospheres. However, the latter failed to expand into iNPC colonies.

The factors responsible for failure in establishing iNPC cultures is unclear. In the first attempt, the failure could be linked to the use of the retrovirus, however when a different batch of retroviruses was used for conversion, it also failed. As both control and patient fibroblasts did not convert into iNPC's it is likely that the protocol requires optimisation. One explanation, as previously, could be the late passage of cells, especially in the case of control 2 and patient 2, which did not reach the state of neurosphere formation. Regrettably, at the time of conversion, earlier passage fibroblasts were not available.

Since retroviral treatment was not effective in converting fibroblasts from the current work into iNPC's, a different approach was used involving Sendai virus treatment. As with the previously mentioned approach, the use of Sendai virus did not result in successful conversion. The reasons behind the failure remain unclear. Nevertheless, one explanation could be the late passage of cells used, which is supported by the fact that control 2 (passage 12) and patient 2 (passage 10) did not form any neurospheres. At the time of conversion, earlier passage fibroblasts were not available.

To overcome these limitations, an additional protocol subsequently to the one used after Sendai virus was considered, which involved mixture of different growth factors to directly convert into iNPC's. Although this method initially seemed promising with

large neurospheres forming by day 15, the neurospheres did not reach the state of being large enough and could not be observed by eye. Therefore, I attempted to select the neurospheres by pipette and expand them further. However, when these were placed in wells pre-coated with laminin, the neurospheres failed to attach, even when the concentration of laminin was increased. It is unclear why the neurospheres did not attach, as the neurospheres were picked from a laminin-coated well. To test whether the coating was unsuitable, other coating reagents could be used in future (Zurita *et al.*, 2016).

It is important to note that in this attempt, controls were not used, therefore it is possible that the reason behind the inability of fibroblasts to successfully convert into iNPC's is due to the nature of *POLG* mutations. The fibroblasts selected for conversion were early passage cells (passage 6) from a patient with a homozygous p.(Ala467Thr) mutation, which is associated with milder phenotype compared to compound heterozygous mutations (Tzoulis *et al.*, 2006; Anagnostou *et al.*, 2016). The fibroblasts from this patient were selected as it was hypothesised that if the homozygous p.(Ala467Thr) mutation has a milder effect, it would be easier to convert the cells into iNPC's for further investigation. Unfortunately, this was not the case, highlighting the difficulty of creating *in vitro* models by direct differentiation methods.

Direct conversion can be a rapid and cost-efficient method to create neurons, however it has its own limitations. These include: restricted proliferative capacity, senescence and limited cell type diversity.

A recent study demonstrated the conversion of homozygous p.(Trp748Ser) fibroblasts into iPSC's (Zurita *et al.*, 2016). Although iPSC's are more expensive and do not convert as rapidly as with direct conversion methodologies, using iPSC's could be an alternative option to produce patient-specific neurons. Using the iPSC approach may be beneficial when considering differentiation into specific neuronal sub-types, given the limited cell type diversity achieved using the direct conversion methods. If neurons are successfully generated, then mitochondrial dysfunction in *POLG*-mutant neurons would be an interesting area to investigate and may result in a suitable model for initial testing of novel therapies.

Finally, since this work could not expand further in the creation of a patient-specific *POLG*-mutant *in vitro* model, post-mortem tissue was selected as an alternative approach.

In the quest to understand the pathogenesis of epilepsy in Alpers' syndrome, the following chapters will discuss the characterisation of mitochondrial dysfunction in post-mortem brain tissue from patients with Alpers.

Chapter 6 Mechanisms of Neurodegeneration in Patients with Alpers and *POLG* Mutations: Assessment of Respiratory Chain Deficiency and MtDNA Damage

6.1 Introduction

Currently, the molecular pathomechanisms underlying *POLG*-related encephalopathy are not well understood. The study of *POLG*-related encephalopathy is limited by the scarcity of brain tissue and the lack of accurate cellular models, particularly given that defects often detected in the tissue are not expressed in cell culture. Similarly, animal models recapitulating the phenotype of *POLG*-related encephalopathy are lacking.

Patients with *POLG* mutations harbour mtDNA defects and respiratory chain deficiencies to a variable extent, depending on the tissue type (see Chapter 3). Most studies have focused on liver, muscle and fibroblasts. Respiratory chain deficiencies involving complexes I-IV and CV defects are common in liver and muscle with evidence of mtDNA depletion (Sarzi *et al.*, 2007; Scalais *et al.*, 2012; Rouzier *et al.*, 2014). However, mtDNA copy number and respiratory chain function in muscle and fibroblasts can often be inconsistent and may appear normal (Kollberg *et al.*, 2006; Tang *et al.*, 2011), even in late disease stage (Schaller *et al.*, 2011). It is important to mention here that most studies are case studies involving a single patient or small number of patients and in the majority of these studies, the molecular investigations performed are not patient or tissue-matched. Therefore, reproducing and correlating the findings remains challenging.

The defects occurring as a result of *POLG* mutations in the central nervous system have not been well characterised due to the lack of post-mortem brain tissue availability. To date, only a few reports exist on human neuronal mtDNA content and deletion levels, respiratory chain protein expression and *POLG* mutations. One study demonstrated a mild decrease (30% mtDNA reduction when compared to the control mean) in the mtDNA copy number in frozen frontal lobe homogenate from a patient with Alpers, harbouring homozygous p.(Ala467Thr) mutations (Ferrari *et al.*, 2005).

Another study by Hakonen and colleagues showed a mild reduction in mtDNA copy number in the cerebellum of a MIRAS patient with homozygous p.(Trp748Ser) mutations but mtDNA copy number was found to be within the normal range of controls in the frontal lobe of the patient (Hakonen *et al.*, 2008). These findings were

coupled with complex I deficiency in neurons from both the cerebellum and frontal cortex. In addition, brain tissue from a patient with homozygous p.(Ala467Thr) mutations showed reduced complex III activity in another study (Blok *et al.*, 2009).

A more recent study described respiratory chain deficiencies involving complex I and to a lesser extent complex IV, associated with mtDNA depletion in brain homogenates and micro-dissected neurons (Tzoulis *et al.*, 2014). Interestingly mtDNA deletions were detected only in patients with late- onset Alpers in the presence of depletion suggesting that deletions may accumulate with age. In agreement, neurons from the dorsal root ganglia from an adult patient with *POLG*-related disorder showed a decrease of 50% in mtDNA content in the presence of deletions and respiratory chain deficiencies involving complexes I and IV (Lax *et al.*, 2012b). More recently Lax and colleagues used a quantitative, quadruple immunofluorescent method to assess complex I and complex IV respiratory chain protein expression in conjunction with mitochondrial mass within GABAergic interneurons of adult patients with mitochondrial disease, including adult patients harbouring *POLG* mutations (Lax *et al.*, 2016). Results revealed extensive respiratory chain deficiencies, which were more profound for complex I, a finding consistent with previous reports (Hakonen *et al.*, 2008; Tzoulis *et al.*, 2014).

GABAergic interneurons are believed to modulate excitation and inhibition in the cerebral cortex. Under normal conditions, interneurons exert their function by modulating pyramidal neurons via GABAergic neurotransmission. The role of interneurons in epileptogenesis has well been characterised, as it has been shown that interneuron loss disrupts neuronal networks in the epileptic hippocampus (Marx *et al.*, 2013). Given their high metabolic activity to sustain oscillatory activity, interneurons are vulnerable to complex I and IV deficiencies, highlighting their dependence on OXPHOS (Kann *et al.*, 2011; Whittaker *et al.*, 2011). The findings from Lax and colleagues suggest mitochondrial dysfunction within GABAergic interneurons, which may contribute to impaired neuronal oscillations leading to the development of the neurological deficits seen in patients (Lax *et al.*, 2016).

Neurological involvement is a prominent feature of Alpers, thus it was hypothesised that mitochondrial dysfunction may underlie impairment of neuronal networks and contribute to epilepsy seen in Alpers. Dr. Hayhurst and Dr. Lax investigated respiratory chain deficiencies within GABAergic interneurons, pyramidal neurons and Purkinje cells from 12 patients with clinically and/or genetically defined Alpers using

the pre-validated protocol by Lax and colleagues (Lax *et al.*, 2016). The occipital lobe was selected, due to the previously documented clinical involvement of this brain region. In addition, respiratory chain deficiency was examined in Purkinje cells of the cerebellum of the patients as this region has been reported to be affected to a variable extent. Results revealed deficiencies involving complex I and to a lesser extent complex IV, in interneurons of the occipital lobe and in Purkinje cells of the cerebellum. Pyramidal neurons of the occipital lobe were found to be complex I and IV deficient, however to a lesser extent when compared to interneurons (courtesy of Hayhurst and Lax).

Patients with Alpers demonstrate mitochondrial respiratory chain deficiencies in the occipital lobe and cerebellum which correlate with the clinical picture. Specifically, the occipital lobe defects are associated with visual loss and epilepsy, and the cerebellum dysfunction explains ataxia seen in patients. The pathology of other brain regions including parietal and frontal lobes from patients with Alpers have rarely been investigated (Hunter *et al.*, 2011; Sofou *et al.*, 2012; Rajakulendran *et al.*, 2016). These areas are important in coordinating cognitive functions and is important to investigate the extent of mitochondrial dysfunction within these regions to better understand the mechanisms of disease progression.

6.2 Aims

This chapter will test the hypothesis that mitochondrial respiratory chain deficiencies in interneurons and pyramidal neurons from the occipital, parietal and frontal lobes contribute to altered neuronal dynamics giving rise to epilepsy and cognitive impairment in patients with Alpers. The contribution of mtDNA damage as an underlying mechanism will also be examined. Cases 8, 13 and 14 have been previously studied by Lax and colleagues (Lax *et al.*, 2016). This work aims to:

1) Confirm a genetic diagnosis of mutations in *POLG* mutations in the cases where one is not available.
2) Assess the degree of respiratory chain deficiencies between different brain regions (occipital, parietal and frontal lobes) using a robust, quantitative, immunofluorescent approach.
3) Quantitatively assess mtDNA abnormalities (depletion and deletions) in brain tissue homogenates from occipital, parietal and frontal lobes from adult patients with *POLG* mutations by qPCR.

4) Correlate mtDNA depletion with respiratory chain deficiencies between different brain regions.

6.3 Results

6.3.1 Molecular Investigations of POLG

DNA was extracted from brain FFPE tissue blocks from patients 1 and 2, for whom a genetic diagnosis of *POLG* mutations had not been confirmed. DNA extraction was performed as described in section 2.5.6. DNA was quantified using the Nanodrop ND-100 Spectrophotometer. DNA appeared to be present in the samples in quantities of 3.2 ng/µl and 5.5ng/µl respectively. However, the PCR reactions performed using the primers for the three most common mutations p.(Ala467Thr), p.(Trp748Ser) and p.(Gly848Ser) did not return positive results (Figure 6.1). Thus, a genetic diagnosis for patients 1 and 2 could not be achieved.

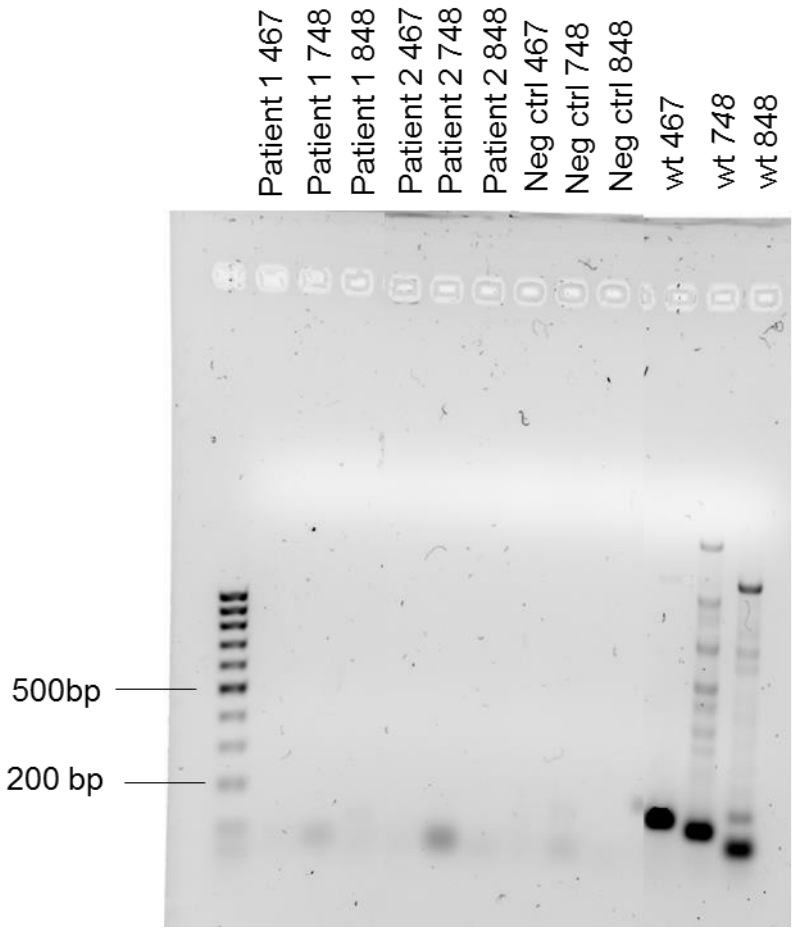

Figure 6.1: Agarose gel electrophoresis showing no amplification of relevant *POLG* DNA regions. The figure is representative of a 1% agarose gel, where the bands were visualised with GelRed™. A first round of PCR was performed spanning the region where the relevant single base mutation is present. A second PCR reaction was performed on the products from the latter in order to obtain more product using a biotinylated primer for each reaction to enable subsequent genotyping by pyrosequencing. The reactions were successful using wild type DNA, which suggests the absence of amplification in patient DNA is due to the poor quality of the DNA obtained after extraction. A negative control (water) for each mutations were tested. The wildtype DNA lanes show positive bands for amplified DNA. The lanes with DNA from patients 1 and 2 do not show positive bands. The negative control DNA lanes are clear. Key: Neg ctrl=negative control; 467= p.(Ala467Thr), 748= p.(Trp748Ser); 848= p.(Gly848Ser); wt= wildtype. A 1bp ladder was used.

6.3.2 Mitochondrial Respiratory Chain Protein Expression within GABAergic Interneurons and Pyramidal Neurons of Patients with Alpers

A previously optimised immunofluorescent assay (Lax *et al.*, 2016) was used to determine the extent of mitochondrial dysfunction in GABAergic interneurons in patients with Alpers' syndrome. The respiratory chain protein expression levels of subunits of complex I and complex IV were measured within GABAergic interneurons and pyramidal neurons within the occipital, parietal and frontal cortices from patients with Alpers' syndrome (see Table 6.1) and controls (see Table 6.2). Different brain regions were examined in different patients due to the lack of available tissue. It is important to mention that the clinical findings including hypsarrhythmia and

hydrocephalus as well as the very early onset for patients 1 and 2 are not representative of classical Alpers phenotype. Taken this into account, as well as the lack of genetic diagnosis of *POLG* mutations in these cases, it is therefore doubtful that these are due to *POLG* mutations and any findings should be interpreted with caution.

To detect mitochondrial respiratory chain protein expression within GABAergic interneurons, antibodies raised to NDUFB8 and COX1 subunit were employed in conjunction with VDAC1/Porin to detect mitochondrial mass within GAD65-67-positive interneurons.

To examine mitochondrial respiratory chain abnormalities in pyramidal neurons, two quantitative triple-based staining protocols were utilised due to conflicting isotype specificity cross-reactivity; in both assays an antibody raised against SMI-32P (non-phosphorylated neurofilaments) was used to visualise pyramidal neurons and hoescht to visualise nuclei, while antibodies raised against NDUFA13 and COX4I2 were used to detect subunits of complex I and mitochondrial mass respectively. COX4I2 levels are comparable in patients and controls, thus this marker can be used to indicate mitochondrial mass. In the second assay, COX1 and VDAC1/Porin were used to visualise complex IV protein abundance and mitochondrial mass respectively.

Downregulation of complex I or IV was observed visually as a loss or absence of NDUFB8/NDUFA13 and COX1 immunoreactivity in the presence of high VDAC1/Porin or COX4I2 immunoreactivity within either interneurons or pyramidal neurons. The optical densities for NDUFB8/NDUFA13, COX1 and Porin/COX4I2 were measured within each GABAergic interneuron (n=40) and pyramidal neuron (n=35) using Volocity software (PerkinElmer), as described in section 2.6.6. The z-scores were derived from the natural logarithm transformation of intensity data for NDUFB8/NDUFA13 vs Porin/COX4I2 and COX1 vs Porin, as detailed in section 2.6.7. The z-scores were then categorised as: overexpression of respiratory chain proteins (z-score>2), normal (z-score<2), low (z-score<-2), deficient (z-score<-3) and severely deficient (z-score<-4). The percentages of interneurons and pyramidal neurons within each category were calculated for patients and controls.

Patient	Age of Onset	Age at Death	Disease Duration	Gender	Genetic Defect	Brain region
Patient 1	2 months	5.5 months	3.5 months	Male	Unknown	Parietal
Patient 2	4 months	13 months	9 months	Male	Unknown	Parietal, frontal
Patient 3	11 months	14 months	3 months	Female	p.(Ala467Thr)/(p.Gly848Ser)	Parietal
Patient 5	11 months	13 months	2 months	Male	p.(Ala467Thr)/p.(Gly303Arg)	Occipital
Patient 6	7.2 months	7.8 months	<1 month	Male	p.(Ala467Thr)/p.(Gly848Ser)	Occipital, frontal
Patient 7	2 years	8 years	6 years	Male	p.(Ala467Thr)/p.(Gly303Arg)	Frontal

Table 6.1: Details of patients used in the study of respiratory chain protein expression. Patients 1 and 2 were clinically diagnosed as Alpers cases, however the clinical findings were not representative of classical Alpers and genetic testing for *POLG* mutations was not available due to the historic nature of these samples.

Control	Age at Death	Cause of Death	Gender	Brain region
Control 1	13 months	Occipital porencephaly	Female	Parietal
Control 2	22 years	Poisoning	Female	Parietal, occipital
Control 3	24 years	Suspension by ligature	Female	Parietal, occipital
Control 4	4.5 months	SIDS	Female	Occipital, frontal
Control 5	1 month	SIDS	Male	Occipital, frontal
Control 6	8 years	Asphyxia	Female	Frontal
Control 7	6 years	Drowning	Female	Frontal
Control 8	16 years	Suspension by ligature	Male	Occipital

Table 6.2: Details of controls used in the study of respiratory chain protein expression. Key: SIDS=sudden infantile death syndrome.

A. Occipital Lobe

In the controls, GABAergic interneurons display equal expression and good co-localisation of NDUFB8, COX1 and Porin. Data from controls 2, 3 and 8 were kindly provided by Dr. Hannah Hayhurst, as part of her project. In patient tissues, there is marked loss of NDUFB8 and COX1 immunoreactivity while Porin is maintained (see Figure 6.2). The quantitative data demonstrate that respiratory chain protein expression within GABAergic interneurons in control tissue is almost 100% normal displaying in the majority a z-score between -2 and +2, with only a minority of interneurons showing low expression (z-score<-2) or overexpression (z-score>2). (see Figure 6.3)

However extensive respiratory chain protein deficiencies involving both complexes I and IV are observed in patients, distinguished by z-score<-3 and -4. Complex I was severely deficient in all four patients. Patient 1 (no *POLG* diagnosis), patient 3 (p.(Ala467Thr)/p.(Gly848Ser)) and patient 6 (p.(Ala467Thr)/p.(Gly848Ser)), with all interneurons displaying z-scores below -3 and -4, suggestive of 100% complex I deficiency. Patient 5 (p.(Ala467Thr)/p.(Gly303Arg)) showed 8% of interneurons with

low complex I expression (z-score<-2), although the remaining were deficient (z-score<-3 and -4) (see Figure 6.3A).

With regards to complex IV expression, all interneurons from patient 5 (p.(Ala467Thr)/p.(Gly303Arg)), showed a z-score<-4 and -3. Interneurons from patient 6 (p.(Ala467Thr)/p.(Gly848Ser)) showed almost 100% deficiency of complex IV deficiency (98% of interneurons with z<-4). Patient 1 (no *POLG* diagnosis) showed also high levels of complex IV deficiency. Patient 3 (p.(Ala467Thr)/p.(Gly848Ser)) showed the milder complex IV deficiency from the patients considered, as a minority of interneurons showed low complex IV expression (z-score<-2 in 11% of interneurons) and normal complex IV expression (z-score<2 in 7% of interneurons) (Figure 6.3B).

Quantitative analysis of respiratory chain deficiencies in pyramidal neurons of the occipital lobe was not feasible due to limited tissue availability.

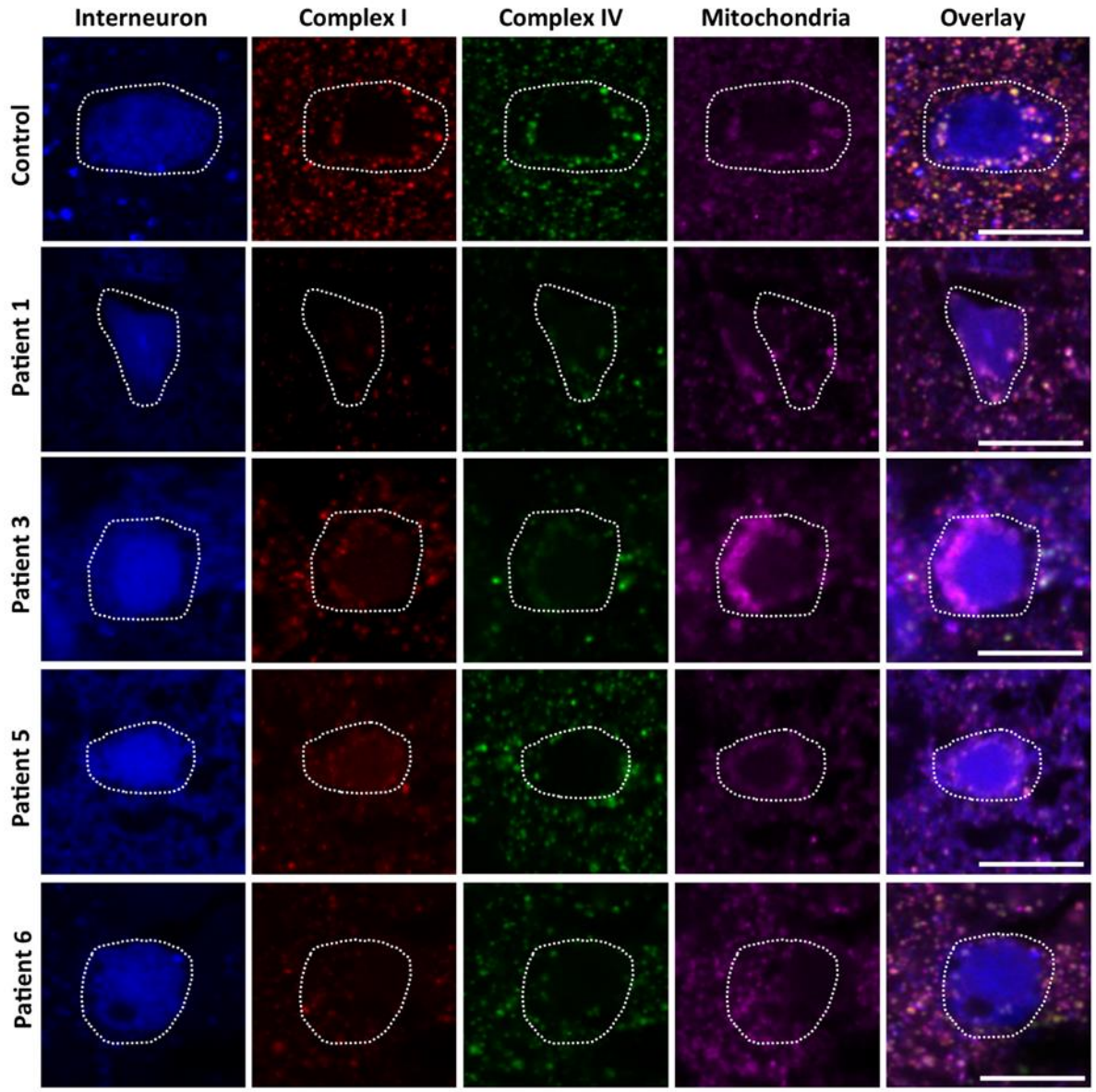

Figure 6.2: Quadruple immunofluorescence showing respiratory chain deficiencies involving complexes I and IV in interneurons of the occipital lobe from patients with Alpers. Sections were stained with GAD65-67 (interneurons), NDUFB8 (complex I subunit), COX1 (complex IV subunit) and Porin (mitochondrial mass). Representative images of the control tissue show a good co-localisation of NDUFB8, COX1 and Porin within the GAD65-67 positive interneurons. All patients show reduced immunoreactivity of NDUFB8 and COX1, while Porin is maintained. Scale bar=10µm.

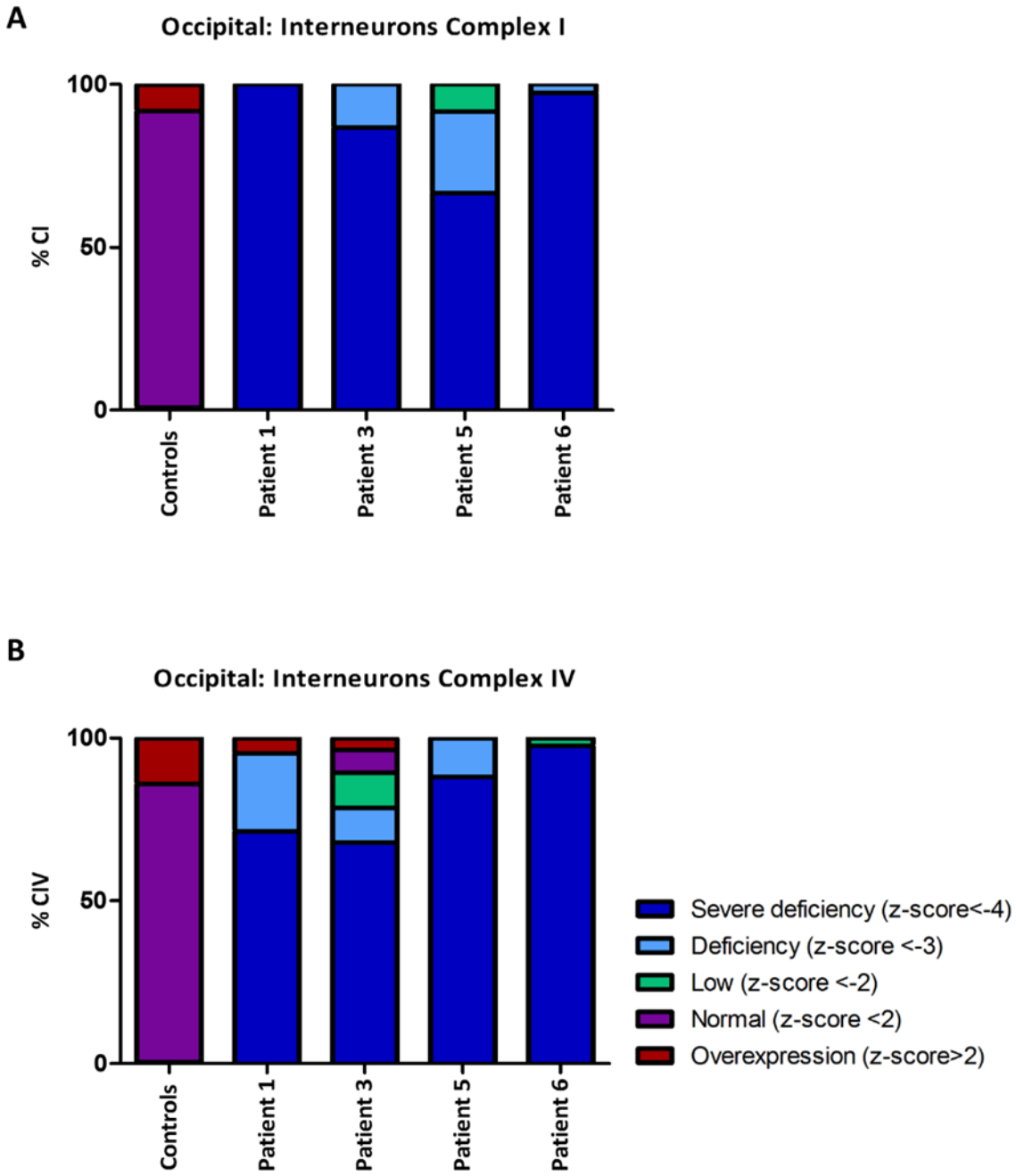

Figure 6.3: Extensive respiratory chain deficiency involving complex I and to a lesser degree complex IV in GABAergic interneurons of the occipital lobe in patients with Alpers. Data are represented as z-scores derived from the quantitative assessment of NDUFB8 and COX1 intensities relative to Porin intensities within GABAergic interneurons in patients and controls. The data demonstrate how much the complex I (A) and complex IV expression (B) deviate from normality. Here, a z-score>2 indicates overexpression, and a z-score<-2 indicates reduced expression. A z-score<-3 shows deficiency and a z-score<-4 indicates severe deficiency. There is a severe complex I deficiency in all patients (A) and to a lesser extent, complex IV (B).

B. Parietal Lobe

In control parietal lobe, GABAergic interneurons showed equal immunoreactivity of NDUFB8, COX1 and Porin and therefore good co-localisation. In patients, there is a marked decrease in NDUFB8 and COX1 while Porin is maintained (see Figure 6.4). Quantitative data demonstrate extensive complex I deficiency in patients 1 and 2 (both without *POLG* diagnosis). The interneurons from patients 1 and 2 (both without *POLG* diagnosis) showed z-score<-3 and -4 in the majority, implying almost 100% complex I deficiency. Patient 3 (p.(Ala467Thr/p.(Gly848Ser)) showed only 21% deficiency (z-score<-3) involving complex I, while the majority of the interneurons showed low expression (60% of interneurons z<-2) and some interneurons expressed complex I at normal levels (19% of interneurons, z-score<2) (see Figure 6.5A).

With regards to complex IV, interneurons of patients showed some degree of complex IV deficiency, however to a lesser extent compared to complex I. Patients 1 and 2 (both without *POLG* diagnosis) had the highest complex IV deficiency as with complex I. In contrast, patient 3 (p.(Ala467Thr)/p.(Gly848Ser)) displayed the lowest degree of complex IV deficiency from all patients analysed (see Figure 6.5B).

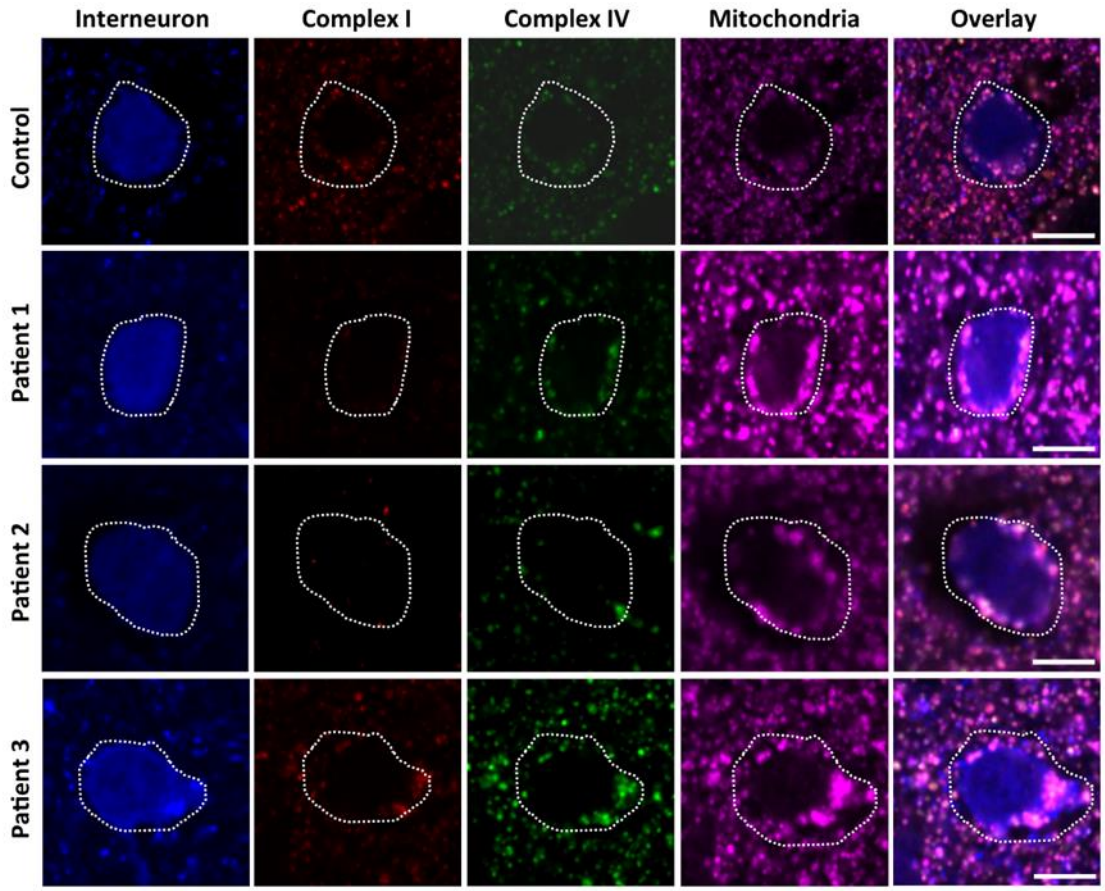

Figure 6.4: Quadruple immunofluorescence demonstrating complex I and IV respiratory chain deficiencies in patient interneurons from the parietal lobe of patients with Alpers. Sections stained with GAD65-67 (interneurons), NDUFB8 (subunit of complex I), COX1 (subunit of complex IV) and Porin (mitochondrial mass). Here, respresentative images show a good co-localisation of NDUFB8, COX1 and Porin within the interneurons of the control tissue. All patients show reduced immunoreactivity of NDUFB8 and COX1, while Porin is maintained. Scale bar=10µm.

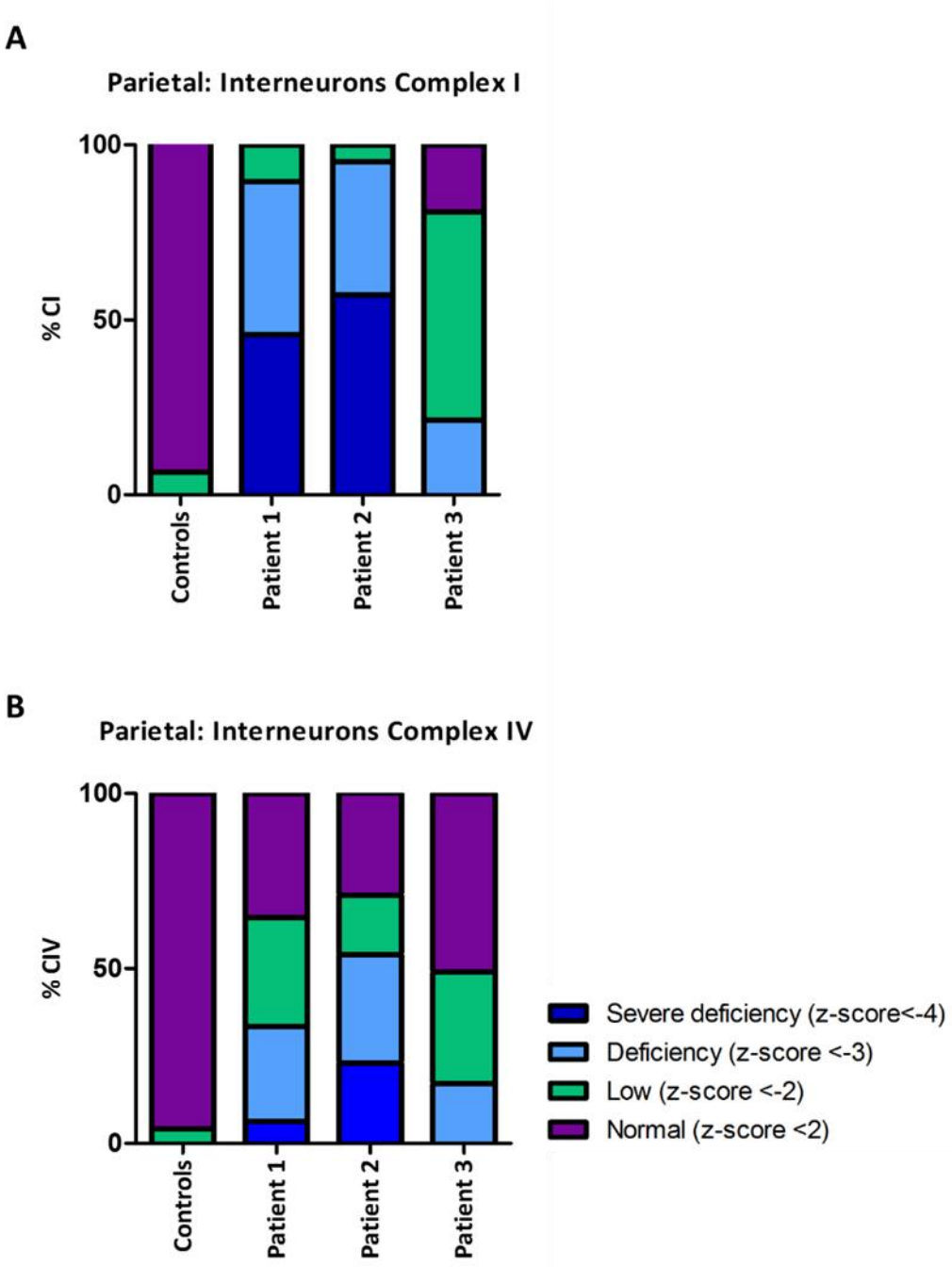

Figure 6.5: Extensive respiratory chain deficiency involving complex I and to a lesser degree, complex IV in GABAergic interneurons from the parietal lobe of patients with Alpers. Data are represented as z-scores derived from the quantitative assessment of NDUFB8 and COX1 intensities relative to Porin intensities, within GABAergic interneurons in patients and controls. The data demonstrate how much the complex I (A) and IV expression (B) (relative to Porin) deviate from normality. Here, a *z*-score <2 is indicative of normal protein expression and a *z*-score lower than −2 indicates reduced expression. A z-score<-3 shows deficiency and a z-score<-4 indicated severe deficiency. There is severe complex I deficiency in all patients (A) and to a lesser extent, complex IV (B).

Pyramidal neurons in the parietal lobe showed equal immunoreactivity of NDUFA13 and COX4I2 or COXI and Porin, which showed good co-localisation. There was a specific loss of NDUFA13 and COX1 in the patients despite the maintained Porin/COX4I2. Patients 1 and 2 (no *POLG* diagnosis) exhibited deficient (z-score<-3) and severely deficient complex I interneurons (z-score<-4), however this was milder compared to the interneurons of the parietal lobe, which were almost 100% complex I deficient. Pyramidal neurons from patient 3 (p.(Ala467Thr)/p.(Gly848Ser)) did not demonstrate any complex I deficiency (see Figures 6.6 and 6.8A).

Complex IV deficiency (z-score<-3) was observed only in Patient 1 (no *POLG* diagnosis) who showed the most extensive complex I deficiency in pyramidal neurons. However complex IV deficiency was milder compared to complex I deficiency. Patient 2 (no *POLG* diagnosis) and Patient 3 (p.(Ala467Thr)/p.(Gly848Ser)) had normal complex IV expression (z-score<2) (see Figures 6.7 and 6.8B).

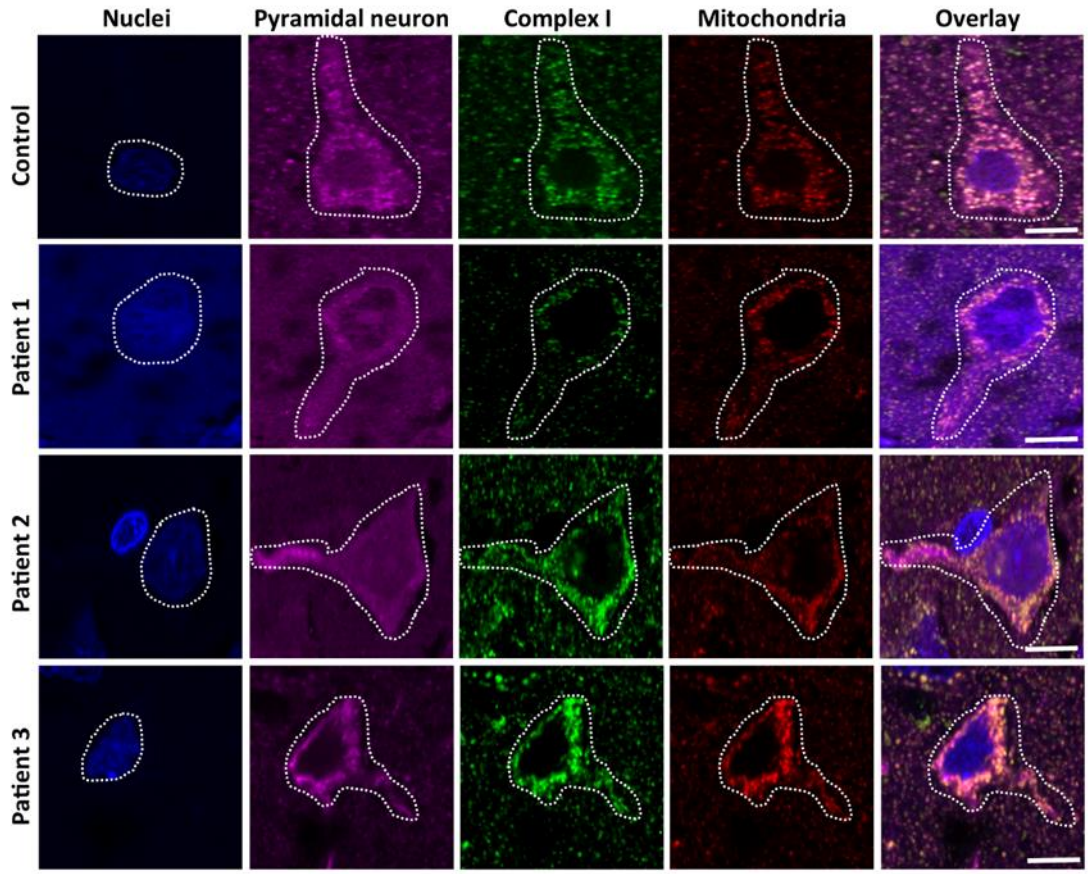

Figure 6.6: Quadruple immunofluorescence demonstrating complex I respiratory chain protein expression in pyramidal neurons from the parietal lobe of patients with Alpers. Sections were stained with Hoechst (nuclei), SMI-32P (pyramidal neurons), NDUFA13 (subunit of complex I) and COX4I2 (as a mitochondrial mass marker). Here, representative images show good co-localisation of NDUFA13 and COX4I2 within the pyramidal neurons of the control tissue. Patients 1 and 2 (both without *POLG* diagnosis) show reduced immunoreactivity of NDUFA13, when COX4I2 is maintained. Patient 3 (p.(Ala467Thr)/p.(Gly848Ser)) shows good co-localisation of NDUFA13 and COX4I2. Scale bar=10µm.

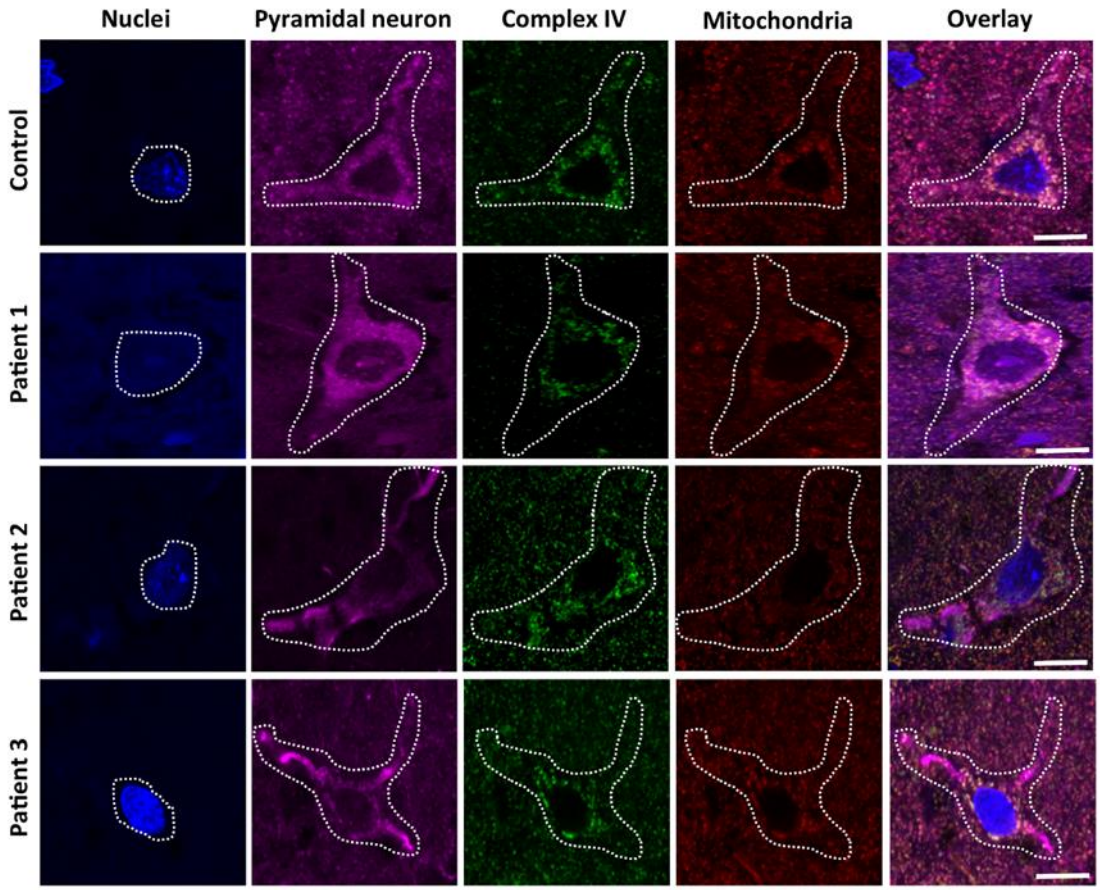

Figure 6.7: Quadruple immunofluorescence demonstrating complex IV respiratory chain protein expression in pyramidal neurons of the parietal lobe from patients with Alpers. Sections were stained with Hoechst (nuclei), SMI-32P (pyramidal neurons), COX1 (subunit of complex IV) and Porin (as a mitochondrial mass marker). Here, representative images show good co-localisation of COX1 and Porin within pyramidal neurons of the control tissue. Patient 1 (no *POLG* diagnosis) shows reduced immunoreactivity of COX1 when Porin is maintained. Patients 2 (no *POLG* diagnosis) and 3 (p.(Ala467Thr)/p.(Gly848Ser)) show equal expression of COX1 compared to controls, when Porin is maintained. Scale bar=10µm.

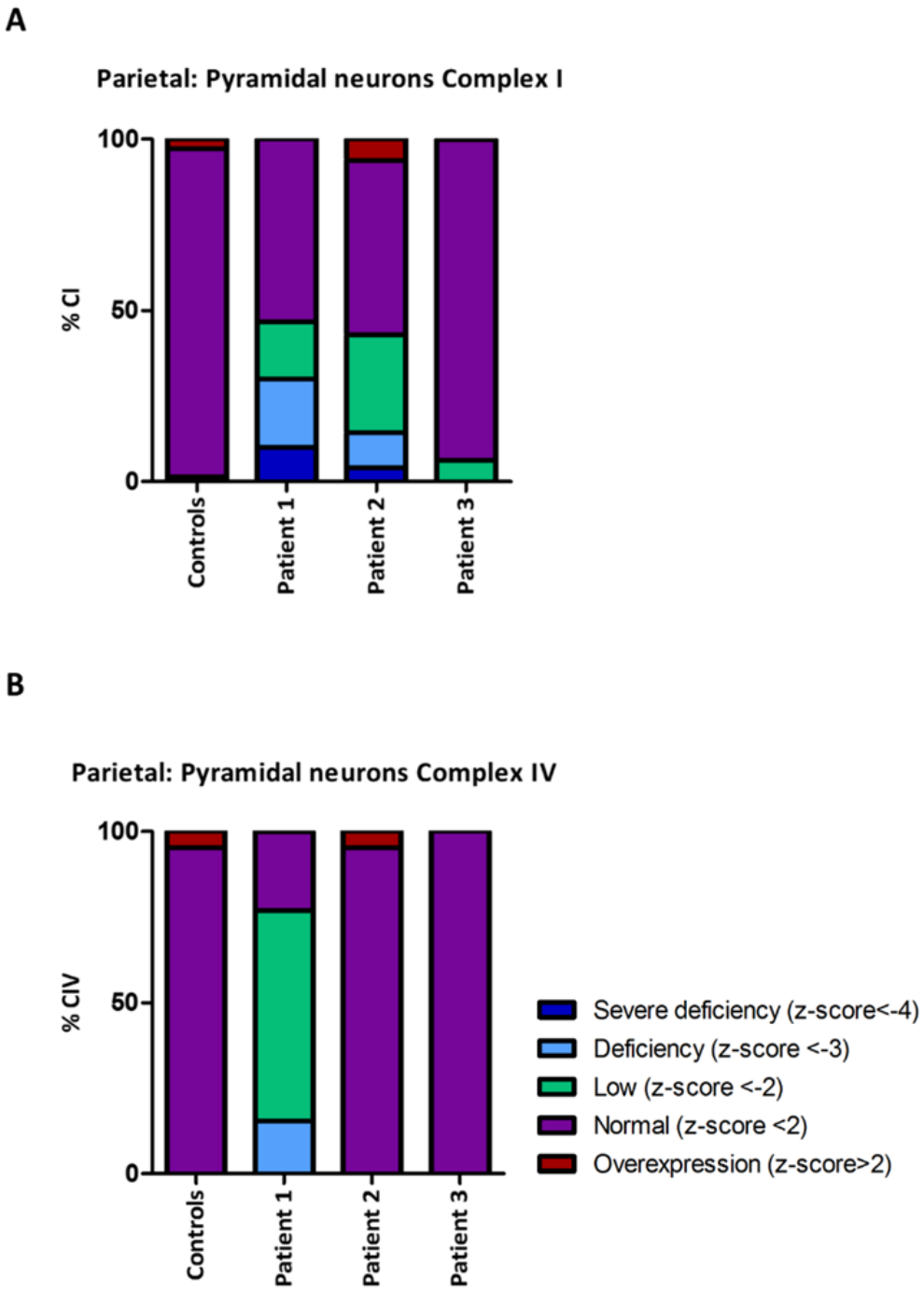

Figure 6.8: Respiratory chain deficiency involving complex I and to a lesser extent, complex IV in pyramidal neurons of the parietal lobe from patients with Alpers. Data are represented as z-scores derived from quantitative assessment of NDUFA13 and COX1 optical densities relative to COX4I2/Porin optical densities within pyramidal neurons in patients and controls. The data demonstrate how much the complex I (A) and complex IV (B) deviate from normality. Here, a z-score<2 is indicative of normal protein expression. A z-score>2 indicates overexpression and a z-score<-2 is indicative of reduced expression. A z-score<-3 shows deficiency and a z-score<-4 indicates severe deficiency. (A) There is severe complex I deficiency in patients 1 and 2 (both without *POLG* diagnosis) but only low levels of complex I expression in patient 3 (p.(Ala467Thr)/p.(Gly848Ser)). (B) Complex IV deficiency and low levels of complex IV expression were evident in the pyramidal neurons of patient 1 (no *POLG* diagnosis), however complex IV deficiency was milder compared to complex I. Pyramidal neurons of patients 2 (no *POLG* diagnosis) and 3 (p.(Ala467Thr)/p.(Gly848Ser)) showed normal complex IV expression.

C. Frontal lobe

In the frontal lobe, the interneurons of control tissue showed good co-localisation of NDUFB8, COX1 and Porin. In controls, complex I and IV expression were almost 100% normal. Patient 2 (no *POLG* diagnosis) showed normal complex I and IV expression (z-score<2), whereas patient 6 (p.(Ala467Thr)/p.(Gly848Ser)) and patient 7 (p.(Ala467Thr)/p.(Gly303Arg)) exhibited deficient (z-score<-3) and severely deficient (z-score<-4) complex I and complex IV interneurons (see Figures 6.9 and 6.10). Patient 6 (p.(Ala467Thr)/p.(Gly848Ser)) exhibited the most severe complex I and complex IV, to a lesser extent, deficient interneurons. Patient 7 (p.(Ala467Thr)/p.(Gly303Arg)) showed a higher percentage of deficient (z-score<-3) and severely deficient (z-score<-4) complex IV interneurons than complex I (see Figures 6.9 and 6.10). This patient had the latest disease onset (2 years) and the longer survival (6 years).

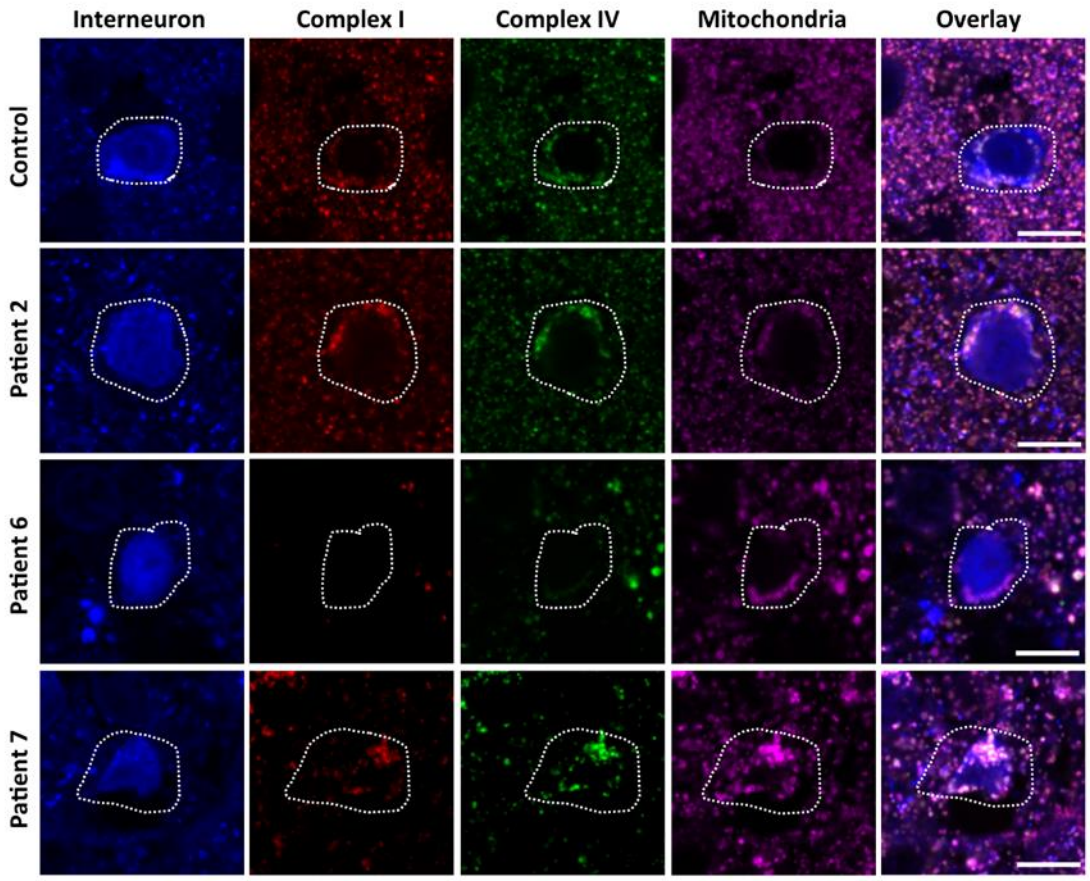

Figure 6.9: Quadruple immunofluorescence demonstrating complex I and complex IV respiratory chain protein deficiencies in GABAergic interneurons from the frontal lobe of patients with Alpers. Sections were stained with GAD65-67 (interneurons), NDUFB8 (subunit of complex I), COXI (subunit of complex IV) and Porin (mitochondrial mass). Representative images show a good co-localisation of NDUFB8, COX1 and Porin within the interneurons of the control tissue and patient 2 (no *POLG* diagnosis). Patient 6 (p.(Ala467Thr)/p.(Gly848Ser)) shows reduced immunoreactivity of NDUFB8 and COX1, while Porin is maintained. Patient 7 (p.(Ala467Thr)/p.(Gly303Arg)) shows decreased immunoreactivity of NDUFB8 and COX1 when Porin is maintained. Scale bar=10µm.

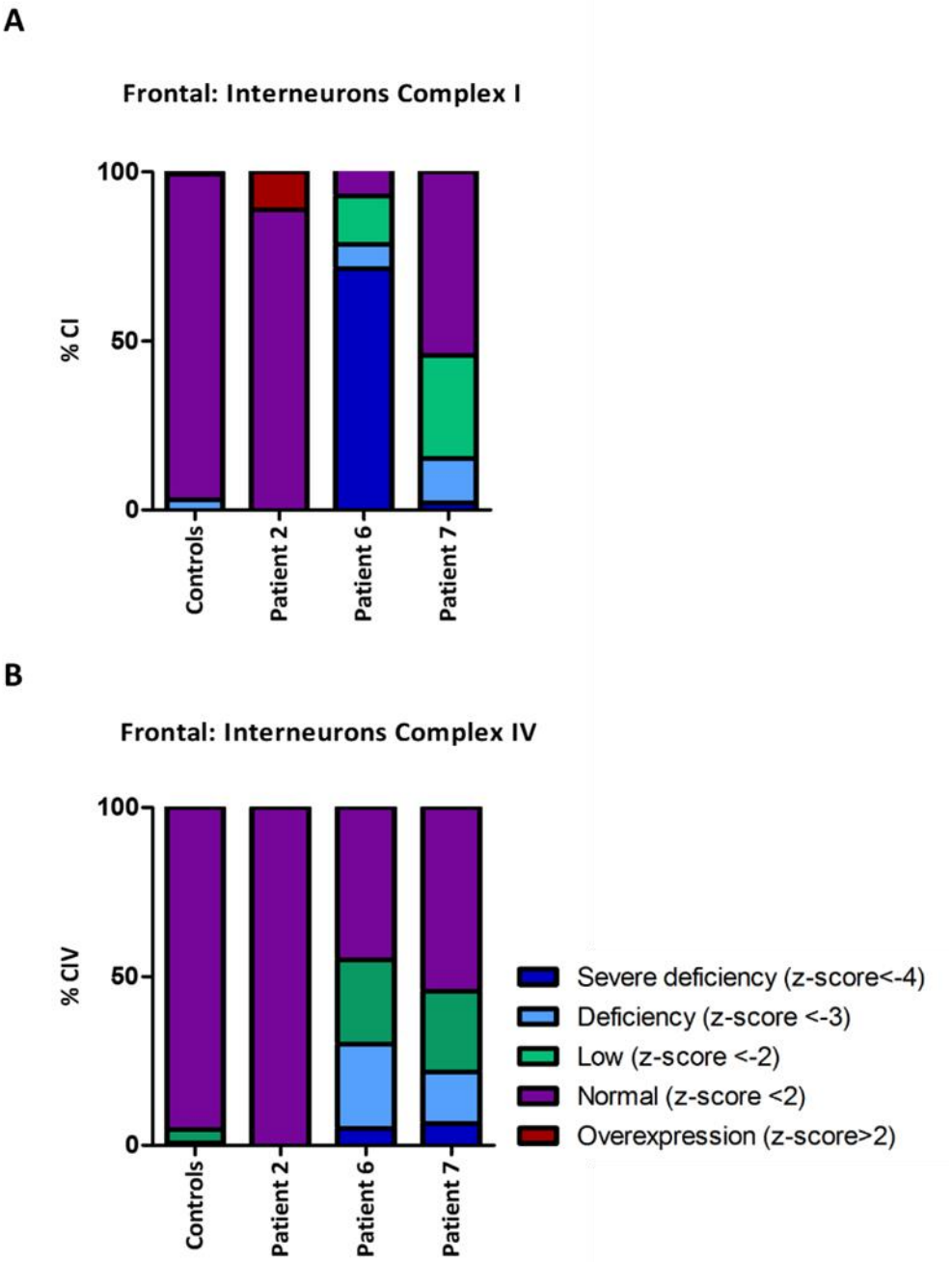

Figure 6.10: Respiratory chain deficiency involving complex I and to a lesser extent, complex IV in GABAergic interneurons of the frontal lobe from patients with Alpers. Data are represented as z-scores derived from the quantitative assessment of NDUFB8 and COX1 intensities relative to Porin intensities within GABAergic interneurons in patients and controls. The data demonstrate how much the complex I (A) and complex IV (B) expression relative to Porin deviate from normality. A z-score<2 is indicative of normal protein expression, a z-score>2 indicates overexpression and a z-score<-2 indicates reduced expression. A z-score<-3 shows deficiency and a z-score<-4 is indicative of severe deficiency. (A) Patient 2 (no *POLG* diagnosis) displays normal complex I expression in the majority of interneurons, with some interneurons exhibiting overexpression. There is severe complex I deficiency in patients 6 (p.(Ala467Thr)/p.(Gly848Ser)) and 7 (p.(Ala467Thr)/p.(Gly303Arg)), however patient 7 (p.(Ala467Thr)/p.(Gly303Arg)) shows complex I deficiency to a lesser extent compared to patient 6 (p.(Ala467Thr)/p.(Gly303Arg)). (B) Complex IV shows normal expression in the interneurons of patient 2 (no *POLG* diagnosis). Complex IV deficiency is evident in the interneurons of patient 6 (p.(Ala467Thr)/p.(Gly848Ser)), however to a lesser extent compared to complex I. Patient 7 (p.(Ala467Thr)/p.(Gly303Arg)) shows complex IV deficiency to similar levels to complex I.

With regards to pyramidal neurons of the frontal lobe, complex I expression was normal in the patients investigated (see Figures 6.11 and 6.13). Patient 7 (p.(Ala467Thr)/p.(Gly303Arg)) exhibited a high degree of overexpressed complex I (48%). Complex I and IV expression was normal in Patient 2 (no *POLG* diagnosis), however patient 7 (p.(Ala467Thr)/p.(Gly303Arg)) exhibited 25% complex IV deficiency (see Figures 6.12 and 6.13). This patient exhibited complex IV deficiency at a similar extent in the interneurons of the frontal lobe. For patient 6 (p.(Ala467Thr)/p.(Gly848Ser)), there was insufficient number of pyramidal neurons, therefore this patient was not included in the analysis.

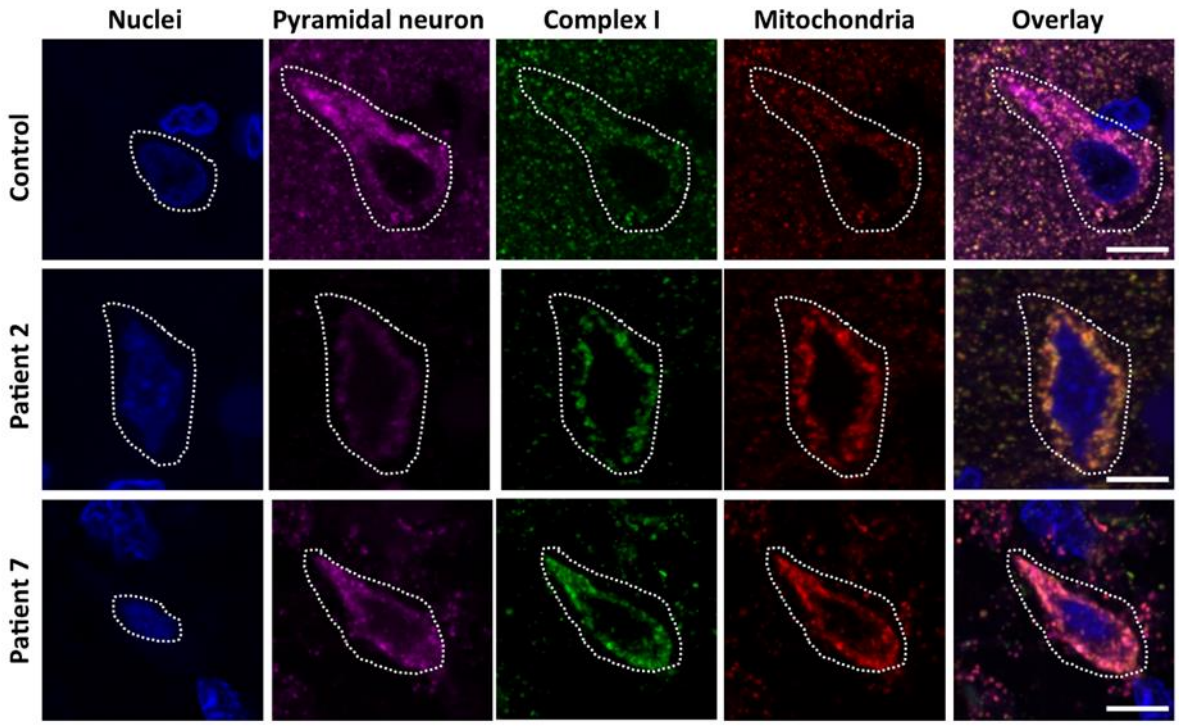

Figure 6.11: Quadruple immunofluorescence demonstrating complex I respiratory chain protein expression in pyramidal neurons from the frontal lobe of patients with Alpers. Sections were stained with Hoechst (nuclei), SMI-32P (pyramidal neurons), NDUFA13 (subunit of complex I) and COX4I2 (as a mitochondrial mass marker). Representative images show good co-localisation of NDUFA13 and COX4I2 within the pyramidal neurons of control and patient tissue. Scale bar=10µm.

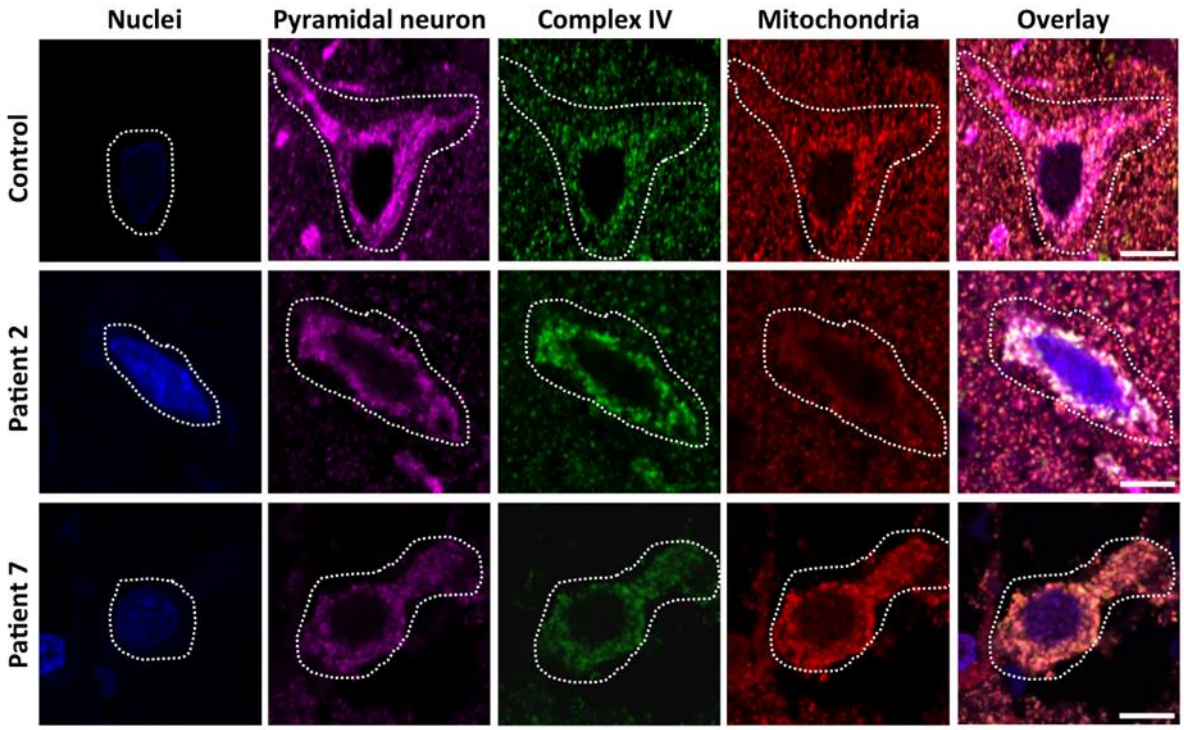

Figure 6.12: Quadruple immunofluorescence demonstrating complex IV respiratory chain protein expression in pyramidal neurons from the frontal lobe of patients with Alpers. Sections were stained with Hoechst (nuclei), SMI-32P (pyramidal neurons), COX1 (subunit of complex IV) and Porin (mitochondrial mass). Here, images show good co-localisation of COX1 and Porin in the pyramidal neurons of control tissue. Patient 2 (no *POLG* diagnosis) shows increased immunoreactivity of COX1 when Porin is maintained. Patient 7 (p.(Ala467Thr))/p.(Gly303Arg)) shows reduced immunoreactivity of COX1, while Porin is maintained. Scale bar=10µm.

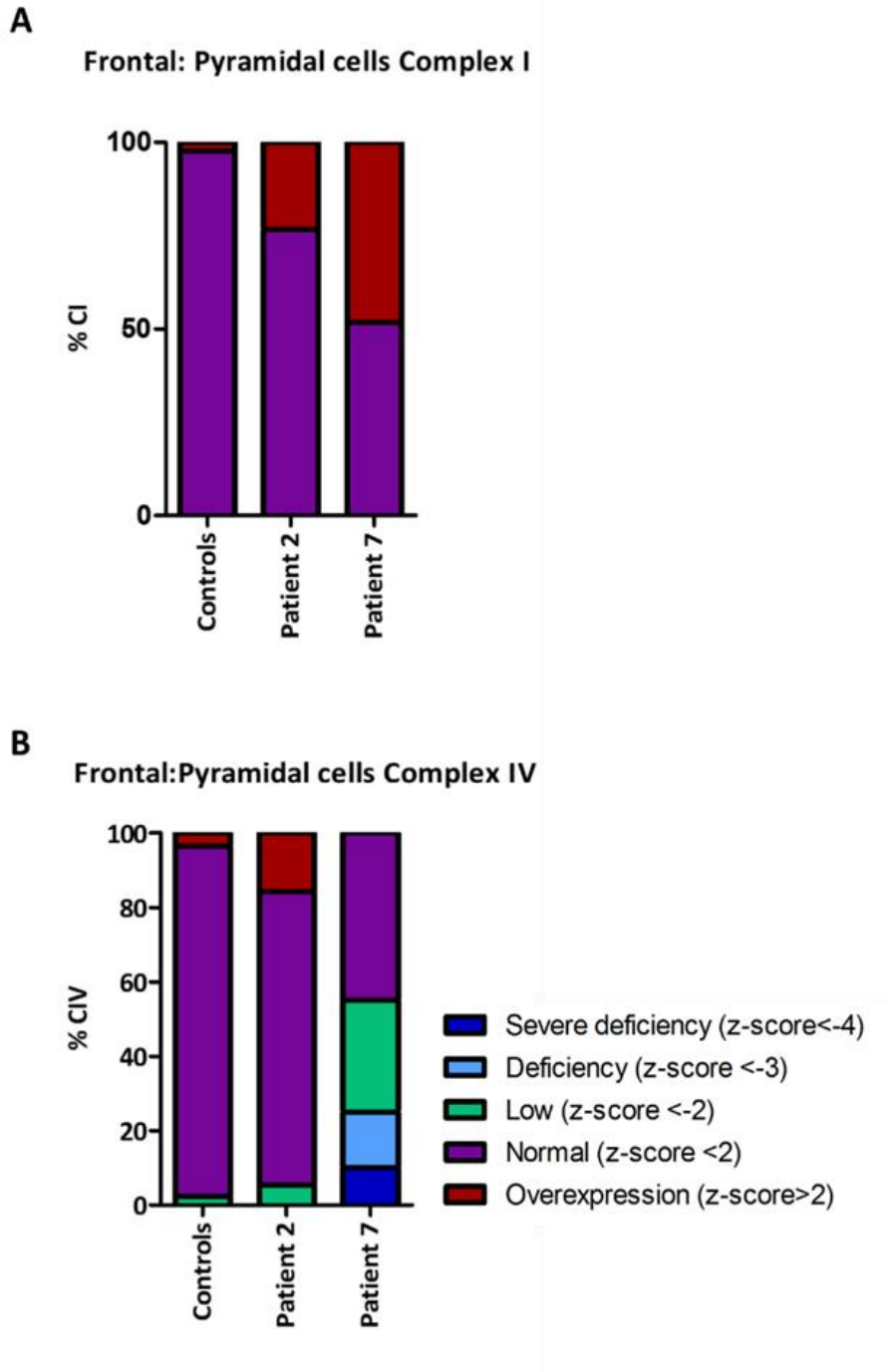

Figure 6.13: Respiratory chain protein expression of complexes I and IV in pyramidal neurons of the frontal lobe from patients with Alpers. Data are shown as z-scores derived from the quantitative assessment of COX1 intensity relative to Porin intensity within pyramidal neurons of patients and controls. The data demonstrate how much complex I expression (A) and complex IV expression (B) deviate from normality. Here, a z-score<2 indicates normal protein expression, a z-score>2 demonstrates overexpression, and a z-score<-2 indicates reduced protein expression. A z-score<-3 indicates deficiency and a z-score<-4 shows severe deficiency. (A) Complex I expression in patient 2 (no *POLG* diagnosis) is normal in the majority of interneurons, with a low number of pyramidal neurons showing overexpression. Patient 7 (p.(Ala467Thr)/p.(Gly303Arg)) shows an equal number of interneurons with normal and overexpressed complex I expression. (B) In patient 2 (no *POLG* diagnosis) complex IV expression is comparable to complex I. Pyramidal neurons from patient 7 (p.(Ala467Thr)/p.(Gly848Ser)) display complex IV deficiency.

6.3.3 *Mitochondrial DNA Copy Number in Brain Tissue*

To test whether mtDNA depletion due to *POLG* mutations is the underlying mechanism of respiratory chain deficiency seen in the brain of patients, mtDNA copy number was assessed in patients with *POLG* mutations and controls. However, the cases examined were adult and not paediatric, as this was the only frozen tissue available (see Table 6.3). Mitochondrial DNA depletion was assessed in brain homogenates from the occipital, parietal and frontal lobes from patients and controls using a quantitative real-time PCR assay. The method involves the amplification of the mitochondrial gene *MT-ND1* and the nuclear gene *B2M* (see section 2.7.10). The mtDNA copy number in brain homogenate tissue from the three different lobes was calculated based on a standard curve from samples with known copy number. The absolute mtDNA copy number per cell was derived.

Patient/Control	Patient Code	Age at Death	Gender	Clinical Phenotype	Genetic Defect	Available Brain Region
Patient 8	2001/0017	24 years	Female	Alpers	p.(Ala467Thr)/p.(Trp748Ser)	Occipital, Parietal, Frontal
Patient 10	4217	45 years	Female	PEO and epilepsy	p.(Ala467Thr)/p.(Trp748Ser)	Frontal
Patient 12	141-97	50 years	Male	CPEO and sensory neuronopathy	p.(Ala467Thr) and p.(X1240Gln)	Occipital
Patient 13	958-10	79 years	Male	CPEO, Ataxia	p.(Thr251Ile)/p.(Pro587Leu) and p.(Ala467Thr)	Occipital
Patient 14	224-11	55 years	Male	CPEO, epilepsy and ataxia	p.(Trp748Ser)/p.(Arg1096Cys) and p.(Glu1143Gly)	Occipital
Patient 9	1997/0064	6 years	Male	Encephalopathy similar to Alpers with liver failure	*IDH3A* p.(Arg178His)/p.(Ala330Val)	Occipital, parietal
Patient 11	110-05	59 years	Male	Parkinsonism	p.(Ser1104Cys)/p.(Gly848Ser)	Occipital
Control 9	1985-647	6 years	Female		N/A	Occipital, Parietal
Control 10	729-10	70 years	Male		N/A	Occipital
Control 11	118-09	55 years	Male		N/A	Occipital
Control 12	891-11	81 years	Male		N/A	Occipital

Control 13	1993-173	19 years	Male		N/A	Parietal, Frontal
Control 14	1993-179	27 years	Male		N/A	Parietal, Frontal

Table 6.3: Details of patients and controls used in the study of mtDNA damage. Key: CPEO=chronic progressive external ophthalmoplegia; *IDH3A*=isocitrate dehydrogenase 3A; N/A=not applicable**.**

A. Occipital Lobe

The mtDNA copy number from five adult patients harbouring compound heterozygous mutations compared to controls and a paediatric patient (6 years old) with an encephalopathy similar to Alpers phenotype, with mutations in *isocitrate dehydrogenase 3A (IDH3A)*, but without evidence of mutations in *POLG*. The mtDNA copy number in four patients with *POLG* mutations was dramatically reduced compared to controls. Patient 8 (p.(Ala467Thr)/p.(Trp748Ser)) and patient 14 (p.(Trp748Ser)/p.(Arg1096Cys)) and p.(Glu1143GGly)) demonstrated mtDNA depletion (<30% of control mean), while patient 12 (p.(Ala467Thr) and p.(X1240Gln)) and patient 13 (p.(Thr251Ile)/p.(Pro587Leu) and p.(Ala467Thr)) showed a severe reduction in the mtDNA copy number. The mtDNA copy number in patient 9 (mutations in *IDH3A*) and patient 11 (p.(Ser1104Cys)/p.(Gly848Ser)) was higher or comparable to controls (see Figure 6.14 and Table 6.4). Interestingly, patient 9 (mutations in *IDH3A*) had encephalopathy similar to Alpers phenotype, with evidence of seizures, but did not harbour *POLG* mutations; whereas patient 11 (p.(Ser1104Cys)/p.(Gly848Ser)) had a clinical picture of cognitive decline and Parkinsonism.

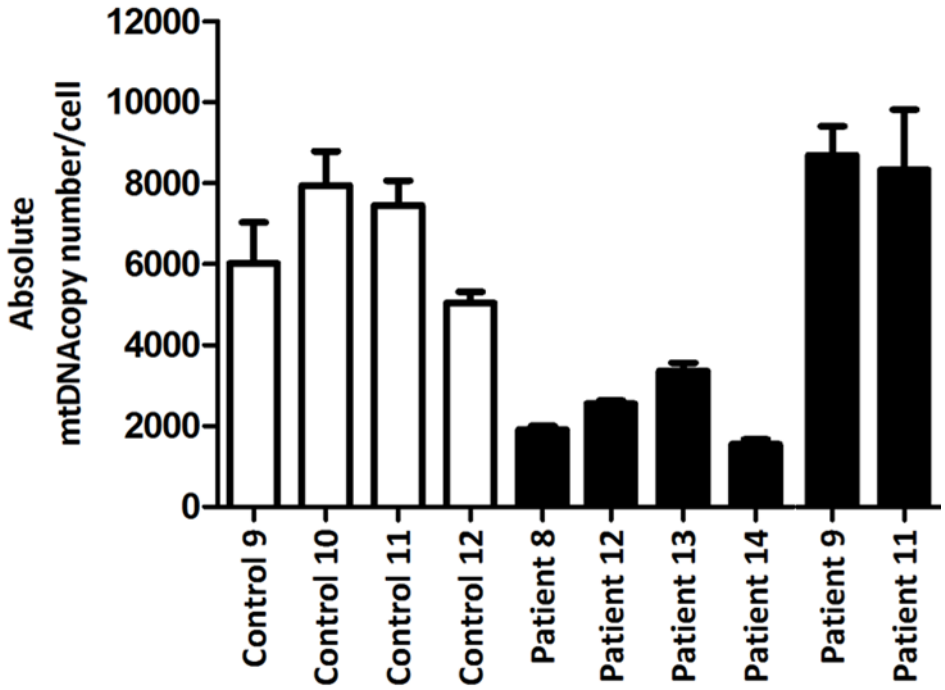

Figure 6.14: MtDNA copy number in the occipital lobe. Patients 8 (p.(Ala467Thr)/p.(Trp748Ser)), 12 (p.(Ala467Thr) and p.(X1240Gln)), 13 (p.(Thr251Ile)/p.(Pro587Leu)) and p.(Ala467Thr))) and 14 (p.(Trp748Ser)/p.(Arg1096Cys) and p.(Glu1143Gly) show a dramatic reduction in the mtDNA copy number compared to the controls. Patients 9 (mutations in *IDH3A*) and 11 (p.(Ser1104Cys)/p.(Gly848Ser)) show higher or similar mtDNA copy number to controls. Data represented as the mean absolute mtDNA copy number per cell ±SD (n=3).

B. Parietal Lobe

With regards to the parietal lobe, the tissue from patients 8 (p.(Ala467Thr)/p.(Trp748Ser)) and 9 (mutations in *IDH3A*) was only available and compared to controls 13 and 14. Patient 8 (p.(Ala467Thr)/p.(Trp748Ser)) shows a moderate reduction (mtDNA copy number 55% of control mean). Patient 9 (mutations in *IDH3A*) shows normal mtDNA copy number (75% of control mean, see Figure 6.15 and Table 6.4). The reduction in the mtDNA copy number in patient 8 (p.(Ala467Thr)/p.(Trp748Ser)) is less severe than in the occipital lobe, where mtDNA is depleted. Patient 9 (mutations in *IDH3A*) showed some decrease in the mtDNA copy number in the parietal lobe, while in the occipital the mtDNA copy number was similar to controls (see Figure 6.15 and Table 6.4).

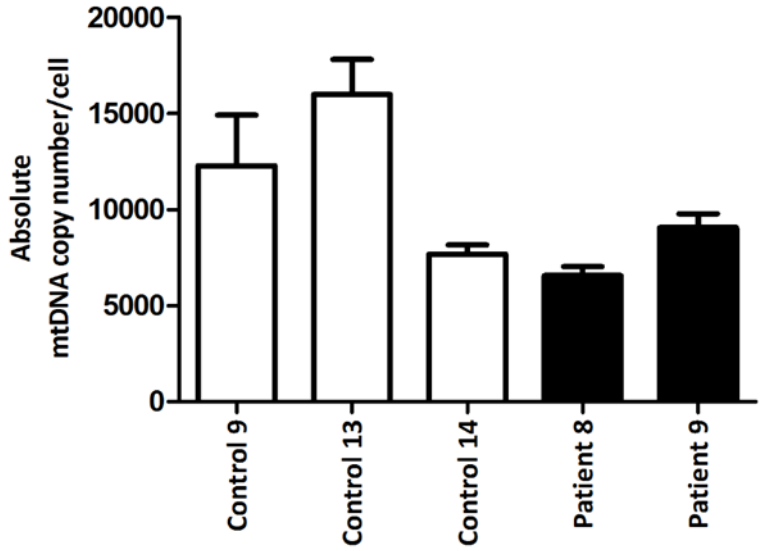

Figure 6.15: MtDNA copy number in the parietal lobe. Patient 8 (p.(Ala467Thr)/p.(Trp748Ser)) shows a moderate decrease in the mtDNA copy number and patient 9 (mutations in *IDH3A*) shows no significant reduction in the mtDNA copy number compared to controls. Data represented as the mean absolute mtDNA copy number per cell ±SD (n=3).

C. Frontal Lobe

In the frontal lobe, patients 8 (p.(Ala467Thr)/p.(Trp748Ser)) and 10 (p.(Ala467Thr)/p.(Trp748Ser)) were examined compared to controls 13 and 14. Both patients showed normal mtDNA copy number (90 and 84% of control mean respectively) compared to controls (Figure 6.16 and Table 6.4).

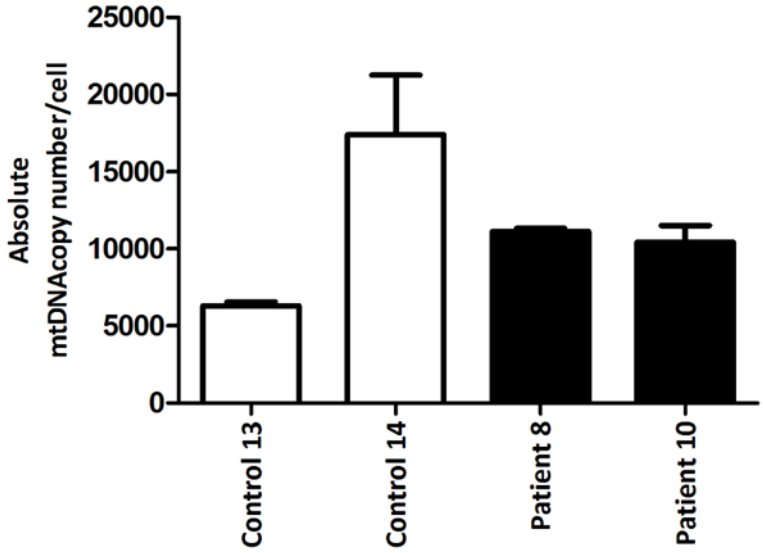

Figure 6.16: MtDNA copy number in the frontal lobe of patients with *POLG* mutations. Patients 8 and 10 (both with (p.(Ala467Thr)/p.(Trp748Ser)) show no significant reduction in the mtDNA copy number when compared to controls. Data represented as mean mtDNA copy number per cell ±SD (n=3).

mtDNA copy number (% of control mean)				
Patient	**Occipital lobe**	**Parietal lobe**	**Frontal lobe**	**Phenotype**
Patient 8	26.93 ± 1.25	54.78 ± 3.86	94.04 ± 1.49	Alpers
Patient 10	N/A	N/A	87.95 ± 9.15	PEO and epilepsy
Patient 12	35.89 ± 1.16	N/A	N/A	CPEO and sensory neuronopathy
Patient 13	47.41 ± 2.79	N/A	N/A	CPEO, ataxia
Patient 14	21.80 ± 1.61	N/A	N/A	CPEO, ataxia and epilepsy
Patient 9	122.55 ± 10.08	75.62 ± 5.94	N/A	Encephalopathy similar to Alpers' and iver failure caused by *IDH3A* mutations
Patient 11	117.39 ± 21.09	N/A	N/A	Parkinsonism

Table 6.4: Calculated percentage (%) mtDNA copy number relative to the control mean for occipital, parietal and frontal lobes. Key: N/A=not applicable.

6.3.4 Mitochondrial DNA Deletions in Brain Tissue

To assess mtDNA deletions a quantitative real-time PCR approach based on Taqman probes was used. This method involves the amplification of mitochondrial genes *MT-ND1* and *MT-ND4*. The percentage of mtDNA deletions in the samples was calculated based on a standard curve and relative proportions of amplified *MT-ND4* to *MT-ND1* (see section 2.7.10). The patients and controls used are summarised in Table 6.3. As with mtDNA copy number, samples from the occipital, parietal and frontal lobes were investigated. This method is inaccurate when measuring low levels of heteroplasmy, below 30% (Spendiff *et al.*, 2013).

A. Occipital Lobe

In the occipital lobe patients 8 (p.(Ala467Thr)/p.(Trp748Ser)), 9p.(Ala467Thr)/p.(Trp748Ser)), 11 (p.(Ser1104Cys)/p.(Gly848Ser)) and 12 (p.(Ala467Thr) and p.(X1240Gln)) showed low levels of *MT-ND4* deletions (within the

experimental error, <30%). All patients were adults with confirmed *POLG* mutations. Patient 9, a 6-year old patient with *IDH3A* mutations and no evidence of *POLG* mutations did not demonstrate any evidence of mtDNA deletions in the occipital lobe. Patient 13 (p.(Thr251Ile)/p.(Pro587Leu)) and p.(Ala467Thr)), showed high levels of mtDNA deletions (>30%). Patient 14 (p.(Trp748Ser)/p.(Arg1096Cys)) and p.(Glu1143Gly)), a showed evidence of *MT-ND1* deletions (see Figure 6.17). The negative values obtained in control samples are indicative of no *MT-ND4* deletions being present.

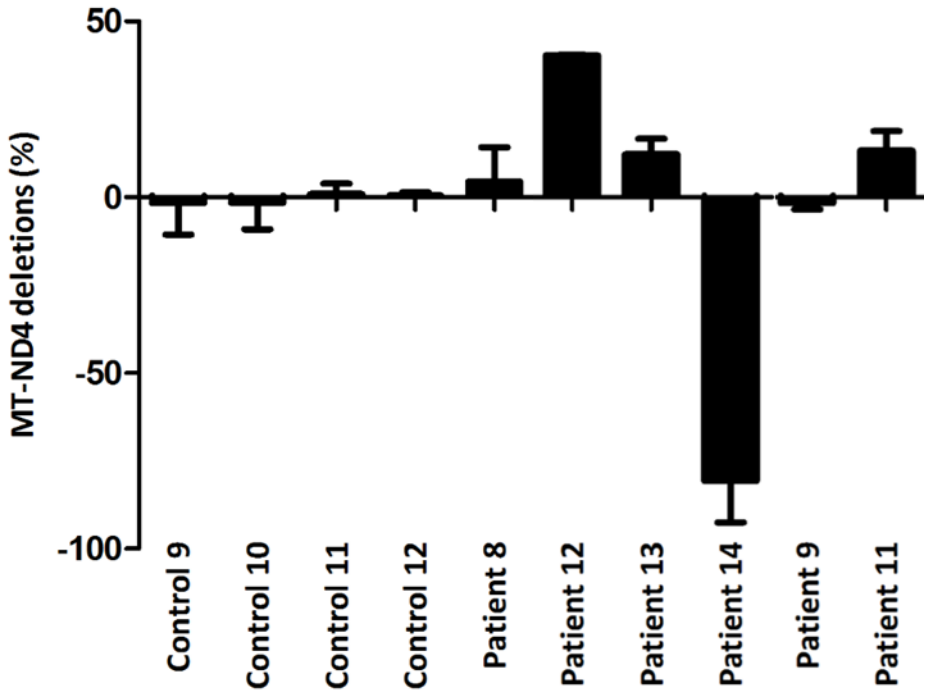

Figure 6.17: *MT-ND4* deletions in the occipital lobe of patients with *POLG* mutations. Patients 8 (p.(Ala467Thr)/p.(Trp748Ser)), 11 (p.(Ser1104Cys)/p.(Gly848Ser)), 12 (p.(Ala467Thr) and p.(X1240Gln) and 13 (p.(Thr251Ile)/p.(Pro587Leu) and p.(Ala467Thr)) demonstrate *MT-ND4* deletions within the experimental error of the assay (<30%). Patient 12 (p.(Ala467Thr) and p.(X1240Gln)) demonstrated a high percentage of *MT-ND4* deletions (>40%). Patient 14 (p.(Trp748Ser)/p.(Arg1096Cys) and p.(Glu1143Gly)) shows evidence of possible *MT-ND1* deletions. Data are represented as % mean *MT-ND4* deletions ± SD (n=3).

B. Parietal Lobe

In the parietal lobe, *MT-ND4* deletions were detected in patient 8 (p.(Ala467Thr)/p.(Trp748Ser)) compared to controls, but at a frequency that was within the experimental error (<30%). The percentage of mtDNA deletions in this patient was higher than in the occipital lobe. Similar to the occipital lobe, patient 9 (mutations in *IDH3A*) did not show evidence of mtDNA deletions compared to controls (see Figure 6.18).

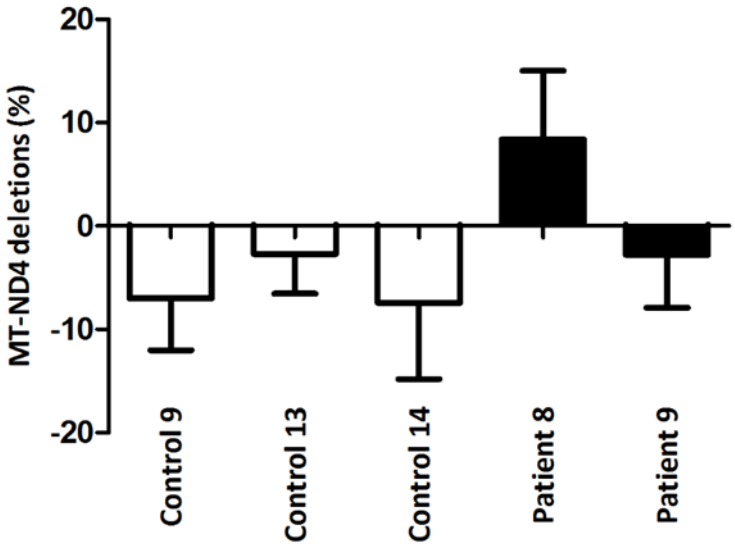

Figure 6.18: *MT-ND4* deletions in the parietal lobe of patients with *POLG* mutations. Patients 8 (p.(Ala467Thr)/p.(Trp748Ser)) demonstrates low levels of *MT-ND4* deletions (<30%), a percentage value within the experimental error of the assay. Patient 9 (mutations in *IDH3A*) did not show any evidence of *MT-ND4* deletions in the parietal lobe. Data are represented as % mean *MT-ND4* deletions ± SD (n=3).

C. Frontal Lobe

With regards to frontal lobe, patient 8 (p.(Ala467Thr)/p.(Trp748Ser)) showed low levels of *MT-ND4* deletions (<30%). Patient 10 (p.(Ala467Thr)/p.(Trp748Ser)) showed evidence of high levels (>40%) *MT-ND4* deletions compared to controls.

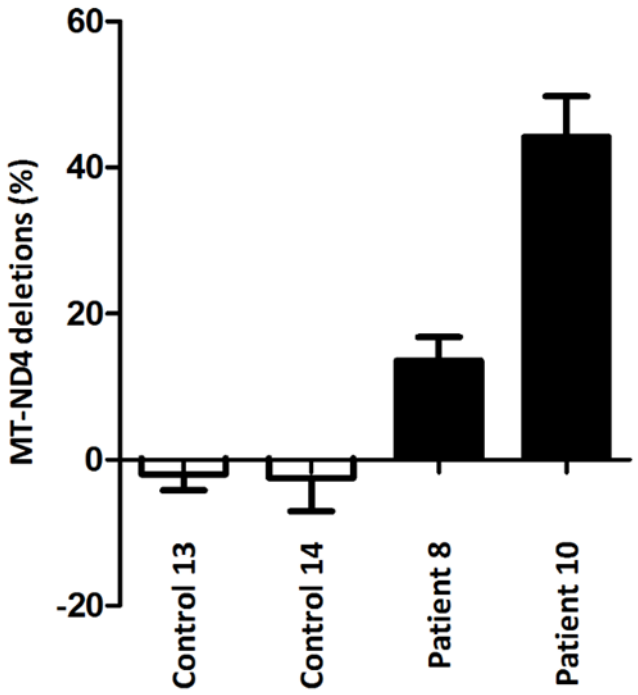

Figure 6.19: *MT-ND4* deletions in the frontal lobe of patients with *POLG* mutations. Patients 8 ((p.(Ala467Thr)/p.(Trp748Ser)) demonstrates low levels of *MT-ND4* deletions (<30%), a percentage value within the experimental error of the assay. Patient 10 (p.(Ala467Thr)/p.(Trp748Ser)) showed high levels of *MT-ND4* deletions (>40%) in the parietal lobe. Data are represented as % mean *MT-ND1* deletions ± SD (n=3).

	Occipital lobe		Parietal lobe		Frontal lobe	
Case	**Copy number (% of control mean)**	***MT-ND4* Deletions**	**Copy number (% of control mean)**	***MT-ND4* Deletions**	**Copy number (% of control mean)**	***MT-ND4* Deletions**
Patient 8	26.93 (depletion)	Low levels (<30%)	54.78	Low levels (<30%)	94.04	Low levels (<30%)
Patient 10	N/A	N/A	N/A	N/A	N/A	High levels (>30%)
Patient 12	35.89	High levels (>30%)	N/A	N/A	87.95	N/A
Patient 13	47.41	Low levels (<30%)	N/A	N/A	N/A	N/A
Patient 14	21.80 (depletion)	High levels of MT-ND1 deletions (>30%)	N/A	N/A	N/A	N/A
Patient 9	122.55	No	75.62	No	N/A	N/A
Patient 11	117.39	Low levels (<30%)	N/A	N/A	N/A	N/A

Table 6.5: Summary of mtDNA copy number and deletions. Key: N/A=not applicable.

6.4 Discussion

This chapter investigated mitochondrial respiratory chain protein expression in the post-mortem brain of six patients with clinically and/or genetically defined Alpers syndrome. The study aimed to unravel the mechanisms causing neurodegeneration through investigating different cortical regions known to have variable involvement in Alpers' syndrome including the occipital, parietal and frontal lobes. GABAergic interneurons of the occipital, parietal and frontal lobes exhibited extensive respiratory chain deficiencies involving complex I, and to a lesser extent, complex IV. The highest degree of respiratory chain deficiency was observed in the interneurons of the occipital lobe, while the frontal lobe demonstrated the lowest levels of respiratory chain deficiency. In pyramidal neurons, deficiencies involving complexes I and IV were observed in the parietal lobe but to a lower extent compared to interneurons. In the frontal lobe, pyramidal neurons generally showed a normal picture of respiratory chain protein expression.

Epilepsy is a major neurological manifestation of mitochondrial disease and constitutes a salient feature of Alpers. However, its underlying aetiology remains unknown. Pathological changes in posterior areas including the occipital lobe and cerebellum have been well described. These changes are consistent with clinical and neuroimaging observations: the occipital lobe is predominantly affected and believed to be a major contributor of epilepsy and visual impairment, while the cerebellum is responsible for coordinating muscle movements. Thus, defects in the cerebellum may explain movement disturbances and ataxia seen in patients.

The parietal and frontal lobes have not commonly been investigated in Alpers. However, pathology of such areas may underlie some common features of Alpers such as psychomotor regression and cognitive decline. Alpers is a rapidly progressive disorder, therefore I aimed to characterise respiratory chain deficiencies in the parietal and frontal lobes of patients to understand disease progression and the mechanism underlying the clinical neurological deficits seen in these patients.

In all areas examined, the research focussed on two neuronal types: GABAergic interneurons and pyramidal neurons. Interneurons are responsible for modulating complex neuronal networks (Haider *et al.*, 2006; Lax *et al.*, 2016). As such they are believed to be the most energy consuming cells of the brain, and they require high expression of complex I and cytochrome *c* oxidase (COX) to maintain their metabolic activity (Kann *et al.*, 2011; Whittaker *et al.*, 2011). Interneuron pathology has been

associated with mitochondrial epilepsy, as interneuron dysfunction is believed to reduce the threshold for seizure generation (Maglóczky and Freund, 2005; Lax *et al.*, 2016). Pyramidal neurons are the major excitatory cells of the brain, which comprise about two thirds of all neurons present in the cerebral cortex and coordinate cognitive functions. In contrast to interneurons, the contribution of pyramidal cells in epilepsy and other neurological deficits seen in patients has not been well characterised.

GABAergic interneurons generally exhibited extensive respiratory chain deficiencies involving both complexes I and IV in all the lobes examined, however these were more prominent in the occipital lobe, which is consistent with the clinical picture observed in patients with Alpers. Given the importance of GABAergic interneurons in generating gamma oscillations and modulating pyramidal cells which are responsible for the transmission of neuronal input to other areas of the cerebral cortex, mitochondrial dysfunction due to respiratory chain deficiencies may result to impaired neuronal oscillations, thereby leading to the neurological deterioration seen in patients with Alpers.

These findings are in concordance with recently documented respiratory chain deficiencies within GABAergic interneurons of patients with mitochondrial disease and *POLG* mutations (Lax *et al.*, 2016). Since all three brain regions were affected by respiratory chain deficiencies, mitochondrial dysfunction within GABAergic interneurons may not only contribute to epilepsy but also to cognitive decline and developmental regression, which characterise Alpers.

Complex I deficiency was generally more severe than complex IV, a finding which is consistent in Alpers (Hakonen *et al.*, 2008; Tzoulis *et al.*, 2014) and other neurological conditions including temporal lobe epilepsy and Parkinson's disease (Schapira *et al.*, 1990; Kunz *et al.*, 2000). The reasons behind preferential vulnerability of complex I is unclear. It has been suggested that it is the most affected complex due to it large size, as it contains the highest number of mtDNA-encoded subunits (Hakonen *et al.*, 2005; Tzoulis *et al.*, 2014). Another hypothesis suggests that complex I may be more vulnerable to deficiency because it functions close to its maximal capacity (Kann *et al.*, 2011). Alternatively, it could serve as a mechanism to compensate for the acquired damage due to respiratory chain deficiency (Tzoulis *et al.*, 2014). It is remarkable that three patients exhibited 100% deficient interneurons in the occipital lobe. As the samples used are post-mortem, limited by the fact they represent end-stage neurological features of Alpers, the observation that all

interneurons demonstrated mitochondrial dysfunction may highlight the importance of GABAergic pathology in end-stage Alpers disease.

It is important to mention that I found severe complex I deficiency in the frontal lobe interneurons of patients 6 (p.(Ala467Thr)/p.(Gly848Ser)) and 7 (p.(Ala467Thr)/p.(Gly303Arg)), which is incompatible with previous studies performed by Tzoulis *et al.,* on the same patients and tissue, where they found 0% deficient neurons. However, I used a quantitative approach which selectively measured complex I expression within interneurons. In contrast, Tzoulis *et al.,* performed semi-quantitative immunohistochemistry approach, which may have underestimated complex I deficiency within neurons (Tzoulis *et al.*, 2014).

Interestingly, interneurons from patients 5 (p.(Ala467Thr)/p.(Gly303Arg)) and 6 (p.(Ala467Thr)/(p.(Gly848Ser)) demonstrated 100% complex IV deficiency when complex I expression was severely compromised (90% and 100% respectively). The highly deficient respiratory chain in the interneurons of both patients may be associated with the short disease duration (less than 1 month and 2 months respectively). In addition, patient 6 (p.(Ala467Thr)/p.(Gly848Ser)) displayed severe complex I deficiency in the interneurons of the frontal lobe, and as this patient has the shortest survival, this finding may be indicative of the rapid disease progression. Patient 7 (p.(Ala467Thr)/p.(Gly303Arg)) exhibited both complex I and IV deficiencies in the interneurons of the frontal lobe. This patient survived for 6 years, however the severe phenotype may be the result of prolonged disease duration, as the tissue is post-mortem and is indicative of end-stage disease. It is intriguing that patients with *POLG* mutations and patients without a confirmed diagnosis exhibited severe respiratory chain deficiencies. However, the limited number of cases did not allow any further correlations.

Respiratory chain deficiencies were quantified in the pyramidal neurons of the parietal and frontal lobes only, as tissue availability was limited with regards to occipital lobe. Respiratory chain deficiencies in pyramidal neurons were milder compared to interneurons in the parietal and frontal lobes of the patients examined. It is important to mention that the respiratory chain deficiency was assessed in the remaining pyramidal cells, thus it is possible that the pyramidal neurons with extensive respiratory chain deficiencies had already died. Alternatively, pyramidal neurons are affected to a lesser extent compared to interneurons. The major limitation regarding respiratory chain protein expression in pyramidal neurons, is that

due to the clash of IgG isotypes, it was not possible to assess complex I and IV at the same time. Therefore, ths data represents respiratory chain protein expression within the same neuronal sub-population but not within the same pyramidal neuron. The study is also limited by the fact that SMI-32P antibody is specific to non-phosphorylated neurofilament, which is not selectively expressed by pyramidal neurons, therefore could detect false positive neurons. However, this antibody was selected for this study because other markers of excitatory proteins such a Calmodulin-dependent protein kinase II (CAMKII) are limited by their incompatibility with human tissue (Personal communication, Dr Nichola Lax).

The findings demonstrate respiratory chain deficiencies involving complex I and to a lesser extent complex IV in the interneurons of the occipital, parietal and frontal lobes of patients with Alpers' syndrome. In addition, some degree of respiratory chain deficiencies within pyramidal cells of the parietal and frontal lobes of the patients were detected. However, these were milder compared to interneurons. A highly robust, and reproducible, quadruple immunofluorescent approach was used, which has been previously described (Lax *et al.*, 2016).

Dysfunction of neuronal sub-populations including interneurons and pyramidal neurons have not been described in Alpers. This is the first evidence of mitochondrial respiratory chain deficiency within interneurons of Alpers patients which may contribute to seizure generation and cognitive impairment. It is intriguing that patient 6 (p.(Ala467Thr)/p.(Gly848Ser)) had no normal complex I and IV in the occipital lobe, while in the frontal lobe the defects were milder. Although this was the only lobe-matched patient. Further, my findings have shown severe respiratory chain deficiencies equally within interneurons of patients with *POLG* mutations and patients without a confirmed genetic diagnosis.

In agreement with clinical observations, I have shown that respiratory chain deficiencies are more severe in the occipital lobe followed by the parietal and frontal lobes, although the lobes examined were not patient-matched. This provides insight into our understanding of disease progression, despite the fact that the post-mortem nature of the tissue used is representative of end-stage disease.

The primary consequence of *POLG* mutations in Alpers is believed to be mtDNA depletion and mtDNA deletions, which are often associated with older patients. In this study both mtDNA depletion and deletions were assessed in brain homogenates from the occipital, parietal and frontal lobes of patients harbouring *POLG* mutations.

The majority of the patients included showed mtDNA depletion or severe mtDNA reduction in brain homogenate from the occipital lobe. The parietal lobe showed similar mtDNA copy number to controls or a moderate reduction. The frontal lobe was the least affected region, as mtDNA copy number was found to be within the normal range of controls. These findings suggest that mtDNA depletion appears to play an important role in *POLG*-related disease and neurons of the occipital lobe seem to be more susceptible, in agreement with the clinical features of Alpers and *POLG*-related epilepsy disorders.

Moreover, the mtDNA copy number reduction appears to correlate with complex I deficiency in interneurons of patients 8 (p.(Ala467Thr)/p.(Trp748Ser)) and 14 (p.(Trp748Ser)/p.(Arg1096Cys)) and p.(Ala467Thr)) (Lax *et al.*, 2016). It is intriguing that patient 13 (p.(Thr251Ile)/p.(Pro587Leu)), who presented with a CPEO phenotype and no evident neurological involvement, showed a severe mtDNA copy number reduction in the occipital lobe and only a 9% complex I deficiency in the interneurons, as demonstrated by Lax *et al* (Lax *et al.,* 2016). Patients 9 (mutations in *IDH3A*) and 11 (p.(Ser1104Cys)/p.(Gly848Ser)) did not show any evidence of mtDNA depletion. Patient 9 (mutations in *IDH3A*) did not harbour *POLG* mutations, while patient 11 (p.(Ser1104Cys)/p.(Gly848Ser)) demonstrated clinical signs of Parkinsonism. These findings suggest that other mechanisms may exist underlying these phenotypes.

To date only a few studies on mtDNA depletion in brain tissue from patients with Alpers and other *POLG*-related epilepsy disorders exist. These studies have shown a non-significant reduction in the mtDNA copy number (70-75% of control mean) in cerebellum and frontal lobe homogenates (Ferrari *et al.*, 2005; Hakonen *et al.*, 2008), consistent with my findings in the frontal lobe of patients with *POLG* mutations. The findings of the current study showed evidence of mtDNA depletion in brain homogenates from the occipital and a non-significant or moderate reduction in the mtDNA copy number or in parietal lobes from patients with *POLG*-related disease.

Tzoulis *et al*., have shown mtDNA depletion in micro-dissected neurons of patients with Alpers and older patients harbouring *POLG* mutations and the depletion remained unchanged regardless disease duration. The mtDNA depletion was significantly more severe compared to brain homogenates (Tzoulis *et al.*, 2014). My study was performed on brain homogenates, as the availability of tissue with similar thickness was limited for further experimentation. Thus, my findings may be an underestimation of the mtDNA defect, as a mixture of neurons and glia, which are

more or less susceptible are included in the sample. Despite this limitation, the findings of the current study support the hypothesis that the occipital lobe is more susceptible to mtDNA depletion compared to the parietal and frontal lobes.

Furthermore, mtDNA deletions have rarely been reported in Alpers and *POLG*-related disease. Deletions were observed only in the older population and not the young infants with Alpers; suggesting that deletions accumulate with age and may be secondary to depletion (Tzoulis *et al.*, 2014). In agreement with this observation I found evidence of deletions in four adult patients with *POLG* mutations. The limited tissue availability did not allow the investigation of younger patients with Alpers, thus it was not possible to compare mtDNA damage between different age groups.

6.4.1 Limitations

This study is limited by the low number of cases, given the rarity of the disease and brain tissue availability. Therefore, a descriptive approach rather than parametric statistics was used in this study. The tissue studied is post-mortem and thus representative of end-stage disease Likewise, the brain regions investigated were not always patient-matched therefore direct correlations were challenging. Similarly, the availability of controls used in the study was limited and these were not always age-matched. With regards to respiratory chain deficiency studies, the tissue used is post-mortem, thus representative of end-stage disease. In addition, two of the controls used for assessment of the occipital lobe were disease controls, who died from sudden infantile death syndrome (SIDS).

In the case of mtDNA damage investigations, frozen tissue was only available for adult patients with *POLG* mutations, thus mtDNA depletion could not be directly correlated with Alpers disease. Despite these limitations, this work achieved to reveal respiratory chain deficiencies in neurons of patients with Alpers and mtDNA depletion in adult *patients with POLG* mutations.

6.4.2 Future work

Other neuropathological features of Alpers include astrocytosis and gliosis. Since astrocytes, and glial cells are important in normal brain functioning, an understanding of mitochondrial dysfunction within those cells may unravel the mechanisms lagging behind impaired neuronal dynamics. Mitochondrial deficiencies within these cells may contribute to the severity of the phenotype (Lax *et al.*, 2016).

In addition, studies on frozen tissue could be used to study mtDNA depletion and levels of mtDNA deletions in micro-dissected interneurons and pyramidal cells using a QPCR protocol. It would be interesting to see whether mtDNA copy number within specific neuronal sub-populations correlate with respiratory chain deficiencies. This approach could be achieved for both young and older patients to unravel any differences in the pathomechanisms of Alpers and *POLG*-related epilepsy.

6.4.3 Conclusions

For the purposes of these study, I used a quantitative quadruple immunofluorescent approach to investigate mitochondrial respiratory chain deficiencies in Alpers. I have shown that GABAergic interneurons demonstrate extensive respiratory chain deficiencies involving complex I, and to a lesser extent, complex IV in the occipital, parietal and frontal lobes of patients with clinically and/or genetically defined Alpers. Defects are most predominant in the occipital lobe.

I have also shown mtDNA depletion in the occipital lobe homogenates of adult *POLG* patients; suggesting that mtDNA depletion is the underlying mechanisms of *POLG*-related disease and may be a common in both young and adult patients.

Overall, my findings support the hypothesis that *POLG* mutations cause respiratory chain deficiencies within interneurons, secondary to mtDNA depletion; leading to impaired neuronal oscillations, giving rise to the neurological deficits seen in patients with Alpers.

Chapter 7 Neuropathological Features in patients with Alpers

7.1 Introduction

The mechanisms underlying neurodegeneration in Alpers remain largely unknown, due to the rarity of post-mortem brain tissue. The first neuropathological report of Alpers was documented by Bernard Alpers in 1931, who described the disorder as 'diffuse progressive degeneration of the grey matter of the cerebrum' accompanied by neuropathological changes including neuronal loss and gliosis (Alpers, 1931).

Since then several reports describing neuropathological changes in Alpers have been published (reviewed in Chapter 3). Macroscopically, Alpers is characterized by atrophy, reduction of cortical thickness and cortical softening predominantly affecting the occipital lobes and to a lesser extent the parietal and frontal lobes (Kollberg *et al.*, 2006; Uusimaa *et al.*, 2008; Sofou *et al.*, 2012). Cerebellar changes and necrotic lesions can be variable. The changes are mostly observed in the grey matter, although recent studies have demonstrated myelin and axonal abnormalities in the white matter (Harding *et al.*, 1995; Simonati *et al.*, 2003; Bao *et al.*, 2008).

Microscopic studies have shown pathological changes including: neuronal loss, spongiosis, Purkinje cell loss and astrogliosis, characteristics often used for diagnosis. The most severe pathology is associated with posterior brain regions (Hunter *et al.*, 2011; Sofou *et al.*, 2012; Rajakulendran *et al.*, 2016) rather than anterior regions, correlating with clinical and neuroimaging findings. Neuronal loss has been qualitatively assessed and the specific sub-neuronal populations affected have not been described in these studies.

More recently, Lax and colleagues demonstrated interneuron loss, secondary to respiratory chain deficiency in adult patients with mitochondrial disease, including patients with *POLG* mutations. It was hypothesized that interneuron pathology may lead to impaired GABAergic neurotransmission, leading to an imbalance between inhibition and excitation, favouring increased excitability and thus seizure generation (Lax *et al.*, 2016).

In the case of Alpers' syndrome, extensive respiratory chain deficiencies involving complexes I and IV in patient neurons from the frontal cortex, hippocampus and substantia nigra has been demonstrated (Tzoulis *et al.*, 2014).

More recent work performed by Dr. Hayhurst and Dr. Lax in interneurons and pyramidal neurons of the occipital lobe as well as Purkinje cells of the cerebellum has shown extensive respiratory chain deficiencies involving complex I and IV coupled with neuron loss. Purkinje cell loss was evident in the cerebellum of patients, however this was to a lesser extent compared to the neuronal loss (including interneurons and pyramidal neurons) observed in the occipital lobe (courtesy of Dr. Hayhurst and Dr. Lax).

The previous chapter demonstrated severe respiratory chain deficiencies involving complexes I, and to a lesser extent complex IV, in the occipital, parietal and frontal lobes of patients with Alpers. Interneurons exhibited more extensive respiratory chain deficiencies than pyramidal neurons. In addition, the work described on the previous chapter showed complex I ad IV deficiencies in the pyramidal neurons of patients, however these were milder compared to the interneurons.

7.2 Aims and Objectives

This chapter focuses on understanding the neuropathological changes underlying neurodegeneration in patients with clinically and/or genetically defined Alpers. The aim of this chapter is to examine the impact of the respiratory chain deficiencies, previously characterised (see Chapter 6), on interneuron and pyramidal neuron pathology and test the hypothesis of an imbalance between inhibition and excitation as a contributor to the neurological involvement seen in patients with Alpers. To this aim the specific objectives are to:

1) Quantitatively assess the extent of interneuron and pyramidal cell loss in the occipital, parietal and frontal lobes of patients with Alpers compared to controls.
2) Semi-quantitatively assess the degree of astrogliosis in patients with Alpers compared to controls.

7.3 Results

7.3.1 Patient Characteristics

The gross neuropathology findings from seven patients with clinically and/or genetically defined Alpers were assessed. Molecular genetic diagnosis of *POLG* mutations confirmed the presence of *POLG* mutations in five patients. For patients 1 and 2 genetic diagnosis was unavailable, as the patients died prior to *POLG* genetic testing. Frozen tissue was not available for these patients, while attempts of DNA extraction from paraffin-embedded tissue did not allow successful PCR amplification. The patient and control details used in this study are summarized in Table 7.1. Control details used in this study are summarized in Table 7.2.

Patient	Age of Onset	Age at Death	Disease Duration	Gender	Genetic Defect	Clinical Symptoms	Brain Region
Patient 1	2 months	5.5 months	3.5 months	Male	Unknown	Epilepsy, developmental regression, heart and respiratory failure.	Parietal
Patient 2	4 months	13 months	9 months	Male	Unknown	Epilepsy and pneumonia.	Parietal, frontal
Patient 3	11 months	14 months	3 months	Female	p.(Ala467Thr)/ p.(Gly848Ser)	Epilepsy, developmental regression, liver failure.	Parietal
Patient 4	17 months	27 months	10 months	Male	p.(Ala467Thr)/ (p.Thr914Pro)	Epilepsy and respiratory failure.	Parietal
Patient 5	11 months	13 months	2 months	Male	p.(Ala467Thr)/ p.(Gly303Arg)	Epilepsy and liver failure.	Occipital (Tzoulis *et al.*, 2014)
Patient 6	7.2 months	7.8 months	<1 month	Male	p.(Ala467Thr)/ p.(Gly848Ser)	Epilepsy and liver failure.	Occipital, frontal (Tzoulis *et al.*, 2014)
Patient 7	2 years	8 years	6 years	Male	p.(Ala467Thr)/ p.(Gly303Arg)	Epilepsy	Frontal (Tzoulis *et al.*, 2014)

Table 7.1: Patient details used in this study.

Control	Age at Death	Gender	Cause of Death	Brain Region
Control 1	13 months	Female	Occipital porencephaly	Parietal
Control 2	22 years	Female	Poisoning	Occipital, parietal
Control 3	24 years	Female	Suspension by ligature	Occipital, parietal
Control 4	4.5 months	Female	SIDS	Occipital, frontal
Control 5	1 month	Male	SIDS	Occipital, frontal
Control 6	6 years	Female	Drowning	Frontal
Control 7	8 years	Female	Asphyxia	Frontal
Control 8	16 years	Male	Suspension by ligature	Occipital

Table 7.2: Control details used in this study. SIDS=sudden infantile death syndrome.

7.3.2 Gross Neuropathology Findings

Grey matter cortical ribbon thinning and neuronal loss was noted in the occipital, parietal and frontal lobes of the patients included. The gross neuropathology findings from qualitative assessment and neuropathology reports are summarized in Table 7.3. In patients 5-7 focal energy-dependent neuronal necrosis (FENN) was observed in CA1 of the hippocampus and in Purkinje cells of the cerebellum. The term FENN was proposed by Tzoulis and colleagues (Tzoulis *et al.,* 2014) and is derived based on neuropathological characteristics of the tissue, with lesions being described as focal, well-demarcated areas featuring neuronal loss and spongiform changes, accompanied by eosinophilia and increased inflammation. FENN lesions have often be referred to as stroke-like lesions due to their resemblance of lesions occurring as a result of an ischaemic stroke. With regards to mitochondrial disease, FENN lesions do not seem to have a vascular aetiology (Tzoulis *et al.,* 2014; Hikmat *et al.,* 2017), however its aetiology remains unclear.

Patient	Occipital lobe	Frontal lobe	Parietal lobe	Cerebellum	Basal Ganglia	Thalamus	Hippocampus
Patient 1	Atrophy of gyri. Severe narrowing of white matter.	N/A	Severe atrophy of gyri. Marked cell loss in layers I and II with marked spongiosis and astrogliosis.	Atrophy with mild to moderate Purkinje cell loss.	Marked gliosis in the putamen. Well preserved globus pallidus.	Mild gliosis.	N/A
Patient 2	Atrophy of gyri. Gliosis.	Atrophy of gyri. Severe neuron loss. Spongiosis.	Atrophy of gyri. Gliosis.	Astrogliosis in dentate nucleus.	Preserved.	Preserved	Atrophic hippocampal formation.
Patient 3	Mild spongiosis.	N/A	Mild spongiosis in superficial layers.	Marked loss of Purkinje cells.	N/A.	N/A	Spongiform changes and marked gliosis.
Patient 4	Atrophic gyri, gliosis and spongiform changes of layers II and III and marked loss of neurons.	N/A	Atrophic gyri, loss of neurons and neuropil degeneration.	Marked loss of Purkinje cells.	Caudate preserved.	N/A	Spongiform changes and marked gliosis.

Patient 5	Atrophy of gyri. Spongiosis, capillary proliferation, neuron loss.	N/A	N/A	FENN in cerebellar cortex with no evidence of gliosis.	N/A	N/A	FENN in CA1.
Patient 6	Severe atrophy of gyri. Neuron loss, spongiosis.	Atrophy of gyri. Spongiosis and neuronal loss.	N/A	Mild neuronal loss and gliosis in cerebellar cortex.	Mild neuronal loss and gliosis in substanti a nigra.	N/A	FENN in CA1.
Patient 7	N/A	Severe atrophy of gyri, marked spongiosis and neuron loss.	N/A	FENN and mild neuronal liss and gliosis in cerebellar cortex.	Mild neuronal loss and gliosis in substanti a nigra	Moderate neuronal loss and gliosis.	FENN in CA1.

Table 7.3: Gross neuropathology findings from patients with Alpers. Key: FENN=focal-energy dependent neuronal necrosis. N/A=not applicable.

7.3.3 Neuron loss

Since respiratory chain deficiency was found in the neurons of the patients in this study, as discussed in Chapter 6, I aimed to investigate the consequences of these deficiencies on the two different neuronal sub-populations. A pre-validated immunohistochemistry protocol was used to detect interneurons (GAD65-67 positive cells) and pyramidal neurons (SMI-32P positive cells) by Dr. Hannah Hayhurst. Cortical neuronal densities encompassing cellular layers I-VI of patients and controls were distinguished as described in the section 2.6.4.

A. Occipital cortex

Occipital lobe tissue was available for patients 5 (p.(Ala467Thr)/p.(Gly303Arg)) and 6 (p.(Ala467Thr)/p.(Gly848Ser)). These patients were compared to two paediatric age-matched disease controls (who died from sudden infantile death syndrome (SIDS). The neuropathology of SIDS is characterised by: morphological changes of the brainstem and cerebellum accompanied by reactive astrocytes and reduced expression of serotonin in neuronal cell bodies (Matturri and Lavezzi, 2011; Mehboob *et al.*, 2017). Since SIDS controls are considered as disease controls, additional control subjects (control, 2, 3 and 8) were included for comparison. The data from these controls were kindly provided by Dr. Hannah Hayhurst, as part of her project.

Positive neurons were identified by dark brown chromogen immunostaining (Figures 7.1 and 7.2). Control subjects 2 and 3 displayed higher neuronal densities compared to SIDS controls 4 and 5, especially in the case of pyramidal neurons (see Figure7.3 and Table 7.4) Patient 5 (p.(Ala467Thr)/p.(Gly303Arg)) showed a marked reduction in interneuron density compared to all controls (28% of control mean). Patient 6 (p.(Ala467Thr)/p.(Gly303Arg)) did not demonstrate interneuron loss when compared to SIDS controls 4 and 5. However when compared to healthy controls 2, 3 and 8 a reduction was observed (see Figure 7.3A). It is relevant to highlight this change particularly as controls 4 and 5 died from SIDS at 4.5 months and 1 month respectively. It is therefore possible that these controls have suffered from neurodevelopmental brain abnormalities including suboptimal neurogenesis, thus having lower neuron densities compared to healthy individuals.

In the case of pyramidal neurons, SMI-32P positive neurons were higher in controls 2, 3 and 8 compared to SIDS controls 4 and 5 (see Figure 7.3B). In patient 5 (p.(Ala467Thr)/p.(Gly303Arg)) pyramidal neuron density was not different to SIDS

controls 4 and 5. However a mild reduction was observed when compared to healthy controls 2, 3 and 8. Patient 6 (p.(Ala467Thr)/p.(Gly848Ser)) displayed a marked reduction in pyramidal neuron density when compared to all controls (13% of control mean) (see Figure 7.3B and Table 7.4).

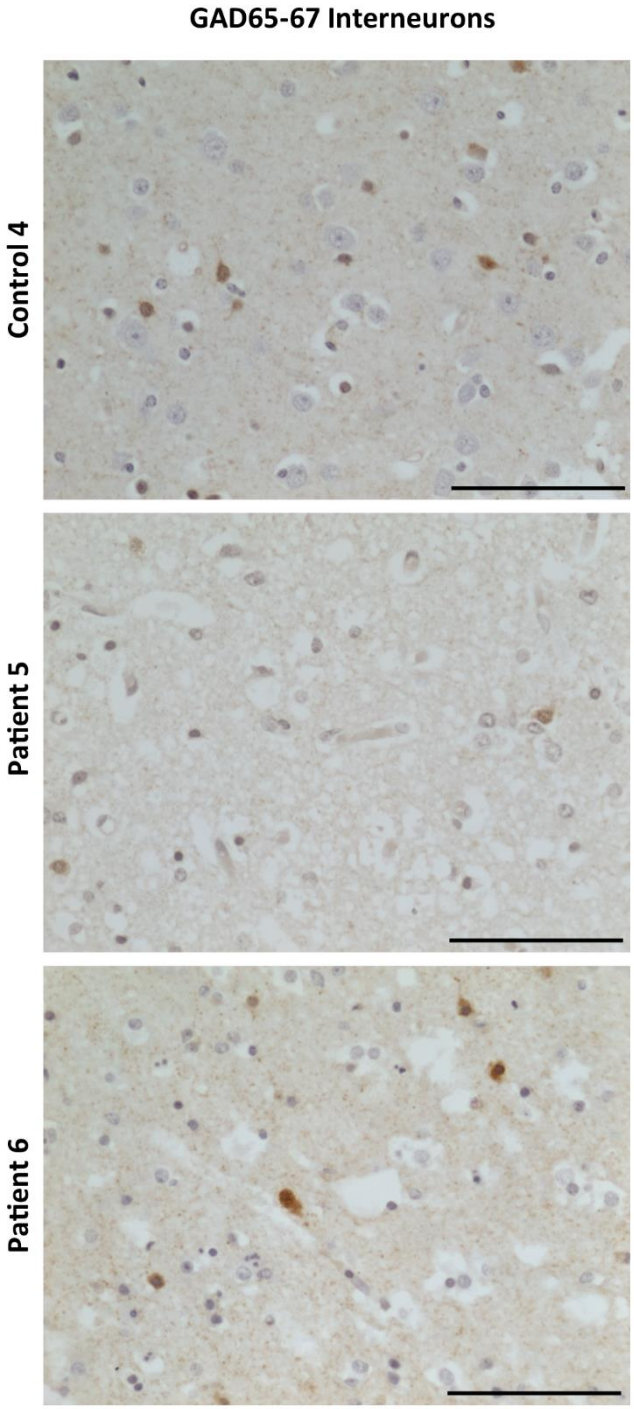

Figure 7.1: GAD65-67 immunostaining in occipital lobe from patients with Alpers.
Representative images captured at 40x magnification from the occipital lobe of patients with Alpers. GAD65-67 positive interneurons are detected by dark brown chromogen immunostaining. There is a marked reduction in the number of positive GAD65-67 interneurons in patient 5 (p.(Ala467Thr)/p.(Gly303Arg)) compared to the control. The number of positive GAD65-67 interneurons in patient 6 (p.(Ala467Thr)/p.(Gly848Ser)) are comparable to the control. Scale bar=100µm.

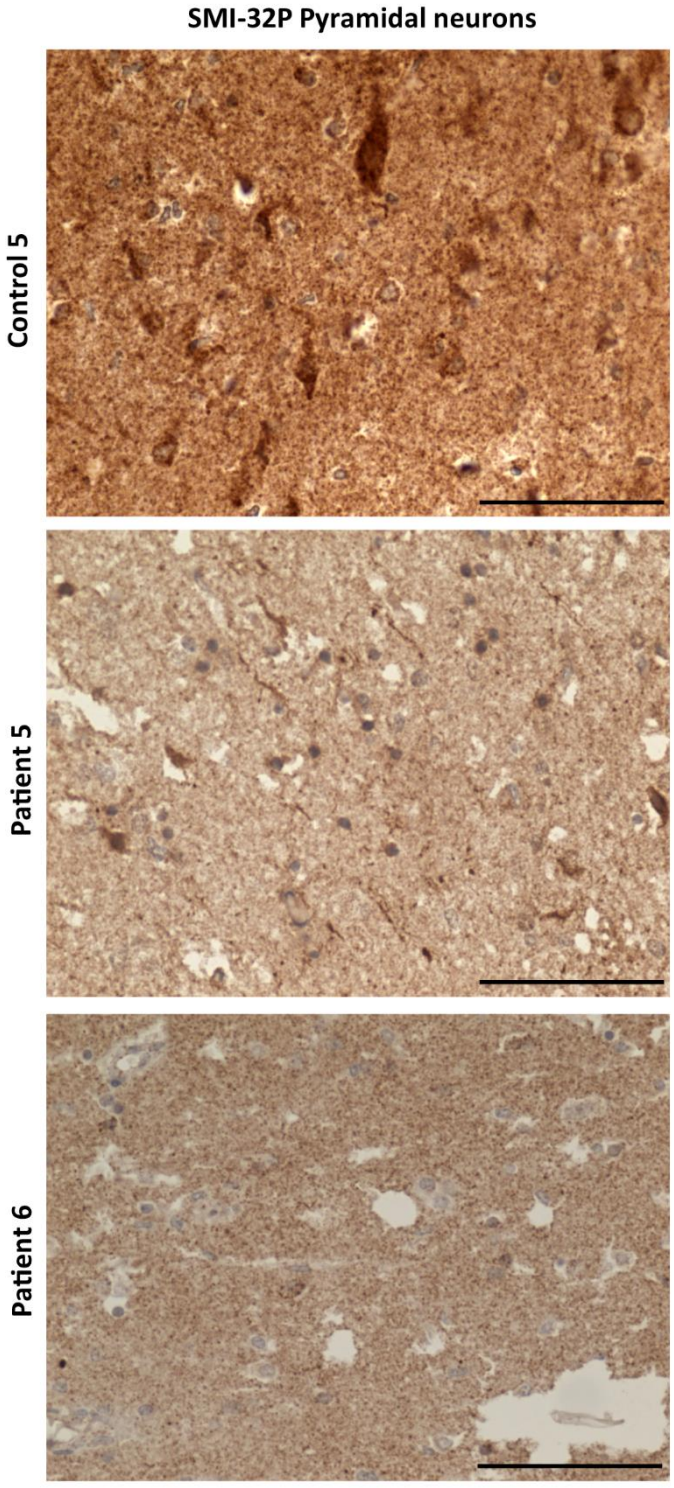

Figure 7.2: SMI-32P immunostaining in the occipital cortex of patients with Alpers.
Representative images of pyramidal neurons at 40x magnification from the occipital cortex of patients with Alpers' syndrome. SMI-32P positive pyramidal neurons are shown by dark brown chromogen immunostaining. The number of positive SMI-32P pyramidal neurons in patient 5 (p.(Ala467Thr)/p.(Gly303Arg)) is comparable to the controls. Patient 6 (p.(Ala467Thr)/p.(Gly848Ser)) shows a severe reduction in the number of positive SMI-32P pyramidal neurons when compared to the control. Scale bar=100µm.

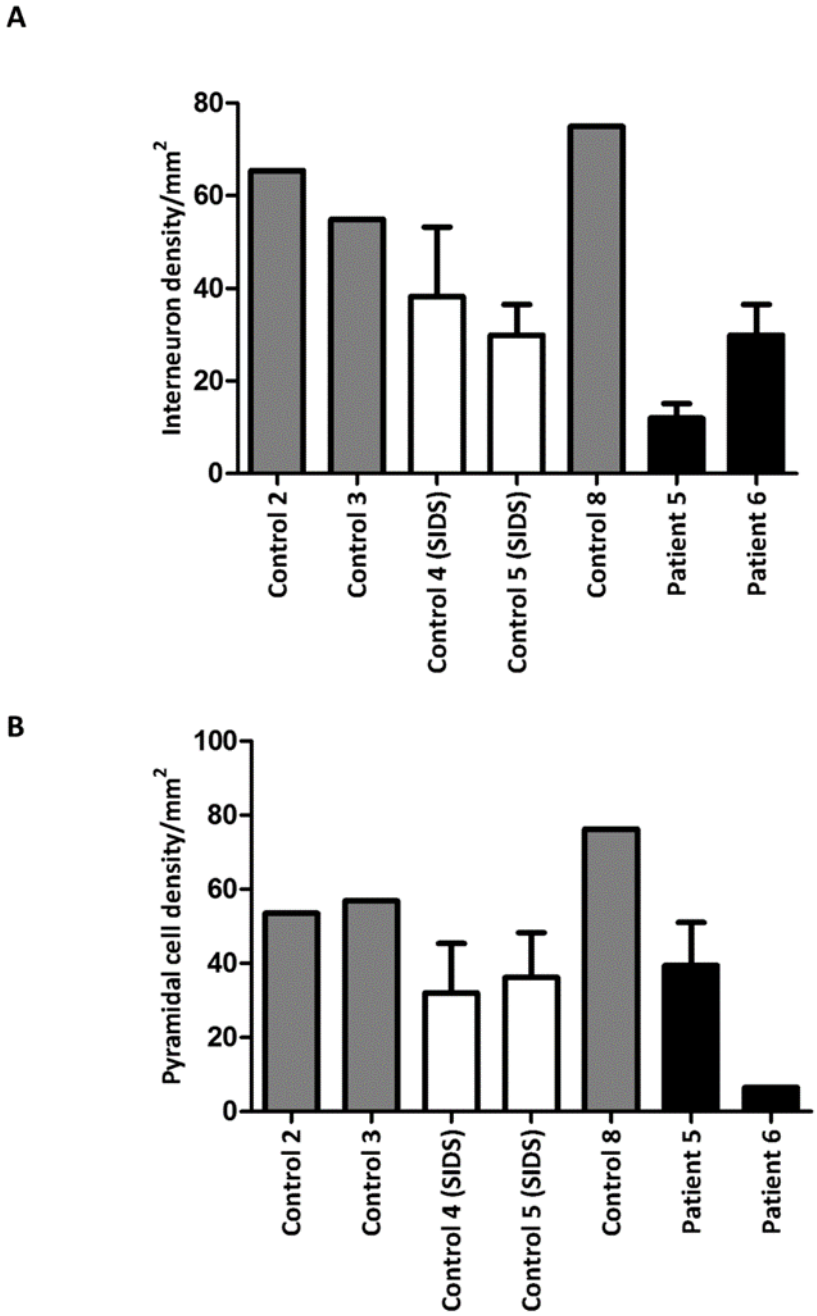

Figure 7.3: Neuronal densities in occipital cortex of patients with Alpers' syndrome. (A) Quantification of interneuron densities in the occipital cortex of patients with Alpers' syndrome. There is a marked reduction of interneuron density in patient 5 (p.(Ala467Thr)/p.(Gly303Arg)) compared to controls. The interneuron density in patient 6 (p.(Ala467Thr)/p.(Gly848Ser)) is comparable to controls. (B) Quantification of pyramidal neuron densities in the occipital cortex of patients with Alpers' syndrome. Pyramidal neuron densities in patient 5 (p.(Ala467Thr)/p.(Gly303Arg)) are not different to controls. Patient 6 (p.(Ala467Thr)/p.(Gly848Ser)) shows a severe reduction in pyramidal neuron densities compared to controls. Neuronal densities are presented as bars with mean ± SD, determined from at least two cortical areas of 10mm^2. For controls 2, 3 and 8 only one cortical area of 10mm^2 was quantified.

B. Parietal cortex

In the parietal cortex, the tissue from three healthy controls and four patients was investigated. Only patient 2 showed a marked reduction in GAD65-67 positive interneurons when compared to all controls (17% of control mean). However, patients 1 (no *POLG* diagnosis), 3 (p.(Ala46Thr)/p(Gly848Ser)) and (p.(Ala467Thr)/p.(Thr914Pro)) were not different when compared to controls (see Figures 7.4 and 7.6A).

Pyramidal neuron density was reduced in all patients relative to controls (see Figures 7.5 and 7.6B). Patients 1 and 2 (both without *POLG* diagnosis) showed the most severe pyramidal neuron loss (8% of control mean). In patient 3 (p.(Ala467Thr)/p.(Gly848Ser)) pyramidal neuron loss was evident as pyramidal neuron density was 20% of the control mean (Figure 7.6B).

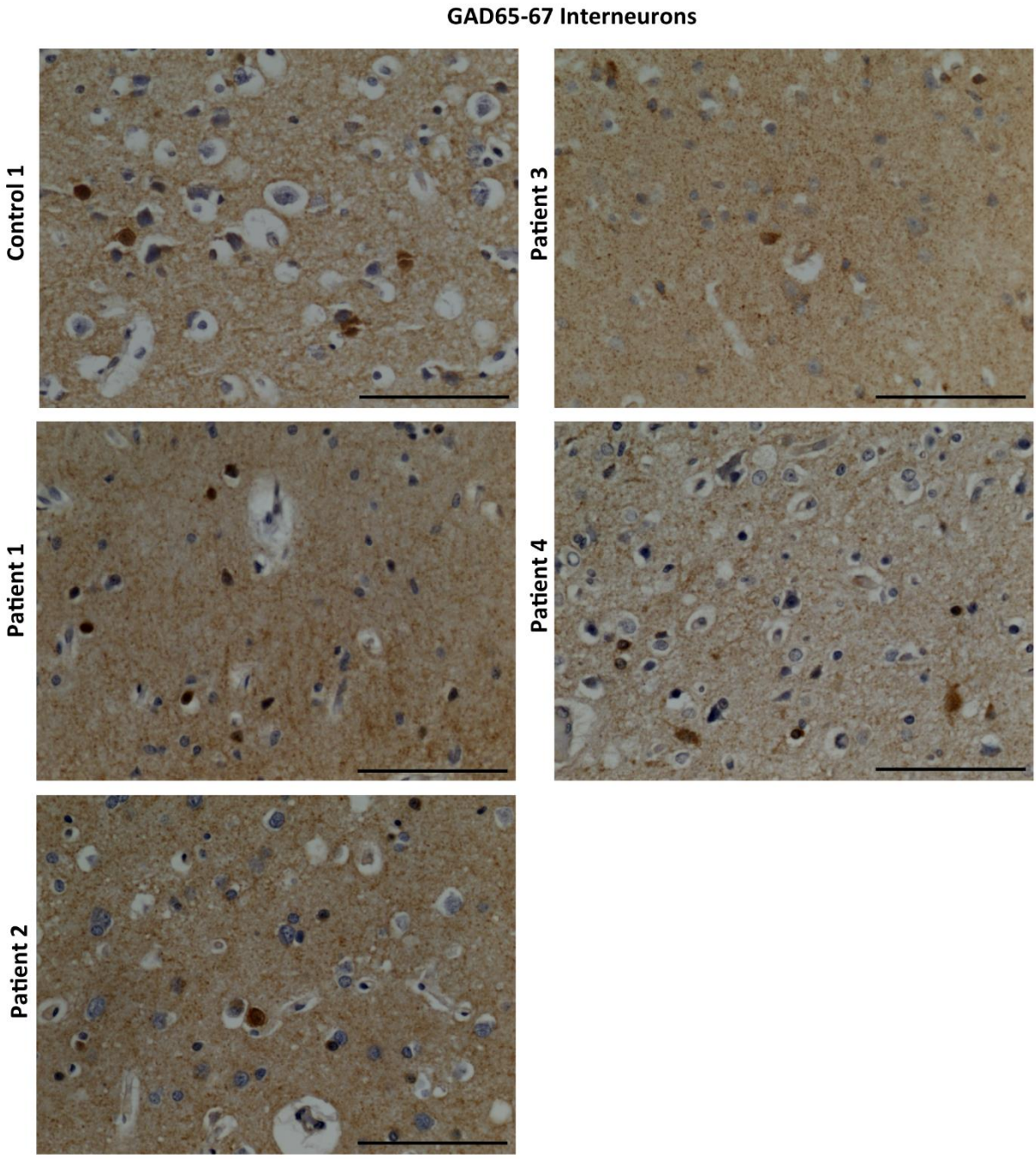

Figure 7.4: GAD65-67 immunostaining in the parietal cortex of patients with Alpers.
Representative images of interneurons captured at 40x magnification from the parietal cortex of patients with Alpers' syndrome. GAD65-67 positive interneurons are shown by brown chromogen immunostaining. Patients 1 (no *POLG* diagnosis), 3 (p.(Ala467Thr)/p.(Gly848Ser)) and 4 (p.(Ala467Thr)/p.(Thr914Pro)) show no difference in GAD65-67 positive interneurons compared to the control. Patient 2 (no *POLG* diagnosis) shows a marked reduction in the number of positive GAD65-67 positive interneurons when compared to the control. Scale bar=100µm.

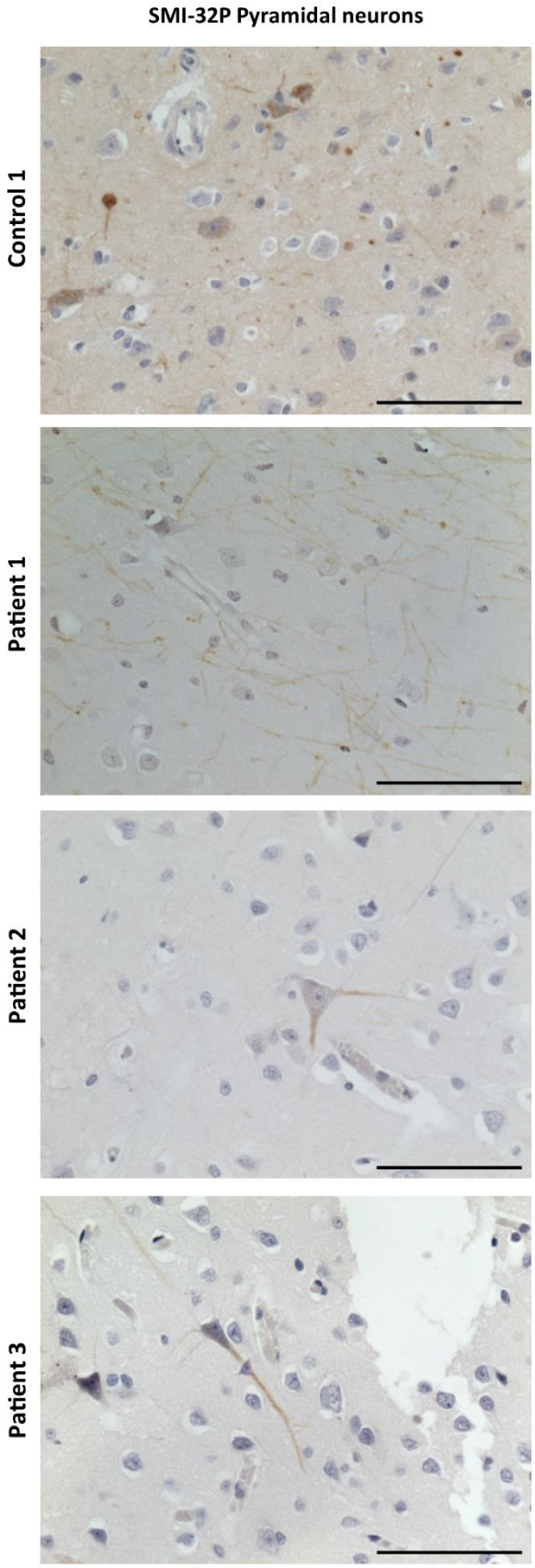

Figure 7.5: SMI-32P immunostaining in the parietal cortex of patients with Alpers.
Representative images of pyramidal neurons captured at 40x magnification (from the parietal cortex of patients with Alpers syndrome. SMI-32P positive pyramidal neurons are shown by brown chromogen immunostaining. There is marked pyramidal neuron in all patients compared to the control. Patients 1 and 2 (both without *POLG* diagnosis) show the most severe pyramidal neuron loss. Scale bar=100µm.

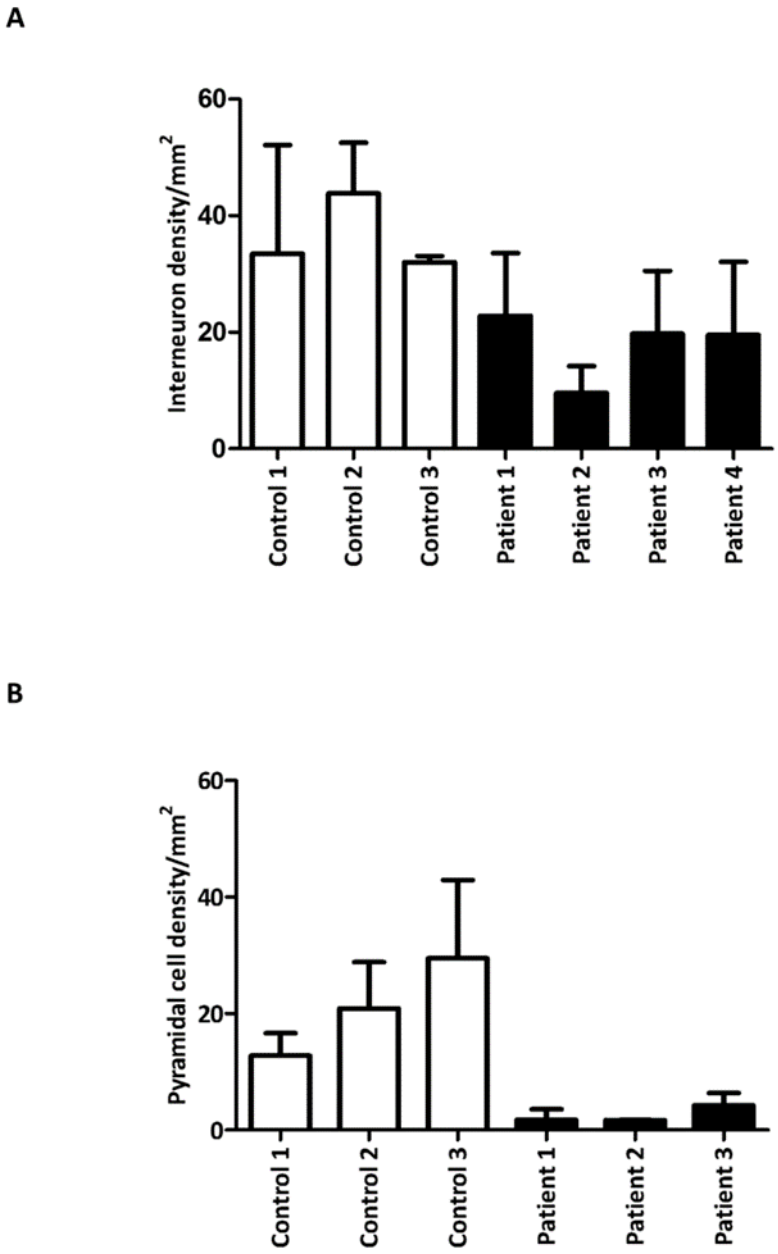

Figure 7.6: Neuronal loss in the parietal cortex of patients with Alpers.(A) Quantification of interneuron densities in the parietal cortex of patients with Alpers. There is a trend of interneuron loss in the patients compared to controls. (B) Quantification of pyramidal neuron densities in the parietal lobe of patients with Alpers. A marked reduction in pyramidal cell densities in the patients is observed, which is more severe compared to interneuron loss. Neuronal densities are presented as bars with mean ± SD, determined from at least two cortical areas of 10mm^2.

C. Frontal cortex

With regards to the frontal lobe, only patient 2 (no *POLG* diagnosis) showed a severe reduction in interneuron density (23% of control mean), suggestive of interneuron loss. Patients 6 (p.(Ala467Thr)/p.(Gly848Ser)) and 7 (p.(Ala467Thr)/p.(Gly303Arg)) did not demonstrate reduction in densities when compared to all controls (Figures 7.7 and 7.8).

Pyramidal neuron densities in the frontal lobe could not be assessed due to limited tissue availability.

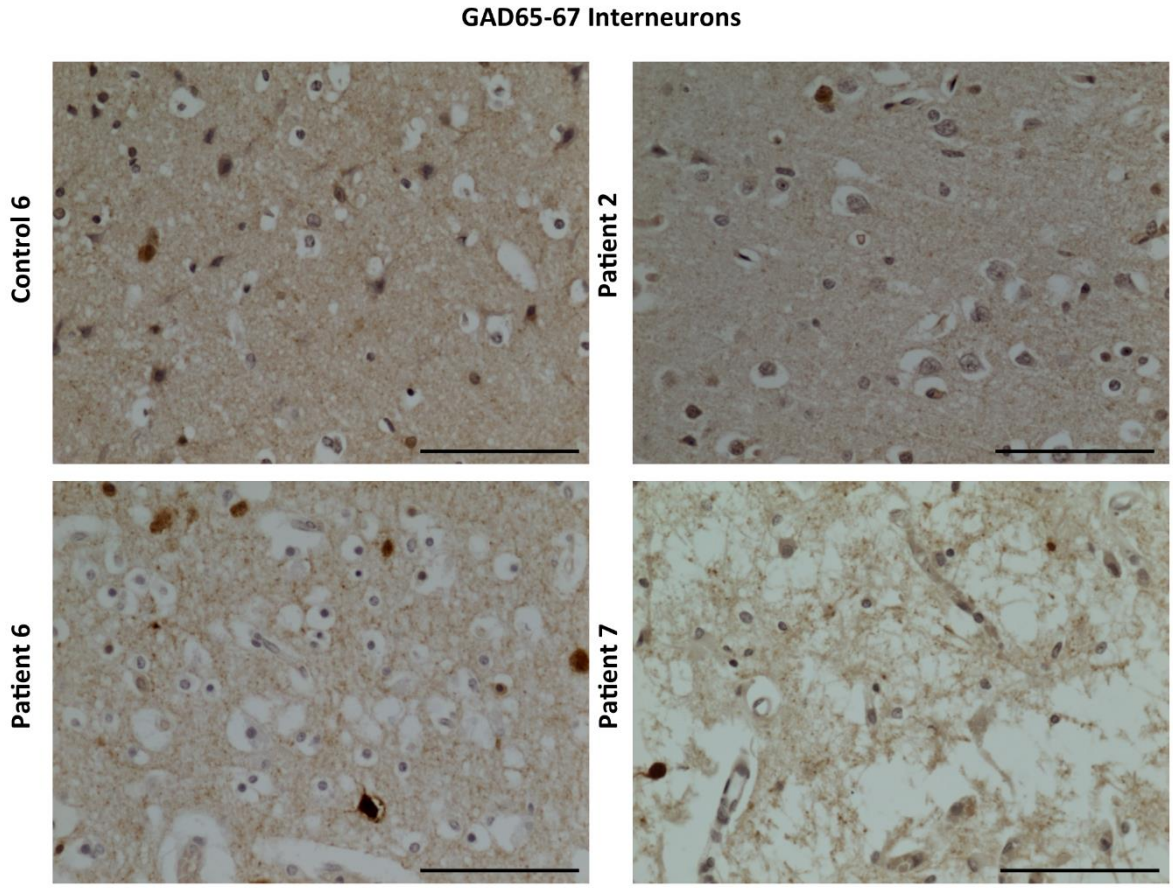

Figure 7.7: GAD65-67 immunostaining in the frontal cortex of patients with Alpers. Here, representative images of GAD65-67 positive interneurons in the frontal cortex of patients with Alpers compared to the control are shown. Patient 2 (no *POLG* diagnosis) shows a marked reduction in the number of GAD65-67 positive interneurons compared to the control. Patients 6 (p.(Ala467Thr)/p.(Gly848Ser)) and 7 (p.(Ala467Thr)/p.(Gly303Arg)) showed no difference compared to the control. Scale bar=100µm.

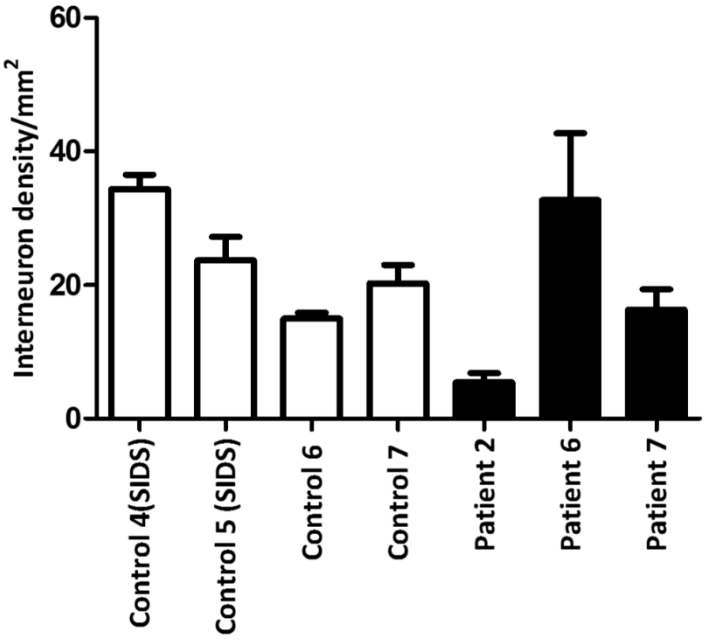

Figure 7.8: Interneuron densities in the frontal cortex from patients with Alpers. Quantitative analysis of interneuron densities showed a marked loss of interneurons in patient 2 (no *POLG* diagnosis), suggestive of interneuron loss. Interneuron densities in patients 6 (p.(Ala467Thr)/p.(Gly848Ser)) and 7 (p.(Ala467Thr)/p.(Gly303Arg)) were no different when compared to controls. Neuronal densities are presented as bars with mean ± SD determined from at least two cortical areas of 10mm^2.

To test the hypothesis of an imbalance between inhibition and excitation, I investigated whether the interneuron to pyramidal cell ratios are altered, as a consequence of neuronal loss.

In the occipital lobe, all controls displayed an interneuron to pyramidal neuron ratio ~1. Patient 5 (p.(Ala467Thr)/p.(Gly303Arg)) showed a decreased interneuron to pyramidal cell ratio compared to the controls, suggesting loss of interneurons. Patient 6 (p.(Ala467Thr)/p.(Gly848Ser)) showed a high interneuron to pyramidal neuron ratio suggesting a loss of pyramidal neurons. In both cases interneuron to pyramidal cell ratios are indicative of an imbalance between inhibition and excitation (see Figure 7.9A).

In the parietal lobe, patients 1 (no *POLG* diagnosis), 2 (no *POLG* diagnosis) and 3 (p.(Ala467Thr))/p.(Gly848Ser)) showed increased GABAergic interneuron density than pyramidal neuron density, as demonstrated by high interneuron to pyramidal neuron ratios, with patient 1 (no *POLG* diagnosis) demonstrating the highest ratio (see Figure 7.9B). The increase in interneuron density is markedly higher compared to the occipital lobe.

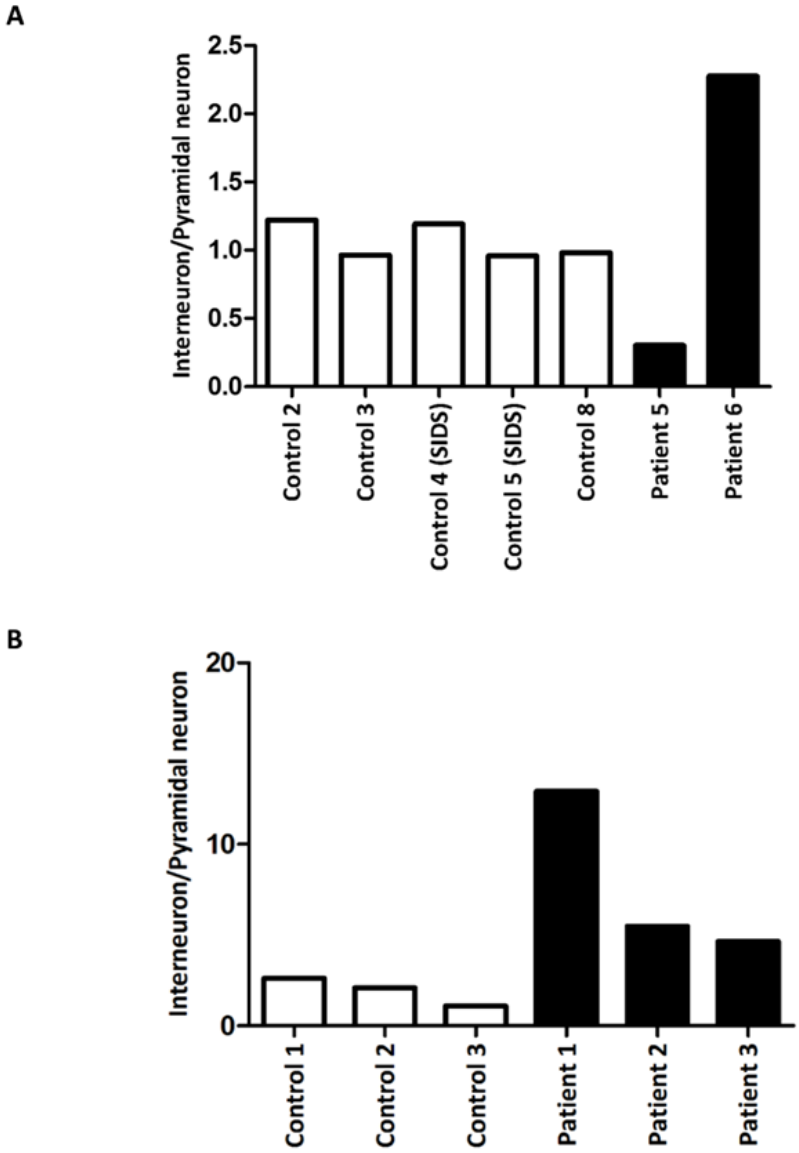

Figure 7.9: Interneuron to pyramidal neuron density ratios in occipital and parietal cortices of patients with Alpers. (A) In the occipital cortex, all controls show a ratio of ~1. Patient 5 (p.(Ala467Thr)/p.(Gly303Arg)) shows a decreased interneuron to pyramidal neuron ratio, suggesting a higher pyramidal neuron density and a loss of inhibitory interneurons. Patient 6 (p.(Ala467Thr)) demonstrates an increased ratio, suggestive of increased interneuron density and a loss of pyramidal neurons. Both cases are indicative of an imbalance between inhibition and excitation. (B) In the parietal cortex, all controls show a ratio of ~1. Patients 1 (no *POLG* diagnosis), patient 2 (no *POLG* diagnosis) and patient 3 (p.(Ala467Thr)/p.(Gly848Ser)) show an increased interneuron to pyramidal neuron density, suggesting loss of pyramidal neurons with patient 1 (no *POLG* diagnosis) showing the highest ratio.

7.3.4 Astrogliosis

Astrocytes are spider-like glial cells of the CNS, which have numerous dendritic projections and make contact to other cells of the CNS. Astrocytes, possess important functions in the CNS such as: repair of damaged tissue and support to neurons. Astrocytes respond to CNS injury via a process known as reactive astrogliosis, a well-characterised pathological feature. Three types of astrocytes exist including: protoplasmic, fibrous and radial. Protoplasmic astrocytes are found in the grey matter and give rise to a 'globoid distribution' (Sofroniew and Vinters, 2010). Fibrous astrocytes are found in the white matter and give rise to a branched network. Both astrocytic sub-types including protoplasmic and fibrous make contact to blood vessels. In contrast, radial glia are bipolar cells responsible for giving rise to progenitor cells (Sofroniew and Vinters, 2010).

Astrogliosis (altered astrocytic morphology) has been reported as a pathological feature of Alpers (Sofou *et al.*, 2012; Montassir *et al.*, 2015). To characterise reactive astrocytic populations in the patients considered in the present study, an antibody against the glial fibrillary acidic protein (GFAP), which is expressed in astrocytes was applied by immunohistochemistry as described in section 2.4.3. A semi-quantitative assessment was performed based on the positive reactive astrocytes observed by dark brown chromogen. In the grey matter the scale -/+/++ was used which is defined as: normal astrocytic morphology (-), mild (+), moderate (++) and severe (+++) astrogliosis.

White matter has higher normal physiological levels of GFAP as it is more densely populated by glial cells. Therefore, control tissue demonstrates a higher immunostaining when compared to the grey matter. As such evidence of high GFAP immunoreactivity was considered as normal astrocytic morphology in controls, and these were compared to the patients. For both grey and white matter, the morphology/size of astrocytes was also considered and compared to controls.

A. Occipital cortex

Control tissue was only available from individuals who died from SIDS. Control 4 showed normal levels of astrogliosis, while control 5 showed mild (+) astrogliosis. In the white matter, normal GFAP immunostaining and normal astrocytic morphology.

In the grey matter, Patient 5 (p.(Ala467Thr)/p.(Gly303Arg)) showed mild astrogliosis (+), however astrocytes demonstrated a swollen morphology (Montassir *et al.*, 2015).

Patient 6 (p.(Ala467Thr)/p.(Gly848Ser)), demonstrated mild astrogliosis (+) in the grey matter, without any observable changes in astrocyte morphology compared to controls (Figure 7.10).

In the white matter both patients showed normal astrocytic morphology (Figure 7.11).

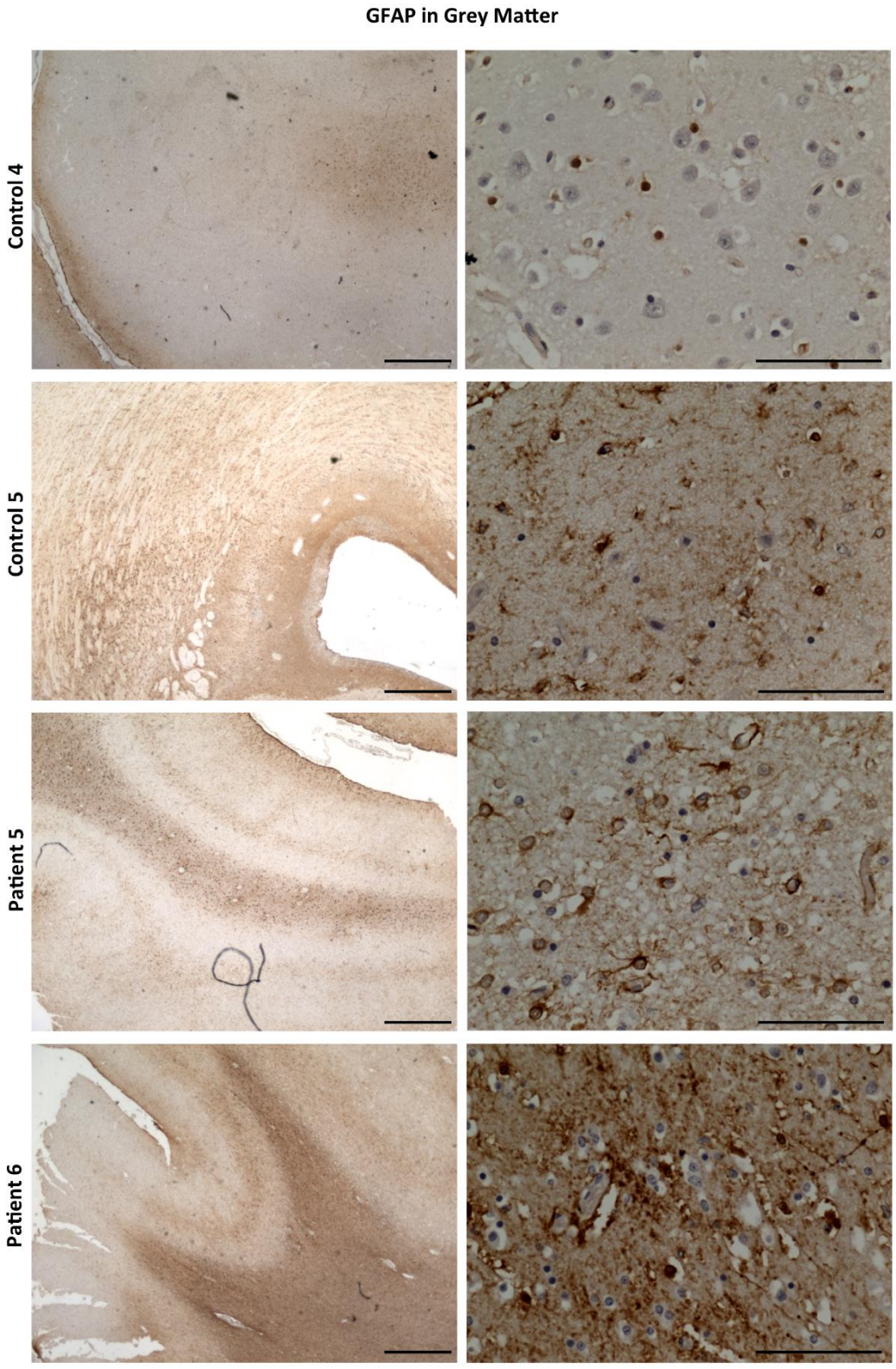

Figure 7.10: Astrogliosis of the grey matter in the occipital lobe of patients with Alpers' syndrome. Representative images take at 2x magnification (left) and at a higher magnification (40x, right) showing astrogliosis in the occipital lobe of patients with Alpers' syndrome. GFAP-positive astrocytes are visualised by dark brown chromogen immunostaining. The control shows normal sdtrocytic morphology. Patient 5 (p.(Ala467Thr)/p.(Gly303Arg)) shows mild astrogliosis (+) compared to the control. Patient 6 (p.(Ala467Thr)/p.(Gly848Ser)) showed mild astrogliosis (+). Scale bar=100µm.

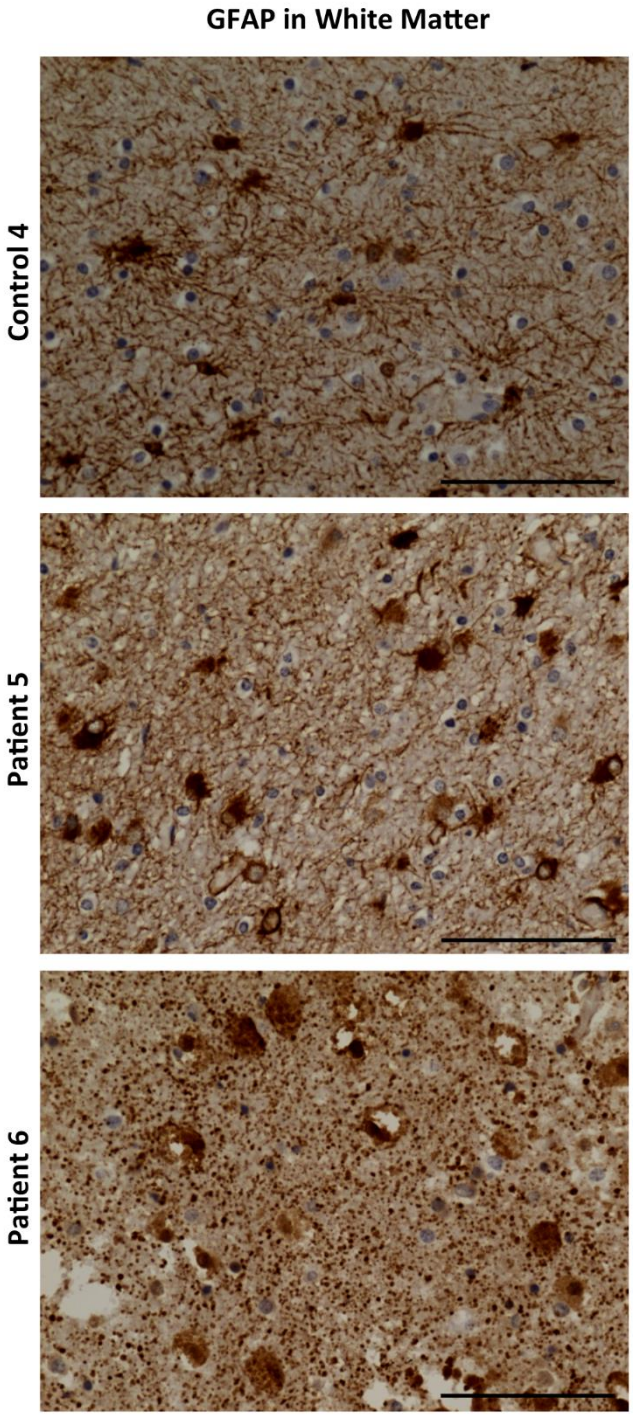

Figure 7.11: Astrogliosis of the white matter in the occipital lobe of patients with Alpers' syndrome. Representative images take at 40x magnification showing astrogliosis in the occipital lobe of patients with Alpers' syndrome. GFAP-positive astrocytes are visualised by dark brown chromogen immunostaining. Both patients showed normal astrocytic morphology in the white matter. Scale bar=100µm.

B. Parietal cortex

Control 3 was only available for assessment, which showed normal astrocytic morphology in the grey matter. Patients 1 (no *POLG* diagnosis) and 3 (p.(Ala467Thr)/p.(Gly848Ser)) showed severe astrogliosis (+++) as evidenced by swollen/hypertrophic astrocytes. Patient 2 (no *POLG* diagnosis) showed normal astrocytic morphology (see Figure 7.12).

In the white matter normal astrocytic morphology was observed in patients 2 and 3 (no *POLG* diagnosis) (Figure 7.13). White matter was not available for analysis for patient 1 (no *POLG* diagnosis).

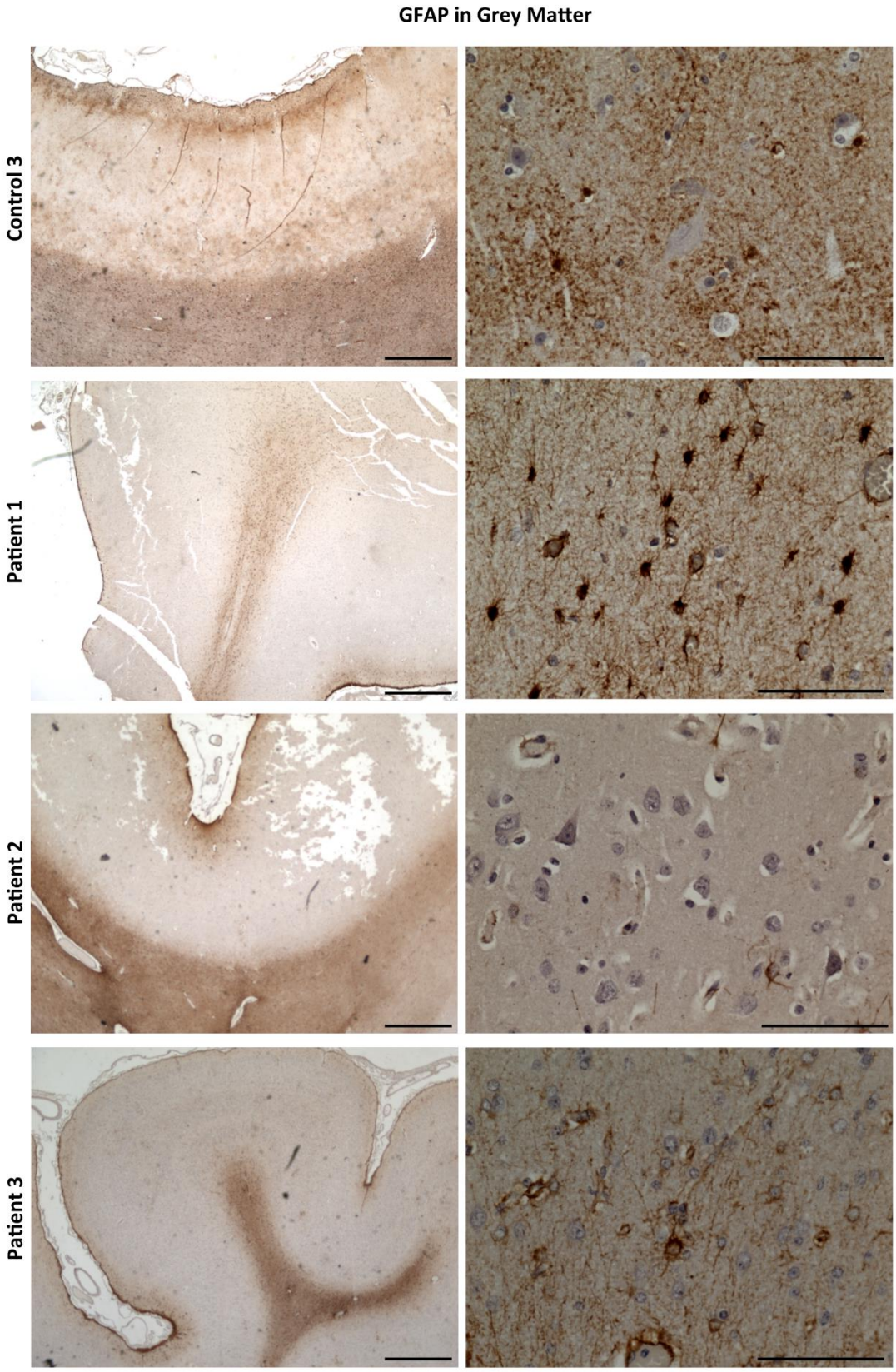

Figure 7.12: Astrogliosis of the grey matter in the parietal lobe of patients with Alpers. Representative images taken at 2x magnification (left) and at a higher magnification (40x, right) showing astrogliosis in the parietal lobe of patients with Alpers. GFAP-positive astrocytes are visualised by dark brown chromogen. Patients 1 (no *POLG* diagnosis) and 3 **(**p.(Ala467Thr)/p.(Gly848Ser)) show severe astrogliosis (+++) compared to the control. Patient 2 (no *POLG* diagnosis) show normal astrocytic morphology. Scale bar=100µm.

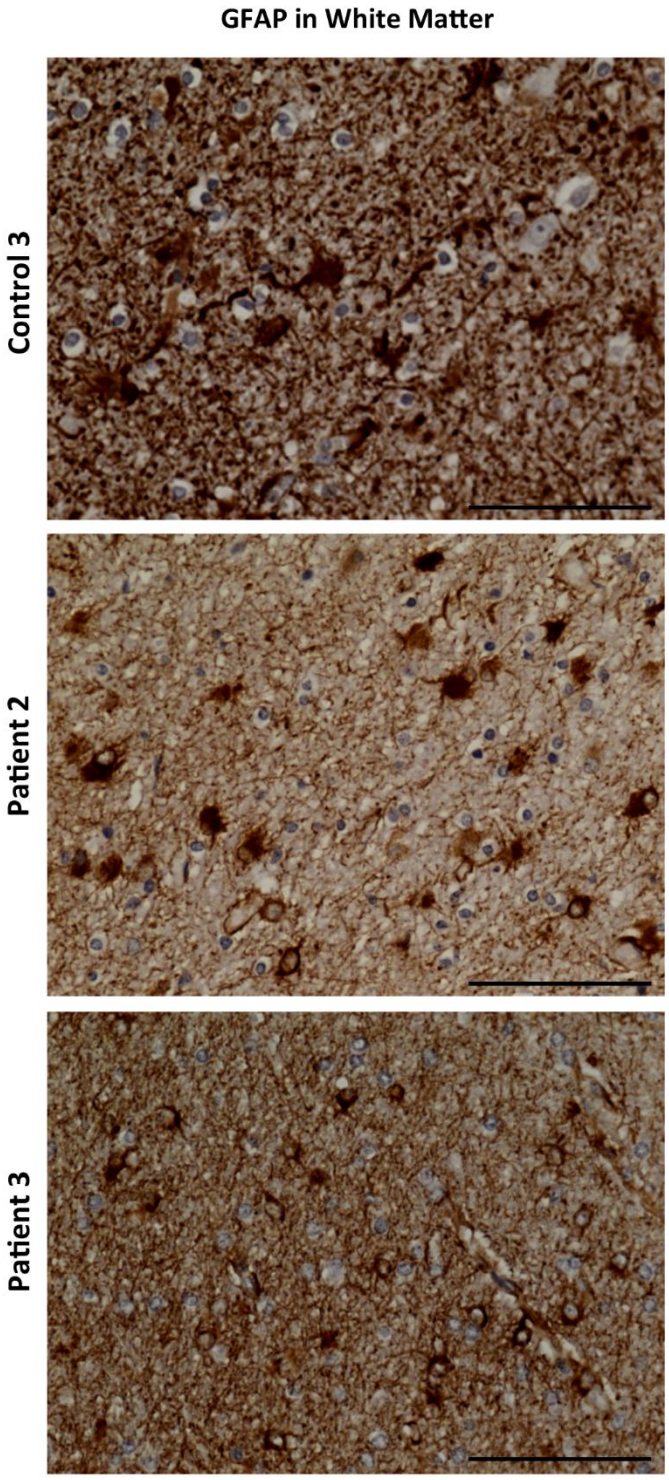

Figure 7.13: Astrogliosis of the white matter in the parietal lobe of patients with Alpers. Representative images take at 40x magnification showing astrogliosis in the white matter of the parietal lobe of patients with Alpers. GFAP-positive astrocytes are visualised by dark brown chromogen. Patients 2 (no *POLG* diagnosis) and 3 (p.(Ala467Thr)/p.(Gly848Ser)) showed normal astrocytic morphology in the white matter. Scale bar=100µm.

C. Frontal cortex

With regards to frontal lobe, controls showed normal astrocytic morphology in the grey matter. Mild astrogliosis (+) was evident in patient 2 (no *POLG* diagnosis). Patient 6 (p.(Ala467Thr)/p.(Gly848Ser)) showed normal astrocytic morphology when compared to the control. Patient 7 (p.(Ala467Thr)/p.(Gly303Arg)) showed severe astrogliosis (+++) in the grey matter (see Figure 7.14)

In the white matter, patients 5 (p.(Ala467Thr)/p.(Gly303Arg)) and 6 (p.(Ala467Thr)/p.(Gly848Ser)) exhibited normal astrocytic morphology. Patient 7 (p.(Ala467Thr)/p.(Gly303Arg)) showed mild astrogliosis (+) as evidenced by swollen astrocytes (see Figure 7.15).

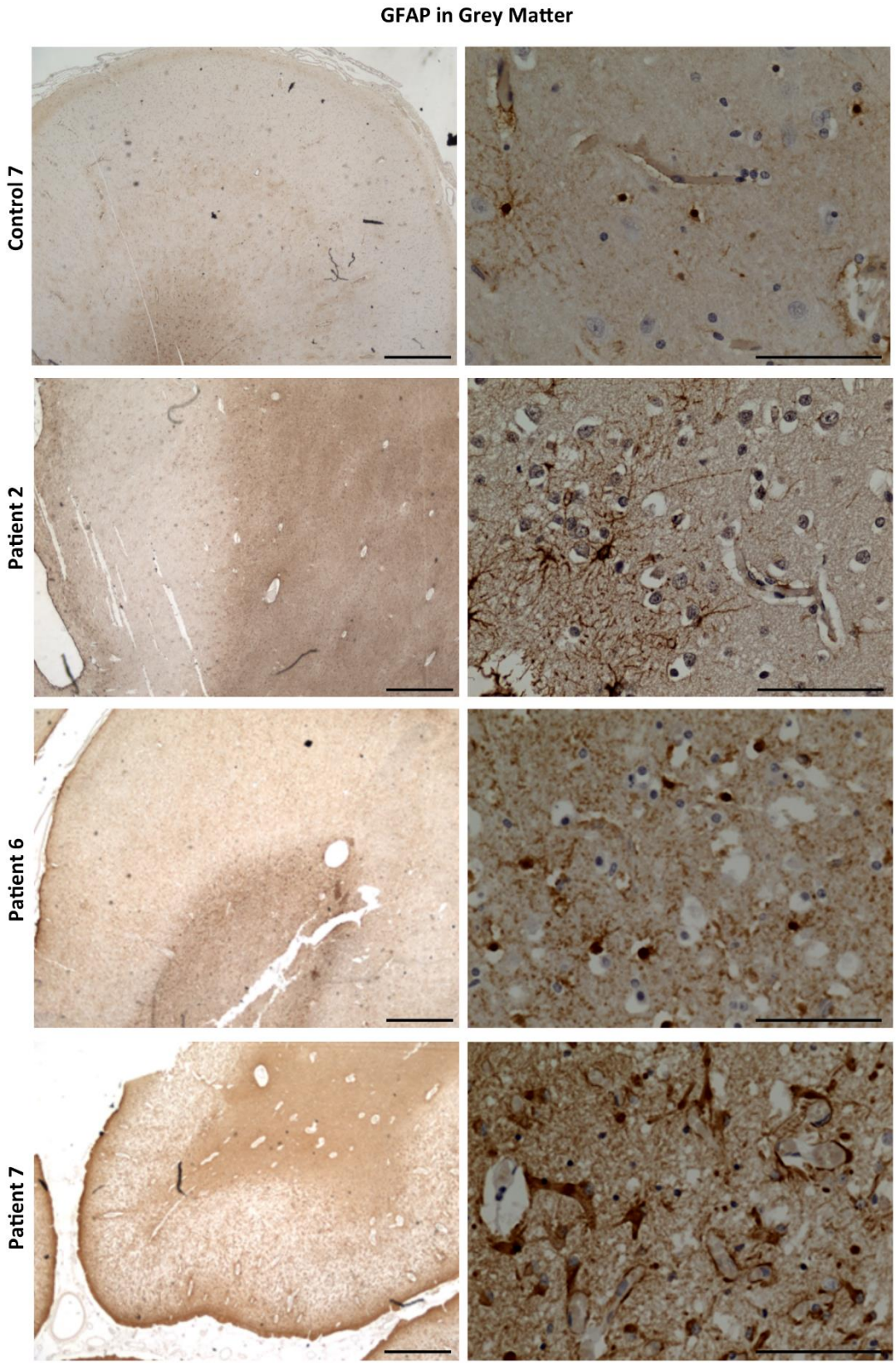

Figure 7.14: Astrogliosis of the grey matter in the frontal lobe of patients with Alpers. Representative images take at 2x magnification (left) and at a higher magnification (40x, right) showing astrogliosis in the parietal lobe of patients with Alpers. GFAP-positive astrocytes are visualised by dark brown chromogen. Patient 2 (no *POLG* mutations) showed mild astroglisosis (+), Patient 6 (p.(Ala467Thr)/p.(Gly848Ser)) showed normal astrocytic morphology. Patient 7 (p.(Ala467Thr)/p.(Gly303Arg)) showed severe astrogliosis (+++) as evidenced by swollen astrocytes. Scale bar=100µm.

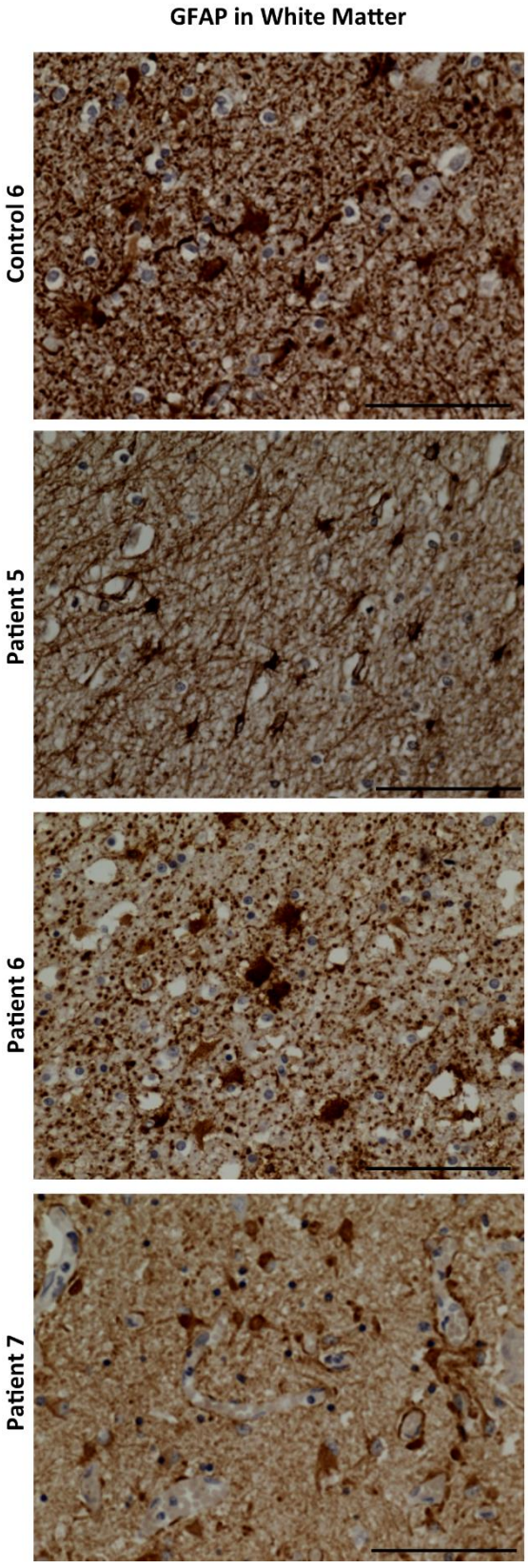

Figure 7.15: Astrogliosis of the white matter in the frontal lobe from patients with Alpers. Representative images taken at 40x magnification showing astrogliosis in the parietal lobe of Alpers patients. GFAP-positive astrocytes are visualised by dark brown chromogen. Controls and patients 5 (p.(Ala467Thr)/p.(Gly303Arg)) and 6 (p.(Ala467Thr)/p.(Gly848Ser)) show normal astrocytic morphology in the white matter. Patient 6 (p.(Ala467Thr)/p.(Gly848Ser)) showed large astrocytes compared to the control. Patient 7 (p.(Ala467Thr)/p.(Gly303Arg)) showed mild astrogliosis as evidenced by swollen astrocytes. Scale bar=100µm.

	Occipital lobe			Parietal lobe			Frontal lobe		
Case	**Mean IN density/ mm^2**	**Mean PC Density/m m^2**	**Astrocytes**	**Mean IN density/mm^2**	**Mean PC density/m m^2**	**Astrocytes**	**Mean IN density/mm^2**	**Mean PC density/mm^2**	**Astrocytes**
Control 1	N/A	N/A	N/A	33.45	12.78	N/A	N/A	N/A	N/A
Control 2	65.44	53.53	N/A	43.82	20.88	N/A	N/A	N/A	N/A
Control 3	54.93	56.89	N/A	32.00	29.46	Normal astrocytic morphology in GM and WM.	N/A	N/A	N/A
Control 4	38.23	22.60	Normal in GM and WM	N/A	N/A	N/A	34.38	N/A	N/A
Control 5	29.90	36.19	Mild astrogliosis in GM. Normal astrocytic morphology in WM.	N/A	N/A	N/A	23.70	N/A	N/A
Control 6	N/A	N/A	N/A	N/A	N/A	N/A	14.95	N/A	Normal astrocytic morphology in GM and WM.
Control 7	N/A	N/A	N/A	N/A	N/A	N/A	20.30	N/A	Normal astrocytic morphology in GM and WM.
Control 8	74.96	76.31	N/A	N/A	N/A	N/A	N/A	N/A	N/A

Patient 1	N/A	N/A	N/A	22.83	1.77	Severe astrogliosis in GM. Normal astrocytic morphology in WM.	N/A	N/A	N/A
Patient 2	N/A	N/A	N/A	9.59	1.75	Mild astrogliosis in GM and normal astrocytic morphology in WM.	5.41	N/A	Mild astrogliosis in GM.
Patient 3	N/A	N/A	N/A	19.71	4.23	Moderate astrogliosis in GM and normal astrocytic morphology in WM.	N/A	N/A	N/A
Patient 4	N/A	N/A	N/A	19.54	N/A	N/A	N/A	N/A	N/A
Patient 5	11.97	39.49	Mild astrogliosis in GM. Normal astrocytic morphology in WM.	N/A	N/A	N/A	N/A	N/A	N/A
Patient 6	29.90	6.57	Mild astrogliosis in GM. Normal astrocytic morphology in WM.	N/A	N/A		32.70	N/A	Normal astrocytic morphology in GM. Normal astrocytic morphology in WM.

Patient 7	N/A	N/A	N/A	N/A	N/A		16.30	N/A	Severe astrogliosis in GM. Mild astrogliosis in WM.

Table 7.4: Summary of neuron loss and astrogliosis. Key: N/A=not applicable.

7.4 Discussion

7.4.1 Introduction

This chapter investigated the neuropathological features of the post-mortem brain tissue from seven patients with clinically and/or genetically defined Alpers. Since respiratory chain deficiencies were evident in the neurons of patients with Alpers (as described in the previous chapter), this work sought to investigate the impact of respiratory chain deficiencies on the gross neuropathology and neuronal densities of these patients. The findings will be discussed for each lobe independently before inferences are made regarding the overall histopathological examination of brain tissue from patients with Alpers.

A. Occipital cortex

Quantitative analysis showed reduced densities of GABAergic interneurons in patient 5 (p.(Ala467Thr)/p.(Gly303Arg)) without any evidence of pyramidal neuron loss. Consequently, the ratio of GABAergic interneurons to pyramidal neurons was also reduced, which suggests that inhibitory neurotransmission is reduced, thus lowering the seizure threshold. The findings reported in this study for patient 5 are in agreement with reduced interneuron densities in a cohort of adult patients with mitochondrial disease, including three patients with *POLG*-related disease (Lax *et al.*, 2016).

Patient 6 (p.(Ala467Thr)/p.(Gly848Ser)) did not show loss of interneurons, however, there was a marked loss of pyramidal neurons. These findings taken at face value are in disagreement of the findings for patient 5 and could be interpreted as suggesting that pyramidal cell loss is independent from interneuron loss.

Nevertheless, interneurons in both patients 5 and 6 have been shown to be highly respiratory chain deficient (Chapter 6), therefore it is likely that even when interneurons have survived the respiratory chain deficiency is sufficient to cause significant synaptic dysfunction and disinhibition. In turn, this would lead to higher excitatory activity and potentially seizures with secondary pyramidal cell loss even without interneuron loss. The theory proposed above has however to be considered with the necessary caution given the fact that it was only possible to examine tissue from two patients.

B. Parietal cortex

In the parietal cortex, I found marked pyramidal neuron loss in all patients (patients 1, 2 and 3), however interneuron loss was only evident in patient 2 (no *POLG* diagnosis). The interneuron to pyramidal cell density is remarkably increased which reflects the significant pyramidal cell loss with mostly preserved interneuron densities.

Consistent with the results found in the occipital lobe, patients 1 and 2 (both without *POLG* diagnosis) had severe respiratory chain deficiencies and patient 3 (p.(Gly8383Ser)) also demonstrated a degree of respiratory chain deficiency, albeit at a lower extent. In contrast, the respiratory chain deficiency in pyramidal cells was milder in patients 1 and 2 (without *POLG* diagnosis) and not present in patient 3 (p.(Ala467Thr)/p.(Gly848Ser)).

The mechanism proposed for loss of pyramidal neurons in the occipital lobe can also be applied to the parietal lobe, with respiratory chain deficiency in interneurons causing synaptic dysfunction and disinhibition followed by higher excitatory states, respiratory chain deficiency in pyramidal cells, seizures and finally pyramidal cell loss. The parietal cortex degeneration, as described above, is likely to contribute not only to epilepsy but also to the cognitive impairment seen in patients with Alpers.

C. Frontal cortex

In the frontal cortex, patient 2 (no *POL*G diagnosis) was the only patient in whom marked interneuron loss was evident. However, respiratory chain deficiency was absent in this patient. It is unclear as to why interneuron loss was seen in patient 2 (no *POLG* diagnosis) without respiratory chain deficiency. However, this observation could result from the limitations of looking at post-mortem tissue and it is possible that respiratory chain deficiency was not identified due to the fact that those interneurons with respiratory chain deficiency were lost before the neuropathological investigation. Therefore, only the ones with normal respiratory chain function survived in this patient.

Patients 6 (p.(Ala467Thr)/(p.(Gly848Ser)) and 7 (p.(Ala467Thr)/p.(Gly303Arg) did not show any significant difference compared to the controls in terms of interneuron density. In contrast to patient 2 (no *POLG* diagnosis), patients 6 (p.(Ala467Thr)/p.(Gly848Ser)) and 7 (p.(Ala467Thr)/p.(Gly303Arg)) showed a picture of respiratory chain deficiency within interneurons. This observation may suggest that

respiratory chain deficiency in interneurons can be tolerated better than in pyramidal neurons, at least in some patients.

7.4.2 Astrogliosis

This study investigated the degree of astrogliosis in patients with Alpers. All patients demonstrated normal astrocytic morphology or astrogliosis. Given the fact that astrogliosis occurs as a response to injury or cell death (Burda and Sofroniew, 2014), I speculate that astrogliosis is a response to neuron loss, which was observed in all lobes examined.

Interestingly, patients showed a picture of swollen, hypertrophic astrocytes in the grey matter independently from the brain region examined, however these do not fulfill the features of the previously described Alzheimer Type II glia (observable by pale nucleus and reduced GFAP immunostaining) in both grey and white matter (Kollberg *et al.*, 2006; Sofou *et al.*, 2012; Montassir *et al.*, 2015). The changes in astrocyte morphology observed in the current study are therefore of unclear pathological significance and will warrant further investigation.

Since astrocytes exert a function in glutamate transport, it can be hypothesized that excessive glutamate may result in astrocytic swelling, which may in turn alter the expression of glutamate transporters and lead to disruption of key astrocytic functions.

Another cause of astrocytic swelling, is hyperammonemia as a result of impaired urea cycle during liver failure. The increase in ammonia will lead to uptake of ammonia by astrocytes which use ammonia to synthesise glutamine from glutamate. As a result, increased levels of glutamine may accumulate in the astrocytes resulting into astrocyte swelling and Alzheimer type II astrocytes a neuropathological feature also described in hepatic encephalopathy (Norenberg, 1987). Thus, the swollen astrocytes seen in patients with Alpers caused by altered glutamate handling may be secondary to liver failure (a predominant feature of Alpers). Alternatively, as shown in other neurodegenerative diseases, reactive astrocytes release inflammatory modulators which may be either neuroprotective or neurotoxic (Phatnani and Maniatis, 2015). Nevertheless, the role of astrocytes in neurodegenerative disease remain unclear.

7.4.3 Limitations

As described above there is a marked degree of variability in the result of neuronal density assessment in the patients examined and this study included a small number of patients and controls. In addition, this work is limited by the availability of lobe-matched patient tissue. Furthermore, the scarcity of controls required that brain tissue from infants who had died from SIDS was included, which could have biased the results as these controls could have neurodevelopmental brain abnormalities including suboptimal neurogenesis.

Consequently, the conclusions and hypothesis resulting from the present study would need further support from additional studies with higher number of patient and control samples. A major limitation of this work is the low number of cases and the unavailability of lobe-matched patient tissue. As such, the findings from this study should be interpreted with caution.

7.4.4 Future work

An important function of astrocytes is glutamate transport, which is the major neurotransmitter required for excitatory synaptic transmission. To assess any alterations in glutamate, the expression of glutamate synthetase could be assessed by immunohistochemistry. Reduced expression of glutamate synthetase may indicate astrocytic dysfunction. Since astrocytes play a role in clearing up the excess glutamate, which results after repetitive firing by pyramidal cells, the assessment of glutamate transporters may also prove beneficial in understanding the role of astrocytes in the brain of patients with Alpers (Trotti *et al.*, 1998).

The present study did not consider white matter abnormalities in the brain of patients with Alpers', as evidence of such abnormalities such as partial demyelination of the occipital lobe, has been reported rarely (Bao *et al.*, 2008). However, to better characterise the neuropathology of Alpers patients it would be interesting in the future to examine myelin expression in the white matter.

7.4.5 Conclusions

Here, I performed a reliable, quantitative assessment of interneuron and pyramidal cell densities in patients with Alpers. My findings show evidence of interneuron loss and pyramidal neuron loss, which is more severe compared to interneurons. This trend was observed in all the three lobes examined.

In addition, I report variable astrogliosis in the grey matter of patients with Alpers, which is most severe in the occipital and frontal lobes examined. Severe astrogliosis is consistent with interneuron and pyramidal neuron loss observed.

Taken together, my findings support the hypothesis of reduced GABAergic neurotransmission, which results in an imbalance between inhibition and excitation, leading to increased excitability; which may contribute significantly to the hallmarks of Alpers including: epilepsy, cognitive decline and psychomotor regression.

This is the first study which reports densities of interneurons and pyramidal neurons in tissue from the same patients with Alpers syndrome.

In general, it has been observed that pyramidal cell loss is more severe than interneuron loss. However, in the majority of cases there is pronounced respiratory chain deficiency in the interneurons. These results are in support of a hypothesized mechanism in which respiratory chain deficiency leads to GABAergic interneuron synaptic dysfunction, thus causing an imbalance between inhibition and excitation, giving rise to neuronal death and the neurological deficits seen in patients with Alpers.

Chapter 8 Final Discussion

8.1 Introduction

Mitochondrial disorders represent the most common group of metabolic diseases, which are characterised by genetic and clinical heterogeneity (Chinnery, 2014). Neurological deficits represent the most common clinical manifestations associated with mitochondrial disease caused by defects in mitochondrial DNA (mtDNA) and nuclear DNA (nDNA). Epilepsy is the most commonly reported neurological deficit in patients with mitochondrial disease (Hikmat *et al.*, 2017b). It has been estimated that seizures are present in 23% of adult and 40% of childhood cases with primary mitochondrial disease during the disease course (Gorman *et al.*, 2015). Although neuropathological investigations have contributed significantly to our understanding of neurodegeneration in mitochondrial disease, the mechanisms underlying mitochondrial epilepsy remain unidentified.

Mitochondrial disorders caused by mutations in the nuclear-encoded POLG represent a common form of mitochondrial disease and are characterised by epilepsy. To date, a total of 128 pathogenic *POLG* variants have been linked to epilepsy, with the majority of the patients harbouring at least one of the three most common mutations including: p.(Ala467Thr), p.(Trp748Ser) and p.(Gly848Ser) (Horvath *et al.*, 2006; Tzoulis *et al.*, 2006; Anagnostou *et al.*, 2016). However, the ever expanding number of pathogenic *POLG* mutations identified and the clinical heterogeneity challenge genotype to phenotype correlations.

Alpers' syndrome results from early-onset autosomal recessive mitochondrial disease and constitutes the most severe form of *POLG*-related disorders (Cohen, 2014). Alpers is characterised by refractory epilepsy and liver dysfunction which eventually progresses to failure (Saneto *et al.*, 2013). Alpers was first described 86 years ago (Alpers, 1931), however the first association with POLG was only established in 1999, when *POLG* mutations were reported to be the underlying genetic defect of Alpers syndrome (Naviaux *et al.*, 1999).

To address the effect of *POLG* mutations on Alpers and human disease, several studies have been performed on different tissue types including liver, brain, muscle, blood and fibroblasts (reviewed in Chapter 3). Evidence suggests that *POLG* mutations cause a tissue specific effect, affecting primarily brain and liver, whereas

muscle, blood and fibroblasts are variably affected and to a lesser extent, which may depend on disease severity and progression (Ashley *et al.*, 2008; Hunter *et al.*, 2011; Schaller *et al.*, 2011; Sofou *et al.*, 2012; Horst *et al.*, 2014). Nevertheless, the majority of the studies published are based on single-case reports.

It has been accepted that *POLG* mutations cause mtDNA depletion and deletions (in post-mitotic tissues) resulting in respiratory chain deficiency, and downstream clinical disease (Tzoulis *et al.*, 2014). However, both the underlying mechanisms and the factors which determine tissue-specificity remain largely unknown.

Consequently, the pathogenesis of Alpers is poorly understood. This is mainly due to the lack of accurate *in vivo* and *in vitro* models and the limitations of post-mortem neuropathological studies. Understanding the mechanisms of epilepsy and neurodegeneration caused by *POLG* mutation will not only inform Alpers pathogenesis but also a wide spectrum of *POLG*-related disorders characterised by neurological deficits.

The aim of this thesis was to further understand the pathogenesis of Alpers caused by *POLG* mutations, using two different approaches. The first approach involved the characterisation of mitochondrial function in *POLG*-mutant fibroblasts from patients with Alpers, prior to its transformation into induced neuronal progenitors (iNPC's), in an effort to create an *in vitro* model of Alpers syndrome.

In addition to *in vitro* studies, a post-mortem neuropathological study was also performed, to explore the mechanisms of epilepsy and neurodegeneration in patients with Alpers and correlate the results with the work performed on fibroblasts. Work focussed on the characterisation of neuronal mtDNA damage, respiratory chain deficiencies and neuropathological features in three different cortical brain regions from patients with Alpers.

8.2 Major Findings

8.2.1 Characterisation of Mitochondrial Function in POLG-mutant Fibroblasts from Patients with Alpers

During the course of this thesis *POLG*-mutant fibroblasts from patients with early-onset and late-onset Alpers harbouring at least one of the common *POLG* pathogenic mutations including the p.(Ala467Thr) and p.(Trp748Ser) were assessed for mitochondrial dysfunction.

Fibroblasts from all patients considered did not reveal any significant changes when compared to controls in terms of mtDNA copy number, mitochondrial nucleoid morphology and dynamic mitochondrial networks, respiratory capacity and steady-state POLG levels. These findings suggest that *POLG* mutations do not interfere significantly with POLG function, therefore POLG is capable of sufficiently synthesising mtDNA to maintain normal respiratory capacity and dynamic mitochondrial networks in fibroblasts. Although previous reports on *POLG*-mutant fibroblasts are limited (Ashley *et al.*, 2008; Schaller *et al.*, 2011; Horst *et al.*, 2014; Rouzier *et al.*, 2014), most are in agreement with the findings of this thesis, further supporting the hypothesis that *POLG* mutations exert their deleterious effects via tissue-specific mechanisms.

This is the first detailed study of *POLG*-mutant fibroblasts which collectively assessed the expression of biochemical defects and baseline mitochondrial function in four patients with Alpers. Previous investigations on *POLG*-mutant fibroblasts have rarely been reported and these are mostly limited on mtDNA copy number quantification.

This study provides evidence that *POLG*-mutant fibroblasts in baseline conditions do not recapitulate the biochemical phenotype of Alpers syndrome, thus *POLG*-mutant fibroblasts do not constitute a good *in vitro* model for the investigation of the molecular pathogenesis of Alpers' syndrome.

The findings of this thesis imply that *POLG* mutations may not exert sufficient dysfunction on fibroblasts for the biochemical defects to be detectable. Given the glycolytic nature of fibroblasts and evidence showing that deprivation of glucose to force energy production through oxidative phosphorylation can unmask mitochondrial defects (Voets *et al.*, 2012; Carelli *et al.*, 2015), *POLG*-mutant fibroblasts could have been cultured in galactose-medium to assess whether mitochondrial dysfunction is triggered by stress. A comparison between *POLG*-mutant fibroblasts cultured in glucose and galactose-medium would have been useful in understanding whether *POLG*-mutant fibroblasts mimic mitochondrial dysfunction seen in Alpers under stress.

An alternative approach for investigating the mechanisms of *POLG*-mutations in fibroblasts may involve the exposure to ethidium bromide, an intercalating agent which causes mtDNA depletion. A report involving ethidium bromide induced mtDNA depletion in *POLG*-mutant fibroblasts has shown impaired mtDNA repopulation by kinetics assessment (Stewart *et al.*, 2011). Therefore, treatment of *POLG*-mutant

fibroblast with ethidium bromide may be particularly useful when exploring mechanisms of mtDNA depletion secondary to *POLG* mutations. This approach may prove useful when dissecting the effect of the location of mutations within the *POLG* gene on its biological function.

Overall the findings of the current work highlight the importance of investigating affected tissues in order to better understand the pathogenesis of Alpers secondary to *POLG* mutations. The development of patient-specific cell-based models through induced pluripotent stem cells (iPSC's) (Li *et al.*, 2015; Zurita *et al.*, 2016) and direct differentiation (Lu *et al.*, 2013; Meyer *et al.*, 2014) technologies may unravel the identification of *POLG* tissue-specific effects and inform novel treatment strategies which are urgently needed.

8.2.2 In vitro Modelling of Alpers Syndrome Secondary to POLG Mutations

Fibroblasts are easily accessible and can be converted into other cell lineages through gene reprogramming in order to be used for disease modelling. This thesis presents a picture of normal baseline mitochondrial function in *POLG*-mutant fibroblasts derived from patients with Alpers.

Given the fact that the central nervous system (CNS) is predominantly affected, it was hypothesised that the effect of *POLG* mutations would be particularly severe in neurons which therefore may express the biochemical dysfunction responsible for Alpers. Hence, *POLG*-mutant fibroblasts were exposed to a direct differentiation approach for transformation into induced neuronal progenitor cells (iNPC's). Direct differentiation was selected over induced pluripotent stem cell (iPSC) technology due to lower cost and time-efficiency.

Although several attempts of converting *POLG*-mutant fibroblasts into iNPC's were performed using two different protocols (see Chapter 5), the experiments failed at the stage of neurosphere expansion and did not yield iNPC colonies for further investigation. The result of this work revealed the influence of fibroblast passage number on direct differentiation, highlighting the need of low-passage fibroblasts when considering direct differentiation. Immortalising fibroblasts may overcome this limitation, however given the time constraints of this PhD this could not have been tested.

Given the opportunity, I would have attempted the use early passage control fibroblasts (passage 1-5) which were not accessible during the course of this thesis,

and for direct differentiation alongside *POLG*-mutant fibroblasts. This would have been beneficial in understanding of whether successful conversion is dependent on early-passage or the nature of *POLG* mutations is responsible for the unsuccessful attempts of fibroblast conversion into iNPC's.

This work highlights the challenge of modelling Alpers using patient-specific fibroblasts harbouring *POLG* mutations. To overcome this challenge and develop *in vitro* models for studying *POLG* mutations in human disease, other routes exist which are beyond the time limits of the current PhD work.

One approach, would involve the conversion of *POLG*-mutant fibroblasts into iPSC's and further differentiation into neurons. Although conversion into iPSC is a lengthy and costly process, it may be used alternatively to iNPC's and yield differentiated neuronal sub-types harbouring the mutations of interest, which could be used for further characterisation.

Alternatively, CRISPR/Cas9 technology could be applied to mutate POLG in commercially available healthy human neurons or hepatocyte cell lines. This approach can result in the induction of specific *POLG* mutations, and thus enable *in vitro* modelling of Alpers. Although hepatocytes would not be useful in modelling the neurological aspects of Alpers in characterising mitochondrial dysfunction in hepatocytes, may unravel tissue-specific mechanisms caused by *POLG*-mutations, especially given the fact that hepatic dysfunction is a common feature of this disease.

8.2.3 Mechanisms of Epilepsy and Neurodegeneration in Alpers

This thesis examined the hypothesis that neuronal energy failure due to respiratory chain deficiency, secondary to mtDNA depletion, represents the primary pathophysiology of Alpers encephalopathy. According to this hypothesis, respiratory chain deficiency would result in impaired neuronal circuitry contributing to an imbalance between inhibition and excitation, resulting in neuronal death, leading to the neurological deficits seen in patients with Alpers.

Severe respiratory chain deficiencies involving complex I, and, to a lesser extent complex IV in all three cortices examined, moreover occipital interneurons showed the most extensive respiratory chain deficiency. This finding is consistent with neuroimaging data, which suggest disease predilection for the occipital lobe in Alpers. Nevertheless, it remains unclear why the occipital lobe is the most severely affected brain region. It has been hypothesised that the occipital lobe is the most

active brain region and thus the most vulnerable to energy failure, although this warrants further investigation (Tzoulis *et al.*, 2014; Hikmat *et al.*, 2017b).

Complex I deficiency was generally more extensive than complex IV in all the cortices examined from patients with Alpers. This finding is consistent with a progressive loss of complex I expression in neurons of patients with *POLG* mutations, suggesting complex I deficiency as a pathological process of *POLG* encephalopathy (Tzoulis *et al.*, 2014). The findings of the current thesis further support suggestions that complex I deficiency, is a contributory factor in the development of epilepsy (Rahman, 2012). It is intriguing that in the occipital lobe, all the interneurons of three patients were complex I deficient. The absence of normal interneurons in these patients is indicative of the vulnerability of the occipital lobe to extensive neuronal dysfunction in end-stage Alpers.

Respiratory chain protein deficiencies in pyramidal neurons were identified in the parietal and frontal lobes of patients with Alpers, however deficiencies were milder compared to those observed in interneurons. It is important to mention that in this study the respiratory chain protein expression of the surviving neurons, consequently deficient pyramidal neurons may have been lost before the neuropathological study was performed, and thus extensive respiratory chain deficiencies involving complexes I and IV were not identified in the post-mortem analyses.

The quantitative nature of the immunofluorescent technique applied, allowed the precise, reproducible and reliable assessment of mitochondrial respiratory chain proteins (Grunewald *et al.*, 2014; Lax *et al.*, 2016), which has not been previously described in Alpers.

Respiratory chain deficiencies within neurons of patients with Alpers were coupled with pyramidal loss in all the brain regions examined, which was particularly severe when compared to interneurons. There was a severe loss of pyramidal neurons but the respiratory chain deficiency within the remaining pyramidal neurons was less profound compared to the interneurons. The basis for this may be that pyramidal neurons are more vulnerable to mitochondrial respiratory chain deficiencies, given their large size and long axons, and consequently die. Therefore, the surviving neurons show lower levels of respiratory chain deficiency.

Interneuron loss was only evident in the occipital lobe of patient 5 (p.(Ala467Thr)/p.(Gly303Arg)) and the parietal and frontal lobes of patient 2 (no

POLG diagnosis), which correlated with more severe respiratory chain deficiencies within the surviving interneurons.

Since interneuron loss is not significant in the majority of the patients but the densities of pyramidal neurons are severely reduced in all lobes, it can be hypothesised interneurons tolerate energy failure better than pyramidal neurons.

Interestingly, patients 5-7 showed a clinical picture of stroke-like episodes, a feature linked to epilepsy. Tzoulis and colleagues (Tzoulis et al., 2014) described lesions which they termed 'FENN' in CA1 and Purkinje cells in these patients. Patients who tend to develop FENN are often those who have epilepsy as part of their neurological condition. The term FENN was proposed to better account for the neuropathological characteristics and underlying mechanisms of their formation. Authors proposed that seizures, which are energy-demanding, increase the energy demand of neurons leading to acute lesions in the hippocampus, which is a driver for seizure generation. It is also suggested that cortical epileptic activity may increase the metabolic activity of the cerebellum, thus making large-sized Purkinje cells vulnerable to focal lesions (Tzoulis *et al.,* 2014).

Although this work provides evidence of interneuron dysfunction, it is unclear whether pyramidal loss is a result from increased excitation due to impaired dynamics or whether pyramidal neurons are more susceptible to respiratory chain deficiency leading to neuronal loss. These hypotheses require further investigation.

MtDNA depletion due to POLG dysfunction has been suggested to be the underlying mechanism of neuronal energy failure. Here, I report a picture of mtDNA depletion in adult patients with *POLG* mutations in brain homogenates from occipital, parietal and frontal lobes. Consistent with energy failure identified in patient interneurons, mtDNA depletion was most evident in the occipital lobe, thereby highlighting the susceptibility of occipital lobe neurons to energy failure, secondary to mtDNA depletion caused by *POLG* mutations.

Although the mtDNA copy number was quantified in tissue from adult patients with *POLG* mutations, the findings support the hypothesis that mtDNA depletion is a shared mechanism in early and late-onset Alpers. Interestingly, patient 9 (mutations in *IDH3A*), who had a clinical picture of Alpers did not demonstrate evidence of mtDNA copy number reduction in the occipital lobe. This finding suggests that

mtDNA copy number reduction is a result of *POLG* mutations in patients with *POLG*-related disease and not a general feature of Alpers syndrome.

Given the available resources within the time frame of this study, I was able to demonstrate a picture of compromised energy production in neurons from patients with Alpers, coupled with mtDNA depletion in brain homogenates of patients with *POLG* mutations. I propose a mechanism of impaired neuronal networks resulting from respiratory chain deficiency within interneurons and pyramidal neurons of patients with, due to mtDNA depletion (see Figure 8.1).

The proposed mechanism involves a cascade of events: mtDNA depletion secondary to *POLG* mutations causes respiratory chain deficiencies within interneurons and pyramidal neurons. Energy failure of neurons coupled with neuronal loss results in impaired neuronal networks giving rise to disinhibition and hyperexcitation, thus triggering seizures. Since seizures increase the energy demands of neurons, many of which are respiratory chain deficient, a vicious cycle is created, where seizures further compromise the metabolic activity of the neurons and thus increase neuronal excitability and neuronal death.

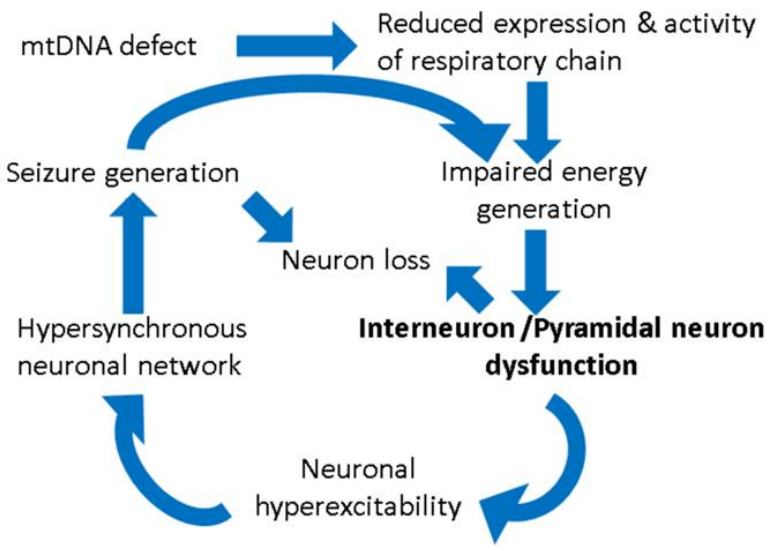

Figure 8.1: Proposed mechanism underlying epilepsy and neurodegeneration in Alpers modified from previously published hypotheses. Loss of mtDNA secondary to POLG dysfunction, results in respiratory chain deficiency leading to energy failure, making interneurons and pyramidal cells dysfunctional. As a result, neuronal oscillations are impaired, disrupting the careful balance of inhibition and excitation in the brain of patients with Alpers. As a consequence, neurons are lost or dysfunctional and disinhibition results in increased excitability, triggering seizure generation. As seizures are energy demanding, these further compromise neuronal function leading to a vicious cycle, further increasing neuronal excitability and neuronal death (Rahman, 2012; Zsurka and Kunz, 2015).

If tissue was available, it would have been beneficial to assess respiratory chain deficiencies in the neurons of all the three lobes examined in the same patients. This would not only provide insight into the mechanisms of neurodegeneration in Alpers but also improve our understanding of disease progression.

Furthermore, the assessment of mtDNA copy number and mtDNA deletions in patients with early-onset Alpers would not only allow comparison between early and late-onset cases but also contribute to our understanding of the mechanisms underlying *POLG*-related encephalopathy. The assessment of mtDNA damage in micro-dissected interneurons and pyramidal neurons would allow correlations with respiratory chain deficiencies within these neuronal populations and thus contribute to our understanding of the mechanisms governing *POLG*-related neurodegeneration.

Despite the limitations of this study, this work presents a picture of interneuron dysfunction in Alpers which has not been reported to date and may be crucial in the pathogenesis of epilepsy seen in these patients. Further, the findings of this work support a disruption of the careful balance between inhibition and excitation (as discussed in Chapter 7), which may not only contribute to the development of epilepsy but also towards cognitive impairment and psychomotor regression, all characteristic features of Alpers.

Understanding neuronal circuitry in post-mortem tissue is extremely challenging. The use of transgenic mouse models may partly address this issue and provide insight into disease progression and impaired neuronal dynamics. Currently, no animal model exists recapitulating the phenotype of *POLG*-related epilepsy and Alpers. Interestingly, a mouse model involving conditional knockout of *NDUFS4*, a gene encoding an important subunit of complex I has been reported to result in a fatal phenotype of encephalopathy and ataxia, accompanied with neuropathological changes including neuron loss, and activation of glia (Quintana *et al.*, 2010; Quintana *et al.*, 2012; Torraco *et al.*, 2015). These features are similar to Alpers thus making this mouse model a potential candidate for future investigations of the mechanisms underlying Alpers neuropathology.

Moreover, *Adenine Nucleotide Translocase* 1 (*Ant1)* knockout mice have been recently used to study mitochondrial dysfunction in interneuron and pyramidal neuron migration, suggesting significant disruption of interneuron migration in the presence of OXPHOS defects. As such the *Ant1* transgenic mice may also be suitable for the

further characterisation of interneuron dysfunction, secondary to mitochondrial defects (Lin-Hendel *et al.*, 2016).

8.3 Limitations

This study provided insight in our understanding of Alpers neuropathology and pathogenesis, however there are important limitations that need to be considered. These include:

1) The *in vitro* studies were limited by the unavailability of early-passage, age-matched, healthy control fibroblasts.
2) Neuropathological investigation was limited by the low number of cases and availability of age-matched controls.
3) Patient tissue was not lobe-matched for every case, therefore evaluation of changes during disease progression were not possible.
4) Neuropathological investigation was based on post-mortem tissue, which is representative of end-stage disease.
5) Neuronal degeneration is an early process, therefore relevant cells may have been lost, prior to the time of the neuropathological evaluation.
6) The genetic diagnosis for two patients was not possible, hence diagnosis of Alpers was based upon the clinical histories and neuropathology findings. Therefore, findings regarding these patients should be interpreted with caution when considering *POLG* mutations as the pathogenic defect.

8.4 Future Work

This work explored mitochondrial function in *POLG*-mutant fibroblasts from patients with Alpers disease and the mechanisms underlying neurodegeneration in post-mortem tissue from patients with clinical and/or genetically defined Alpers. Not all patients included in this study had confirmed *POLG* mutations.

To validate the findings of the current study and better understand disease progression and neurodegeneration in Alpers, future work should focus on investigating multiple brain cortices from a larger cohort of patients with Alpers and confirmed *POLG* mutations.

Moreover, to better understand the pathogenesis of Alpers, future work should include investigating the role of astrocytes. Since astrogliosis and Type II Alzheimer glia are neuropathological features of Alpers, it would be interesting to assess whether mitochondrial defects in astrocytes contribute to neurological impairments

seen in patients with Alpers. Specifically, astrocytes could be assessed for respiratory chain deficiency using a similar approach used in interneurons and pyramidal neurons.

In addition, the assessment of mtDNA defects in microdissected interneurons, pyramidal neurons and astrocytes (from frozen tissue obtained from patients with Alpers) would provide insight into the molecular pathogenesis of Alpers caused by *POLG*-mutations.

Cell-based studies, including iPSC and direct differentiation technologies (i.e. iNPC's) may prove beneficial in understanding the mechanisms underlying respiratory chain deficiency. Direct differentiation technologies may allow the differentiation of interneurons, pyramidal neurons and glial cells with the potential of exploring *in vitro* mitochondrial dysfunction and interplay of neurons with glial cells in Alpers.

8.5 Concluding Remarks

In conclusion, the findings of the work presented in this thesis advance our understanding of the neuropathology and pathogenesis of Alpers. The mtDNA damage in brain homogenates from different brain cortices combined with extensive respiratory chain deficiencies within interneurons and pyramidal cells observed, and coupled with neuron loss and astrogliosis found in the tissue examined provide insight into the current understanding of *POLG*-specific mechanisms associated with intractable epilepsy and cognitive decline in patients with Alpers.

Alpers' syndrome is an incurable, devastating disease. Understanding brain micro-circuitry in Alpers would provide insight into better understanding of the disease pathogenesis and may inform potential treatments.

Appendix A

CRITICAL REVIEW AND INVITED COMMENTARY

Epilepsy due to mutations in the mitochondrial polymerase gamma (*POLG*) gene: A clinical and molecular genetic review

[1]Maria-Eleni Anagnostou, [1]Yi Shiau Ng, Robert W. Taylor, and Robert McFarland

Epilepsia, 57(10):1531–1545, 2016
doi: 10.1111/epi.13508

Maria-Eleni Anagnostou is a doctoral student and her research project is funded by Ryan Stanford Appeal.

Dr. Yi Shiau Ng is a clinical research fellow with a research interest in phenotyping of mitochondrial disorders.

Summary

We performed a systematic review of the clinical, molecular, and biochemical features of polymerase gamma (*POLG*)–related epilepsy and current evidence on seizure management. Patients were identified from a combined electronic search of articles using Ovid Medline and Scopus databases, published from January 2000 to January 2015. Only patients with a confirmed genetic diagnosis of *POLG* mutations were considered. Seventy-two articles were included for analysis. We identified 128 pathogenic variants in 372 patients who had *POLG*-related epilepsy. Among these, 84% of the cases harbored at least one of these pathogenic variants: p.Ala467Thr, p.Trp748Ser, and p.Gly848Ser. A bimodal distribution of disease onset was present in early childhood (<5 years) and adolescence; female patients had a later presentation than male patients (median age 4.00 vs. 1.83 years, p-value = 0.041). Focal-onset seizure including convulsive, myoclonus, and occipital seizures was common at the outset and was refractory to pharmacotherapy. We confirmed that homozygous pathogenic variants located in the linker region of *POLG* were associated with later age of onset and longer survival compared to compound heterozygous variants. In addition, biochemical and molecular heterogeneities in different tissues were frequently observed. *POLG*-related epilepsy is clinically heterogeneous, and the prognosis is, in part, influenced by the location of the variants in the gene and the presence of hepatic involvement. Normal muscle and fibroblast studies do no exclude the diagnosis of *POLG*-related mitochondrial disease and direct sequencing of the *POLG* gene should be the gold standard when investigating suspected cases.

KEY WORDS: **Mitochondrial disease, Status epilepticus, Stroke-like lesion, mtDNA copy number, Treatment.**

Accepted July 26, 2016; Early View publication August 24, 2016.
Wellcome Trust Centre for Mitochondrial Research, Institute of Neuroscience, Newcastle University, Newcastle upon Tyne, United Kingdom
Address correspondence to Dr. Robert McFarland, Wellcome Trust Centre for Mitochondrial Research, Institute of Neuroscience, Newcastle University, Framlington Place, Newcastle upon Tyne, NE2 4HH, U.K. E-mail: robert.mcfarland@newcastle.ac.uk
[1]These authors contribute equally.

Key Points

- 128 pathogenic variants were identified in 372 patients with *POLG*-related epilepsy
- Eighty-four percent of the cases harbored at least one of the following pathogenic variants: p.Ala467Thr, p.Trp748Ser, and p.Gly848Ser
- Homozygous variants located in the linker domain of the *POLG* gene correlated with later age of onset and longer survival compared to compound heterozygous variants
- Variable expression of biochemical and molecular features was frequently observed among different tissue types
- Diagnosis should be based on direct sequencing of the whole *POLG* gene

The enzyme polymerase gamma (POLG), the only DNA polymerase thought to exist in mammalian mitochondria, plays a vital role in replication and repair of mitochondrial DNA (mtDNA). In humans, POLG exists as a heterotrimer (195 kDa), consisting of a catalytic subunit (p140, encoded by *POLG* on chromosome 15q25) and two identical accessory subunits (p55, encoded by *POLG2* on chromosome 17q25), which are absolutely essential for processive DNA synthesis.[1,2] The *POLG* gene consists of 22 coding exons and performs two distinct functions including an N-terminal 3′–5′ exonuclease (proofreading) connected to a C-terminal 5′–3′ polymerase activity (synthesising and lyase function)[1] through a linker region that structurally supports and enhances the processivity of the holoenzyme.[3]

The first *POLG* pathogenic variant was reported in 2001,[4] and since then >180 variants have been identified.[5] Two pathogenic variants, the p.Ala467Thr and p.Trp748Ser have been identified as the most common in the Caucasian population, with an estimated carrier prevalence 0.5–1%.[6] Disease resulting from mutations in *POLG* exhibits either autosomal recessive or autosomal dominant inheritance, with the latter often leading to a less severe phenotype.

Alpers syndrome, or Alpers-Huttenlocher syndrome (AHS), is the most severe clinical phenotype of *POLG*-related mitochondrial disease, characterized by a clinical triad of drug resistant, mixed-type seizures; episodic psychomotor regression; and hepatopathy with or without acute liver failure. Harding et al. comprehensively described postmortem brain and liver pathology in cases of AHS (progressive neuronal degeneration of childhood with liver disease) in the late 1980s.[7] The link between mtDNA depletion and deficiency of POLG activity was made by Naviaux and colleagues in 1999.[8] The clinical, pathologic, and diagnostic criteria of AHS were subsequently proposed.[9] Myocerebrohepatopathy spectrum (MCHS) has been reported as a different clinical entity based on the presence of prominent hypotonia or myopathy and lack of characteristic liver pathologic changes in AHS.[10] Other *POLG*-related clinical phenotypes include myoclonic epilepsy myopathy sensory ataxia (MEMSA), ataxia neuropathy spectrum (ANS), and autosomal recessive/dominant progressive external ophthalmoplegia (arPEO, adPEO). Although the mechanisms remain unclear, mutations in *POLG* can result in mtDNA depletion (quantitative loss of mtDNA copy number) and/or multiple deletions (qualitative change in mtDNA) in affected tissues. These defects in mtDNA lead to respiratory chain deficiency, which in turn precipitates the development of disease.

In this review, we aim to systematically evaluate the clinical, therapeutic, genetic, and molecular aspects of *POLG*-related seizure disorders. Furthermore, we intend to determine the putative prognostic factors.

Methods

Search strategy and study selection

A systematic and independent electronic search for the terms "POLG," "polymerase gamma," and "POLG1" was performed using Ovid Medline and Scopus databases by two researchers (MEA and YSN). We limited the search on articles written in the English language and on humans published from January 2000 to January 2015. Articles were excluded if the article title and/or abstract did not include any of the following terms: seizures, epilepsy, status epilepticus, Alpers syndrome/disease, hepatocerebral syndrome, encephalopathy, or liver/hepatic failure. To clarify the pathogenicity of any given rare, private allelic variant, cross-reference to the Human DNA Polymerase Gamma (POLG) Mutation Database webpage (http://tools.niehs.nih.gov/polg/), ClinVar (http://www.ncbi.nlm.nih.gov/clinvar/) and predictor software (Alamut Visual version 2.7.1) were performed. Only patients with pathogenic recessive *POLG* variants in either a homozygous or compound heterozygous state were considered. Patients who harbored a single, heterozygous variant with adPEO, PEO, and/or Parkinsonism were excluded.

Data extraction

Data were extracted from individual articles regarding the number of patients, clinical details (age of disease onset, age of death, seizure types, imaging and electroencephalography [EEG] findings, and treatment), pathogenic variants, histopathologic findings, mtDNA content, and mitochondrial respiratory chain (RC) biochemistry in various tissue types.

Statistical analysis

Statistical analysis was performed using the IBM SPSS Statistic version 22.0 software and Minitab version 17.

Epilepsia, 57(10):1531–1545, 2016
doi: 10.1111/epi.13508

Descriptive statistics were used to provide summative information of the findings. Continuous data were presented in the mean value ± standard deviation (SD), and median value for the nonparametric data. Kaplan-Meier survival analysis was performed and the statistical significance level was determined at $p < 0.05$.

Results

Systematic search results

The initial search from combined databases returned 64,272 articles (Ovid = 22,721 and Scopus = 41,551). A total of 276 articles met the inclusion criteria and were used for further evaluation. After removing the duplicates and including only cases with two pathogenic variants in the *POLG* gene, 372 patients from 72 articles were selected for analysis (Fig. S1 and Table S1).

Pathogenic variants associated with *POLG*-related epilepsy

There are 128 pathogenic variants associated with *POLG*-related epilepsy, and the 10 most common variants are illustrated in Figure 1A. Eighty-four percent of cases had at least one of the three common pathogenic variants: p.Ala467Thr, p.Trp748Ser, and p.Gly848Ser (Fig. 1B). The most common type of variant is missense (77%), followed by splicing variants (9%), nonsense (stop codon) variants (8%), deletions, and insertion and duplication (collectively 6%). In addition, a complete deletion of a *POLG* allele has been reported.[11]

Age at onset, age at death, and genotypes

The age at onset of *POLG*-related epilepsy ranged from infancy to late adulthood (<30 days to 64 years, n = 265), and the median age was 2 years (first quartile (Q1) = 0.75 and third quartile (Q3) = 13.50). The distribution of the age at onset was positively skewed (skewness = 2.08, kurtosis = 5.68), with the largest peak occurring at <5 years old with a second, smaller peak evident in adolescence (12.50–17.50) (Fig. 1C). Female patients have a higher median age at disease onset than male patients do (4.00 vs. 1.83 years, p-value =0.041) (Fig. 1D).

We identified 177 deaths (median age at onset was 1.33 years, range was at birth to 50, Q1 = 0.58 and Q3 = 7.00) recorded in the literature, and the age at death was available in 92% of cases. The median age at death is 3.5 years (range 0.33–55.00, Q1 = 1.25 and Q3 = 17.00), and there is no statistically significant difference between the sexes ($p = 0.545$). The median interval between disease onset and death is 1 year (n = 149, range <30 days to 50 years, Q1 = 0.50 and Q3 = 5.69).

Comparison of age at onset and age at death between the common genotypes is summarized in Table 1. Patients with homozygous p.Ala467Thr and homozygous p.Trp748Ser present later than those with other genotypes and have a longer survival ($p < 0.001$) (Fig. 2). Individuals who harbor both pathogenic variants located in the linker domain (e.g. homozygous p.Ala467Thr, homozygous p.Trp748Ser, and compound heterozygous p.Ala467Thr and p.Trp748Ser) have significant later clinical manifestation and longer survival ($p < 0.001$). The occurrence of both variants in the exonuclease domain (EE) or the polymerase and linker domains (PL) is associated with the earliest median age of onset and median age of death. Both variants located in EE were identified in only 3% of cases (n = 15).

Presenting clinical manifestations

Seizure was the first, presenting clinical manifestation in 50% of all cases. In the pediatric population, 26% of the patients presented, prior to the development of a seizure disorder, with one of the following clinical features: developmental delay, failure to thrive, or hypotonia. Rarely, hepatic dysfunction (causing jaundice and/or hypoglycaemia) was the earliest manifestation (5%) (Fig. S2). The median age of individual presenting feature is summarized in Table S2. AHS or Alpers-lile disease was reported in 48% of cases (n = 180).

Seizure semiology and EEG findings

Description of seizure was available for further analysis in 229 patients. Focal motor seizure (64%) and/or myoclonus (58%) involving limbs, shoulders, or necks were identified at the outset of disease, and often progressed into generalized status epilepticus (49%) or focal motor status with or without altered awareness (34%). Positive and/or negative visual phenomena were recognized as the onset of epilepsy with occipital focus in some adult patients.[12] Other concomitant clinical features associated with seizure were psychomotor regression, vomiting, headache, hemianopia, cortical blindness, or other focal neurologic deficit. Hepatic involvement commonly manifested following a protracted period of drug-resistant seizure; often it heralded the terminal event and was associated with exposure to sodium valproate (VPA) in >50% of the cases.

In terms of EEG findings (n = 72), focal abnormality (including epileptic discharges, rhythmic high amplitude delta with superimposed spikes [RHAD],[13–16] and slowing, Fig. S3) was most commonly identified in occipital area/posterior quadrant (61%) followed by frontal (6%) and temporal (2%) regions. Multifocal abnormality was evident in 23% of EEG studies, and location of changes was not specified in 7% of the cases. The myoclonic jerks did not always correlate with EEG changes, suggesting that these may have subcortical origin.[17,18]

Imaging findings

Brain imaging data were available for analysis in 136 patients (Table 2). The most common imaging finding was stroke-like lesion (43%), manifesting as confluent T_2/FLAIR (fluid-attenuation inversion recovery)

Table 1. Comparison of age at onset (n = 268), age at death (n = 163), and disease duration (n = 150) in different genotypes

Genotype	Total number of patients	Number of patients with age of onset	Median age at disease onset	Q1–Q3	Number of deaths	Number of patients with age at death	Median age at death	Q1–Q3	Number of patients with disease duration	Median disease duration	Q1–Q3
Homozygous p.Ala467Thr	72	59	14.00	9.00–17.00	38	36	20.00	17.00–43.50	32	10.50	1.00–19.50
Compound heterozygous p.Ala467Thr	144	108	1.00	0.67–2.00	76	72	1.88	1.09–3.73	67	0.78	0.42–2.50
Homozygous p.Trp748Ser	33	22	17.00	14.75–28.25	13	8	25.00	18.50–35.75	8	7.00	4.00–18.00
Compound heterozygous p.Trp748Ser	37	26	1.33	0.48–6.13	15	15	3.00	1.08–10.00	13	1.50	0.66–2.92
Homozygous p.Gly848Ser	1	0	1.00	–	1	0	–	–	0	–	–
Compound heterozygous p.Gly848Ser	7	2	0.21	–	2	2	0.58	–	2	0.88	0.67–2.07
Compound heterozygous p.Trp748Ser and p.Gly848Ser	15	12	1.04	0.73–5.00	11	11	4.30	1.67–7.75	10	1.085	0.75–3.10
Compound heterozygous p.[Thr251Ile; Pro587Leu]	5	4	0.29	0.19–0.46	1	1	0.46	–	1	0.29	–
Other	58	35	1.00	0.42–9.00	20	18	1.44	0.98–10.44	17	0.92	0.50–3.25

Q1, 25th quartile; Q3, 75th quartile. Kruskal-Wallis (nonparametric) test shows that the medians of the age at disease onset, age at death, and disease duration are significantly larger in homozygous p.Ala467Thr and p.Trp748Ser groups compared to other genotypes ($p < 0.001$).

Epilepsia, 57(10):1531–1545, 2016
doi: 10.1111/epi.13508

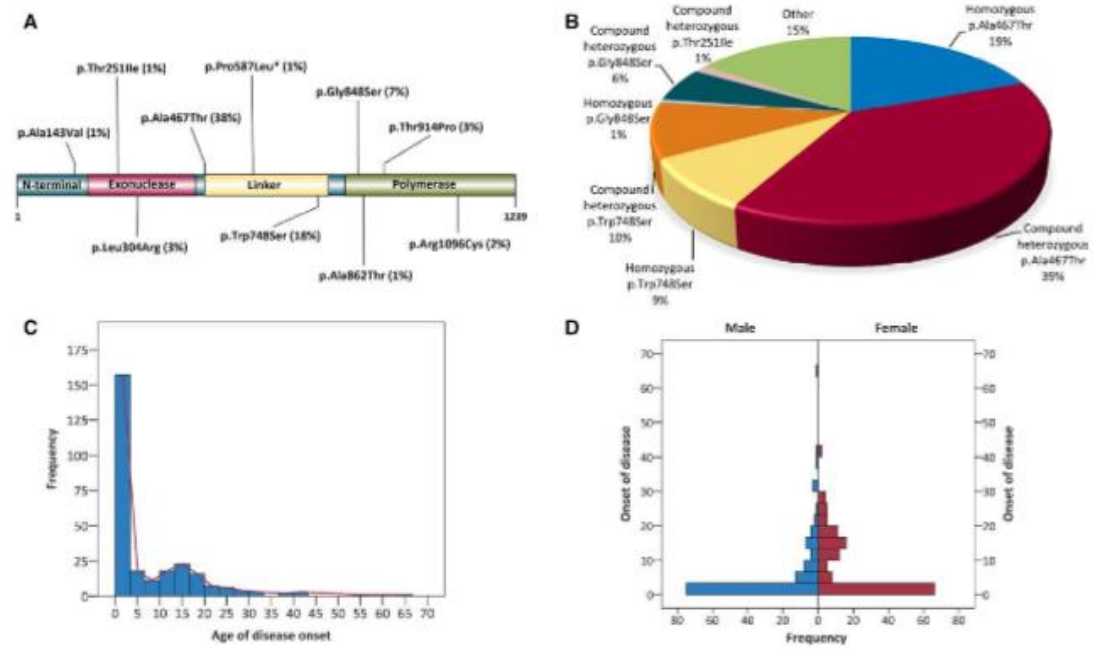

Figure 1.

(**A**) Ten common pathogenic variants associated with *POLG*-related epilepsy. *p.Thr251Ile and p.Pro587Leu frequently present in the same allele. (**B**) Frequency of genotypes. (**C**) Age at disease onset in *POLG*-related epilepsy. (**D**) Histograms show the distribution of the age at disease onset in male and female patients.

Epilepsia © ILAE

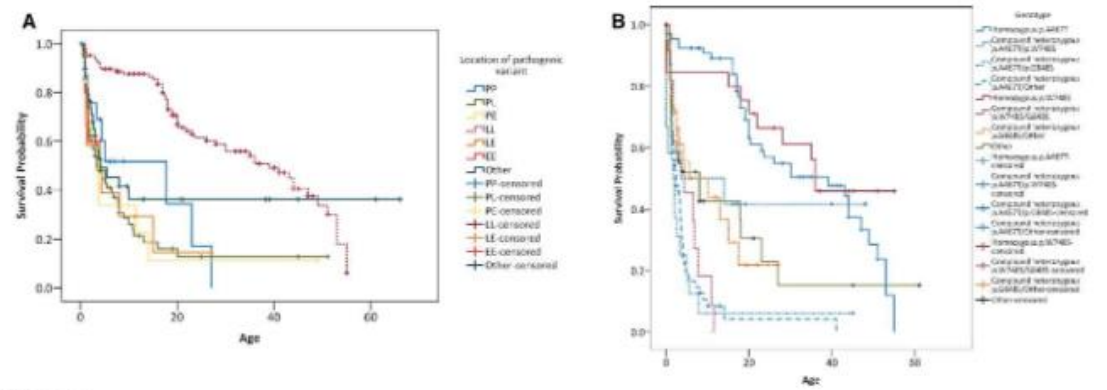

Figure 2.

Kaplan-Meier survival curves (**A**) based on the combination of the location of pathogenic variants (P, polymerase domain; L, linker domain; E, exonuclease), and (**B**) based on different genotypes. Hom, homozygous; Com, compound heterozygous. Censored data (representing the number of patients that were still alive when reported in the literature) are shown as crosses (+).

Epilepsia © ILAE

hyperintensities involving cortical and subcortical areas, of which occipital lobe is more commonly affected compared to other parts of cerebral hemisphere (Fig. S4). These lesions could have cytotoxic, vasogenic, or mixed changes (often depending on timing of the imaging in relation to onset of symptoms) and very rarely could be accompanied by hemorrhagic changes.[19] T_2-hyperintense thalamic lesions (37%), often bilateral, are another common finding observed in cases with drug-resistant seizures. Unusual imaging appearances such as enhancement of bilateral

Table 2. Summary of radiologic findings (n = 136)

Radiologic findings	Frequency
Stroke-like lesion	59 (43%)
Occipital lobe	51
Bilateral	15
Unilateral	36
Parietal lobe	12
Frontal	4
Temporal	1
Thalamic lesion	50 (37%)
Bilateral	30
Unilateral	20
Cerebral/cerebellar atrophy	38 (28%)
Cerebellar lesion	23 (17%)
Basal ganglia lesion	19 (14%)
Cerebral white matter change	10 (7.4%)

Stroke-like lesion refers to confluent T_2/FLAIR (fluid-attenuated inversion recovery) hyperintensities involving cortical and subcortical areas.

cranial nerves (III, V, to X) and cervical nerve roots,[20] and T_2-hyperintensity in inferior colliculus (a midbrain nucleus) have also been reported.[21] Overall, brainstem signal abnormality is extremely uncommon.

Seizure management

No randomized or open-labeled pharmacologic trial has been performed on patients with *POLG*-related seizure disorders to date. Seizure management was discussed in 29 publications, involving 51 patients (Table 3). The median number of antiepileptic drugs (AEDs) used was 3 (range 1–10), and overall 24 different AEDs had been tried. Details on general anesthetic agents were provided in 16 cases; midazolam (n = 11) and pentobarbital (n = 7) were the most commonly used drugs. Possible efficacious treatments for seizure were identified in 18 cases: ketogenic diet/low glycemic diet (n = 3),[15,18,22] phenobarbital (n = 3),[23] combined midazolam and thiopentone with other AEDs (n = 2),[24,25] magnesium infusion (n = 2),[26] combined propofol and thiopentone (n = 1),[16] ketamine infusion (n = 1),[27] folinic acid (n = 1),[28] and carnitine for hepatic encephalopathy (n = 1)[29] (Table 3). Palliative hemispherectomy was performed in a single patient.[14] A case series consisting entirely of adult patients with *POLG*-related occipital epilepsy (n = 19) suggested that a combination of sodium channel blocker (carbamazepine, oxcarbazepine, lamotrigine, and phenytoin) and benzodiazepine was effective for generalized tonic–clonic seizure, whereas myoclonus was better controlled with topiramate, phenobarbital, or clonazepam.[12]

Histopathology

Brain

Neuropathology reports were available for 28 patients, of whom 21 were infants/children (0–9 years) and seven were adolescents/young adults (12–18 years).[13,21,24,25,30–37] These samples were mainly postmortem, although three were brain biopsies.[24,34,37]

Macroscopic abnormalities of postmortem brain tissue were identified in nine patients: six infants/children (0–5 years)[30–32] and three adolescents/young adults (14–18 years).[25,33] The younger group showed decreased cortical thickness (n = 5), which was most prominent in the occipital lobes.[31,32] Similar changes were observed in the parietal lobes of two patients.[31,32] The older group demonstrated mild atrophy in the cerebellar vermis[25] and ischemic changes in the cerebrum and thalamus,[25] whereas the cerebellar/cerebral hemispheres and grey nuclei of substantia nigra were well preserved in another patient.[33]

Microscopically, the posterior areas of the brain, including gray and white matter, were more frequently affected compared to anterior parts of the brain. Neuronal loss, gliosis, capillary proliferation, spongiosis, and astrocytosis were commonly observed in the cerebral cortex,[13,21,24,25,30–32,34,36,37] and they were most prominent in the occipital lobes (n = 5).[13,31,32,34,37] Similar changes were also identified in the gray and white matter of substantia nigra, basal ganglia, hippocampus, thalamus, and brainstem to a lesser extent.[21,31,32,35–37] The cerebellum of 16 patients was affected by Purkinje cell loss and type II Alzheimer glia.[13,21,25,30–32,35] Severe degeneration of the spinal cord was evident in only three pediatric cases (0–12 years).[35] Variable complex I and IV deficiency in different brain regions has been observed.[35] Abnormal mitochondrial morphology was identified by electron microscopy (EM) in one brain biopsy (Table 4).[24]

Liver

Histologic findings from 30 patients were reviewed. A total of 11 liver biopsies and 2 postmortem liver samples were identified. Tissue source for 17 patients was not specified.[9,13,30,31,36,38–43] Of the patients reviewed, there were 28 infants/children (range 0–8.5 years), one 12-year-old adolescent, and a 39-year-old adult.[41]

Microvesicular fatty changes, microvesicular steatosis, fibrosis, and cirrhosis were prominent features.[9,13,30,38,40,42] Other changes have been reported, although uncommonly detected[9,13,39,40] It is intriguing that one pediatric patient who had AHS clinically had histologically normal liver on postmortem.[13] A number of mitochondrial abnormalities were observed (Table 4).[13,38,43] A mosaic of cytochrome *c* oxidase (COX) activity was reported in the liver of six infants (0–5 years)[31,35,38,41] and two older patients (12- and 39-years-old, respectively).[41] "Ragged-red" changes (increased density of mitochondria accumulating at the periphery of the hepatocytes) were detected in only the two older patients, suggesting that these changes may be uncommon in the younger population.[41]

Table 3. Summary of seizure types, antiepileptic treatments, and treatment efficacy (n = 51)

Ref	Case	Seizure onset	Death	Death age	Genotype	Alpers	Focal	Generalized	Myoclonus	SE	EPC	SLE	Liver	VPA	AEDs	Anesthetic agents	Other treatment	Efficacy
17	1		+	1.02	Compound heterozygous p.Ala467Thr	+	+		+		+		+		Diazepam, lorazepam, paraldehyde, PBT, fosphenytoin, LEV, CBZ	Midazolam, thiopental	Corticosteroids, IVIG	Drug resistant to treatment
34	16	9	–		Other	+	+	+	–	+	+	+	+	+	PBT, CBZ, TOP, LTG, clonazepam		Corticosteroids, IVIG	Drug resistant to treatment
36	1	5	+	17.25	Homozygous p.Ala467Thr	+	+	+	+	+	+		+	+	Benzodiazepine, PBT	Non-specified		Drug resistant to treatment
29	1	7	–		Homozygous p.Ala467Thr	–	+					+	+	+	VPA (caused hepatic encephalopathy)		Carnitine for hepatic encephalopathy	Possible efficacious
18		1.17	+	1.58	Other	+	+		+		+		+	–		Pentobarbital	Ketogenic diet	Possible efficacious
62	1	1	+	2.25	Compound heterozygous p.Ala467Thr	+	+	+	+	+	+	+	+		CBZ (worsened myoclonus)		Ketogenic diet	Drug resistant to treatment
62	2	1.33	+	4.17	Compound heterozygous p.Trp748Ser	+		+	+	+			+	+			Ketogenic diet	Did not tolerate ketogenic diet
55	1	0.83	+	2.5	Compound heterozygous p.Trp748Ser	+	+		+				+	–	TOP, clobazam, phenylbarbiturate			Drug resistant to treatment
55	7	1.33	+	2	Compound heterozygous p.Ala467Thr	+	+	+		+	+		+	+	CBZ, OXC			Drug resistant to treatment
66	7	3	–		Other	+		+	+				+		PBT			Drug resistant to treatment
19	1	23	–		Compound heterozygous p.Ala467Thr	–	+	+				+	–	–	LEV, PHT, primidone			Drug resistant to treatment
28		3.5	+	5.5	Compound heterozygous p.Ala467Thr	+	+	+		+	+	–	–		PBT + VIG		Folinic acid (Leucovorin) PO 0.25 mg/kg/body weight × 2 and increased to 4 mg/kg/ body weight × 2	Possible efficacious with folinic acid replacement
57	1	0.75	+	1.17	Compound heterozygous p.Ala467Thr	+	+	+		+	+	+	+		Numerous drugs		IVIG, steroids, transcranial magnetic stimulation	Drug resistant to treatment
31	1	1	+	4.33	Compound heterozygous p.Ala467Thr	+	+	+	+	+	+	+	+	+	PBT			Drug resistant to treatment
31	2	0.58	+	1.17	Compound heterozygous p.Ala467Thr	+	+	+	+	+	+	+	+	+	PBT	Thiopental		Drug resistant to treatment
31	5	13	–		Compound heterozygous p.Trp748Ser	–		+	+			+	–	–	LTG, clonazepam			Possible efficacious
14	1	4	+	5	Compound heterozygous p.Ala467Thr	+	+	–	+	+	+	+	+	–	OXC, PHT, PBT, LEV, clonazepam, TOP	Pentobarbital, midazolam	Methylprednisolone, ketogenic diet (4:1). had functional right hemispherectomy and deemed	Drug resistant to treatment; functional hemispherectomy appeared to

Continued

Table 3. Continued.

Ref.	Case	Seizure onset	Death	Death age	Genotype	Alpers	Focal	Generalized	Myoclonus	SE	EPC	SLE	Liver	VPA	AEDs	Anesthetic agents	Other treatment	Efficacy
50	2		+	2.08	Compound heterozygous p.Ala467Thr	+		+		+		+	+	–	PBT, fosphenytoin, lorazepam, diazepam, TOP, LEV	Pentobarbital, midazolam	successfully controlled seizure for 2 months before fatal infection and liver failure	control seizure for 2 months
15	1	26	–		Homozygous p.Trp748Ser	–	+	+	–	+	–	+	–	–	PHT, OXC, LEV	None	Low glycemic diet (LGI)	Possible efficacious
16	1	1.42	+	1.42	Compound heterozygous p.Ala467Thr	+	+				+		+		Lorazepam, fosphenytoin, PBT	Midazolam; propofol + thiopentone		Possible efficacious with propofol and thiopentone
16	4	3.58	–		Compound heterozygous p.Ala467Thr	+	+	+		+	+		–		Lorazepam, PBT, PHT; CBZ	Midazolam		Possible efficacious
23	1	0.42	+		Other	+	+						+	+	PBT			Possible efficacious
23	3	4	–		Other	+	+					+	–		PBT, TOP, clobazam			Possible efficacious
23	8	0.42	–		Other	+	+					–	–		PBT			Possible efficacious
24	1	16	+	17.5	Compound heterozygous p.Trp748Ser	–	+	+	+	+	+		–	+	PBT, PHT, LEV, OXC, VIG	Thiopental	Plasmapheresis, methylprednisoline, cyclosporine, etanercept	Drug resistant to treatment
24	2	17	–		Compound heterozygous p.Trp748Ser	–	+	+	+	+			–	–	LEV, PHT, clobazam, TOP,	Thiopental, midazolam	L-carnitine	Possible efficacious with thiopental and midazolam
76	1	15	–		Compound heterozygous p.Ala467Thr	–	+	+		+		+	–	+	Ineffective: OXC, LEV, ZNS, TOP (cognitive side effect), PHT + LTG		Resolution of SE with PHT, 10% dextrose with L-carnitine + co-enzyme Q10	Possible efficacious with PHT and LTG
77	II.2		+	27	Other	–	+	+	+	+			–	–	LTG			Possible efficacious
27,77	II.3	17	+	23	Other	–	+	+	+	+			–	+	Primidone, lorazepam, PHT, LEV, TOP	Thiopental, propofol, Ketamine bolus and midazolam, ketamine infusion for 14 days (cumulative dose of 32 g)		Drug resistant to most treatments; possible efficacious with ketamine infusion
54	II-1	14	+	18.5	Other	+	+						+	+	OXC, PHT			Drug resistant to treatment
78	1	45	–		Compound heterozygous p.Ala467Thr	–	–	+	+		–	–	–	–	Clonazepam, LEV	None		Unknown

Continued

Table 3. Continued.

Ref	Case	Seizure onset	Death	Death age	Genotype	Alpers	Focal	Generalized	Myoclonus	SE	EPC	SLE	Liver	VPA	AEDs	Anesthetic agents	Other treatment	Efficacy
25	1	14	+	15	Homozygous p.Trp748Ser	+	+	+	+	+	+	+	+	+	Controlled with OXC & VPA			Possible efficacious
25	3	15	+	20	Homozygous p.Trp748Ser	+	+	+					+	+	OXC, LTG, diazepam, clonazepam, TOP, GBP, fosphenytoin	Midazolam, thiopentone		Possible efficacious with midazolam and thiopentone
59	29		–		Homozygous p.Ala467Thr		+	+	+			–	+	+	Clonazepam, LTG			Unknown
33	B1,B3	18	+	39	Homozygous p.Ala467Thr	–		+	+	+			–	+	PHT, LEV			Drug resistant to treatment
37	1	17	+	17.75	Other	+	+	+		+		+	+	+	PHT, CBZ, LTG, benzodiazepine, TOP, GBP, PBT	Midazolam		Drug resistant to treatment
10	1	15	+	23.5	Homozygous p.Ala467Thr	+	+		+		+	–	+	+	LTG, LEV	None		Drug resistant to treatment
10	8	6	–		Compound heterozygous p.Ala467Thr	+		+				–	+	–	CBZ, OXC, LTG, ZNS, LEV, TPM			Drug resistant to treatment
10	11	2.8	+	3.33	Compound heterozygous p.Ala467Thr	+	+		+		+	–	+	+	OXC			Unknown
22	1	2.58	+	5.5	Compound heterozygous p.Trp748Ser	+	+				+	–	+	–	Lorazepam, PHT, PBT, CBZ, clobazam, clonazepam, nitrazepam, TOP, LEV, ETHO	Midazolam	Methylprednisolone 30 mg/kg for 3/7; ketogenic diet	Possible efficacious with ketogenic diet and midazolam
79	1	21	–		Other	–	+	+	+	+	+	+	–	+	PHT, CBZ, PBT, LEV			Drug resistant to treatment
80	1a		+		Homozygous p.Ala467Thr	–			+	–			+	–	LTG, clonazepam			
80	2a	17	–		Homozygous p.Ala467Thr	–	+	+	+	+	+	+	–	–	OXC, LEV, clonazepam			
80	4b	17	+		Homozygous p.Ala467Thr	–			+				+	–	PHT, clonazepam			
80	18		+	30	Homozygous p.Trp748Ser	–	+	+	+	+	+	+	+	+	VPA for 14 years			
80	22	18	–		Homozygous p.Trp748Ser	–	+	+	+	+	+	+	–	–	OXC, PHT, clonazepam, PBT, diazepam			
80	23		–		Homozygous p.Trp748Ser	–	+	+	+	+	+	+	–	–	LTG, PBT, clonazepam			
80	24		–		Homozygous p.Trp748Ser	–		+	–	–	–	+	–	–	LTG, Clobazam			
80	25		–		Homozygous p.Trp748Ser	–		+	+	+	+	+	–	–	CBZ, Clobazam, TOP			
80	26	19	–		Homozygous p.Trp748Ser		+	+	+	+	+		+	+	Clonazepam, LEV, liver transplant			

Continued

Epilepsia, 57(10):1531–1545, 2016
doi: 10.1111/epi.13508

Table 3. Continued.

Ref	Case	Seizure onset	Death	Death age	Genotype	Alpers	Focal	Generalized	Myoclonus	SE	EPC	SLE	Liver	VPA	AEDs	Anesthetic agents	Other treatment	Efficacy
26	1	20	+	20.17	Homozygous p.Ala467Thr	+	+				+	+	–	–	PHT, clonazepam, clobazam, LEV, TOP	Midazolam	Magnesium infusion	Possible efficacious with magnesium infusion
26	2	17	+	17.67	Homozygous p.Ala467Thr	+	+				+	+	–	–	PHT, LEV	Midazolam	Magnesium infusion	Possible efficacious with magnesium infusion

SE, status epilepticus; EPC, epilepsia partialis continua; SLE, stroke-like episodes; VPA, exposure to sodium valproate; AEDs, antiepileptic drugs; PBT, phenobarbitone; LEV, levetiracetam; CBZ, carbamazepine; IVIG, intravenous immunoglobulin; LTG, lamotrigine; TOP, topiramate; OXC, oxcarbazepine; PHT, phenytoin; VIG, vigabatrin; ZNS, zonisamide; GBP, gabapentin; ETHO, ethosuximide.

Muscle

With regard to muscle, biopsies or postmortem tissue were analyzed from 38 patients, of whom 36 were children. Normal muscle histology was evident for 10 patients (26%), of whom one was an adolescent (17-year-old) and 9 were infants/children.[13,16,32,40,44–46] Of interest, two infants had normal muscle findings in the presence of severe liver abnormalities.[13,40] Similar to in liver, nonspecific microscopic changes and mitochondrial abnormalities were observed (n = 28)[13,18,24,25,31–33,39–41,45–47] (Table 4). Among these patients, abnormalities in both muscle and liver were detected in seven.[13,31,39–41]

Mitochondrial DNA content

To better understand the tissue-specific impact of *POLG* variants on the mtDNA content, we reviewed the mtDNA copy number of liver, brain, muscle, blood, and cultured fibroblasts from a total of 109 patients. The mtDNA copy number was expressed as a percentage relative to the control mean. As defined previously, a value <30% was considered diagnostic of mtDNA depletion.[48] The presence of multiple mtDNA deletions, another observed consequence of a disorder of mtDNA maintenance, was also considered.

Liver was the most severely affected tissue followed by muscle, blood, and cultured fibroblasts (Table 4). The mtDNA copy number from biopsy or postmortem liver was available for 37 patients. In liver, mtDNA copy number was reduced severely in all cases. Depletion of mtDNA copy number was found in 34 (92.5%) of 37 patients (3–28% of control mean),[13,21,30,36,37,42,49–54] and 3 patients showed a significant mtDNA copy number loss (30–36% of control mean).[46,49]

The mtDNA copy number from brain tissue has been rarely reported. Postmortem frontal cortex from a single patient revealed a 30% mtDNA copy number reduction,[55] whereas single microdissected neurons from multiple brain regions of five patients showed variable mtDNA copy number loss, ranging from moderate to severe.[35]

The findings of mtDNA copy number in the muscle of 42 patients, of whom 39 were pediatric (0–16 years) and 3 were adults (18–66 years) was highly variable (Table 4). Among the patients considered, only four samples (0–9 years) were within the normal range (70–93% of control mean).[31,34,52,54] A total of 18 patients exhibited mtDNA depletion,[21,31,40,46,49,51,53,54,56] whereas 14 showed mild to moderate reduction (32–65% of control mean).[36,46,49,54] Of interest, five patients (0–16 years) showed mtDNA copy number increase (108–174% of control mean).[31,49,54] The mtDNA copy number in six patients was generally higher in muscle than in liver.[36,49,51,54]

The mtDNA copy number of blood and fibroblasts was less consistent compared to muscle. Blood mtDNA copy number data were available for 49 patients.[54,57] Only five samples were mtDNA depleted (15–27% of control mean), whereas 13 had normal mtDNA copy number (70–100% of

Table 4. Summary of histopathologic findings, mtDNA content, and RC biochemistry from biopsies or postmortem brain, liver, and muscle tissues

Tissue	Histopathology	mtDNA content	RC Biochemistry	Total number of patients	References
Brain	Microscopic changes: (n = 28), neuronal loss, gliosis, capillary proliferation, spongiosis and astrocytosis in the cerebral cortex (most prominent in occipital lobes and cerebellum), substantia nigra, basal ganglia, hippocampus, thalamus, and brainstem, degeneration of spinal cord, variable CI and CIV deficiency EM microscopy: (n = 1), enlarged mitochondria with short/curved cristae and deep invaginations of outer membrane	Rearrangements/deletions: not reported mtDNA copy number: (n = 6), 15–56% of control mean	RCD: CIII (n = 1)	30 (27 postmortem, 3 biopsies)	13,21,24,25,30–33
Liver	Normal histology: (n = 1) Microscopic changes: (n = 28), macro/microvesicular steatosis, fibrosis, cirrhosis, necrosis, bile duct proliferation Histochemistry: mosaic COX-deficient fibers (n = 8), "Ragged-red" fiber-like structures (n = 2) EM microscopy: (n = 9), granule loss, enlarged/abnormally shaped mitochondria with pale matrix, cristae displacement	Rearrangements/deletions: not reported mtDNA copy number: (n = 37), 3–36% of control mean	Normal: (n = 3) RCD: (n = 26), multi-complex (n = 22, 85%), single complex (n = 4) CIII (n = 1), CIV (n = 3) CV deficiency: (n = 3), with RCD (n = 2), without RCD (n = 1)	61 (4 postmortem, 31 biopsies, 26 unspecified source)	9,13,21,30,31,36–38
Muscle	Normal histology: (n = 10, 26%) Microscopic changes: (n = 18), mild to moderate lipid accumulation, type II atrophy, myopathy, increased lipofuscin/glycogen, steatosis Histochemistry: mosaic COX-negative fibers (n = 10), "Ragged-red" fibres (n = 7) EM microscopy: (n = 5), enlarged mitochondria with abnormal shape and clustering, cristae displacement	Rearrangements/deletions: multiple deletions (n = 12) mtDNA copy number: (n = 42), 3–175% of control mean	Normal: (n = 34, 56%) RCD: (n = 27): multi-complex (n = 16, 59%), single complex (n = 8) CI (n = 3), CIV (n = 4), CIII (n = 1), no specific complex defect reported (n = 3) CV deficiency: (n = 3) with RCD	110 (4 postmortem, 90 biopsies, 16 unspecified source)	9,13,16,18–22

EM, electron microscopy; RCD, respiratory chain deficiency; CI, complex I; CIII, complex III; CIV, complex IV; CV, complex V; COX = cytochrome oxidase; n, number of patients.

control mean). As with muscle, an mtDNA copy number increase (101–167%) was detected in nine patients (0–60 years).[54] The mtDNA copy number from cultured fibroblasts of five pediatric patients (0–4 years) ranged from 37 to 98.43%.[49,52]

Compared to depletion, multiple deletions in the muscle of 12 patients have been reported of whom 9 were pediatric (0–15 years) and three adults (20–48 years).[19,31,32,36,41,58,59] Among these patients only three (1–5 years) had deletions in the presence of depletion.[31,32,36] With regard to brain, mtDNA deletions were not detectable in the patients considered.

Mitochondrial Respiratory chain (RC)

The RC activity from liver (n = 29), muscle (n = 61), brain biopsy (n = 1), and cultured fibroblasts (n = 16) from 76 patients was evaluated. The RC activity was highly variable among different tissues. Normal RC activity[9,21,22,28,32,37,39,40,44–46,51,52,60–64] and a number of RC defects (isolated and multicomplex deficiencies)[9,13,20,21,30,32,37,38,40,46,50–52,56,57,61–66] were detected. Complex V defects were rarely reported in muscle and liver samples[20,46,51,57] (Table 4). Complex III deficiency was identified in fibroblasts obtained from a single patient.[20] The RC activity of liver (n = 8) was deficient when RC activity in muscle was normal.[9,21,46,51,61,63] Conversely, both the liver and muscle from five patients showed RC deficiency.[46,50–52,62] As with fibroblasts, a single brain biopsy was reported to show isolated complex III deficiency.[63]

Discussion

Over 80% of patients affected by *POLG*-related epilepsy harbored at least one of the three common pathogenic variants, which are p.Ala467Thr, p.Trp748Ser, and p.Gly848Ser. Although we have identified 128 variants in the *POLG* gene related to seizure manifestation in the literature, many of them have been based only on single case reports or a small number of pedigrees. Differentiating rare pathogenic variant from single nucleotide polymorphisms often imposes diagnostic difficulty, particularly without the supportive functional work in the clinical practice.[67] More recently, a clustering prediction tool using a POLG molecular model has emerged as a potential method to assess pathogenicity of new variants to address this challenge.[68]

Homozygous variants located in the linker region of *POLG* are associated with better prognosis compared to compound heterozygous variants of different domains; this observation concurs with the analysis reported elsewhere.[68] The milder phenotype exhibited in homozygous or compound heterozygous linker p.Ala467Thr and p.Trp748Ser variants suggests that defective replication and repair of mtDNA caused by homozygous p.Ala467Thr variant or p.Trp748Ser remain unclear. Furthermore, we found that homozygous or compound heterozygous variants located in EE were very rare (3%) and associated with very severe disease and early death. This raises a possibility that EE variants are incompatible with life. Of interest, mice with exonuclease-deficient POLG are viable and exhibited only a premature aging phenotype with no evidence of seizures.[69]

Our result is consistent with previous observations of a predisposition for occipital lobe involvement in *POLG*-related epilepsy, especially among those with juvenile and adult onset, in terms of clinical, radiologic, and histopathologic findings; however, the precise explanation of such preferential involvement remains enigmatic.[12,70] The stroke-like lesions in *POLG*-related epilepsy appear to overlap in those observed in mitochondrial encephalomyopathy, lactic acidosis, and stroke-like episodes (MELAS) caused by the m.3243A>G mutation and other primary pathogenic mtDNA mutations.[29] However, thalamic (37%) and cerebellar lesions with restricted diffusion are more commonly observed in cases with *POLG* mutations compared to the m.3243A>G mutation. These may reflect the drug-resistant and prolonged nature of the seizure activity associated with *POLG* variants as well as the inherent role of the epileptogenesis in these structures.[35]

The seizure management in patients who harbor *POLG* variants is extremely challenging, and often futile in those presented with recurrent status epilepticus and progressive encephalopathy. It remains unclear whether earlier recognition of seizure and aggressive treatment with combined AEDs as well as general anesthesia could alter the clinical outcome in all patients with *POLG* variants, as a significant number of patients especially pediatric cases with Alpers disease eventually succumbed to hepatic failure. Efficacious treatments reported in the case reports are anecdotal, and such evidence is limited by small number of patients. However, VPA is an absolute contraindication in patients with *POLG*-related epilepsy.

A better understanding of the epileptogenesis in *POLG*-related disorders and other mitochondrial disorders is crucial for developing better or novel therapies. Several hypotheses explaining seizure development in mitochondrial disease have been proposed.[71] More recently, a postmortem study of patients with mitochondrial epilepsy suggested that γ-aminobutyric acid (GABA)ergic interneurons exhibit more severe mitochondrial respiratory chain deficiencies, thereby resulting in imbalance of neuronal inhibition and excitation and development of seizure.[72]

Liver involvement is rarely observed as a presenting symptom and is most often associated with preterminal disease stage. Severe mtDNA depletion and oxidative phosphorylation dysfunction are accompanied by microscopic abnormalities indicative of liver failure, which are essential for the diagnosis of AHS.[9] However, these results may reflect the bias of the postmortem tissue studied or the liver biopsies, which were taken late in the disease course when

the liver was severely affected. It is notable that a prospective study revealed that a single, heterozygous variant in *POLG* (p.Gln1236His) was strongly associated with VPA-induced hepatotoxicity (odds ratio [OD] 23.6, p-value $=5.1 \times 10^{-7}$), as the result of non-apoptotic cell death that was not mediated through the mtDNA defect or impairment of the fatty acid oxidation.[73] A recent study using hepatocytes from the induced pluripotent stem cells (iPSCs) with p.Ala467Thr variant demonstrated that VPA led to increased apoptosis through a mitochondrial-transition pore-opening pathway. More importantly, supplementation of carnitine or *N*-acetylcysteine appeared to rescue VPA-induced toxicity, suggesting that this iPSC model may serve as a promising tool for evaluating potential therapeutic agents.[74]

In accordance with the normal muscle histology observed in many pediatric cases, we found that myopathy was not a common clinical feature in *POLG*-related epilepsy. Furthermore, normal muscle mtDNA content has been reported especially in this group of patients, highlighting the caveat that *POLG*-related mitochondrial disease cannot be reliably excluded based on muscle biopsy alone.

The mtDNA abnormalities in blood and cultured fibroblasts were less consistent. A possible explanation would be the high mitotic rate, which may mask any mtDNA abnormalities. Although it is still unclear, it seems that a process of negative selection favors replication of cells with higher levels of mtDNA.[75] Therefore, it is not surprising that fibroblasts did not recapitulate the biochemical features of the disease phenotype, even when the liver was severely affected.[52]

The major limitation of our findings is the retrospective nature of the study design and data extrapolation from a number of case studies with different emphasis on clinical or molecular findings. We were unable to perform multivariate Cox regression analysis to identify prognostic factors that might explain the discrepancy in survival between the different genotypes due to incomplete data set and the inherent bias associated with case reports. Other limitations are that the tissue examined was not patient matched in all cases, and there was limited documentation about the number of age-/gender-matched controls used for molecular/biochemical investigations.

Conclusions

POLG-related epilepsy has a bimodal disease onset in early childhood and adolescence, although onset in late adulthood is rare. Normal muscle biopsy findings do not exclude the diagnosis of *POLG*-related mitochondrial disease, and direct sequencing of the *POLG* gene should be the gold standard when investigating suspected cases. Mixed seizure types are common and often highly drug resistant to conventional pharmacologic treatments. The overall prognosis appears to be, in part, correlated with the genotype, although what determines tissue specificity and disease phenotype remains elusive. Recent advances in new technologies and model systems will improve our understanding of the pathophysiology of *POLG*-related epilepsy. As the number of *POLG* variants likely to be pathogenic is ever-expanding, prospective, multicenter cohort studies and randomized controlled trials are necessary to understand the natural history of the individual genotype and determine better treatment strategies.

Acknowledgments

We would like to thank Charlotte L. Alston for her help in verifying the pathogenicity of certain variants using predictor software (Alamut Visual version 2.7.1). This work was supported by the Wellcome Trust (096919Z/11/Z, R.W.T.), The Medical Research Council (G0601943, G0800674, R.M., R.W.T.), The Lily Foundation, and the UK NHS Specialized Services and Newcastle upon Tyne Hospitals NHS Foundation Trust supporting the "Rare Mitochondrial Disorders of Adults and Children" Diagnostic Service (http://www.newcastle-mitochondria.com/). MEA receives funding from the charity Ryan Stanford Appeal for her PhD study and YSN is funded by the MRC Centre for Neuromuscular Diseases.

Disclosure

None of the authors has any conflict of interest to disclose. We confirm that we have read the Journal's position on issues involved in ethical publication and affirm that this report is consistent with those guidelines.

References

1. Ropp PA, Copeland WC. Cloning and characterization of the human mitochondrial DNA polymerase, DNA polymerase gamma. *Genomics* 1996;36:449–458.
2. Yakubovskaya E, Chen Z, Carrodeguas JA, et al. Functional human mitochondrial DNA polymerase γ forms a heterotrimer. *J Biol Chem* 2006;281:374–382.
3. Lee Y-S, Kennedy WD, Yin YW. Structural insights into human mitochondrial DNA replication and disease-related polymerase mutations. *Cell* 2009;139:312–324.
4. Van Goethem G, Dermaut B, Lofgren A, et al. Mutation of POLG is associated with progressive external ophthalmoplegia characterized by mtDNA deletions. *Nat Genet* 2001;28:211–212.
5. Saneto RP, Cohen BH, Copeland WC, et al. Alpers-Huttenlocher syndrome. *Pediatr Neurol* 2013;48:167–178.
6. Hakonen AH, Davidzon G, Salemi R, et al. Abundance of the POLG disease mutations in Europe, Australia, New Zealand, and the United States explained by single ancient European founders. *Eur J Hum Genet* 2007;15:779–783.
7. Harding BN, Egger J, Portmann B, et al. Progressive neuronal degeneration of childhood with liver disease. A pathological study. *Brain* 1986;109:181–206.
8. Naviaux RK, Nyhan WL, Barshop BA, et al. Mitochondrial DNA polymerase gamma deficiency and mtDNA depletion in a child with Alpers' syndrome. *Ann Neurol* 1999;45:54–58.
9. Nguyen KV, Ostergaard E, Ravn SH, et al. POLG mutations in Alpers syndrome. *Neurology* 2005;65:1493–1495.
10. Wong LJ, Naviaux RK, Brunetti-Pierri N, et al. Molecular and clinical genetics of mitochondrial diseases due to POLG mutations. *Hum Mutat* 2008;29:E150–E172.
11. Naess K, Barbaro M, Bruhn H, et al. Complete deletion of a POLG1 allele in a patient with Alpers syndrome. *JIMD Rep* 2012;4:67–73.
12. Engelsen BA, Tzoulis C, Karlsen B, et al. POLG1 mutations cause a syndromic epilepsy with occipital lobe predilection. *Brain* 2008;131:818–828.

13. Hunter MF, Peters H, Salemi R, et al. Alpers syndrome with mutations in POLG: clinical and investigative features. *Pediatr Neurol* 2011;45:311–318.
14. Lupashko S, Malik S, Donahue D, et al. Palliative functional hemispherectomy for treatment of drug resistant status epilepticus associated with Alpers' disease. *Childs Nerv Syst* 2011;27:1321–1323.
15. Martikainen MH, Paivarinta M, Jaaskelainen S, et al. Successful treatment of POLG-related mitochondrial epilepsy with antiepileptic drugs and low glycaemic index diet. *Epileptic Disord* 2012;14:438–441.
16. McCoy B, Owens C, Howley R, et al. Partial status epilepticus – rapid genetic diagnosis of Alpers' disease. *Eur J Paediatr Neurol* 2011;15:558–562.
17. Allen NM, Winter T, Shahwan A, et al. Explosive onset non-epileptic jerks and profound hypotonia in an infant with Alpers-Huttenlocher syndrome. *Seizure* 2014;23:237–239.
18. Cardenas JF, Amato RS. Compound heterozygous polymerase gamma gene mutation in a patient with Alpers disease. *Semin Pediatr Neurol* 2010;17:62–64.
19. Hansen N, Zwarg T, Wanke I, et al. MELAS/SANDO overlap syndrome associated with POLG1 mutations. *Neurol Sci* 2012;33:209–212.
20. Horst DM, Ruess L, Rusin JA, et al. Cranial nerve and cervical root enhancement in an infant with polymerase gamma mutation mitochondrial disease. *Pediatr Neurol* 2014;51:734–736.
21. Scalais E, Francois B, Schlesser P, et al. Polymerase gamma deficiency (POLG): clinical course in a child with a two stage evolution from infantile myocerebrohepatopathy spectrum to an Alpers syndrome and neuropathological findings of Leigh's encephalopathy. *Eur J Paediatr Neurol* 2012;16:542–548.
22. Joshi CN, Greenberg CR, Mhanni AA, et al. Ketogenic diet in Alpers-Huttenlocher syndrome. *Pediatr Neurol* 2009;40:314–316.
23. Mohamed K, Fathallah W, Ahmed E. Gender variability in presentation with Alpers' syndrome: a report of eight patients from the UAE. *J Inherit Metab Dis* 2011;34:439–441.
24. Nolte KW, Trepels-Kottek S, Honnef D, et al. Early muscle and brain ultrastructural changes in polymerase gamma 1-related encephalomyopathy. *Neuropathology* 2013;33:59–67.
25. Uusimaa J, Hinttala R, Rantala H, et al. Homozygous W748S mutation in the POLG1 gene in patients with juvenile-onset Alpers syndrome and status epilepticus. *Epilepsia* 2008;49:1038–1045.
26. Visser NA, Braun KP, Leijten FS, et al. Magnesium treatment for patients with drug resistant status epilepticus due to POLG1-mutations. *J Neurol* 2011;258:218–222.
27. Pruss H, Holtkamp M. Ketamine successfully terminates malignant status epilepticus. *Epilepsy Res* 2008;82:219–222.
28. Hasselmann O, Blau N, Ramaekers VT, et al. Cerebral folate deficiency and CNS inflammatory markers in Alpers disease. *Mol Genet Metab* 2010;99:58–61.
29. Brinjikji W, Swanson JW, Zabel C, et al. Stroke and stroke-like symptoms in patients with mutations in the POLG1 gene. *JIMD Rep* 2011;1:89–96.
30. Montassir H, Maegaki Y, Murayama K, et al. Myocerebrohepatopathy spectrum disorder due to POLG mutations: a clinicopathological report. *Brain Dev* 2015;37:719–724.
31. Kollberg G, Moslemi AR, Darin N, et al. POLG1 mutations associated with progressive encephalopathy in childhood. *J Neuropathol Exp Neurol* 2006;65:758–768.
32. Sofou K, Moslemi AR, Kollberg G, et al. Phenotypic and genotypic variability in Alpers syndrome. *Eur J Paediatr Neurol* 2012;16:379–389.
33. Van Goethem G, Luoma P, Rantamaki M, et al. POLG mutations in neurodegenerative disorders with ataxia but no muscle involvement. *Neurology* 2004;63:1251–1257.
34. Bao X, Wu Y, Wong LJ, et al. Alpers syndrome with prominent white matter changes. *Brain Dev* 2008;30:295–300.
35. Tzoulis C, Tran GT, Coxhead J, et al. Molecular pathogenesis of polymerase gamma-related neurodegeneration. *Ann Neurol* 2014;76:66–81.
36. Boes M, Bauer J, Urbach H, et al. Proof of progression over time: finally fulminant brain, muscle, and liver affection in Alpers syndrome associated with the A467T POLG1 mutation. *Seizure* 2009;18:232–234.
37. Wiltshire E, Davidzon G, DiMauro S, et al. Juvenile Alpers disease. *Arch Neurol* 2008;65:121–124.
38. Roels F, Verloo P, Eyskens F, et al. Mitochondrial mosaics in the liver of 3 infants with mtDNA defects. *BMC Clin Pathol* 2009;9:4.
39. Simon M, Chang RC, Bali DS, et al. Abnormalities in glycogen metabolism in a patient with alpers' syndrome presenting with hypoglycemia. *JIMD Rep* 2014;14:29–35.
40. Uusimaa J, Gowda V, McShane A, et al. Prospective study of POLG mutations presenting in children with intractable epilepsy: prevalence and clinical features. *Epilepsia* 2013;54:1002–1011.
41. Stewart JD, Tennant S, Powell H, et al. Novel POLG1 mutations associated with neuromuscular and liver phenotypes in adults and children. *J Med Genet* 2009;46:209–214.
42. Davidzon G, Mancuso M, Ferraris S, et al. POLG mutations and Alpers syndrome. *Ann Neurol* 2005;57:921–923.
43. Mangalat N, Tatevian N, Bhattacharjee M, et al. Alpers syndrome: an unusual etiology of failure to thrive. *Ultrastruct Pathol* 2012;36:219–221.
44. McFarland R, Hudson G, Taylor RW, et al. Reversible valproate hepatotoxicity due to mutations in mitochondrial DNA polymerase gamma (POLG1). *Arch Dis Child* 2008;93:151–153.
45. Isohanni P, Hakonen AH, Euro L, et al. POLG1 manifestations in childhood. *Neurology* 2011;76:811–815.
46. Rouzier C, Chaussenot A, Serre V, et al. Quantitative multiplex PCR of short fluorescent fragments for the detection of large intragenic POLG rearrangements in a large French cohort. *Eur J Hum Genet* 2014;22:542–550.
47. Cheldi A, Ronchi D, Bordoni A, et al. POLG1 mutations and stroke like episodes: a distinct clinical entity rather than an atypical MELAS syndrome. *BMC Neurol* 2013;13:8.
48. Vu TH, Sciacco M, Tanji K, et al. Clinical manifestations of mitochondrial DNA depletion. *Neurology* 1998;50:1783–1790.
49. Ashley N, O'Rourke A, Smith C, et al. Depletion of mitochondrial DNA in fibroblast cultures from patients with POLG1 mutations is a consequence of catalytic mutations. *Hum Mol Genet* 2008;17:2496–2506.
50. Lutz RE, Dimmock D, Schmitt ES, et al. De novo mutations in POLG presenting with acute liver failure or encephalopathy. *J Pediatr Gastroenterol Nutr* 2009;49:126–129.
51. Sarzi E, Bourdon A, Chretien D, et al. Mitochondrial DNA depletion is a prevalent cause of multiple respiratory chain deficiency in childhood. *J Pediatr* 2007;150:531–534, 534.e531-536.
52. Schaller A, Hahn D, Jackson CB, et al. Molecular and biochemical characterisation of a novel mutation in POLG associated with Alpers syndrome. *BMC Neurol* 2011;11:4.
53. Taanman JW, Rahman S, Pagnamenta AT, et al. Analysis of mutant DNA polymerase gamma in patients with mitochondrial DNA depletion. *Hum Mutat* 2009;30:248–254.
54. Tang S, Wang J, Lee NC, et al. Mitochondrial DNA polymerase gamma mutations: an ever expanding molecular and clinical spectrum. *J Med Genet* 2011;48:669–681.
55. Ferrari G, Lamantea E, Donati A, et al. Infantile hepatocerebral syndromes associated with mutations in the mitochondrial DNA polymerase-gammaA. *Brain* 2005;128:723–731.
56. Navarro-Sastre A, Tort F, Garcia-Villoria J, et al. Mitochondrial DNA depletion syndrome: new descriptions and the use of citrate synthase as a helpful tool to better characterise the patients. *Mol Genet Metab* 2012;107:409–415.
57. Khan A, Trevenen C, Wei XC, et al. Alpers syndrome: the natural history of a case highlighting neuroimaging, neuropathology, and fat metabolism. *J Child Neurol* 2012;27:636–640.
58. Naimi M, Bannwarth S, Procaccio V, et al. Molecular analysis of ANT1, TWINKLE and POLG in patients with multiple deletions or depletion of mitochondrial DNA by a dHPLC-based assay. *Eur J Hum Genet* 2006;14:917–922.
59. Van Goethem G, Schwartz M, Lofgren A, et al. Novel POLG mutations in progressive external ophthalmoplegia mimicking mitochondrial neurogastrointestinal encephalomyopathy. *Eur J Hum Genet* 2003;11:547–549.
60. de Vries MC, Rodenburg RJ, Morava E, et al. Normal biochemical analysis of the oxidative phosphorylation (OXPHOS) system in a child with POLG mutations: a cautionary note. *J Inherit Metab Dis* 2008;31 (Suppl. 2):S299–S302.

Epilepsia, 57(10):1531–1545, 2016
doi: 10.1111/epi.13508

61. Kurt B, Jaeken J, Van Hove J, et al. A novel POLG gene mutation in 4 children with Alpers-like hepatocerebral syndromes. *Arch Neurol* 2010;67:239–244.
62. Mousson de Camaret B, Chassagne M, Mayencon M, et al. POLG exon 22 skipping induced by different mechanisms in two unrelated cases of Alpers syndrome. *Mitochondrion* 2011;11:223–227.
63. Blok MJ, van den Bosch BJ, Jongen E, et al. The unfolding clinical spectrum of POLG mutations. *J Med Genet* 2009;46:776–785.
64. de Vries MC, Rodenburg RJ, Morava E, et al. Multiple oxidative phosphorylation deficiencies in severe childhood multi-system disorders due to polymerase gamma (POLG1) mutations. *Eur J Pediatr* 2007;166:229–234.
65. Witters P, Pirenne J, Aerts R, et al. Alpers syndrome presenting with anatomopathological features of fulminant autoimmune hepatitis. *J Inherit Metab Dis* 2010;33:451.
66. Ferreira M, Evangelista T, Almeida LS, et al. Relative frequency of known causes of multiple mtDNA deletions: two novel POLG mutations. *Neuromuscul Disord* 2011;21:483–488.
67. Prasun P. Rare variant of unknown significance in POLG1 and diagnostic dilemma. *J Neurol* 2014;261:2218–2220.
68. Farnum GA, Nurminen A, Kaguni LS. Mapping 136 pathogenic mutations into functional modules in human DNA polymerase gamma establishes predictive genotype-phenotype correlations for the complete spectrum of POLG syndromes. *Biochim Biophys Acta* 2014;1837:1113–1121.
69. Trifunovic A, Wredenberg A, Falkenberg M, et al. Premature ageing in mice expressing defective mitochondrial DNA polymerase. *Nature* 2004;429:417–423.
70. Janssen W, Quaegebeur A, Van Goethem G, et al. The spectrum of epilepsy caused by POLG mutations. *Acta Neurol Belg* 2016;116:17–25.
71. Zsurka G, Kunz WS. Mitochondrial dysfunction and seizures: the neuronal energy crisis. *Lancet Neurol* 2015;14:956–966.
72. Lax NZ, Grady J, Laude A, et al. Extensive respiratory chain defects in inhibitory interneurones in patients with mitochondrial disease. *Neuropathol Appl Neurobiol* 2016;42:180–193.
73. Stewart JD, Horvath R, Baruffini E, et al. Polymerase gamma gene POLG determines the risk of sodium valproate-induced liver toxicity. *Hepatology* 2010;52:1791–1796.
74. Li S, Guo J, Ying Z, et al. Valproic acid-induced hepatotoxicity in Alpers syndrome is associated with mitochondrial permeability transition pore opening-dependent apoptotic sensitivity in an induced pluripotent stem cell model. *Hepatology* 2015;61:1730–1739.
75. van den Heuvel LP, Smeitink JA, Rodenburg RJ. Biochemical examination of fibroblasts in the diagnosis and research of oxidative phosphorylation (OXPHOS) defects. *Mitochondrion* 2004;4:395–401.
76. Roshal D, Glosser D, Zangaladze A. Parieto-occipital lobe epilepsy caused by a POLG1 compound heterozygous A467T/W748S genotype. *Epilepsy Behav* 2011;21:206–210.
77. Stricker S, Pruss H, Horvath R, et al. A variable neurodegenerative phenotype with polymerase gamma mutation. *J Neurol Neurosurg Psychiatry* 2009;80:1181–1182.
78. Tuladhar AM, Meijer FJ, van de Warrenburg BP. POLG mutation presenting with late-onset jerky torticollis. *J Neurol* 2013;260:903–905.
79. Woodbridge P, Liang C, Davis RL, et al. POLG mutations in Australian patients with mitochondrial disease. *Intern Med J* 2013;43:150–156.
80. Tzoulis C, Engelsen BA, Telstad W, et al. The spectrum of clinical disease caused by the A467T and W748S POLG mutations: a study of 26 cases. *Brain* 2006;129:1685–1692.

Supporting Information

Additional Supporting Information may be found in the online version of this article:

Figure S1. Flow chart of literature search and articles included for analysis.

Figure S2. First clinical manifestation of *POLG*-related epilepsy.

Figure S3. (**A**) EEG from an 11-month-old infant with left-sided facial twitching, and asynchronous twitching of both arms and legs. The background was dominated by high-amplitude posterior-predominant delta with low amplitude frequent spikes and polyspikes seen centered over the temporol regions bilateraly; these were suggestive of rhythmic high-amplitude delta with superimposed spikes (RHADS) but not entirely typical. (**B**) EEG from a 2.5-year-old boy with continuous jerking of right-sided shoulder and arm with retained consciousness; EEG changes were consistent with epilepsia partialis continua (EPC). (**C**) and (**D**) are EEG studies performed on a female teenager admitted to intensive care unit with status epilepticus. Persistent sharp slow wave complexes were identified in the right posterior quadrant, (**C**) and ictal focus migrated to left frontotemporal regions (**D**) 2 weeks later.

Figure S4. Axial FLAIR sequence of MRI of the head.

Table S1. Total number of patients identified in literature and number of patients included in this review.

Table S2. Comparison of median and mean age at disease onset in different presenting clinical features (n = 265).

Appendix B

Reference	Number of patients in article	Number of patients fulfilled criteria	Patient case
(Allen *et al.*, 2014)	1	1	1
(Ashley *et al.*, 2008)	24	18	A,B,C,E,F,G,H,I,K,L,N,O,Q,R,S,V,W,X
(Bao *et al.*, 2008)	1	1	16
(Bijarnia-Mahay *et al.*, 2014)	1	1	1
(Blok *et al.*, 2009)	21	13	1,6,7,8,9,10,11,12,15,17,18,19,20
(Boes *et al.*, 2009)	1	1	1
(Brinjikji *et al.*, 2011)	2	2	1,2
(Cardenas and Amato, 2010)	1	1	1
(Cheldi *et al.*, 2013)	1	1	1
(Davidzon *et al.*, 2005)	4	4	1,2,3,4
(Mousson de Camaret *et al.*, 2011)	2	2	1,2
(de Vries *et al.*, 2007)	8	8	1,2,3,4,5,6,7,8
(de Vries *et al.*, 2008)	2	2	Patient-A, Patient-B
(Dhamija *et al.*, 2011)	1	1	1
(Engelsen *et al.*, 2008)	19	19	1,2,3,4,5,6,7,8,9,10,11,12,13,14,15,16,17,18,19
(Ferrari *et al.*, 2005)	9	9	1,2,3,4,5,6,7,8,9

(Ferreira *et al.*, 2011)	10	2	7, 8
(Hakonen *et al.*, 2005)	19	10	D1,D1S, D2,D2S,V,D6,D8,121,III-7,III-4
(Hansen *et al.*, 2012)	1	1	1
(Hasselmann *et al.*, 2010)	1	1	1
(Hinnell *et al.*, 2012)	1	1	1
(Horst *et al.*, 2014)	1	1	1
(Horvath *et al.*, 2006)	38	17	1,2,3,4,5,6,7,8,9,10,11,12,13,14,22,23,37,38
(Hunter *et al.*, 2011)	31	12	1,2,3,4,5,6,7,8,9,10,11,12
(Joshi *et al.*, 2009)	1	1	1
(Isohanni *et al.*, 2011)	7	7	1,2,3,4,5,6,7
(Khan *et al.*, 2012)	1	1	1
(Kollberg *et al.*, 2006)	7	6	1,2,3,4,5,6
(Komulainen *et al.*, 2010)	5	1	B1
(Kurt *et al.*, 2010)	4	4	1,2,3,4
(London *et al.*, 2017)	1	1	1
(Lupashko *et al.*, 2011)	1	1	1
(Lutz *et al.*, 2009)	2	2	1,2
(Mangalat *et al.*, 2012)	1	1	1

(Martikainen *et al.*, 2012)	1	1	1
(McCoy *et al.*, 2011)	4	4	1,2,3,4
(McFarland *et al.*, 2009)	1	1	1
(Mohamed *et al.*, 2011)	8	8	1,2,3,4,5,6,7,8
(Montassir *et al.*, 2015)	1	1	1
(Naess *et al.*, 2012)	1	1	1
(Naimi *et al.*, 2006)	8	3	PE, PL,PO
(Navarro-Sastre *et al.*, 2012)	2	2	P9,P10
(Naviaux and Nguyen, 2004)	3	3	K1-II-1, K2-II-1, K2-II-2
(Neeve *et al.*, 2012)	68	37	1,2,6,8,9,10,11,16, 17,18,19,20,21,23, 24,25,27,33,34,36, 37,38,39,42,44,45, 46,48,50,51,52,53, 54,55,58,60,64
(Nguyen *et al.*, 2005)	6	6	A4.II.2,A3.II.4,A3.II .3,A5.II.1,A6.II.1,A 6.II.3
(Nolte *et al.*, 2013)	2	2	1,2
(Roels *et al.*, 2009)	2	1	2
(Roshal *et al.*, 2011)	1	1	1
(Rouzier *et al.*, 2014)	8	5	8,9,10a,10b,12
(Sarzi *et al.*, 2007)	9	7	10,11,33,34,35,37, 38
(Scalais *et al.*, 2012)	1	1	1

(Schaller *et al.*, 2011)	1	1	1
(Simon *et al.*, 2014)	1	1	1
(Sofou *et al.*, 2012)	6	6	1,2,3,4,5,6
(Spinazzola *et al.*, 2006)	19	2	4,8
(Stewart *et al.*, 2009)	14	8	4,6,9,10,11,12,13, 14
(Stricker *et al.*, 2009)	2	2	II.2, II.3
(Taanman *et al.*, 2009)	6	3	P2,P5,P6
(Tang *et al.*, 2011)	73	57	II-1, II-2,II-3, II-6,II-7,II-9,II-10,II-11,II-13,II-18,II-19,II-20,II-21,II-22,II-24, II-26,II-29, II-31,II-32,II-33,II-34,II-35,II-37,II-38,II-40,II-42,II-45,II-46,II-47,II-48,II-49,II-50,II-51,II-52,II-56,II-57,II-58,II-59,II-61,II-63,II-65,II-66,II-69,II-71,II-72,II-74,II-75,II-76,II-77,II-78,II-79,II-80,II-83,II-84,II-85,II-90
(Tuladhar *et al.*, 2013)	1	1	1
(Tzoulis *et al.*, 2010)	32	2	WS-6A,WS-7B
(Tzoulis *et al.*, 2014)	15	5	AT-1A,WS-8A,AL-1A,Al-1B, AL-2A
(Uusimaa *et al.*, 2008)	3	3	1,2,3
(Uusimaa *et al.*, 2013)	8	8	1,2,3,4,5,6,7,8

(Van Goethem *et al.*, 2003)	2	1	II-1
(Van Goethem *et al.*, 2004)	10	4	B1.II.3,B1.II.4,F1.III.4,F1.III.7
(Visser *et al.*, 2011)	1	1	1
(Wiltshire *et al.*, 2008)	1	1	1
(Witters *et al.*, 2010)	1	1	1
(Wolf *et al.*, 2009)	5	5	1,2,3,4,5
(Wong *et al.*, 2008)	33	21	1,3,4,5,6,7,8,9,10,11,12,13,14,15,17,18,19,20,21,22,23
(Woodbridge *et al.*, 2013)	3	1	1
(Zabalza *et al.*, 2014)	2	1	I-1

Bibliography

Acin-Perez, R., Fernandez-Silva, P., Peleato, M.L., Perez-Martos, A. and Enriquez, J.A. (2008) 'Respiratory active mitochondrial supercomplexes', Mol Cell, 32(4), pp. 529-39.

Aguer, C., Gambarotta, D., Mailloux, R.J., Moffat, C., Dent, R., McPherson, R. and Harper, M.-E. (2011) 'Galactose Enhances Oxidative Metabolism and Reveals Mitochondrial Dysfunction in Human Primary Muscle Cells', PLOS ONE, 6(12), p. e28536.

Aldridge, D.R., Tranah, E.J. and Shawcross, D.L. (2015) 'Pathogenesis of Hepatic Encephalopathy: Role of Ammonia and Systemic Inflammation', Journal of Clinical and Experimental Hepatology, 5(Suppl 1), pp. S7-S20.

Alexander, C., Votruba, M., Pesch, U.E., Thiselton, D.L., Mayer, S., Moore, A., Rodriguez, M., Kellner, U., Leo-Kottler, B., Auburger, G., Bhattacharya, S.S. and Wissinger, B. (2000) 'OPA1, encoding a dynamin-related GTPase, is mutated in autosomal dominant optic atrophy linked to chromosome 3q28', Nat Genet, 26(2), pp. 211-5.

Allen, N.M., Winter, T., Shahwan, A. and King, M.D. (2014) 'Explosive onset non-epileptic jerks and profound hypotonia in an infant with Alpers-Huttenlocher syndrome', Seizure, 23(3), pp. 237-9.

Almalki, A., Alston, C.L., Parker, A., Simonic, I., Mehta, S.G., He, L., Reza, M., Oliveira, J.M., Lightowlers, R.N., McFarland, R., Taylor, R.W. and Chrzanowska-Lightowlers, Z.M. (2014) 'Mutation of the human mitochondrial phenylalanine-tRNA synthetase causes infantile-onset epilepsy and cytochrome c oxidase deficiency', Biochim Biophys Acta, 1842(1), pp. 56-64.

Alpers, B.J. (1931) 'Diffuse progressive degeneration of the gray matter of the cerebrum', Archives of Neurology & Psychiatry, 25(3), pp. 469-505..

Anagnostou, M.E., Ng, Y.S., Taylor, R.W. and McFarland, R. (2016) 'Epilepsy due to mutations in the mitochondrial polymerase gamma (POLG) gene: A clinical and molecular genetic review', Epilepsia, 57(10), pp. 1531-1545.

Anderson, S., Bankier, A.T., Barrell, B.G., de Bruijn, M.H., Coulson, A.R., Drouin, J., Eperon, I.C., Nierlich, D.P., Roe, B.A., Sanger, F., Schreier, P.H., Smith, A.J.,

Staden, R. and Young, I.G. (1981) 'Sequence and organization of the human mitochondrial genome', Nature, 290(5806), pp. 457-65.

Andrews, B., Carroll, J., Ding, S., Fearnley, I.M. and Walker, J.E. (2013) 'Assembly factors for the membrane arm of human complex I', Proc Natl Acad Sci U S A, 110(47), pp. 18934-9.

Andrews, R.M., Kubacka, I., Chinnery, P.F., Lightowlers, R.N., Turnbull, D.M. and Howell, N. (1999) 'Reanalysis and revision of the Cambridge reference sequence for human mitochondrial DNA', Nat Genet, 23(2), p. 147.

Arpa, J., Cruz-Martinez, A., Campos, Y., Gutierrez-Molina, M., Garcia-Rio, F., Perez-Conde, C., Martin, M.A., Rubio, J.C., Del Hoyo, P., Arpa-Fernandez, A. and Arenas, J. (2003) 'Prevalence and progression of mitochondrial diseases: a study of 50 patients', Muscle Nerve, 28(6), pp. 690-5.

Ashley, N., O'Rourke, A., Smith, C., Adams, S., Gowda, V., Zeviani, M., Brown, G.K., Fratter, C. and Poulton, J. (2008) 'Depletion of mitochondrial DNA in fibroblast cultures from patients with POLG mutations is a consequence of catalytic mutations', Hum Mol Genet, 17(16), pp. 2496-506.

Bacman, S.R., Williams, S.L. and Moraes, C.T. (2009) 'Intra- and inter-molecular recombination of mitochondrial DNA after in vivo induction of multiple double-strand breaks', Nucleic Acids Res, 37(13), pp. 4218-26.

Bao, X., Wu, Y., Wong, L.J., Zhang, Y., Xiong, H., Chou, P.C., Truong, C.K., Jiang, Y., Qin, J., Yuan, Y., Lin, Q. and Wu, X. (2008) 'Alpers syndrome with prominent white matter changes', Brain Dev, 30(4), pp. 295-300.

Bereiter-Hahn, J. (1990) 'Behavior of mitochondria in the living cell', Int Rev Cytol, 122, pp. 1-63.

Bertrand, E., Lewandowska, E., Szpak, G.M., Hoogenraad, T., Blaauwgers, H.G., Czlonkowska, A. and Dymecki, J. (2001) 'Neuropathological analysis of pathological forms of astroglia in Wilson's disease', Folia Neuropathol, 39(2), pp. 73-9.

Beth, A.Z.-K. and Emily, S. (2008) 'An Overview of the Ketogenic Diet for Pediatric Epilepsy', Nutrition in Clinical Practice, 23(6), pp. 589-596.

Betts-Henderson, J., Jaros, E., Krishnan, K.J., Perry, R.H., Reeve, A.K., Schaefer, A.M., Taylor, R.W. and Turnbull, D.M. (2009) 'Alpha-synuclein pathology and

Parkinsonism associated with POLG mutations and multiple mitochondrial DNA deletions', Neuropathol Appl Neurobiol, 35(1), pp. 120-4.

Bezawork-Geleta, A., Rohlena, J., Dong, L., Pacak, K. and Neuzil, J. (2017) 'Mitochondrial Complex II: At the Crossroads', Trends in Biochemical Sciences, 42(4), pp. 312-325.

Bijarnia-Mahay, S., Mohan, N., Goyal, D. and Verma, I.C. (2014) 'Mitochondrial DNA depletion syndrome causing liver failure', Indian Pediatr, 51(8), pp. 666-8.

Bindoff, L.A. and Engelsen, B.A. (2012) 'Mitochondrial diseases and epilepsy', Epilepsia, 53 Suppl 4, pp. 92-7.

Birky, J.C.W. (1994) 'Relaxed and Stringent Genomes: Why Cytoplasmic Genes Don't Obey Mendel's Laws', Journal of Heredity, 85(5), pp. 355-365.

Blackwood, W., Buxton, P.H., Cumings, J.N., Robertson, D.J. and Tucker, S.M. (1963) 'Diffuse cerebral degeneration in infancy (Alpers disease)', Arch Dis Child, 38, pp. 193-204.

Bleazard, W., McCaffery, J.M., King, E.J., Bale, S., Mozdy, A., Tieu, Q., Nunnari, J. and Shaw, J.M. (1999) 'The dynamin-related GTPase Dnm1 regulates mitochondrial fission in yeast', Nat Cell Biol, 1(5), pp. 298-304.

Blok, M.J., van den Bosch, B.J., Jongen, E., Hendrickx, A., de Die-Smulders, C.E., Hoogendijk, J.E., Brusse, E., de Visser, M., Poll-The, B.T., Bierau, J., de Coo, I.F. and Smeets, H.J. (2009) 'The unfolding clinical spectrum of POLG mutations', J Med Genet, 46(11), pp. 776-85.

Boes, M., Bauer, J., Urbach, H., Elger, C.E., Frank, S., Baron, M., Zsurka, G., Kunz, W.S. and Kornblum, C. (2009) 'Proof of progression over time: finally fulminant brain, muscle, and liver affection in Alpers syndrome associated with the A467T POLG mutation', Seizure, 18(3), pp. 232-4.

Bonnen, Penelope E., Yarham, John W., Besse, A., Wu, P., Faqeih, Eissa A., Al-Asmari, Ali M., Saleh, Mohammad A., Eyaid, W., Hadeel, A., He, L., Smith, F., Yau, S., Simcox, Eve M., Miwa, S., Donti, T., Abu-Amero, Khaled K., Wong, L.-J., Craigen, William J., Graham, Brett H., Scott, Kenneth L., McFarland, R. and Taylor, Robert W. (2013) 'Mutations in FBXL4 Cause Mitochondrial Encephalopathy and a Disorder of Mitochondrial DNA Maintenance', American Journal of Human Genetics, 93(3), pp. 471-481.

Bose, A. and Beal, M.F. (2016) 'Mitochondrial dysfunction in Parkinson's disease', J Neurochem, 139 Suppl 1, pp. 216-231.

Brinjikji, W., Swanson, J.W., Zabel, C., Dyck, P.J., Tracy, J.A. and Gavrilova, R.H. (2011) 'Stroke and Stroke-Like Symptoms in Patients with Mutations in the POLG Gene', JIMD Rep, 1, pp. 89-96.

Brown, W.M., George, M., Jr. and Wilson, A.C. (1979) 'Rapid evolution of animal mitochondrial DNA', Proc Natl Acad Sci U S A, 76(4), pp. 1967-71.

Burda, J.E. and Sofroniew, M.V. (2014) 'Reactive gliosis and the multicellular response to CNS damage and disease', Neuron, 81(2), pp. 229-248.

Calvo, S.E., Clauser, K.R. and Mootha, V.K. (2016) 'MitoCarta2.0: an updated inventory of mammalian mitochondrial proteins', Nucleic Acids Res, 44(D1), pp. D1251-7.

Cardenas, J.F. and Amato, R.S. (2010) 'Compound heterozygous polymerase gamma gene mutation in a patient with Alpers disease', Semin Pediatr Neurol, 17(1), pp. 62-4.

Carelli, V., Musumeci, O., Caporali, L., Zanna, C., La Morgia, C., Del Dotto, V., Porcelli, A.M., Rugolo, M., Valentino, M.L., Iommarini, L., Maresca, A., Barboni, P., Carbonelli, M., Trombetta, C., Valente, E.M., Patergnani, S., Giorgi, C., Pinton, P., Rizzo, G., Tonon, C., Lodi, R., Avoni, P., Liguori, R., Baruzzi, A., Toscano, A. and Zeviani, M. (2015) 'Syndromic parkinsonism and dementia associated with OPA1 missense mutations', Ann Neurol, 78(1), pp. 21-38.

Cecchini, G. (2003) 'Function and structure of complex II of the respiratory chain', Annu Rev Biochem, 72, pp. 77-109.

Chan, D.C. (2012) 'Fusion and fission: interlinked processes critical for mitochondrial health', Annu Rev Genet, 46, pp. 265-87.

Chan, S.S., Longley, M.J. and Copeland, W.C. (2005a) 'The common A467T mutation in the human mitochondrial DNA polymerase (POLG) compromises catalytic efficiency and interaction with the accessory subunit', J Biol Chem, 280(36), pp. 31341-6.

Chan, S.S., Longley, M.J. and Copeland, W.C. (2006) 'Modulation of the W748S mutation in DNA polymerase gamma by the E1143G polymorphismin mitochondrial disorders', Hum Mol Genet, 15(23), pp. 3473-83.

Chan, S.S., Longley, M.J., Naviaux, R.K. and Copeland, W.C. (2005b) 'Mono-allelic POLG expression resulting from nonsense-mediumted decay and alternative splicing in a patient with Alpers syndrome', DNA Repair (Amst), 4(12), pp. 1381-9.

Cheldi, A., Ronchi, D., Bordoni, A., Bordo, B., Lanfranconi, S., Bellotti, M.G., Corti, S., Lucchini, V., Sciacco, M., Moggio, M., Baron, P., Comi, G.P., Colombo, A. and Bersano, A. (2013) 'POLG mutations and stroke like episodes: a distinct clinical entity rather than an atypical MELAS syndrome', BMC Neurol, 13, p. 8.

Chen, H., Detmer, S.A., Ewald, A.J., Griffin, E.E., Fraser, S.E. and Chan, D.C. (2003a) 'Mitofusins Mfn1 and Mfn2 coordinately regulate mitochondrial fusion and are essential for embryonic development', J Cell Biol, 160(2), pp. 189-200.

Chen, Q., Vazquez, E.J., Moghaddas, S., Hoppel, C.L. and Lesnefsky, E.J. (2003b) 'Production of reactive oxygen species by mitochondria: central role of complex III', J Biol Chem, 278(38), pp. 36027-31.

Chinnery, P.F. (2014) Mitochondrial Disorders Overview.

Chinnery, P.F. and Hudson, G. (2013) 'Mitochondrial genetics', Br Med Bull, 106, pp. 135-59.

Chinnery, P.F. and Samuels, D.C. (1999) 'Relaxed replication of mtDNA: A model with implications for the expression of disease', Am J Hum Genet, 64(4), pp. 1158-65.

Cho, J.S., Kim, S.H., Kim, H.Y., Chung, T., Kim, D., Jang, S., Lee, S.B., Yoo, S.K., Shin, J., Kim, J.I., Kim, H., Hwang, H., Chae, J.H., Choi, J., Kim, K.J. and Lim, B.C. (2017) 'FARS2 mutation and epilepsy: Possible link with early-onset epileptic encephalopathy', Epilepsy Res, 129, pp. 118-124.

Cipolat, S., Martins de Brito, O., Dal Zilio, B. and Scorrano, L. (2004) 'OPA1 requires mitofusin 1 to promote mitochondrial fusion', Proc Natl Acad Sci U S A, 101(45), pp. 15927-32.

Clayton, D.A. (1982) 'Replication of animal mitochondrial DNA', Cell, 28(4), pp. 693-705.

Cohen, B.H. (2014) POLG-related Disorders

Copeland, B. (n.d.) Human DNA Polymerase gamma Mutation Database. Available at: https://www.ncbi.nlm.nih.gov/pubmed/23149385 (Accessed: 20 Aug 2017).

Coughlin, C.R., 2nd, Scharer, G.H., Friederich, M.W. and Yu, H.C. (2015) 'Mutations in the mitochondrial cysteinyl-tRNA synthase gene, CARS2, lead to a severe epileptic encephalopathy and complex movement disorder', 52(8), pp. 532-40.

Craig, K., Young, M.J., Blakely, E.L., Longley, M.J., Turnbull, D.M., Copeland, W.C. and Taylor, R.W. (2012) 'A p.R369G POLG2 mutation associated with adPEO and multiple mtDNA deletions causes decreased affinity between polymerase gamma subunits', Mitochondrion, 12(2), pp. 313-9.

Craven, L., Tuppen, H.A., Greggains, G.D., Harbottle, S.J., Murphy, J.L., Cree, L.M., Murdoch, A.P., Chinnery, P.F., Taylor, R.W., Lightowlers, R.N., Herbert, M. and Turnbull, D.M. (2010) 'Pronuclear transfer in human embryos to prevent transmission of mitochondrial DNA disease', Nature, 465(7294), pp. 82-5.

Darin, N., Oldfors, A., Moslemi, A.R., Holme, E. and Tulinius, M. (2001) 'The incidence of mitochondrial encephalomyopathies in childhood: clinical features and morphological, biochemical, and DNA abnormalities', Ann Neurol, 49(3), pp. 377-83.

Davidzon, G., Mancuso, M., Ferraris, S., Quinzii, C., Hirano, M., Peters, H.L., Kirby, D., Thorburn, D.R. and DiMauro, S. (2005) 'POLG mutations and Alpers syndrome', Ann Neurol, 57(6), pp. 921-3.

Davis, A.F., Ropp, P.A., Clayton, D.A. and Copeland, W.C. (1996) 'Mitochondrial DNA polymerase gamma is expressed and translated in the absence of mitochondrial DNA maintenance and replication', Nucleic Acids Res, 24(14), pp. 2753-9.

de Vries, M.C., Rodenburg, R.J., Morava, E., Lammens, M., van den Heuvel, L.P., Korenke, G.C. and Smeitink, J.A. (2008) 'Normal biochemical analysis of the oxidative phosphorylation (OXPHOS) system in a child with POLG mutations: a cautionary note', J Inherit Metab Dis, 31 Suppl 2, pp. S299-302.

de Vries, M.C., Rodenburg, R.J., Morava, E., van Kaauwen, E.P., ter Laak, H., Mullaart, R.A., Snoeck, I.N., van Hasselt, P.M., Harding, P., van den Heuvel, L.P. and Smeitink, J.A. (2007) 'Multiple oxidative phosphorylation deficiencies in severe childhood multi-system disorders due to polymerase gamma (POLG) mutations', Eur J Pediatr, 166(3), pp. 229-34.

Debray, F.G., Lambert, M., Chevalier, I., Robitaille, Y., Decarie, J.C., Shoubridge, E.A., Robinson, B.H. and Mitchell, G.A. (2007) 'Long-term outcome and clinical

spectrum of 73 pediatric patients with mitochondrial diseases', Pediatrics, 119(4), pp. 722-33.

Delarue, A., Paut, O., Guys, J.M., Montfort, M.F., Lethel, V., Roquelaure, B., Pellissier, J.F., Sarles, J. and Camboulives, J. (2000) 'Inappropriate liver transplantation in a child with Alpers-Huttenlocher syndrome misdiagnosed as valproate-induced acute liver failure', Pediatr Transplant, 4(1), pp. 67-71.

Deluca, H.F. and Engstrom, G.W. (1961) 'Calcium uptake by rat kidney mitochondria', Proc Natl Acad Sci U S A, 47, pp. 1744-50.

Dennerlein, S., Wang, C. and Rehling, P. (2017) 'Plasticity of Mitochondrial Translation', Trends in Cell Biology, 27(10), pp. 712-721.

Deschauer, M., Tennant, S., Rokicka, A., He, L., Kraya, T., Turnbull, D.M., Zierz, S. and Taylor, R.W. (2007) 'MELAS associated with mutations in the POLG gene', Neurology, 68(20), pp. 1741-2.

Dhamija, R., Moseley, B.D. and Wirrell, E.C. (2011) 'Clinical reasoning: a 10-month-old boy with myoclonic status epilepticus', Neurology, 76(5), pp. e22-5.

Dimmock, D., Tang, L.Y., Schmitt, E.S. and Wong, L.J. (2010) 'Quantitative evaluation of the mitochondrial DNA depletion syndrome', Clin Chem, 56(7), pp. 1119-27.

Distelmaier, F., Koopman, W.J., van den Heuvel, L.P., Rodenburg, R.J., Mayatepek, E., Willems, P.H. and Smeitink, J.A. (2009) 'Mitochondrial complex I deficiency: from organelle dysfunction to clinical disease', Brain, 132(Pt 4), pp. 833-42.

el-Khamisy, S.F. and Caldecott, K.W. (2007) 'DNA single-strand break repair and spinocerebellar ataxia with axonal neuropathy-1', Neuroscience, 145(4), pp. 1260-6.

Elson, J.L., Samuels, D.C., Turnbull, D.M. and Chinnery, P.F. (2001) 'Random intracellular drift explains the clonal expansion of mitochondrial DNA mutations with age', Am J Hum Genet, 68(3), pp. 802-6.

Engelsen, B.A., Tzoulis, C., Karlsen, B., Lillebo, A., Laegreid, L.M., Aasly, J., Zeviani, M. and Bindoff, L.A. (2008) 'POLG mutations cause a syndromic epilepsy with occipital lobe predilection', Brain, 131(Pt 3), pp. 818-28.

Enns, G.M., Kinsman, S.L., Perlman, S.L., Spicer, K.M., Abdenur, J.E., Cohen, B.H., Amagata, A., Barnes, A., Kheifets, V., Shrader, W.D., Thoolen, M., Blankenberg, F.

and Miller, G. (2012) 'Initial experience in the treatment of inherited mitochondrial disease with EPI-743', Mol Genet Metab, 105(1), pp. 91-102.

Euro, L., Farnum, G.A., Palin, E., Suomalainen, A. and Kaguni, L.S. (2011) 'Clustering of Alpers disease mutations and catalytic defects in biochemical variants reveal new features of molecular mechanism of the human mitochondrial replicase, Pol gamma', Nucleic Acids Res, 39(21), pp. 9072-84.

Farge, G., Pham, X.H., Holmlund, T., Khorostov, I. and Falkenberg, M. (2007) 'The accessory subunit B of DNA polymerase gamma is required for mitochondrial replisome function', Nucleic Acids Res, 35(3), pp. 902-911.

Farnum, G.A., Nurminen, A. and Kaguni, L.S. (2014) 'Mapping 136 Pathogenic Mutations into Functional Modules in Human DNA Polymerase γ Establishes Predictive Genotype-phenotype Correlations for the Complete Spectrum of POLG Syndromes', Biochimica et biophysica acta, 1837(7), pp. 1113-1121.

Feely, S.M., Laura, M., Siskind, C.E., Sottile, S., Davis, M., Gibbons, V.S., Reilly, M.M. and Shy, M.E. (2011) 'MFN2 mutations cause severe phenotypes in most patients with CMT2A', Neurology, 76(20), pp. 1690-6.

Ferrari, G., Lamantea, E., Donati, A., Filosto, M., Briem, E., Carrara, F., Parini, R., Simonati, A., Santer, R. and Zeviani, M. (2005) 'Infantile hepatocerebral syndromes associated with mutations in the mitochondrial DNA polymerase-gammaA', Brain, 128(Pt 4), pp. 723-31.

Ferreira, M., Evangelista, T., Almeida, L.S., Martins, J., Macario, M.C., Martins, E., Moleirinho, A., Azevedo, L., Vilarinho, L. and Santorelli, F.M. (2011) 'Relative frequency of known causes of multiple mtDNA deletions: two novel POLG mutations', Neuromuscul Disord, 21(7), pp. 483-8.

Flemming, K., Ulmer, S., Duisberg, B., Hahn, A. and Jansen, O. (2002) 'MR spectroscopic findings in a case of Alpers-Huttenlocher syndrome', AJNR Am J Neuroradiol, 23(8), pp. 1421-3.

Ford, F.R., Livingston, S. and Pryles, C. (1951) 'Familial degeneration of the cerebral gray matter in childhood with convulsions, myoclonus, spasticity, cerebellar ataxia, choreoathetosis, dementia, and death in status epilepticus; differentiation of infantile and juvenile types', J Pediatr, 39(1), pp. 33-43.

Formosa, L.E., Dibley, M.G., Stroud, D.A. and Ryan, M.T. (2017) 'Building a complex complex: Assembly of mitochondrial respiratory chain complex I', Seminars in Cell & Developmental Biology.

Fuste, J.M., Wanrooij, S., Jemt, E., Granycome, C.E., Cluett, T.J., Shi, Y., Atanassova, N., Holt, I.J., Gustafsson, C.M. and Falkenberg, M. (2010) 'Mitochondrial RNA polymerase is needed for activation of the origin of light-strand DNA replication', Mol Cell, 37(1), pp. 67-78.

Gai, X., Ghezzi, D., Johnson, Mark A., Biagosch, Caroline A., Shamseldin, Hanan E., Haack, Tobias B., Reyes, A., Tsukikawa, M., Sheldon, Claire A., Srinivasan, S., Gorza, M., Kremer, Laura S., Wieland, T., Strom, Tim M., Polyak, E., Place, E., Consugar, M., Ostrovsky, J., Vidoni, S., Robinson, Alan J., Wong, L.-J., Sondheimer, N., Salih, Mustafa A., Al-Jishi, E., Raab, Christopher P., Bean, C., Furlan, F., Parini, R., Lamperti, C., Mayr, Johannes A., Konstantopoulou, V., Huemer, M., Pierce, Eric A., Meitinger, T., Freisinger, P., Sperl, W., Prokisch, H., Alkuraya, Fowzan S., Falk, Marni J. and Zeviani, M. (2013) 'Mutations in FBXL4, Encoding a Mitochondrial Protein, Cause Early-Onset Mitochondrial Encephalomyopathy', American Journal of Human Genetics, 93(3), pp. 482-495.

Gautheron, D.C. (1984) 'Mitochondrial oxidative phosphorylation and respiratory chain: review', J Inherit Metab Dis, 7 Suppl 1, pp. 57-61.

Gordon, N. (2006) 'Alpers syndrome: progressive neuronal degeneration of children with liver disease', Dev Med Child Neurol, 48(12), pp. 1001-3.

Gorman, G.S., Schaefer, A.M., Ng, Y., Gomez, N., Blakely, E.L., Alston, C.L., Feeney, C., Horvath, R., Yu-Wai-Man, P., Chinnery, P.F., Taylor, R.W., Turnbull, D.M. and McFarland, R. (2015) 'Prevalence of nuclear and mitochondrial DNA mutations related to adult mitochondrial disease', Ann Neurol, 77(5), pp. 753-9.

Grady, J.P., Murphy, J.L., Blakely, E.L., Haller, R.G., Taylor, R.W., Turnbull, D.M. and Tuppen, H.A.L. (2014) 'Accurate Measurement of Mitochondrial DNA Deletion Level and Copy Number Differences in Human Skeletal Muscle', PLoS ONE, 9(12), p. e114462.

Graziewicz, M.A., Longley, M.J. and Copeland, W.C. (2006) 'DNA polymerase gamma in mitochondrial DNA replication and repair', Chem Rev, 106(2), pp. 383-405.

Greaves, L.C., Reeve, A.K., Taylor, R.W. and Turnbull, D.M. (2012) 'Mitochondrial DNA and disease', J Pathol, 226(2), pp. 274-86.

Grunewald, A., Lax, N.Z., Rocha, M.C., Reeve, A.K., Hepplewhite, P.D., Rygiel, K.A., Taylor, R.W. and Turnbull, D.M. (2014) 'Quantitative quadruple-label immunofluorescence of mitochondrial and cytoplasmic proteins in single neurons from human midbrain tissue', J Neurosci Methods, 232, pp. 143-9.

Guerrero-Castillo, S., Baertling, F., Kownatzki, D., Wessels, H.J., Arnold, S., Brandt, U. and Nijtmans, L. (2017) 'The Assembly Pathway of Mitochondrial Respiratory Chain Complex I', Cell Metabolism, 25(1), pp. 128-139.

Gustafsson, C.M., Falkenberg, M. and Larsson, N.G. (2016) 'Maintenance and Expression of Mammalian Mitochondrial DNA', Annu Rev Biochem, 85, pp. 133-60.

Haider, B., Duque, A., Hasenstaub, A.R. and McCormick, D.A. (2006) 'Neocortical network activity in vivo is generated through a dynamic balance of excitation and inhibition', J Neurosci, 26(17), pp. 4535-45.

Hakonen, A.H., Davidzon, G., Salemi, R., Bindoff, L.A., Van Goethem, G., Dimauro, S., Thorburn, D.R. and Suomalainen, A. (2007) 'Abundance of the POLG disease mutations in Europe, Australia, New Zealand, and the United States explained by single ancient European founders', Eur J Hum Genet, 15(7), pp. 779-83.

Hakonen, A.H., Goffart, S., Marjavaara, S., Paetau, A., Cooper, H., Mattila, K., Lampinen, M., Sajantila, A., Lonnqvist, T., Spelbrink, J.N. and Suomalainen, A. (2008) 'Infantile-onset spinocerebellar ataxia and mitochondrial recessive ataxia syndrome are associated with neuronal complex I defect and mtDNA depletion', Hum Mol Genet, 17(23), pp. 3822-35.

Hakonen, A.H., Heiskanen, S., Juvonen, V., Lappalainen, I., Luoma, P.T., Rantamaki, M., Goethem, G.V., Lofgren, A., Hackman, P., Paetau, A., Kaakkola, S., Majamaa, K., Varilo, T., Udd, B., Kaariainen, H., Bindoff, L.A. and Suomalainen, A. (2005) 'Mitochondrial DNA polymerase W748S mutation: a common cause of autosomal recessive ataxia with ancient European origin', Am J Hum Genet, 77(3), pp. 430-41.

Hance, N., Ekstrand, M.I. and Trifunovic, A. (2005) 'Mitochondrial DNA polymerase gamma is essential for mammalian embryogenesis', Hum Mol Genet, 14(13), pp. 1775-83.

Hansen, N., Zwarg, T., Wanke, I., Zierz, S., Kastrup, O. and Deschauer, M. (2012) 'MELAS/SANDO overlap syndrome associated with POLG mutations', Neurol Sci, 33(1), pp. 209-12.

Harding, B.N. (1990) 'Progressive neuronal degeneration of childhood with liver disease (Alpers-Huttenlocher syndrome): a personal review', J Child Neurol, 5(4), pp. 273-87.

Harding, B.N., Alsanjari, N., Smith, S.J., Wiles, C.M., Thrush, D., Miller, D.H., Scaravilli, F. and Harding, A.E. (1995) 'Progressive neuronal degeneration of childhood with liver disease (Alpers disease) presenting in young adults', Journal of Neurology, Neurosurgery, and Psychiatry, 58(3), pp. 320-325.

Harris, J.J., Jolivet, R. and Attwell, D. (2012) 'Synaptic energy use and supply', Neuron, 75(5), pp. 762-77.

Hasselmann, O., Blau, N., Ramaekers, V.T., Quadros, E.V., Sequeira, J.M. and Weissert, M. (2010) 'Cerebral folate deficiency and CNS inflammatory markers in Alpers disease', Mol Genet Metab, 99(1), pp. 58-61.

Hegde, M.L., Izumi, T. and Mitra, S. (2012) 'Oxidized Base Damage and Single-Strand Break Repair in Mammalian Genomes: Role of Disordered Regions and Posttranslational Modifications in Early Enzymes', Progress in molecular biology and translational science, 110, pp. 123-153.

Herrera, A.S., Del, C.A.E.M., Md Ashraf, G., Zamyatnin, A.A. and Aliev, G. (2015) 'Beyond mitochondria, what would be the energy source of the cell?', Cent Nerv Syst Agents Med Chem, 15(1), pp. 32-41.

Hikmat, O., Charalampos, T., Klingenberg, C., Rasmussen, M., Tallaksen, C.M.E., Brodtkorb, E., Fiskerstrand, T., McFarland, R., Rahman, S. and Bindoff, L.A. (2017a) 'The presence of anaemia negatively influences survival in patients with POLG disease', J Inherit Metab Dis.

Hikmat, O., Eichele, T., Tzoulis, C. and Bindoff, L.A. (2017b) 'Understanding the Epilepsy in POLG Related Disease', International Journal of Molecular Sciences, 18(9), p. 1845.

Hinnell, C., Haider, S., Delamont, S., Clough, C., Hadzic, N. and Samuel, M. (2012) 'Dystonia in mitochondrial spinocerebellar ataxia and epilepsy syndrome associated with novel recessive POLG mutations', Mov Disord, 27(1), pp. 162-3.

Holt, I.J., Harding, A.E. and Morgan-Hughes, J.A. (1988) 'Deletions of muscle mitochondrial DNA in patients with mitochondrial myopathies', Nature, 331(6158), pp. 717-9.

Holt, I.J., He, J., Mao, C.C., Boyd-Kirkup, J.D., Martinsson, P., Sembongi, H., Reyes, A. and Spelbrink, J.N. (2007) 'Mammalian mitochondrial nucleoids: organizing an independently minded genome', Mitochondrion, 7(5), pp. 311-21.

Holt, I.J., Lorimer, H.E. and Jacobs, H.T. (2000) 'Coupled leading- and lagging-strand synthesis of mammalian mitochondrial DNA', Cell, 100(5), pp. 515-24.

Horst, D.M., Ruess, L., Rusin, J.A. and Bartholomew, D.W. (2014) 'Cranial nerve and cervical root enhancement in an infant with polymerase gamma mutation mitochondrial disease', Pediatr Neurol, 51(5), pp. 734-6.

Horvath, R., Hudson, G., Ferrari, G., Futterer, N., Ahola, S., Lamantea, E., Prokisch, H., Lochmuller, H., McFarland, R., Ramesh, V., Klopstock, T., Freisinger, P., Salvi, F., Mayr, J.A., Santer, R., Tesarova, M., Zeman, J., Udd, B., Taylor, R.W., Turnbull, D., Hanna, M., Fialho, D., Suomalainen, A., Zeviani, M. and Chinnery, P.F. (2006) 'Phenotypic spectrum associated with mutations of the mitochondrial polymerase gamma gene', Brain, 129(Pt 7), pp. 1674-84.

Huang, P., Galloway, C.A. and Yoon, Y. (2011) 'Control of mitochondrial morphology through differential interactions of mitochondrial fusion and fission proteins', PLoS One, 6(5), p. e20655.

Huang, P., Zhang, L., Gao, Y., He, Z., Yao, D., Wu, Z., Cen, J., Chen, X., Liu, C., Hu, Y., Lai, D., Hu, Z., Chen, L., Zhang, Y., Cheng, X., Ma, X., Pan, G., Wang, X. and Hui, L. (2014) 'Direct reprogramming of human fibroblasts to functional and expandable hepatocytes', Cell Stem Cell, 14(3), pp. 370-84.

Hughes, S.D., Kanabus, M., Anderson, G., Hargreaves, I.P., Rutherford, T., O'Donnell, M., Cross, J.H., Rahman, S., Eaton, S. and Heales, S.J. (2014) 'The ketogenic diet component decanoic acid increases mitochondrial citrate synthase and complex I activity in neuronal cells', J Neurochem, 129(3), pp. 426-33.

Humble, M.M., Young, M.J., Foley, J.F., Pandiri, A.R., Travlos, G.S. and Copeland, W.C. (2013) 'Polg2 is essential for mammalian embryogenesis and is required for mtDNA maintenance', Hum Mol Genet, 22(5), pp. 1017-25.

Hunter, M.F., Peters, H., Salemi, R., Thorburn, D. and Mackay, M.T. (2011) 'Alpers syndrome with mutations in POLG: clinical and investigative features', Pediatr Neurol, 45(5), pp. 311-8.

Huttenlocher, P.R., Solitare, G.B. and Adams, G. (1976) 'Infantile diffuse cerebral degeneration with hepatic cirrhosis', Arch Neurol, 33(3), pp. 186-92.

Hyslop, L.A., Blakeley, P., Craven, L., Richardson, J., Fogarty, N.M., Fragouli, E., Lamb, M., Wamaitha, S.E., Prathalingam, N., Zhang, Q., O'Keefe, H., Takeda, Y., Arizzi, L., Alfarawati, S., Tuppen, H.A., Irving, L., Kalleas, D., Choudhary, M., Wells, D., Murdoch, A.P., Turnbull, D.M., Niakan, K.K. and Herbert, M. (2016) 'Towards clinical application of pronuclear transfer to prevent mitochondrial DNA disease', Nature, 534(7607), pp. 383-6.

Iborra, F.J., Kimura, H. and Cook, P.R. (2004) 'The functional organization of mitochondrial genomes in human cells', BMC Biol, 2, p. 9.

Isohanni, P., Hakonen, A.H., Euro, L., Paetau, I., Linnankivi, T., Liukkonen, E., Wallden, T., Luostarinen, L., Valanne, L., Paetau, A., Uusimaa, J., Lonnqvist, T., Suomalainen, A. and Pihko, H. (2011) 'POLG manifestations in childhood', Neurology, 76(9), pp. 811-5.

Iwata, S., Lee, J.W., Okada, K., Lee, J.K., Iwata, M., Rasmussen, B., Link, T.A., Ramaswamy, S. and Jap, B.K. (1998) 'Complete structure of the 11-subunit bovine mitochondrial cytochrome bc1 complex', Science, 281(5373), pp. 64-71.

Janssen, W., Quaegebeur, A., Van Goethem, G., Ann, L., Smets, K., Vandenberghe, R. and Van Paesschen, W. (2015) 'The spectrum of epilepsy caused by POLG mutations', Acta Neurol Belg.

Jin, S.M. and Youle, R.J. (2012) 'PINK1- and Parkin-mediumted mitophagy at a glance', J Cell Sci, 125(Pt 4), pp. 795-9.

Johnson, A.A. and Johnson, K.A. (2001) 'Exonuclease proofreading by human mitochondrial DNA polymerase', J Biol Chem, 276(41), pp. 38097-107.

Jonckheere, A.I., Smeitink, J.A.M. and Rodenburg, R.J.T. (2012) 'Mitochondrial ATP synthase: architecture, function and pathology', Journal of Inherited Metabolic Disease, 35(2), pp. 211-225.

Jornayvaz, F.R. and Shulman, G.I. (2010) 'Regulation of mitochondrial biogenesis', Essays Biochem, 47, pp. 69-84.

Joshi, C.N., Greenberg, C.R., Mhanni, A.A. and Salman, M.S. (2009) 'Ketogenic diet in Alpers-Huttenlocher syndrome', Pediatr Neurol, 40(4), pp. 314-6.

Kaguni, L.S. (2004) 'DNA polymerase gamma, the mitochondrial replicase', Annu Rev Biochem, 73, pp. 293-320.

Kann, O., Huchzermeyer, C., Kovacs, R., Wirtz, S. and Schuelke, M. (2011) 'Gamma oscillations in the hippocampus require high complex I gene expression and strong functional performance of mitochondria', Brain, 134(Pt 2), pp. 345-58.

Karbowski, M., Jeong, S.Y. and Youle, R.J. (2004) 'Endophilin B1 is required for the maintenance of mitochondrial morphology', J Cell Biol, 166(7), pp. 1027-39.

Kasiviswanathan, R., Longley, M.J., Chan, S.S. and Copeland, W.C. (2009) 'Disease mutations in the human mitochondrial DNA polymerase thumb subdomain impart severe defects in mitochondrial DNA replication', J Biol Chem, 284(29), pp. 19501-10.

Kayihan, N., Nennesmo, I., Ericzon, B.G. and Nemeth, A. (2000) 'Fatal deterioration of neurological disease after orthotopic liver transplantation for valproic acid-induced liver damage', Pediatr Transplant, 4(3), pp. 211-4.

Kelaini, S., Cochrane, A. and Margariti, A. (2014) 'Direct reprogramming of adult cells: avoiding the pluripotent state', Stem Cells Cloning, 7, pp. 19-29.

Khan, A., Trevenen, C., Wei, X.C., Sarnat, H.B., Payne, E. and Kirton, A. (2012) 'Alpers syndrome: the natural history of a case highlighting neuroimaging, neuropathology, and fat metabolism', J Child Neurol, 27(5), pp. 636-40.

Khurana, D.S., Salganicoff, L., Melvin, J.J., Hobdell, E.F., Valencia, I., Hardison, H.H., Marks, H.G., Grover, W.D. and Legido, A. (2008) 'Epilepsy and respiratory chain defects in children with mitochondrial encephalopathies', Neuropediatrics, 39(1), pp. 8-13.

Kirichok, Y., Krapivinsky, G. and Clapham, D.E. (2004) 'The mitochondrial calcium uniporter is a highly selective ion channel', Nature, 427(6972), pp. 360-4.

Kollberg, G., Moslemi, A.R., Darin, N., Nennesmo, I., Bjarnadottir, I., Uvebrant, P., Holme, E., Melberg, A., Tulinius, M. and Oldfors, A. (2006) 'POLG mutations associated with progressive encephalopathy in childhood', J Neuropathol Exp Neurol, 65(8), pp. 758-68.

Komulainen, T., Hinttala, R., Karppa, M., Pajunen, L., Finnila, S., Tuominen, H., Rantala, H., Hassinen, I., Majamaa, K. and Uusimaa, J. (2010) 'POLG p.R722H mutation associated with multiple mtDNA deletions and a neurological phenotype', BMC Neurol, 10, p. 29.

Koopman, W.J., Distelmaier, F., Smeitink, J.A. and Willems, P.H. (2013) 'OXPHOS mutations and neurodegeneration', Embo j, 32(1), pp. 9-29.

Koopman, W.J., Willems, P.H. and Smeitink, J.A. (2012) 'Monogenic mitochondrial disorders', N Engl J Med, 366(12), pp. 1132-41.

Korhonen, J.A., Pham, X.H., Pellegrini, M. and Falkenberg, M. (2004) 'Reconstitution of a minimal mtDNA replisome in vitro', The EMBO Journal, 23(12), pp. 2423-2429.

Kunz, W.S., Kudin, A.P., Vielhaber, S., Blumcke, I., Zuschratter, W., Schramm, J., Beck, H. and Elger, C.E. (2000) 'Mitochondrial complex I deficiency in the epileptic focus of patients with temporal lobe epilepsy', Ann Neurol, 48(5), pp. 766-73.

Kurt, B., Jaeken, J., Van Hove, J., Lagae, L., Lofgren, A., Everman, D.B., Jayakar, P., Naini, A., Wierenga, K.J., Van Goethem, G., Copeland, W.C. and DiMauro, S. (2010) 'A novel POLG gene mutation in 4 children with Alpers-like hepatocerebral syndromes', Arch Neurol, 67(2), pp. 239-44.

Larsson, N.G. and Clayton, D.A. (1995) 'Molecular genetic aspects of human mitochondrial disorders', Annu Rev Genet, 29, pp. 151-78.

Lax, N.Z., Gorman, G.S. and Turnbull, D.M. (2017) 'Review: Central nervous system involvement in mitochondrial disease', Neuropathol Appl Neurobiol, 43(2), pp. 102-118.

Lax, N.Z., Grady, J., Laude, A., Chan, F., Hepplewhite, P.D., Gorman, G., Whittaker, R.G., Ng, Y., Cunningham, M.O. and Turnbull, D.M. (2016) 'Extensive respiratory chain defects in inhibitory interneurones in patients with mitochondrial disease', Neuropathol Appl Neurobiol, 42(2), pp. 180-93.

Lax, N.Z., Hepplewhite, P.D., Reeve, A.K., Nesbitt, V., McFarland, R., Jaros, E., Taylor, R.W. and Turnbull, D.M. (2012a) 'Cerebellar ataxia in patients with mitochondrial DNA disease: a molecular clinicopathological study', J Neuropathol Exp Neurol, 71(2), pp. 148-61.

Lax, N.Z., Whittaker, R.G., Hepplewhite, P.D., Reeve, A.K., Blakely, E.L., Jaros, E., Ince, P.G., Taylor, R.W., Fawcett, P.R. and Turnbull, D.M. (2012b) 'Sensory

neuronopathy in patients harbouring recessive polymerase gamma mutations', Brain, 135(Pt 1), pp. 62-71.

Lazarow, A. and Cooperstein, S.J. (1953) 'Studies on the enzymatic basis for the Janus green B staining reaction', J Histochem Cytochem, 1(4), pp. 234-41.

Lecrenier, N., Van Der Bruggen, P. and Foury, F. (1997) 'Mitochondrial DNA polymerases from yeast to man: a new family of polymerases', Gene, 185(1), pp. 147-52.

Lee, H.R. and Johnson, K.A. (2006) 'Fidelity of the human mitochondrial DNA polymerase', J Biol Chem, 281(47), pp. 36236-40.

Lee, Y.S., Kennedy, W.D. and Yin, Y.W. (2009) 'Structural insight into processive human mitochondrial DNA synthesis and disease-related polymerase mutations', Cell, 139(2), pp. 312-24.

Lee, Y.S., Lee, S., Demeler, B., Molineux, I.J., Johnson, K.A. and Yin, Y.W. (2010) 'Each monomer of the dimeric accessory protein for human mitochondrial DNA polymerase has a distinct role in conferring processivity', J Biol Chem, 285(2), pp. 1490-9.

Lemasters, J.J. and Holmuhamedov, E. (2006) 'Voltage-dependent anion channel (VDAC) as mitochondrial governator--thinking outside the box', Biochim Biophys Acta, 1762(2), pp. 181-90.

Lestienne, P. (1987) 'Evidence for a direct role of the DNA polymerase gamma in the replication of the human mitochondrial DNA in vitro', Biochemical and Biophysical Research Communications, 146(3), pp. 1146-1153.

Li, S., Guo, J., Ying, Z., Chen, S., Yang, L., Chen, K., Long, Q., Qin, D., Pei, D. and Liu, X. (2015) 'Valproic acid-induced hepatotoxicity in Alpers syndrome is associated with mitochondrial permeability transition pore opening-dependent apoptotic sensitivity in an induced pluripotent stem cell model', Hepatology, 61(5), pp. 1730-9.

Lill, R., Hoffmann, B., Molik, S., Pierik, A.J., Rietzschel, N., Stehling, O., Uzarska, M.A., Webert, H., Wilbrecht, C. and Muhlenhoff, U. (2012) 'The role of mitochondria in cellular iron-sulfur protein biogenesis and iron metabolism', Biochim Biophys Acta, 1823(9), pp. 1491-508.

Lin-Hendel, E.G., McManus, M.J., Wallace, D.C., Anderson, S.A. and Golden, J.A. (2016) 'Differential mitochondrial requirements for radially and non-radially migrating

cortical neurons: Implications for mitochondrial disorders', Cell reports, 15(2), pp. 229-237.

Liu, Y. and Levine, B. (2015) 'Autosis and autophagic cell death: the dark side of autophagy', Cell Death Differ, 22(3), pp. 367-76.

Lodish, H., Berk, A. and Zipursky, S. (2000) 'Electron Transport and Oxidative Phosphorylation', in York, N. (ed.) Molecular Cell Biology. 4th edn.

Loeb, L.A., Wallace, D.C. and Martin, G.M. (2005) 'The mitochondrial theory of aging and its relationship to reactive oxygen species damage and somatic mtDNA mutations', Proc Natl Acad Sci U S A, 102(52), pp. 18769-70.

London, F., Hadhoum, N., Outteryck, O., Vermersch, P. and Zéphir, H. (2017) 'Late-onset of Alpers-Huttenlocher syndrome: an unusual cause of refractory epilepsy and liver failure', Acta Neurologica Belgica, 117(1), pp. 399-401.

Longley, M.J., Clark, S., Yu Wai Man, C., Hudson, G., Durham, S.E., Taylor, R.W., Nightingale, S., Turnbull, D.M., Copeland, W.C. and Chinnery, P.F. (2006) 'Mutant POLG2 disrupts DNA polymerase gamma subunits and causes progressive external ophthalmoplegia', Am J Hum Genet, 78(6), pp. 1026-34.

Longley, M.J., Prasad, R., Srivastava, D.K., Wilson, S.H. and Copeland, W.C. (1998) 'Identification of 5'-deoxyribose phosphate lyase activity in human DNA polymerase gamma and its role in mitochondrial base excision repair in vitro', Proc Natl Acad Sci U S A, 95(21), pp. 12244-8.

Lu, J., Liu, H., Huang, C.T., Chen, H., Du, Z., Liu, Y., Sherafat, M.A. and Zhang, S.C. (2013) 'Generation of integration-free and region-specific neural progenitors from primate fibroblasts', Cell Rep, 3(5), pp. 1580-91.

Lundgaard, I., Osório, M.J., Kress, B., Sanggaard, S. and Nedergaard, M. (2014) 'White matter astrocytes in health and disease', Neuroscience, 0, pp. 161-173.

Luoma, P.T., Luo, N., Loscher, W.N., Farr, C.L., Horvath, R., Wanschitz, J., Kiechl, S., Kaguni, L.S. and Suomalainen, A. (2005) 'Functional defects due to spacer-region mutations of human mitochondrial DNA polymerase in a family with an ataxia-myopathy syndrome', Hum Mol Genet, 14(14), pp. 1907-20.

Lupashko, S., Malik, S., Donahue, D., Hernandez, A. and Perry, M.S. (2011) 'Palliative functional hemispherectomy for treatment of refractory status epilepticus

associated with Alpers disease', Child's nervous system : ChNS : official journal of the International Society for Pediatric Neurosurgery, 27(8), pp. 1321-1323.

Lutz, R.E., Dimmock, D., Schmitt, E.S., Zhang, Q., Tang, L.Y., Reyes, C., Truemper, E., McComb, R.D., Hernandez, A., Basinger, A. and Wong, L.J. (2009) 'De novo mutations in POLG presenting with acute liver failure or encephalopathy', J Pediatr Gastroenterol Nutr, 49(1), pp. 126-9.

Macaskill, A.F., Rinholm, J.E., Twelvetrees, A.E., Arancibia-Carcamo, I.L., Muir, J., Fransson, A., Aspenstrom, P., Attwell, D. and Kittler, J.T. (2009) 'Miro1 is a calcium sensor for glutamate receptor-dependent localization of mitochondria at synapses', Neuron, 61(4), pp. 541-55.

Maglóczky, Z. and Freund, T.F. (2005) 'Impaired and repaired inhibitory circuits in the epileptic human hippocampus', Trends in Neurosciences, 28(6), pp. 334-340.

Mandavilli, B.S., Santos, J.H. and Van Houten, B. (2002) 'Mitochondrial DNA repair and aging', Mutat Res, 509(1-2), pp. 127-51.

Mandel, H., Szargel, R., Labay, V., Elpeleg, O., Saada, A., Shalata, A., Anbinder, Y., Berkowitz, D., Hartman, C., Barak, M., Eriksson, S. and Cohen, N. (2001) 'The deoxyguanosine kinase gene is mutated in individuals with depleted hepatocerebral mitochondrial DNA', Nat Genet, 29(3), pp. 337-41.

Mangalat, N., Tatevian, N., Bhattacharjee, M. and Rhoads, J.M. (2012) 'Alpers syndrome: an unusual etiology of failure to thrive', Ultrastruct Pathol, 36(4), pp. 219-21.

Maranzana, E., Barbero, G., Falasca, A.I., Lenaz, G. and Genova, M.L. (2013) 'Mitochondrial respiratory supercomplex association limits production of reactive oxygen species from complex I', Antioxid Redox Signal, 19(13), pp. 1469-80.

Margulis, L. (1975) 'Symbiotic theory of the origin of eukaryotic organelles; criteria for proof', Symp Soc Exp Biol, (29), pp. 21-38.

Martikainen, M.H., Paivarinta, M., Jaaskelainen, S. and Majamaa, K. (2012) 'Successful treatment of POLG-related mitochondrial epilepsy with antiepileptic drugs and low glycaemic index diet', Epileptic Disord, 14(4), pp. 438-41.

Martin, W. and Mentel, P. (2010) 'The origin of mitochondria', Natl Edu, 3(9), p. 58.

Martin, W. and Muller, M. (1998) 'The hydrogen hypothesis for the first eukaryote', Nature, 392(6671), pp. 37-41.

Marx, M., Haas, C.A. and Haussler, U. (2013) 'Differential vulnerability of interneurons in the epileptic hippocampus', Front Cell Neurosci, 7, p. 167.

Mason, P.A., Matheson, E.C., Hall, A.G. and Lightowlers, R.N. (2003) 'Mismatch repair activity in mammalian mitochondria', Nucleic Acids Research, 31(3), pp. 1052-1058.

Mattson, M.P. and Partin, J. (1999) 'Evidence for mitochondrial control of neuronal polarity', J Neurosci Res, 56(1), pp. 8-20.

Matturri, L. and Lavezzi, A.M. (2011) 'Unexplained stillbirth versus SIDS: Common congenital diseases of the autonomic nervous system—pathology and nosology', Early Human Development, 87(3), pp. 209-215.

McCoy, B., Owens, C., Howley, R., Ryan, S., King, M., Farrell, M.A. and Lynch, B.J. (2011) 'Partial status epilepticus - rapid genetic diagnosis of Alpers disease', Eur J Paediatr Neurol, 15(6), pp. 558-62.

McFarland, R., Hudson, G., Taylor, R.W., Green, S.H., Hodges, S., McKiernan, P.J., Chinnery, P.F. and Ramesh, V. (2009) 'Reversible valproate hepatotoxicity due to mutations in mitochondrial DNA polymerase gamma (POLG)', BMJ Case Rep, 2009.

McKinney, E.A. and Oliveira, M.T. (2013) 'Replicating animal mitochondrial DNA', Genet Mol Biol, 36(3), pp. 308-15.

Mehboob, R., Kabir, M., Ahmed, N. and Ahmad, F.J. (2017) 'Towards Better Understanding of the Pathogenesis of Neuronal Respiratory Network in Sudden Perinatal Death', Frontiers in Neurology, 8, p. 320.

Mertens, J., Marchetto, M.C., Bardy, C. and Gage, F.H. (2016) 'Evaluating cell reprogramming, differentiation and conversion technologies in neuroscience', Nat Rev Neurosci, 17(7), pp. 424-437.

Meyer, K., Ferraiuolo, L., Miranda, C.J., Likhite, S., McElroy, S., Renusch, S., Ditsworth, D., Lagier-Tourenne, C., Smith, R.A., Ravits, J., Burghes, A.H., Shaw, P.J., Cleveland, D.W., Kolb, S.J. and Kaspar, B.K. (2014) 'Direct conversion of patient fibroblasts demonstrates non-cell autonomous toxicity of astrocytes to motor neurons in familial and sporadic ALS', Proc Natl Acad Sci U S A, 111(2), pp. 829-32.

Mick, D.U., Fox, T.D. and Rehling, P. (2011) 'Inventory control: cytochrome c oxidase assembly regulates mitochondrial translation', Nat Rev Mol Cell Biol, 12(1), pp. 14-20.

Mimaki, M., Wang, X., McKenzie, M., Thorburn, D.R. and Ryan, M.T. (2012) 'Understanding mitochondrial complex I assembly in health and disease', Biochimica et Biophysica Acta (BBA) - Bioenergetics, 1817(6), pp. 851-862.

Mitchell, P. (1961) 'Coupling of phosphorylation to electron and hydrogen transfer by a chemi-osmotic type of mechanism', Nature, 191, pp. 144-8.

Mitchell, P. (1975) 'The protonmotive Q cycle: a general formulation', FEBS Lett, 59(2), pp. 137-9.

Mitochondrial Dysfunction in Neurodegenerative Disorders. (2016).

Mohamed, K., Fathallah, W. and Ahmed, E. (2011) 'Gender variability in presentation with Alpers syndrome: a report of eight patients from the UAE', J Inherit Metab Dis, 34(2), pp. 439-41.

Montassir, H., Maegaki, Y., Murayama, K., Yamazaki, T., Kohda, M., Ohtake, A., Iwasa, H., Yatsuka, Y., Okazaki, Y., Sugiura, C., Nagata, I., Toyoshima, M., Saito, Y., Itoh, M., Nishino, I. and Ohno, K. (2015) 'Myocerebrohepatopathy spectrum disorder due to POLG mutations: A clinicopathological report', Brain Dev, 37(7), pp. 719-24.

Morris, A.A.M., Singh-Kler, R., Perry, R.H., Griffiths, P.D., Burt, A.D., Chee Piau, W., Gardner-Medwin, D. and Tumbull, D.M. (1996) 'Respiratory Chain Dysfunction in Progressive Neuronal Degeneration of Childhood With Liver Disease', Journal of Child Neurology, 11(5), pp. 417-419.

Morse, W.I., 2nd (1949) 'Hereditary myoclonus epilepsy; two cases with pathological findings', Bull Johns Hopkins Hosp, 84(2), pp. 116-33.

Mousson de Camaret, B., Chassagne, M., Mayencon, M., Padet, S., Crehalet, H., Clerc-Renaud, P., Rouvet, I., Zabot, M.T., Rivier, F., Sarda, P., des Portes, V. and Bozon, D. (2011) 'POLG exon 22 skipping induced by different mechanisms in two unrelated cases of Alpers syndrome', Mitochondrion, 11(1), pp. 223-7.

Muller, F.L., Liu, Y. and Van Remmen, H. (2004) 'Complex III releases superoxide to both sides of the inner mitochondrial membrane', J Biol Chem, 279(47), pp. 49064-73.

Naess, K., Barbaro, M., Bruhn, H., Wibom, R., Nennesmo, I., von Dobeln, U., Larsson, N.G., Nemeth, A. and Lesko, N. (2012) 'Complete Deletion of a POLG Allele in a Patient with Alpers Syndrome', JIMD Rep, 4, pp. 67-73.

Naimi, M., Bannwarth, S., Procaccio, V., Pouget, J., Desnuelle, C., Pellissier, J.F., Rotig, A., Munnich, A., Calvas, P., Richelme, C., Jonveaux, P., Castelnovo, G., Simon, M., Clanet, M., Wallace, D. and Paquis-Flucklinger, V. (2006) 'Molecular analysis of ANT1, TWINKLE and POLG in patients with multiple deletions or depletion of mitochondrial DNA by a dHPLC-based assay', Eur J Hum Genet, 14(8), pp. 917-22.

Navarro-Sastre, A., Tort, F., Garcia-Villoria, J., Pons, M.R., Nascimento, A., Colomer, J., Campistol, J., Yoldi, M.E., Lopez-Gallardo, E., Montoya, J., Unceta, M., Martinez, M.J., Briones, P. and Ribes, A. (2012) 'Mitochondrial DNA depletion syndrome: new descriptions and the use of citrate synthase as a helpful tool to better characterise the patients', Mol Genet Metab, 107(3), pp. 409-15.

Naviaux, R.K. and Nguyen, K.V. (2004) 'POLG mutations associated with Alpers syndrome and mitochondrial DNA depletion', Ann Neurol, 55(5), pp. 706-12.

Naviaux, R.K., Nyhan, W.L., Barshop, B.A., Poulton, J., Markusic, D., Karpinski, N.C. and Haas, R.H. (1999) 'Mitochondrial DNA polymerase gamma deficiency and mtDNA depletion in a child with Alpers syndrome', Ann Neurol, 45(1), pp. 54-8.

Neeve, V.C., Samuels, D.C., Bindoff, L.A., van den Bosch, B., Van Goethem, G., Smeets, H., Lombes, A., Jardel, C., Hirano, M., Dimauro, S., De Vries, M., Smeitink, J., Smits, B.W., de Coo, I.F., Saft, C., Klopstock, T., Keiling, B.C., Czermin, B., Abicht, A., Lochmuller, H., Hudson, G., Gorman, G.G., Turnbull, D.M., Taylor, R.W., Holinski-Feder, E., Chinnery, P.F. and Horvath, R. (2012) 'What is influencing the phenotype of the common homozygous polymerase-gamma mutation p.Ala467Thr?', Brain, 135(Pt 12), pp. 3614-26.

Nguyen, K.V., Ostergaard, E., Ravn, S.H., Balslev, T., Danielsen, E.R., Vardag, A., McKiernan, P.J., Gray, G. and Naviaux, R.K. (2005) 'POLG mutations in Alpers syndrome', Neurology, 65(9), pp. 1493-5.

Nguyen, K.V., Sharief, F.S., Chan, S.S., Copeland, W.C. and Naviaux, R.K. (2006) 'Molecular diagnosis of Alpers syndrome', J Hepatol, 45(1), pp. 108-16.

Nijtmans, L.G.J., Ugalde, C., van den Heuvel, L.P. and Smeitink, J.A.M. (2004) 'Function and dysfunction of the oxidative phosphorylation system', in Mitochondrial Function and Biogenesis. Berlin, Heidelberg: Springer Berlin Heidelberg, pp. 149-176.

Nolte, K.W., Trepels-Kottek, S., Honnef, D., Weis, J., Bien, C.G., van Baalen, A., Ritter, K., Czermin, B., Rudnik-Schoneborn, S., Wagner, N. and Hausler, M. (2013) 'Early muscle and brain ultrastructural changes in polymerase gamma 1-related encephalomyopathy', Neuropathology, 33(1), pp. 59-67.

Nordli, D.R., Jr., Kuroda, M.M., Carroll, J., Koenigsberger, D.Y., Hirsch, L.J., Bruner, H.J., Seidel, W.T. and De Vivo, D.C. (2001) 'Experience with the ketogenic diet in infants', Pediatrics, 108(1), pp. 129-33.

Norenberg, M.D. (1987) 'The role of astrocytes in hepatic encephalopathy', Neurochem Pathol, 6(1-2), pp. 13-33.

Olson, M.W. and Kaguni, L.S. (1992) '3'-->5' exonuclease in Drosophila mitochondrial DNA polymerase. Substrate specificity and functional coordination of nucleotide polymerization and mispair hydrolysis', J Biol Chem, 267(32), pp. 23136-42.

Orrenius, S. (2004) 'Mitochondrial regulation of apoptotic cell death', Toxicol Lett, 149(1-3), pp. 19-23.

Palade, G.E. (1953) 'An electron microscope study of the mitochondrial structure', J Histochem Cytochem, 1(4), pp. 188-211.

Paleologou, E., Ismayilova, N. and Kinali, M. (2017) 'Use of the Ketogenic Diet to Treat Intractable Epilepsy in Mitochondrial Disorders', Journal of Clinical Medicine, 6(6), p. 56.

Palinsky, M., Kozinn, P.J. and Zahtz, H. (1954) 'Acute familial infantile heredodegenerative disorder of the central nervous system', J Pediatr, 45(5), pp. 538-45.

Pan, X., Liu, J., Nguyen, T., Liu, C., Sun, J., Teng, Y., Fergusson, M.M., Rovira, II, Allen, M., Springer, D.A., Aponte, A.M., Gucek, M., Balaban, R.S., Murphy, E. and Finkel, T. (2013) 'The physiological role of mitochondrial calcium revealed by mice lacking the mitochondrial calcium uniporter', Nat Cell Biol, 15(12), pp. 1464-72.

Pang, Z.P., Yang, N., Vierbuchen, T., Ostermeier, A., Fuentes, D.R., Yang, T.Q., Citri, A., Sebastiano, V., Marro, S., Sudhof, T.C. and Wernig, M. (2011) 'Induction of human neuronal cells by defined transcription factors', Nature, 476(7359), pp. 220-3.

Paradkar, P.N., Zumbrennen, K.B., Paw, B.H., Ward, D.M. and Kaplan, J. (2009) 'Regulation of mitochondrial iron import through differential turnover of mitoferrin 1 and mitoferrin 2', Mol Cell Biol, 29(4), pp. 1007-16.

Pearce, S.F., Rebelo-Guiomar, P., D'Souza, A.R., Powell, C.A., Van Haute, L. and Minczuk, M. (2017) 'Regulation of Mammalian Mitochondrial Gene Expression: Recent Advances', Trends in Biochemical Sciences, 42(8), pp. 625-639.

Pfeiffer, T., Schuster, S. and Bonhoeffer, S. (2001) 'Cooperation and competition in the evolution of ATP-producing pathways', Science, 292(5516), pp. 504-7.

Phatnani, H. and Maniatis, T. (2015) 'Astrocytes in neurodegenerative disease', Cold Spring Harb Perspect Biol, 7(6).

Pinz, K.G. and Bogenhagen, D.F. (1998) 'Efficient repair of abasic sites in DNA by mitochondrial enzymes', Mol Cell Biol, 18(3), pp. 1257-65.

Pradelli, L.A., Beneteau, M. and Ricci, J.E. (2010) 'Mitochondrial control of caspase-dependent and -independent cell death', Cell Mol Life Sci, 67(10), pp. 1589-97.

Puigserver, P., Wu, Z., Park, C.W., Graves, R., Wright, M. and Spiegelman, B.M. (1998) 'A cold-inducible coactivator of nuclear receptors linked to adaptive thermogenesis', Cell, 92(6), pp. 829-39.

Quintana, A., Kruse, S.E., Kapur, R.P., Sanz, E. and Palmiter, R.D. (2010) 'Complex I deficiency due to loss of Ndufs4 in the brain results in progressive encephalopathy resembling Leigh syndrome', Proc Natl Acad Sci U S A, 107(24), pp. 10996-1001.

Quintana, A., Zanella, S., Koch, H., Kruse, S.E., Lee, D., Ramirez, J.M. and Palmiter, R.D. (2012) 'Fatal breathing dysfunction in a mouse model of Leigh syndrome', J Clin Invest, 122(7), pp. 2359-68.

Rahman, S. (2012) 'Mitochondrial disease and epilepsy', Dev Med Child Neurol, 54(5), pp. 397-406.

Rajakulendran, S., Pitceathly, R.D.S., Taanman, J.-W., Costello, H., Sweeney, M.G., Woodward, C.E., Jaunmuktane, Z., Holton, J.L., Jacques, T.S., Harding, B.N., Fratter, C., Hanna, M.G. and Rahman, S. (2016) 'A Clinical, Neuropathological and Genetic Study of Homozygous A467T POLG-Related Mitochondrial Disease', PLoS ONE, 11(1), p. e0145500.

Reznick, R.M., Zong, H., Li, J., Morino, K., Moore, I.K., Yu, H.J., Liu, Z.X., Dong, J., Mustard, K.J., Hawley, S.A., Befroy, D., Pypaert, M., Hardie, D.G., Young, L.H. and Shulman, G.I. (2007) 'Aging-associated reductions in AMP-activated protein kinase activity and mitochondrial biogenesis', Cell Metab, 5(2), pp. 151-6.

Richter, C., Park, J.W. and Ames, B.N. (1988) 'Normal oxidative damage to mitochondrial and nuclear DNA is extensive', Proc Natl Acad Sci U S A, 85(17), pp. 6465-7.

Rizzuto, R., De Stefani, D., Raffaello, A. and Mammucari, C. (2012) 'Mitochondria as sensors and regulators of calcium signalling', Nat Rev Mol Cell Biol, 13(9), pp. 566-78.

Rodenburg, R.J.T. (2011) 'Biochemical diagnosis of mitochondrial disorders', Journal of Inherited Metabolic Disease, 34(2), pp. 283-292.

Roels, F., Verloo, P., Eyskens, F., Francois, B., Seneca, S., De Paepe, B., Martin, J.J., Meersschaut, V., Praet, M., Scalais, E., Espeel, M., Smet, J., Van Goethem, G. and Van Coster, R. (2009) 'Mitochondrial mosaics in the liver of 3 infants with mtDNA defects', BMC Clin Pathol, 9, p. 4.

Roestenberg, P., Manjeri, G.R., Valsecchi, F., Smeitink, J.A., Willems, P.H. and Koopman, W.J. (2012) 'Pharmacological targeting of mitochondrial complex I deficiency: the cellular level and beyond', Mitochondrion, 12(1), pp. 57-65.

Ropp, P.A. and Copeland, W.C. (1996) 'Cloning and characterization of the human mitochondrial DNA polymerase, DNA polymerase gamma', Genomics, 36(3), pp. 449-58.

Roshal, D., Glosser, D. and Zangaladze, A. (2011) 'Parieto-occipital lobe epilepsy caused by a POLG compound heterozygous A467T/W748S genotype', Epilepsy Behav, 21(2), pp. 206-10.

Rötig, A. and Poulton, J. (2009) 'Genetic causes of mitochondrial DNA depletion in humans', Biochimica et Biophysica Acta (BBA) - Molecular Basis of Disease, 1792(12), pp. 1103-1108.

Rouault, T.A. (2012) 'Biogenesis of iron-sulfur clusters in mammalian cells: new insights and relevance to human disease', Dis Model Mech, 5(2), pp. 155-64.

Rouzier, C., Chaussenot, A., Serre, V., Fragaki, K., Bannwarth, S., Ait-El-Mkadem, S., Attarian, S., Kaphan, E., Cano, A., Delmont, E., Sacconi, S., Mousson de Camaret, B., Rio, M., Lebre, A.S., Jardel, C., Deschamps, R., Richelme, C., Pouget, J., Chabrol, B. and Paquis-Flucklinger, V. (2014) 'Quantitative multiplex PCR of short fluorescent fragments for the detection of large intragenic POLG rearrangements in a large French cohort', Eur J Hum Genet, 22(4), pp. 542-50.

Rutter, J., Winge, D.R. and Schiffman, J.D. (2010) 'Succinate dehydrogenase - Assembly, regulation and role in human disease', Mitochondrion, 10(4), pp. 393-401.

Safdar, A., Bourgeois, J.M., Ogborn, D.I., Little, J.P., Hettinga, B.P., Akhtar, M., Thompson, J.E., Melov, S., Mocellin, N.J., Kujoth, G.C., Prolla, T.A. and Tarnopolsky, M.A. (2011) 'Endurance exercise rescues progeroid aging and induces systemic mitochondrial rejuvenation in mtDNA mutator mice', Proc Natl Acad Sci U S A, 108(10), pp. 4135-40.

Sandbank, U. and Lerman, P. (1972) 'Progressive cerebral poliodystrophy--Alpers disease. Disorganized giant neuronal mitochondria on electron microscopy', J Neurol Neurosurg Psychiatry, 35(6), pp. 749-55.

Saneto, R.P. and Naviaux, R.K. (2010) 'Polymerase gamma disease through the ages', Dev Disabil Res Rev, 16(2), pp. 163-74..

Saneto, R.P., Cohen, B.H., Copeland, W.C. and Naviaux, R.K. (2013) 'Alpers-Huttenlocher syndrome', Pediatr Neurol, 48(3), pp. 167-78.

Saraste, M. (1999) 'Oxidative phosphorylation at the fin de siecle', Science, 283(5407), pp. 1488-93.

Sarzi, E., Bourdon, A., Chretien, D., Zarhrate, M., Corcos, J., Slama, A., Cormier-Daire, V., de Lonlay, P., Munnich, A. and Rotig, A. (2007) 'Mitochondrial DNA depletion is a prevalent cause of multiple respiratory chain deficiency in childhood', J Pediatr, 150(5), pp. 531-4, 534.e1-6.

Scalais, E., Francois, B., Schlesser, P., Stevens, R., Nuttin, C., Martin, J.J., Van Coster, R., Seneca, S., Roels, F., Van Goethem, G., Lofgren, A. and De Meirleir, L. (2012) 'Polymerase gamma deficiency (POLG): clinical course in a child with a two stage evolution from infantile myocerebrohepatopathy spectrum to an Alpers syndrome and neuropathological findings of Leigh's encephalopathy', Eur J Paediatr Neurol, 16(5), pp. 542-8.

Schafer, E., Seelert, H., Reifschneider, N.H., Krause, F., Dencher, N.A. and Vonck, J. (2006) 'Architecture of active mammalian respiratory chain supercomplexes', J Biol Chem, 281(22), pp. 15370-5.

Schagger, H. and Pfeiffer, K. (2000) 'Supercomplexes in the respiratory chains of yeast and mammalian mitochondria', Embo j, 19(8), pp. 1777-83.

Schaller, A., Hahn, D., Jackson, C.B., Kern, I., Chardot, C., Belli, D.C., Gallati, S. and Nuoffer, J.M. (2011) 'Molecular and biochemical characterisation of a novel mutation in POLG associated with Alpers syndrome', BMC Neurol, 11, p. 4.

Schapira, A.H.V., Cooper, J.M., Dexter, D., Clark, J.B., Jenner, P. and Marsden, C.D. (1990) 'Mitochondrial Complex I Deficiency in Parkinson's Disease', Journal of Neurochemistry, 54(3), pp. 823-827.

Schwartz, M. and Vissing, J. (2002) 'Paternal inheritance of mitochondrial DNA', N Engl J Med, 347(8), pp. 576-80.

Sciacco, M., Bonilla, E., Schon, E.A., DiMauro, S. and Moraes, C.T. (1994) 'Distribution of wild-type and common deletion forms of mtDNA in normal and respiration-deficient muscle fibers from patients with mitochondrial myopathy', Hum Mol Genet, 3(1), pp. 13-9.

Sena, L.A. and Chandel, N.S. (2012) 'Physiological roles of mitochondrial reactive oxygen species', Mol Cell, 48(2), pp. 158-67.

Shadel, G.S. and Clayton, D.A. (1997) 'Mitochondrial DNA maintenance in vertebrates', Annu Rev Biochem, 66, pp. 409-35.

Sheng, Z.H. (2014) 'Mitochondrial trafficking and anchoring in neurons: New insight and implications', J Cell Biol, 204(7), pp. 1087-98.

Sheng, Z.H. and Cai, Q. (2012) 'Mitochondrial transport in neurons: impact on synaptic homeostasis and neurodegeneration', Nat Rev Neurosci, 13(2), pp. 77-93.

Simon, M., Chang, R.C., Bali, D.S., Wong, L.-J., Peng, Y. and Abdenur, J.E. (2014) 'Abnormalities in Glycogen Metabolism in a Patient with Alpers Syndrome Presenting with Hypoglycemia', JIMD Reports, 14, pp. 29-35.

Simonati, A., Filosto, M., Savio, C., Tomelleri, G., Tonin, P., Dalla Bernardina, B. and Rizzuto, N. (2003) 'Features of cell death in brain and liver, the target tissues of progressive neuronal degeneration of childhood with liver disease (Alpers-Huttenlocher disease)', Acta Neuropathol, 106(1), pp. 57-65.

Skladal, D., Halliday, J. and Thorburn, D.R. (2003) 'Minimum birth prevalence of mitochondrial respiratory chain disorders in children', Brain, 126(Pt 8), pp. 1905-12.

Smith, P.M., Fox, J.L. and Winge, D.R. (2012) 'Reprint of: Biogenesis of the cytochrome bc1 complex and role of assembly factors', Biochimica et Biophysica Acta (BBA) - Bioenergetics, 1817(6), pp. 872-882.

Sofou, K., Kollberg, G., Holmstrom, M., Davila, M., Darin, N., Gustafsson, C.M., Holme, E., Oldfors, A., Tulinius, M. and Asin-Cayuela, J. (2015) 'Whole exome sequencing reveals mutations in NARS2 and PARS2, encoding the mitochondrial asparaginyl-tRNA synthetase and prolyl-tRNA synthetase, in patients with Alpers syndrome', Mol Genet Genomic Med, 3(1), pp. 59-68.

Sofou, K., Moslemi, A.R., Kollberg, G., Bjarnadottir, I., Oldfors, A., Nennesmo, I., Holme, E., Tulinius, M. and Darin, N. (2012) 'Phenotypic and genotypic variability in Alpers syndrome', Eur J Paediatr Neurol, 16(4), pp. 379-89.

Sofroniew, M.V. and Vinters, H.V. (2010) 'Astrocytes: biology and pathology', Acta Neuropathologica, 119(1), pp. 7-35.

Song, S., Pursell, Z.F., Copeland, W.C., Longley, M.J., Kunkel, T.A. and Mathews, C.K. (2005) 'DNA precursor asymmetries in mammalian tissue mitochondria and possible contribution to mutagenesis through reduced replication fidelity', Proc Natl Acad Sci U S A, 102(14), pp. 4990-5.

Spendiff, S., Reza, M., Murphy, J.L., Gorman, G., Blakely, E.L., Taylor, R.W., Horvath, R., Campbell, G., Newman, J., Lochmuller, H. and Turnbull, D.M. (2013) 'Mitochondrial DNA deletions in muscle satellite cells: implications for therapies', Hum Mol Genet, 22(23), pp. 4739-47.

Spinazzola, A., Viscomi, C., Fernandez-Vizarra, E., Carrara, F., D'Adamo, P., Calvo, S., Marsano, R.M., Donnini, C., Weiher, H., Strisciuglio, P., Parini, R., Sarzi, E., Chan, A., DiMauro, S., Rotig, A., Gasparini, P., Ferrero, I., Mootha, V.K., Tiranti, V. and Zeviani, M. (2006) 'MPV17 encodes an inner mitochondrial membrane protein and is mutated in infantile hepatic mitochondrial DNA depletion', Nat Genet, 38(5), pp. 570-5.

Stewart, J.D., Schoeler, S., Sitarz, K.S., Horvath, R., Hallmann, K., Pyle, A., Yu-Wai-Man, P., Taylor, R.W., Samuels, D.C., Kunz, W.S. and Chinnery, P.F. (2011) 'POLG mutations cause decreased mitochondrial DNA repopulation rates following induced depletion in human fibroblasts', Biochimica et Biophysica Acta (BBA) - Molecular Basis of Disease, 1812(3), pp. 321-325.

Stewart, J.D., Tennant, S., Powell, H., Pyle, A., Blakely, E.L., He, L., Hudson, G., Roberts, M., du Plessis, D., Gow, D., Mewasingh, L.D., Hanna, M.G., Omer, S., Morris, A.A., Roxburgh, R., Livingston, J.H., McFarland, R., Turnbull, D.M., Chinnery,

P.F. and Taylor, R.W. (2009) 'Novel POLG mutations associated with neuromuscular and liver phenotypes in adults and children', J Med Genet, 46(3), pp. 209-14.

Stierum, R.H., Dianov, G.L. and Bohr, V.A. (1999) 'Single-nucleotide patch base excision repair of uracil in DNA by mitochondrial protein extracts', Nucleic Acids Res, 27(18), pp. 3712-9.

Stricker, S., Pruss, H., Horvath, R., Baruffini, E., Lodi, T., Siebert, E., Endres, M., Zschenderlein, R. and Meisel, A. (2009) 'A variable neurodegenerative phenotype with polymerase gamma mutation', J Neurol Neurosurg Psychiatry, 80(10), pp. 1181-2.

Stumpf, J.D., Saneto, R.P. and Copeland, W.C. (2013) 'Clinical and molecular features of POLG-related mitochondrial disease', Cold Spring Harb Perspect Biol, 5(4), p. a011395.

Sykora, P., Kanno, S., Akbari, M., Kulikowicz, T., Baptiste, B.A., Leandro, G.S., Lu, H., Tian, J., May, A., Becker, K.A., Croteau, D.L., Wilson, D.M., 3rd, Sobol, R.W., Yasui, A. and Bohr, V.A. (2017) 'DNA polymerase beta participates in mitochondrial DNA repair', Mol Cell Biol.

Szczepanowska, K. and Foury, F. (2010) 'A cluster of pathogenic mutations in the 3'-5' exonuclease domain of DNA polymerase gamma defines a novel module coupling DNA synthesis and degradation', Hum Mol Genet, 19(18), pp. 3516-29.

Taanman, J.W., Rahman, S., Pagnamenta, A.T., Morris, A.A., Bitner-Glindzicz, M., Wolf, N.I., Leonard, J.V., Clayton, P.T. and Schapira, A.H. (2009) 'Analysis of mutant DNA polymerase gamma in patients with mitochondrial DNA depletion', Hum Mutat, 30(2), pp. 248-54.

Takahashi, K. and Yamanaka, S. (2013) 'Induced pluripotent stem cells in medicine and biology', Development, 140(12), pp. 2457-61.

Takahashi, K., Tanabe, K., Ohnuki, M., Narita, M., Ichisaka, T., Tomoda, K. and Yamanaka, S. (2007) 'Induction of pluripotent stem cells from adult human fibroblasts by defined factors', Cell, 131(5), pp. 861-72.

Tang, S., Wang, J., Lee, N.C., Milone, M., Halberg, M.C., Schmitt, E.S., Craigen, W.J., Zhang, W. and Wong, L.J. (2011) 'Mitochondrial DNA polymerase gamma mutations: an ever expanding molecular and clinical spectrum', J Med Genet, 48(10), pp. 669-81.

Taylor, R.W. and Turnbull, D.M. (2005) 'Mitochondrial DNA mutations in human disease', Nat Rev Genet, 6(5), pp. 389-402.

Tong, W.H., Jameson, G.N., Huynh, B.H. and Rouault, T.A. (2003) 'Subcellular compartmentalization of human Nfu, an iron-sulfur cluster scaffold protein, and its ability to assemble a [4Fe-4S] cluster', Proc Natl Acad Sci U S A, 100(17), pp. 9762-7.

Torraco, A., Peralta, S., Iommarini, L. and Diaz, F. (2015) 'MITOCHONDRIAL DISEASES PART I: MOUSE MODELS OF OXPHOS DEFICIENCIES CAUSED BY DEFECTS ON RESPIRATORY COMPLEX SUBUNITS OR ASSEMBLY FACTORS', Mitochondrion, 0, pp. 76-91.

Trifunovic, A., Hansson, A., Wredenberg, A., Rovio, A.T., Dufour, E., Khvorostov, I., Spelbrink, J.N., Wibom, R., Jacobs, H.T. and Larsson, N.G. (2005) 'Somatic mtDNA mutations cause aging phenotypes without affecting reactive oxygen species production', Proc Natl Acad Sci U S A, 102(50), pp. 17993-8.

Trifunovic, A., Wredenberg, A., Falkenberg, M., Spelbrink, J.N., Rovio, A.T., Bruder, C.E., Bohlooly-Y, M., Gidlof, S., Oldfors, A., Wibom, R., Tornell, J., Jacobs, H.T. and Larsson, N.-G. (2004) 'Premature ageing in mice expressing defective mitochondrial DNA polymerase', Nature, 429(6990), pp. 417-423.

Trifunovic, A., Wredenberg, A., Falkenberg, M., Spelbrink, J.N., Rovio, A.T., Bruder, C.E., Bohlooly-Y, M., Gidlof, S., Oldfors, A., Wibom, R., Tornell, J., Jacobs, H.T. and Larsson, N.-G. (2004) 'Premature ageing in mice expressing defective mitochondrial DNA polymerase', Nature, 429(6990), pp. 417-423.

Trotti, D., Danbolt, N.C. and Volterra, A. (1998) 'Glutamate transporters are oxidant-vulnerable: a molecular link between oxidative and excitotoxic neurodegeneration?', Trends Pharmacol Sci, 19(8), pp. 328-34.

Tsukihara, T., Aoyama, H., Yamashita, E., Tomizaki, T., Yamaguchi, H., Shinzawa-Itoh, K., Nakashima, R., Yaono, R. and Yoshikawa, S. (1996) 'The whole structure of the 13-subunit oxidized cytochrome c oxidase at 2.8 A', Science, 272(5265), pp. 1136-44.

Tuladhar, A.M., Meijer, F.J. and van de Warrenburg, B.P. (2013) 'POLG mutation presenting with late-onset jerky torticollis', J Neurol, 260(3), pp. 903-5.

Tuppen, H.A., Blakely, E.L., Turnbull, D.M. and Taylor, R.W. (2010) 'Mitochondrial DNA mutations and human disease', Biochim Biophys Acta, 1797(2), pp. 113-28.

Tzoulis, C., Engelsen, B.A., Telstad, W., Aasly, J., Zeviani, M., Winterthun, S., Ferrari, G., Aarseth, J.H. and Bindoff, L.A. (2006) 'The spectrum of clinical disease caused by the A467T and W748S POLG mutations: a study of 26 cases', Brain, 129(Pt 7), pp. 1685-92.

Tzoulis, C., Neckelmann, G., Mork, S.J., Engelsen, B.E., Viscomi, C., Moen, G., Ersland, L., Zeviani, M. and Bindoff, L.A. (2010) 'Localized cerebral energy failure in DNA polymerase gamma-associated encephalopathy syndromes', Brain, 133(Pt 5), pp. 1428-37.

Tzoulis, C., Tran, G.T., Coxhead, J., Bertelsen, B., Lilleng, P.K., Balafkan, N., Payne, B., Miletic, H., Chinnery, P.F. and Bindoff, L.A. (2014) 'Molecular Pathogenesis of Polymerase Gamma–Related Neurodegeneration', Annals of Neurology, 76(1), pp. 66-81.

Ugalde, C., Vogel, R., Huijbens, R., Van Den Heuvel, B., Smeitink, J. and Nijtmans, L. (2004) 'Human mitochondrial complex I assembles through the combination of evolutionary conserved modules: a framework to interpret complex I deficiencies', Hum Mol Genet, 13(20), pp. 2461-72.

Uusimaa, J., Gowda, V., McShane, A., Smith, C., Evans, J., Shrier, A., Narasimhan, M., O'Rourke, A., Rajabally, Y., Hedderly, T., Cowan, F., Fratter, C. and Poulton, J. (2013) 'Prospective study of POLG mutations presenting in children with intractable epilepsy: prevalence and clinical features', Epilepsia, 54(6), pp. 1002-11.

Uusimaa, J., Hinttala, R., Rantala, H., Paivarinta, M., Herva, R., Roytta, M., Soini, H., Moilanen, J.S., Remes, A.M., Hassinen, I.E. and Majamaa, K. (2008) 'Homozygous W748S mutation in the POLG gene in patients with juvenile-onset Alpers syndrome and status epilepticus', Epilepsia, 49(6), pp. 1038-45.

van den Heuvel, L.P., Smeitink, J.A. and Rodenburg, R.J. (2004) 'Biochemical examination of fibroblasts in the diagnosis and research of oxidative phosphorylation (OXPHOS) defects', Mitochondrion, 4(5-6), pp. 395-401.

Van Goethem, G., Dermaut, B., Lofgren, A., Martin, J.J. and Van Broeckhoven, C. (2001) 'Mutation of POLG is associated with progressive external ophthalmoplegia characterized by mtDNA deletions', Nat Genet, 28(3), pp. 211-2.

Van Goethem, G., Luoma, P., Rantamaki, M., Al Memar, A., Kaakkola, S., Hackman, P., Krahe, R., Lofgren, A., Martin, J.J., De Jonghe, P., Suomalainen, A., Udd, B. and Van Broeckhoven, C. (2004) 'POLG mutations in neurodegenerative disorders with ataxia but no muscle involvement', Neurology, 63(7), pp. 1251-7.

Van Goethem, G., Schwartz, M., Lofgren, A., Dermaut, B., Van Broeckhoven, C. and Vissing, J. (2003) 'Novel POLG mutations in progressive external ophthalmoplegia mimicking mitochondrial neurogastrointestinal encephalomyopathy', Eur J Hum Genet, 11(7), pp. 547-9.

Vasileiou, P.V.S., Mourouzis, I. and Pantos, C. (2017) 'Principal Aspects Regarding the Maintenance of Mammalian Mitochondrial Genome Integrity', International Journal of Molecular Sciences, 18(8), p. 1821.

Vierbuchen, T., Ostermeier, A., Pang, Z.P., Kokubu, Y., Sudhof, T.C. and Wernig, M. (2010) 'Direct conversion of fibroblasts to functional neurons by defined factors', Nature, 463(7284), pp. 1035-41.

Visser, N.A., Braun, K.P., Leijten, F.S., van Nieuwenhuizen, O., Wokke, J.H. and van den Bergh, W.M. (2011) 'Magnesium treatment for patients with refractory status epilepticus due to POLG-mutations', J Neurol, 258(2), pp. 218-22.

Voets, A.M., Lindsey, P.J., Vanherle, S.J., Timmer, E.D., Esseling, J.J., Koopman, W.J.H., Willems, P.H.G.M., Schoonderwoerd, G.C., De Groote, D., Poll-The, B.T., de Coo, I.F.M. and Smeets, H.J.M. (2012) 'Patient-derived fibroblasts indicate oxidative stress status and may justify antioxidant therapy in OXPHOS disorders', Biochimica et Biophysica Acta (BBA) - Bioenergetics, 1817(11), pp. 1971-1978.

Walker, R.L., Anziano, P. and Meltzer, P.S. (1997) 'A PAC containing the human mitochondrial DNA polymerase gamma gene (POLG) maps to chromosome 15q25', Genomics, 40(2), pp. 376-8.

Wang, J. and Pantopoulos, K. (2011) 'Regulation of cellular iron metabolism', Biochem J, 434(3), pp. 365-81.

Whittaker, R.G., Devine, H.E., Gorman, G.S., Schaefer, A.M., Horvath, R., Ng, Y., Nesbitt, V., Lax, N.Z., McFarland, R., Cunningham, M.O., Taylor, R.W. and Turnbull, D.M. (2015) 'Epilepsy in adults with mitochondrial disease: A cohort study', Ann Neurol, 78(6), pp. 949-57.

Whittaker, R.G., Turnbull, D.M., Whittington, M.A. and Cunningham, M.O. (2011) 'Impaired mitochondrial function abolishes gamma oscillations in the hippocampus through an effect on fast-spiking interneurons', Brain, 134(7), pp. e180-e180.

Wiltshire, E., Davidzon, G., DiMauro, S., Akman, H.O., Sadleir, L., Haas, L., Zuccollo, J., McEwen, A. and Thorburn, D.R. (2008) 'Juvenile Alpers disease', Arch Neurol, 65(1), pp. 121-4.

Winterthun, S., Ferrari, G., He, L., Taylor, R.W., Zeviani, M., Turnbull, D.M., Engelsen, B.A., Moen, G. and Bindoff, L.A. (2005) 'Autosomal recessive mitochondrial ataxic syndrome due to mitochondrial polymerase gamma mutations', Neurology, 64(7), pp. 1204-8.

Witters, P., Pirenne, J., Aerts, R., Monbaliu, D., Nevens, F., Verslype, C., Laleman, W., Roskams, T., Desmet, L., Vlasselaers, D., Marien, P., Hoffman, I., Lombaerts, R., Goethals, E., Jaeken, J., Meersseman, W. and Cassiman, D. (2010) 'Alpers syndrome presenting with anatomopathological features of fulminant autoimmune hepatitis', J Inherit Metab Dis, 33(4), p. 451.

Wolf, N.I., Rahman, S., Schmitt, B., Taanman, J.W., Duncan, A.J., Harting, I., Wohlrab, G., Ebinger, F., Rating, D. and Bast, T. (2009) 'Status epilepticus in children with Alpers disease caused by POLG mutations: EEG and MRI features', Epilepsia, 50(6), pp. 1596-607.

Wong, L.J., Naviaux, R.K., Brunetti-Pierri, N., Zhang, Q., Schmitt, E.S., Truong, C., Milone, M., Cohen, B.H., Wical, B., Ganesh, J., Basinger, A.A., Burton, B.K., Swoboda, K., Gilbert, D.L., Vanderver, A., Saneto, R.P., Maranda, B., Arnold, G., Abdenur, J.E., Waters, P.J. and Copeland, W.C. (2008) 'Molecular and clinical genetics of mitochondrial diseases due to POLG mutations', Hum Mutat, 29(9), pp. E150-72.

Woodbridge, P., Liang, C., Davis, R.L., Vandebona, H. and Sue, C.M. (2013) 'POLG mutations in Australian patients with mitochondrial disease', Intern Med J, 43(2), pp. 150-6.

Xue, Y., Ouyang, K., Huang, J., Zhou, Y., Ouyang, H., Li, H., Wang, G., Wu, Q., Wei, C., Bi, Y., Jiang, L., Cai, Z., Sun, H., Zhang, K., Zhang, Y., Chen, J. and Fu, X.-D. (2013) 'Direct Conversion of Fibroblasts to Neurons by Reprogramming PTB-Regulated microRNA Circuits', Cell, 152(1-2), pp. 82-96.

Yakubovskaya, E., Chen, Z., Carrodeguas, J.A., Kisker, C. and Bogenhagen, D.F. (2006) 'Functional human mitochondrial DNA polymerase gamma forms a heterotrimer', J Biol Chem, 281(1), pp. 374-82.

Yang, M.Y., Bowmaker, M., Reyes, A., Vergani, L., Angeli, P., Gringeri, E., Jacobs, H.T. and Holt, I.J. (2002) 'Biased incorporation of ribonucleotides on the mitochondrial L-strand accounts for apparent strand-asymmetric DNA replication', Cell, 111(4), pp. 495-505.

Yasui, A., Yajima, H., Kobayashi, T., Eker, A.P. and Oikawa, A. (1992) 'Mitochondrial DNA repair by photolyase', Mutat Res, 273(2), pp. 231-6.

Yasukawa, T., Reyes, A., Cluett, T.J., Yang, M.Y., Bowmaker, M., Jacobs, H.T. and Holt, I.J. (2006) 'Replication of vertebrate mitochondrial DNA entails transient ribonucleotide incorporation throughout the lagging strand', Embo j, 25(22), pp. 5358-71.

Yoneda, M., Miyatake, T. and Attardi, G. (1995) 'Heteroplasmic mitochondrial tRNA(Lys) mutation and its complementation in MERRF patient-derived mitochondrial transformants', Muscle Nerve Suppl, 3, pp. S95-101.

Yoshida, M., Muneyuki, E. and Hisabori, T. (2001) 'ATP synthase--a marvellous rotary engine of the cell', Nat Rev Mol Cell Biol, 2(9), pp. 669-77.

Young, M.J., Longley, M.J., Li, F.Y., Kasiviswanathan, R., Wong, L.J. and Copeland, W.C. (2011) 'Biochemical analysis of human POLG2 variants associated with mitochondrial disease', Hum Mol Genet, 20(15), pp. 3052-66.

Yu, J., Vodyanik, M.A., Smuga-Otto, K., Antosiewicz-Bourget, J., Frane, J.L., Tian, S., Nie, J., Jonsdottir, G.A., Ruotti, V., Stewart, R., Slukvin, I.I. and Thomson, J.A. (2007) 'Induced Pluripotent Stem Cell Lines Derived from Human Somatic Cells', Science, 318(5858), p. 1917.

Zabalza, R., Nurminen, A., Kaguni, L.S., Garesse, R., Gallardo, M.E. and Bornstein, B. (2014) 'Co-occurrence of four nucleotide changes associated with an adult mitochondrial ataxia phenotype', BMC Res Notes, 7, p. 883.

Zhu, X., Perry, G., Smith, M.A. and Wang, X. (2013) 'Abnormal mitochondrial dynamics in the pathogenesis of Alzheimer's disease', J Alzheimers Dis, 33 Suppl 1, pp. S253-62.

Zsurka, G. and Kunz, W.S. (2015) 'Mitochondrial dysfunction and seizures: the neuronal energy crisis', Lancet Neurol, 14(9), pp. 956-66.

Zuchner, S., Mersiyanova, I.V., Muglia, M., Bissar-Tadmouri, N., Rochelle, J., Dadali, E.L., Zappia, M., Nelis, E., Patitucci, A., Senderek, J., Parman, Y., Evgrafov, O., Jonghe, P.D., Takahashi, Y., Tsuji, S., Pericak-Vance, M.A., Quattrone, A., Battaloglu, E., Polyakov, A.V., Timmerman, V., Schroder, J.M. and Vance, J.M. (2004) 'Mutations in the mitochondrial GTPase mitofusin 2 cause Charcot-Marie-Tooth neuropathy type 2A', Nat Genet, 36(5), pp. 449-51.

Zurita, F., Galera, T., Gonzalez-Paramos, C., Moreno-Izquierdo, A., Schneiderat, P., Fraga, M.F., Fernandez, A.F., Garesse, R. and Gallardo, M.E. (2016) 'Generation of a human iPSC line from a patient with a defect of intergenomic communication', Stem Cell Res, 16(1), pp. 120-3.